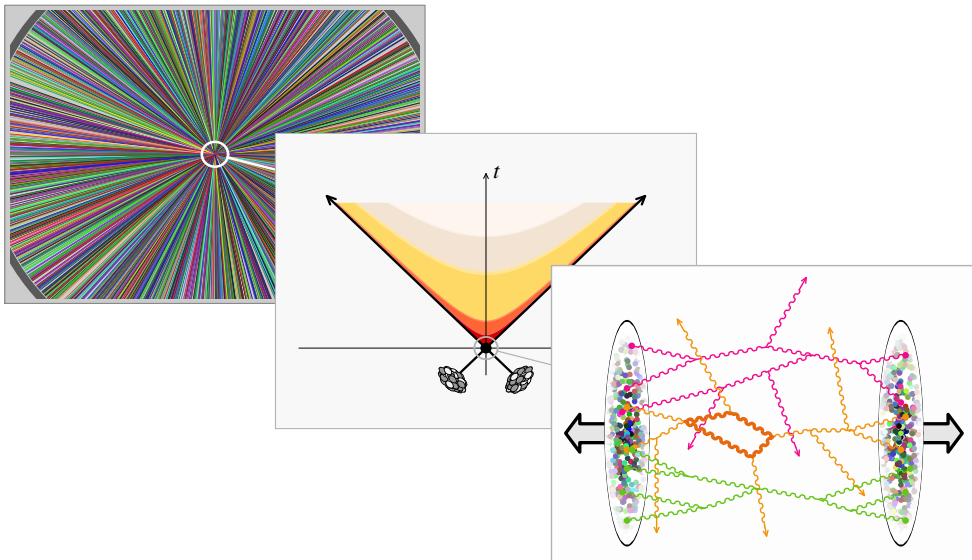


The Initial Stages of High Energy Heavy Ion Collisions

FRANÇOIS GELIS



Abstract



In this manuscript, we review the description of the initial stages of high energy heavy ion collisions in the Color Glass Condensate framework. The primary goal of this work is to provide a first principles approach, based on Quantum Chromo-Dynamics, to the calculation of initial conditions for the subsequent hydrodynamical evolution of the matter produced in heavy ion collisions such as those studied at RHIC or at the LHC.

In the first part, we develop some general tools and results that are useful in any quantum field theory coupled to strong external sources. We show how to organize the expansion in powers of the coupling constant in these theories, with a particular emphasis on the simplifications that arise when one considers inclusive observables.

In the second part, we apply these techniques to the Color Glass Condensate. We show that the dependence of inclusive observables on the collision energy arises from logarithmic terms that can be factorized into universal distributions that describe the color charge content of high energy nuclei. We then present some phenomenological applications of this factorization theorem, and confront these predictions with measurements performed at RHIC.

In the last part, we focus on the final state evolution of the system, with emphasis on the issue of thermalization of the matter produced in heavy ion collisions. Starting from the existence of instabilities in the classical Yang-Mills equations, that lead to secular divergences in observables when higher order corrections are included, we develop a resummation scheme that collects all the dominant secular terms and leads to finite expressions. Finally, we show on the example of a scalar field theory that this resummation has also the virtue of making the system relax towards thermal equilibrium.

Keywords



Quantum-Chromo-Dynamics,
Heavy ion collisions,
Gluon saturation, Color Glass Condensate,
Classical fields, Factorization,
Secular divergence, Thermalization

Relevant works

- [1] *Gluon propagation inside a high-energy nucleus*,
F. Gelis, Y. Mehtar-Tani,
Phys. Rev. **D73**, 034019 (2006).
- [2] *Particle production in field theories coupled to strong external sources, I: Formalism and main results*,
F. Gelis, R. Venugopalan,
Nucl. Phys. **A776**, 135 (2006).
- [3] *Particle production in field theories coupled to strong external sources, II: Generating functions*,
F. Gelis, R. Venugopalan,
Nucl. Phys. **A779**, 177 (2006).
- [4] *Initial singularity of the Little Bang*,
K. Fukushima, F. Gelis, L. McLerran,
Nucl. Phys. **A786**, 107 (2007).
- [5] *High energy factorization in nucleus-nucleus collisions, I: General results*,
F. Gelis, T. Lappi, R. Venugopalan,
Phys. Rev. **D78**, 054019 (2008).
- [6] *High energy factorization in nucleus-nucleus collisions, II: Multigluon correlations*,
F. Gelis, T. Lappi, R. Venugopalan,
Phys. Rev. **D78**, 054020 (2008).
- [7] *High energy factorization in nucleus-nucleus collisions, III: Long range rapidity correlations*,
F. Gelis, T. Lappi, R. Venugopalan,
Phys. Rev. **D79**, 094017 (2009).
- [8] *Glasma flux tubes and the near side ridge phenomenon at RHIC*,
A. Dumitru, F. Gelis, L. McLerran, R. Venugopalan,
Nucl. Phys. **A810**, 91 (2008).
- [9] *Long range two-particle rapidity correlations in A+A collisions from high energy QCD evolution*,

K. Dusling, F. Gelis, T. Lappi, R. Venugopalan,
Nucl. Phys. **A836**, 159 (2010).

[10] *Glittering Glasma*,
F. Gelis, T. Lappi, L. McLerran,
Nucl. Phys. **A828**, 149 (2009).

[11] *The role of quantum fluctuations in a system of strong fields:
Onset of hydrodynamical flow*,
K. Dusling, T. Epelbaum, F. Gelis, R. Venugopalan,
Nucl. Phys. **A850**, 69 (2011).

[12] *The evolving Glasma*,
K. Fukushima, F. Gelis,
arXiv:1106.1396, to appear in Nucl. Phys. **A**.

[13] *The initial spectrum of fluctuations in the little bang*,
K. Dusling, F. Gelis, R. Venugopalan,
Nucl. Phys. **A872**, 161 (2011).

[14] *The role of quantum fluctuations in a system of strong fields:
Spectral properties and Thermalization*,
T. Epelbaum, F. Gelis,
Nucl. Phys. **A872**, 210 (2011).

Prologue



Heavy Ion collisions, at least in their early stages, should in principle be amenable to a description in terms of Quantum Chromo-Dynamics since they involve only interactions among quarks and gluons. However, they present very interesting challenges for QCD. Firstly, it is a priori not obvious that the typical momentum transfer in the partonic collisions is large enough compared to the confinement scale in order to allow a perturbative approach. Another difficulty is that heavy ion collisions involve a very large number of constituents (mostly gluons) in the initial state, while standard perturbative techniques are designed to treat rare processes involving very few particles. Moreover, the kinematics of particle production in heavy ion collisions is such that they are dominated by constituents that carry a very small fraction of the momentum of their parent nucleon. In this regime, the parton densities are large and receive non-linear corrections due to gluon recombination, an effect known as *gluon saturation*. The standard parton model, completed by the DGLAP or BFKL evolution equations for the parton distributions, does not take these non-linear corrections into account. The two issues are in fact closely related, since the non-linear interactions among the gluons dynamically generate a semi-hard scale that enables an expansion in powers of the coupling.

My first encounter with the questions addressed in this manuscript goes back to 2000, while a postdoc in the Nuclear Theory group at Brookhaven National Laboratory. L. McLerran had told me about a recent work of him and A. Baltz [15], in which they had derived a neat formula for the production of e^+e^- pairs in peripheral collisions of high energy nuclei, in terms of retarded solutions of Dirac's equation in the electro-magnetic field of the two moving nuclei. Since in this approach the fast nuclei act as strong sources, it was natural to obtain an answer in terms of classical solutions of the field equations of motion, but there was still some confusion concerning their boundary conditions. In a work with A. Peshier [16], we proved that inclusive observables are given by retarded boundary conditions, but that this is incorrect for exclusive observables. A typical exclusive observable in this context is the probability P_n for producing exactly n electron-positron pairs, while the mean number of produced pairs $\langle N \rangle \equiv \sum_n n P_n$ is an inclusive observable. Loosely speaking, time-ordered amplitudes (i.e. standard Feynman diagrams) lead to $P_{1,2,\dots}$, while $\langle N \rangle$ is directly given by retarded amplitudes.

We employed similar techniques in 2004 with J.-P. Blaizot and R. Venugopalan [17–19] to compute the yield of gluons and quark-antiquark pairs in proton-nucleus collisions. The complications related to the choice of the boundary conditions are not essential in this problem, thanks to the presence of one weak source – which implies that $P_1 \approx \langle N \rangle \ll 1$ and therefore that we need not distinguish so carefully between inclusive and exclusive observables. Nevertheless, this problem was another instance where the approach in terms of retarded classical fields proved superior to the direct computation of Feynman graphs, because it simplified considerably the calculations.

We went back to the problem of heavy ion collisions in 2006 with R. Venugopalan in a series of two papers [2, 3]. A lot of work, mostly numerical, had already been done by A. Krasnitz, R. Venugopalan, Y. Nara [20–25] and T. Lappi [26] on the computation of the gluon yield in nucleus-nucleus collisions, using the Color Glass Condensate framework. In this approach, the gluon yield is obtained by solving the classical Yang-Mills equations with null boundary conditions in the remote past. Here also, the choice of the boundary conditions had remained rather mysterious. In these two papers, we addressed several aspects of the following question: *In a field theory coupled to strong time-dependent sources, what can be said of the distribution of produced particles?* In particular, we noticed a general relationship between the inclusiveness of an observable and the boundary conditions of the classical fields that are needed for its evaluation. We showed that, at leading and next-to-leading orders, inclusive moments of the particle distribution involve retarded boundary conditions. Moreover, we developed in these papers tools that were sufficiently powerful to extend the computation of the gluon yield beyond leading order.

Next-to-leading order corrections to an observable contain terms that are enhanced by large logarithms of the collision energy. For the Color Glass Condensate to be a consistent effective theory, one should be able to factorize these logarithms into universal distributions that represent the two projectiles. Proving this factorization requires to know analytically these logarithms – a daunting task given the non-perturbative nature of the classical solutions of the Yang-Mills equations. A crucial step to go around this difficulty was made during the summer 2006 with T. Lappi: we managed to relate the NLO and LO gluon yields by the action of an operator that involves only perturbative quantities. Moreover, the structure of this operator was quite similar to that of the JIMWLK Hamiltonian that drives the evolution of the source distributions in the Color Glass Condensate framework. Therefore, this expression of the NLO corrections seemed to be a promising starting point to establish factorization.

Eventually, the logarithmic part of this operator was indeed proven to be identical to the JIMWLK Hamiltonian [5]. Once this is established, the factorizability of the logarithms of energy in the gluon spectrum becomes almost trivial. We then generalized this factorization result to the case of the inclusive multigluon spectra [6, 7]. Moreover, these results for correlations and fluctuations proved to be relevant for the phenomenology of heavy ion collisions, since they can be applied to some experimental observations made at RHIC [8, 10] and possibly even in proton-proton collisions at the LHC [27].

The JIMWLK factorization resums all the leading singularities that arise from the evolution of the projectiles prior to their collision. The next question that arises is that of the thermalization of the matter produced in heavy ion collisions. Here also, thanks to a rather large saturation scale, one may hope to address the problem in a weak coupling setting. It turns out that the final state evolution is plagued with secular divergences, and there is abundant speculation [28–52] that they may play a role in the thermalization. We investigated this issue in recent works [11, 13, 14], first by developing a resummation scheme that cures these secular divergences, and secondly by showing via the example of a simpler toy model that this leads indeed to the relaxation of the system towards the equation of state expected at equilibrium. This is by no means a settled issue. Whether the same occurs in QCD in the realistic conditions of a high energy heavy ion collision is still open for debate, and even if the same applies to QCD it is unclear at the moment whether the system reaches full local thermal equilibrium or not.

Acknowledgements



he results presented in this manuscript owe a lot to my collaborators, in particular Raju Venugopalan and Tuomas Lappi with whom the main results have been obtained. Working and discussing with them, about these and many other questions, was a great source of inspiration and insight. Adrian Dumitru, Kevin Dusling, Thomas Epelbaum, Kenji Fukushima and Yacine Mehtar-Tani also greatly contributed to some of the works discussed in this manuscript.

I should also thank warmly Larry McLerran, who introduced me to these issues ten years ago while I was a postdoc at BNL and taught me a good deal of what I know about QCD at small x . Even after this postdoctoral stay, the support of the Nuclear Theory group at BNL, extended to me during many subsequent visits, was instrumental in getting many of these works started or completed.

I am equally indebted to my former PhD supervisor, Patrick Aurenche, who taught me a lot about physics in general and about the Schwinger-Keldysh formalism in particular. Some of the tricks used in this manuscript are directly inspired by his retarded-advanced formalism at finite temperature.

Of course, I'm indebted to many others, who contributed indirectly to the works presented here by their discussions, insightful questions or criticisms – among them Javier Albacete, Emil Avsar, Ian Balitsky, Joachim Bartels, Guillaume Beuf, Jean-Paul Blaizot, Hiro Fujii, Yoshi Hatta, Edmond Iancu, Kazunori Itakura, Jamal Jalilian-Marian, Sangyong Jeon, Keijo Kajantie, Dima Kharzeev, Yuri Kovchegov, Alex Kovner, Julien Laidet, Andrei Leonidov, Jinfeng Liao, Matt Luzum, Cyrille Marquet, Guilherme Milhano, Al Mueller, Stéphane Nonnenmacher, Jean-Yves Ollitrault, Robi Peschanski, André Peshier, Rob Pisarski, Andreas Shafer, Dam Son, Gregory Soyez, Anna Stasto, Dionysis Triantafyllopoulos, Heribert Weigert...

I would also like to thank all the experimentalists involved in the study of heavy ion collisions at RHIC and at the LHC, with a special mention to Alexandre Charpy, Magdalena Malek and Cynthia Hadjidakis from the IPN in Orsay, with whom I've had numerous discussions about the phenomenological aspects of gluon saturation.

Finally, I should thank my home institution, the Institut de Physique Théorique at CEA, Saclay, for providing us a great work environment, combining a very competent support staff and a highly stimulating research atmosphere.



Reality is that which, when you stop believing in it, doesn't go away.

PHILIP K. DICK

Contents

Abstract	i
Relevant works	iii
Prologue	v
Acknowledgements	vii
I Quantum Field Theory with Strong External Sources	1
1 Quantum Chromo-Dynamics in heavy ion collisions	5
1.1 Kinematics	7
1.2 Nucleon structure at high energy	8
1.3 Gluon saturation	10
1.4 McLerran-Venugopalan model	12
1.5 Color Glass Condensate	15
2 Particle production from strong classical sources	17
2.1 Power counting	18
2.2 Generic features of the particle distribution	20
2.3 Generating functional	29
2.4 Inclusive moments at leading order	34
2.5 Exclusive quantities at leading order	36
2.6 Next-to-Leading Order corrections	37
II Initial State Factorization in Heavy Ion Collisions	47
3 Inclusive gluon spectra at Leading Log accuracy	51
3.1 Gluon spectrum at Leading Order	52
3.2 Leading logarithms in the single gluon spectrum	59
3.3 Logarithms in the energy-momentum tensor	81
3.4 Multigluon correlations at Leading Log accuracy	84

4	RHIC phenomenology	91
4.1	Glasma and color flux tubes	91
4.2	Long range rapidity correlations	94
4.3	Multiplicity fluctuations	107
III	Final State Evolution, Thermalization?	117
5	Unstable modes; Secular Terms Resummation	121
5.1	Unstable modes in Yang-Mills equations	121
5.2	Resummation of the secular divergences	123
5.3	Initial spectrum of fluctuations	128
5.4	Time evolution of the distribution of initial conditions	133
6	Toy model study: Scalar fields in a box	137
6.1	Model setup	138
6.2	Toy calculation with uniform fluctuations	144
6.3	Equation of state	148
6.4	Spectral properties and thermalization	153
	Conclusions and Perspectives	181
IV	Appendices	183
A	Schwinger-Keldysh formalism	185
A.1	Standard perturbation theory	185
A.2	Schwinger-Keldysh perturbation theory	187
A.3	Relation between the functionals $Z[\eta]$ and $Z^{\text{sk}}[\eta]$	190
A.4	Propagators in a background field	191
B	Green's formulas	195
B.1	Green's formula for a retarded classical scalar field	195
B.2	Extension to a generic initial surface	197
B.3	Green's formula for small field fluctuations	199
B.4	Schwinger-Keldysh formalism	201
B.5	Summing tree diagrams using Green's formulas	203

C	Small fluctuations in a background field	207
C.1	Basis of retarded small fluctuations	207
C.2	Completeness relations	208
C.3	$\mathcal{G}_{+-}(x, y) = \mathcal{G}_{-+}(x, y)$ for $(x - y)^2 < 0$	209
D	Light-cone coordinates, Light-cone gauge	213
D.1	Light-cone coordinates	213
D.2	Gluon propagator in LC gauge	214
D.3	Green's formulas in LC gauge	215
D.4	Propagation through a shockwave background	218
E	Laplacian Green's function in two dimensions	221
E.1	Definition	221
E.2	Derivatives of the Green's function	221
E.3	Useful identities	223
F	Liouville equation	225
F.1	Hamilton's equations	225
F.2	Liouville's equation	226
F.3	Basic properties	226
	Bibliography	227
	Index	235

Part I

Quantum Field Theory with Strong External Sources

Introduction



In the first chapter, we present a brief overview of heavy ion collisions, focusing on the QCD aspects that are essential in their study. We then present the McLerran-Venugopalan (MV) model, proposed as an effective description of gluon saturation. Then, we end the chapter with a brief account of the Color Glass Condensate (CGC), that improves over the MV model by providing a renormalization group evolution equation.

The major feature of the CGC effective theory is that it couples quantum fields to an external time-dependent classical source. Moreover, this external source is strong, which makes calculations non-perturbative. In the chapter 2, we study the main features of such a theory, focusing on aspects related to particle production. Since our intent is to focus on the specificities of having a strong external source, we use a simpler toy scalar theory instead of QCD in this discussion.

We end the chapter by some expressions for the inclusive spectra at Next-to-Leading Order. This is a crucial step for our study of factorization in heavy ion collisions, discussed in the second part of this manuscript. In particular, we derive a master formula, easily generalizable to QCD, that expresses the NLO corrections in a form that already contains the essence of factorization.

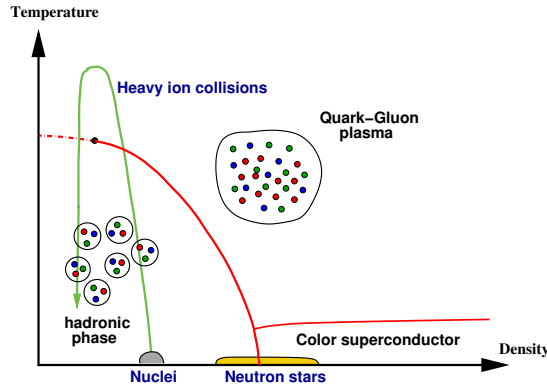
Chapter 1

Quantum Chromo-Dynamics in heavy ion collisions



attice simulations¹ of Quantum Chromo-Dynamics (QCD) indicate the existence of a transition at high temperature, from a phase where quarks and gluons are bound into hadrons and chiral symmetry is spontaneously broken to a phase where the quarks and gluons are deconfined and the chiral symmetry is restored. QCD predicts that this transition occurs when the nuclear matter reaches a critical energy density around $\epsilon_c \approx 1 \text{ GeV/fm}^3$. A sketch of the phase diagram of nuclear matter is represented in the figure 1.1. Note however that only the region of very small baryonic den-

Figure 1.1: QCD phase diagram.



sity has been studied quantitatively by lattice simulations. At non-zero baryonic density, the Euclidian QCD action is complex valued, making Monte-Carlo evaluations of the partition function unpractical². High energy collisions of large nuclei are a way to make an incursion

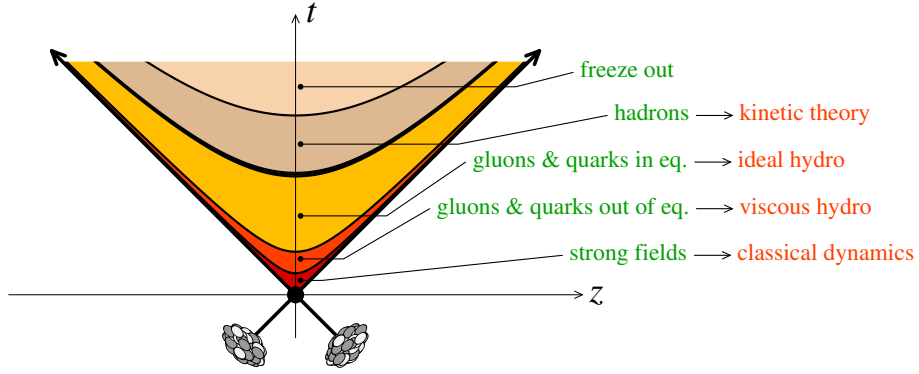
¹See [53] for recent lattice results on the QCD equation of state.

²Several methods have been explored in the past years in order to overcome this difficulty. The principal strategies that have been used are the analytic continuation from an imaginary baryonic chemical potential μ_B , the Taylor

into the deconfined region. In these collisions, one tries to infer the properties of the deconfined phase from features of the final products – such as their momentum spectra, chemical composition, or correlations.

Due to the macroscopic nature of heavy ion collisions (compared to the typical hadronic size), it makes sense to talk about the spatio-temporal development of the system created in such a collision. In fact, experimental techniques such as Hanbury-Brown-Twiss intensity interferometry give (to a limited extent) access to this history. The main stages of a heavy ion collision are illustrated in the figure 1.2. A particularly successful description of this evolution

Figure 1.2: Stages of a heavy ion collision.



is to treat it as the expansion of a fluid in empty space, via hydrodynamical equations [54–56]. Furthermore, it appears that this fluid is nearly perfect in the sense that it flows with almost zero dissipation – in other words, it has a very small viscosity [57].

QCD enters at several places in this description. The equation of state of the quark gluon plasma can be predicted from QCD lattice simulations [53], or even perturbative calculations at a large enough temperature [58, 59]. Moreover, the hydrodynamical evolution needs some initial conditions for the energy density, pressure and velocity fields. In collisions at high energy, it is possible to calculate these initial conditions by a perturbative expansion³. This statement is far from trivial: indeed, if most of the energy deposited in the collision were in modes near the QCD confinement scale Λ_{QCD} , then calculating the initial value of the energy-momentum tensor would not be tractable by weak coupling methods. As we shall see, a weak coupling treatment of this problem is made possible by the emergence of a dynamical scale, called the *saturation momentum* and denoted Q_s , where all the relevant dynamics take place. Most of the energy deposited in the collision is in momentum modes near Q_s . Moreover, the saturation momentum increases with the energy of the collision, and is much larger than Λ_{QCD} in high energy collisions. Since Q_s is also the relevant scale for the QCD coupling, this explains why this problem can be treated as a weak coupling problem, thanks to asymptotic freedom.

expansion at small μ_B , or reweighting techniques to compute expectation values at non-zero μ_B from an ensemble of gauge configurations obtained at $\mu_B = 0$. However, there is still a large uncertainty on the localization of the critical point (where the first order transition line ends), or even on its existence.

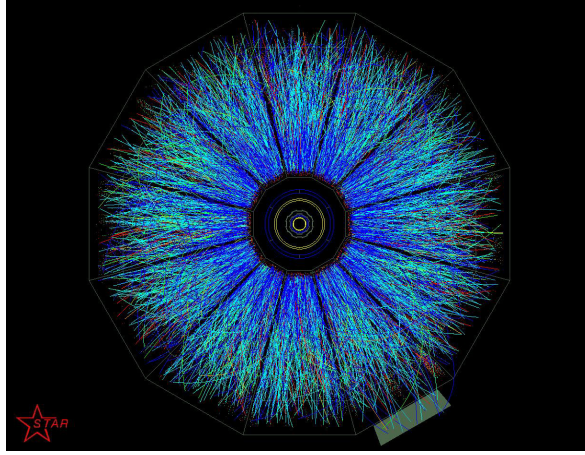
³As we shall see later in this manuscript, the initial energy density has a well defined expansion in powers of the QCD coupling α_s . However, the calculation of a given order in this expansion requires to resum an infinite set of graphs, and in that sense bears some non-perturbative features.

The projectile modes that matter the most in a high energy collision are those that carry only a very small fraction of the longitudinal momentum of the incoming projectiles. These modes have a large occupation number, which makes their interactions important – a phenomenon known as *gluon saturation*. The saturation momentum mentioned in the previous paragraph originates in fact from these interactions. In this chapter, we describe qualitatively the main aspects of gluon saturation, and present the *Color Glass Condensate* (CGC), an effective theory based on QCD that enables quantitative calculations in the saturated regime.

1.1 Kinematics

The figure 1.3 shows a typical collision at small impact parameter between two heavy nuclei, performed at RHIC ($\sqrt{s} = 200$ GeV per nucleon pair). A striking feature of such a collision

Figure 1.3: *Event display of a central heavy ion collision in the STAR detector.*



is the very high particle multiplicity in the final state, of the order of 1000 charged particles per unit rapidity at this energy. Another important property is that most of these particles carry a small transverse momentum, below 2 GeV. At a microscopic level, a nucleus-nucleus collision is made of many elementary collisions between the quarks and gluons contained in the incoming nuclei. For the sake of the argument, let us assume that a gluon moving in the $+z$ direction, with 4-momentum $p_1^\mu = (p_1, 0, 0, p_1)$, collides with a gluon moving in the opposite direction, with 4-momentum $p_2^\mu = (p_2, 0, 0, -p_2)$, producing a final state of 4-momentum P^μ . From the conservation of energy and momentum, we have

$$p_1^\mu + p_2^\mu = P^\mu . \quad (1.1)$$

Thus, $p_1 + p_2 = P^0$ and $p_1 - p_2 = P^3$ (while $P^1 = P^2 = 0$). It is convenient to parameterize the energy P^0 of the final state and its longitudinal momentum P^3 in terms of its transverse mass M_\perp and rapidity Y :

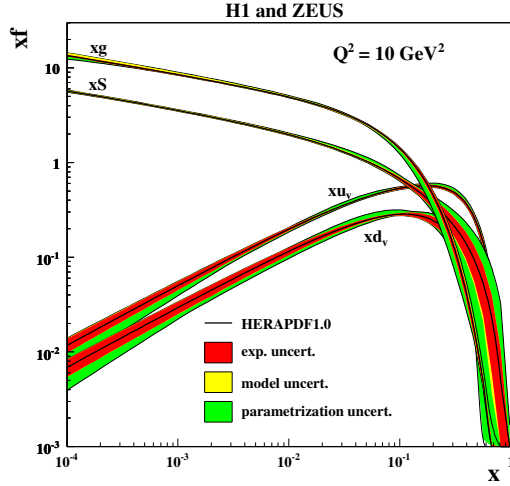
$$P^0 \equiv M_\perp \cosh Y \quad , \quad P^3 \equiv M_\perp \sinh Y , \quad (1.2)$$

so that we have

$$p_1 = \frac{M_\perp}{2} e^\gamma, \quad p_2 = \frac{M_\perp}{2} e^{-\gamma}. \quad (1.3)$$

The longitudinal momentum of a nucleon is $\sqrt{s}/2$ for a collision where the center of mass

Figure 1.4: *Parton distributions in a proton. From [60].*



energy per nucleon pair is \sqrt{s} . Therefore, the two colliding gluons carry the following fractions of the longitudinal momentum of their parent nucleon:

$$x_1 \equiv \frac{2p_1}{\sqrt{s}} = \frac{M_\perp}{\sqrt{s}} e^\gamma, \quad x_2 \equiv \frac{2p_2}{\sqrt{s}} = \frac{M_\perp}{\sqrt{s}} e^{-\gamma}. \quad (1.4)$$

Since the typical transverse momentum scale for the produced particles is of the order of a couple of GeVs, the corresponding longitudinal momentum fraction is

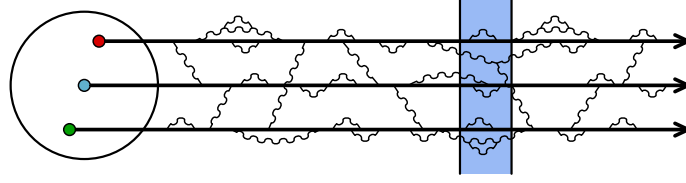
$$\begin{aligned} x &\sim 10^{-2} && \text{at RHIC } (\sqrt{s} = 200 \text{ GeV}), \\ x &\sim 4 \cdot 10^{-4} && \text{at the LHC } (\sqrt{s} = 5.5 \text{ TeV}). \end{aligned} \quad (1.5)$$

Thus, the partonic collisions that produce most of the particles in high energy heavy ion collisions involve partons that carry a very small fraction of the momentum of their parent nucleon. From measurements of the parton distributions in a proton (see the figure 1.4), we see that at these values of x , the vast majority of these partons are gluons.

1.2 Nucleon structure at high energy

Before we discuss in more detail the physics that drives the gluon content of a nucleon at small x , let us start with a qualitative description of the structure of a nucleon. A nucleon

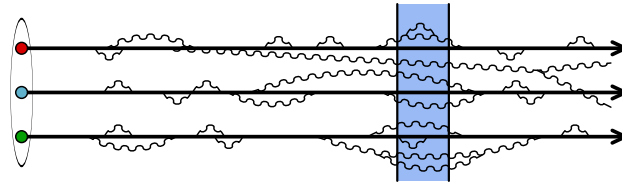
Figure 1.5: Nucleon at low energy.



is a bound state of three *valence* quarks, and the binding force comes from gluon exchanges between these quarks. In addition, vacuum fluctuations are also present, that for instance turn momentarily a quark into a quark and a gluon. A cartoon of this structure is shown in the figure 1.5. In this figure, the horizontal axis represents the time, and we have shown several gluon exchanges between the valence quarks, and some vacuum fluctuations. These fluctuations can exist on any space-time scale smaller than the nucleon size, but the very small ones are not visible in a typical reaction. Indeed, when the nucleon is probed by an external object (e.g. the virtual photon in Deep Inelastic Scattering), this probe is characterized by certain time and length scales (the photon frequency and wavelength in the case of DIS). Only the fluctuations that are longer lived and larger than the characteristic scales of the probe are accessible to that probe.

This basic picture of a nucleon goes a long way into explaining the *parton model* for nucleon interactions at high energy. At low energy, the main issue is that the non-perturbative dynamics going on inside the nucleon mixes with the interaction with the external probe, because the two have similar space-time scales. Let us now consider the same process with a nucleon at a much higher energy, in a frame where the probe is unchanged (i.e. all the boost is applied to the nucleon). All the internal time-scales of the nucleon are dilated by the Lorentz factor of the boost: interactions among the constituents take much longer, and quantum fluctuations are much longer lived. The main simplification is that the constituents of the nucleon no longer interact significantly over the time-scale seen by the external probe (represented in blue in the figure 1.6). Thus, at high energy, a nucleon appears as a collection of *quasi free constituents*. The other outcome of the boost is that, by increasing the lifetime

Figure 1.6: Nucleon at high energy.



of the fluctuations, it made a larger number of them accessible to the probe. If the lifetime of a fluctuation is large compared to the characteristic time-scale of the probe, this fluctuation is seen as an extra on-shell gluon. Thus, the number of gluons (and also of sea quarks, not represented on the figures 1.5 and 1.6) in a nucleon appears to increase as its energy increases. The new gluons uncovered by the boost have smaller and smaller momentum fractions x : this

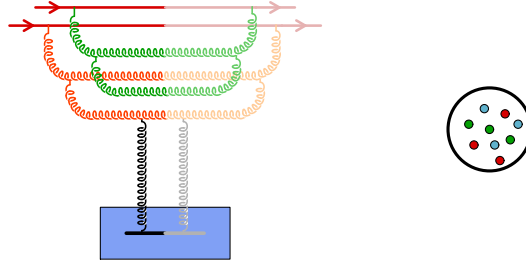
is the qualitative explanation for the rise at small x of the gluon distribution that one can see in the figure 1.4.

Another consequence of the boost is that the fluctuations that were already visible before the boost are now very long lived: their time evolution is slowed down by the boost, and they can be considered as static for the duration of the interaction process with the probe. The only relevant information about these fast modes is the color current they carry. This remark about the fast partons is at the basis of the McLerran-Venugopalan model and of the Color Glass Condensate, that we shall introduce later in this chapter.

1.3 Gluon saturation

The previous discussion of the evolution of the nucleon structure under a boost suggests that the gluon content evolves at small x via cascades such as those displayed in the figure 1.7: each valence quark starts its own cascade of gluons, that have increasingly small longitudinal momenta as one moves down in the cascade. As long as these gluon cascades do not

Figure 1.7: *Linear evolution: gluons do not overlap in the transverse plane, and gluon cascades evolve independently.*



interact, the evolution can be described by a linear equation for the gluon distribution: the Balitsky-Fadin-Kuraev-Lipatov (BFKL) equation [61, 62], that provides the x -dependence of the *non-integrated* (i.e. transverse momentum dependent) gluon distribution. The kernel of this equation has positive eigenvalues, which are responsible for the increase of the gluon distribution when $x \rightarrow 0$ – and its solutions behave roughly as a positive power of $1/x$.

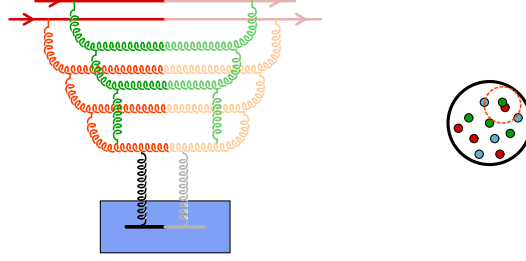
However, this increase of the gluon density cannot continue forever. When the gluons become densely packed in the wavefunction of a nucleon, the interactions between gluons from different cascades cannot be neglected anymore, as illustrated in the figure 1.8. These mergings of gluons from different cascades slow down⁴ the increase of the gluon distribution at small x , by adding a term quadratic in the gluon density, with a negative coefficient, to the BFKL equation. This effect is known as *gluon saturation*. Very schematically, the modified equation reads⁵:

$$\underbrace{\frac{\partial n(x, k_{\perp})}{\partial \ln(1/x)}}_{\text{BFKL}} = a \frac{\partial^2 n}{\partial k_{\perp}^2} + b n - c \alpha_s n^2, \quad (1.6)$$

⁴It has also been argued that an uninterrupted rise of the gluon distribution of the form $x^{-\lambda}$ would eventually violate unitarity bounds –such as the Froissart bound [63]– for hadronic cross-sections.

⁵The actual equation is more complicated than eq. (1.6). In particular, it has a non local kernel in transverse momentum, which is mimicked here by a diffusion term.

Figure 1.8: Non-linear evolution: gluons overlap in the transverse plane, and mergings from different cascades occur.



where a, b and c are of order unity, and where the diffusion term in transverse momentum mimics the actual behavior of the BFKL equation. The extra power of α_s in front of the quadratic term reflects the fact that the merging of two gluon cascades requires two extra powers of the strong coupling g . Thus, we expect on the basis of this toy model that this non-linear correction becomes important when the gluon density is of order $1/\alpha_s$.

A more precise criterion for gluon saturation has been derived by Gribov, Levin and Ryskin in [64], in terms of the transverse momentum of these gluons. First of all, the relevant density here is the number of gluons per unit of transverse area. Indeed, the boost in the longitudinal direction turns the nucleon into a thin pancake due to Lorentz contraction. The wavelength of the probe being held fixed, it becomes larger than the thickness of the Lorentz contracted nucleon, and the probe therefore cannot resolve the gluon distribution in the longitudinal direction: it sees only the number of gluons integrated over the z axis. This surface density can be estimated by:

$$\mathcal{N} \sim \frac{xG(x, k_\perp^2)}{\pi R^2}, \quad (1.7)$$

where R is the radius of the nucleon. To decide whether this density is large enough to have gluon mergings, it should be compared to the cross-section for the recombination of two gluons, that can be estimated as

$$\sigma \sim \frac{\alpha_s}{k_\perp^2}. \quad (1.8)$$

When $\mathcal{N}\sigma \geq 1$, gluon recombination cannot be neglected anymore. This condition can be rewritten as an inequality for the transverse momentum of the gluons,

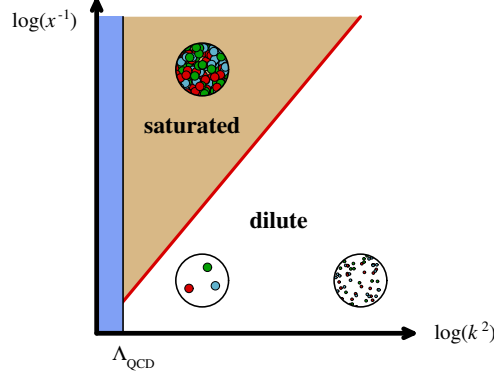
$$k_\perp \leq Q_s(x), \quad (1.9)$$

where $Q_s(x)$ is the *saturation momentum* and is defined in terms of the gluon distribution as

$$Q_s^2(x) \sim \frac{\alpha_s xG(x, Q_s^2)}{\pi R^2}. \quad (1.10)$$

From the inequality (1.9), one can divide the (x, k_\perp) plane in two domains: respectively dilute and saturated, as illustrated in the figure 1.9 (the red line separating the domains corresponds to the equality $k_\perp = Q_s(x)$).

Figure 1.9: Dilute (high k_\perp and high x) and saturated (low k_\perp and low x) domains. The strip at $k_\perp \leq \Lambda_{\text{QCD}}$ is dominated by confinement physics, and not accessible via weak coupling techniques.



The x dependence of the saturation momentum follows that of the gluon distribution. One has roughly $Q_s^2 \sim x^{-\lambda}$, where phenomenologically $\lambda \approx 0.3$ [65, 66]. Note also that nothing in the above derivation of the saturation condition is specific to a nucleon: the same condition applies to a nucleus, provided that one replaces in the saturation momentum the gluon distribution and the radius by the appropriate ones. The gluon distribution of a nucleus is approximately proportional to the mass number A , and its radius to $A^{1/3}$. Thus, the saturation momentum squared of a nucleus is proportional to $A^{1/3}$ [67] and $x^{-0.3}$,

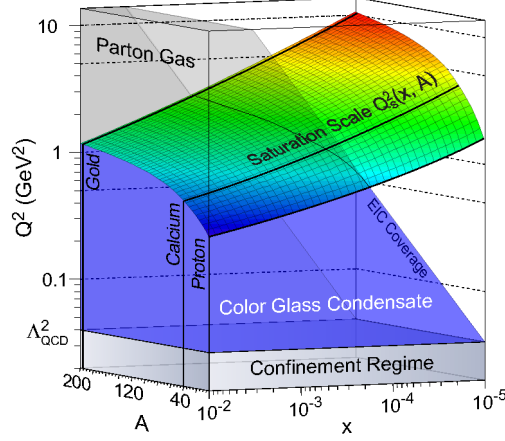
$$Q_s^2(x) \sim A^{1/3} \frac{1}{x^{0.3}}. \quad (1.11)$$

For large nuclei like the ones employed in heavy ion collisions (Gold at RHIC and Lead at the LHC), the nuclear enhancement of the saturation momentum is $A^{1/3} \approx 6$. From fits to existing data on deep inelastic scattering on various targets, one can get a more precise idea of the numerical value of the saturation momentum. This has been done in the references [67, 68], and the result is shown in the figure 1.10. Given the inequality (1.9), it is obvious that a larger saturation momentum means that saturation effects exist in a wider kinematical range. From eq. (1.11), we conclude that gluon saturation should be more prominent for heavy ion collisions at high energy. In fact, estimates of the saturation momentum for Gold nuclei at $x \approx 10^{-2}$ (RHIC kinematics) give $Q_s \approx 1.2$ GeV [67], indicated that the bulk of particle production at RHIC is affected by saturation. At the LHC, this value could thus reach $Q_s \approx 2$ GeV (at $x \approx 4 \cdot 10^{-4}$), making saturation even more important.

1.4 McLerran-Venugopalan model

Up to now, we have described gluon saturation at a very qualitative level. An important step towards a theoretical description of this phenomenon was provided by the McLerran-Venugopalan (MV) model [70–72]. In order to have a technically tractable model of a nucleon or nucleus, it is necessary to simplify the dynamics in the valence region, since this is the part where confinement effects make a full QCD treatment impossible. Once one has a handle

Figure 1.10: Numerical value of the saturation momentum, as a function of the longitudinal momentum fraction x and of the atomic number A . From [69].



on the fast partons, it is easy to compute how slower partons are radiated by bremsstrahlung. The main idea of the MV model is to replace the fast quanta in a nucleon or nucleus by simpler degrees of freedom that retain only the aspects that are essential in order to compute bremsstrahlung, while continuing to treat the slow gluons as full fledged gauge fields. As we have noted before, time dilation means that the fast quanta are quasi-static over the time-scales relevant in an interaction process. Moreover, in order to calculate the radiation of the slower gluons from the fast ones, one needs only to know the color current associated with the fast partons.

Thus, the MV model introduces a cutoff Λ^+ in the longitudinal momentum k^+ of partons. Partons that have $k^+ > \Lambda^+$ are replaced by a color current J_a^μ , of the form:

$$J_a^\mu(x) = \delta^{\mu+} \delta(x^-) \rho_a(\mathbf{x}_\perp) . \quad (1.12)$$

This current has only a nonzero $+$ component in light-cone coordinates (in ordinary Cartesian coordinates, this current has equal 0 and 3 components and vanishing transverse components). The factor ρ_a is a density of color charge per unit of transverse area. The static nature of these degrees of freedom translates into the fact that J_a^μ does not depend on x^+ . The delta function in x^- is motivated by the Lorentz contraction⁶.

The slow gluons, for which $k^+ < \Lambda^+$, are still described by the usual gauge fields A_a^μ , and their action is the standard Yang-Mills action⁷. Because of the time-scale separation between the fast and slow degrees of freedom, the coupling between them is Eikonal and appears in the action of the MV model as a term

$$\int d^4x J_a^\mu(x) A_{\mu a}(x) . \quad (1.13)$$

⁶It is not crucial to have exactly a $\delta(x^-)$, nor to have factorized x^- and \mathbf{x}_\perp dependences. Physical results are insensitive to the details of the x^- dependence, provided it is peaked around $x^- = 0$, on scales that are small compared to the physical longitudinal length scales.

⁷At small x , one usually disregards the quarks.

What is missing at this point is a theory or model for the color density ρ_a . ρ_a describes the distribution of the partons that have momentum k^+ larger than the cutoff Λ^+ . In a nucleon or nucleus, their distribution varies in time⁸ and their configuration at the time of a collision is a snapshot of this fluctuating distribution. Thus, one should treat ρ_a as a stochastic quantity, and complement the MV model with a statistical distribution $W[\rho_a]$ for the ρ_a 's.

The MV model goes one step further by proposing a model of the functional $W[\rho_a]$ for a large nucleus. First of all, the MV model assumes that the values of the color charge density at two distinct points in the transverse plane are not correlated. This assumption can be seen as a consequence of confinement: two color charges belonging to different nucleons are uncorrelated. Secondly, at a given \mathbf{x}_\perp , $\rho_a(\mathbf{x}_\perp) d^2\mathbf{x}_\perp$ is made up of all the color charges in a longitudinal tube of cross-section $d^2\mathbf{x}_\perp$. These charges are also random and uncorrelated, and there is a large number of them in a large nucleus (proportional to $A^{1/3}$) – thus, ρ_a is an incoherent sum of many random variables. The *Central Limit Theorem* implies that the statistical distribution of $\rho_a(\mathbf{x}_\perp)$ is a Gaussian distribution, characterized by a 2-point correlator of the form:

$$\langle \rho_a(\mathbf{x}_\perp) \rho_b(\mathbf{y}_\perp) \rangle = \mu^2 \delta_{ab} \delta(\mathbf{x}_\perp - \mathbf{y}_\perp) . \quad (1.14)$$

Under these assumptions, the distribution $W[\rho_a]$ reads:

$$W[\rho_a] = \exp \left[- \int d^2\mathbf{x}_\perp \frac{\rho_a(\mathbf{x}_\perp) \rho_a(\mathbf{x}_\perp)}{2\mu^2} \right] . \quad (1.15)$$

Given the distribution $W[\rho_a]$, the calculation of the expectation value of some observable \mathcal{O} in the MV model is performed as follows:

- i. Compute the observable in an arbitrary configuration ρ_a of the color sources, $\mathcal{O}[\rho_a]$. In the saturated regime, the power counting should be done by assuming that $\rho_a \sim g^{-1}$. In this regime, non-linearities in ρ_a are important even at Leading Order, which is the reason why this model is suitable to describe gluon saturation. At Leading Order, the sum of the relevant contributions can be resummed by solving the classical Yang-Mills equations,

$$[\mathcal{D}_\mu, \mathcal{F}^{\mu\nu}] = J^\nu . \quad (1.16)$$

- ii. Average $\mathcal{O}[\rho_a]$ over the distribution $W[\rho_a]$:

$$\langle \mathcal{O} \rangle = \int [D\rho_a] W[\rho_a] \mathcal{O}[\rho_a] . \quad (1.17)$$

To close this section, let us add a remark about gauge invariance. The distribution in eq. (1.15) is invariant under gauge transformations⁹, as well as the functional measure $[D\rho_a]$. Therefore, if \mathcal{O} is a gauge invariant operator, then the expectation value $\langle \mathcal{O} \rangle$ defined in eq. (1.17) is also gauge invariant.

⁸It appears static only over the short duration of the collision process.

⁹Under a gauge transformation, ρ_a transforms as

$$\rho_a(\mathbf{x}) t^a \rightarrow \Omega^\dagger(\mathbf{x}) [\rho_a(\mathbf{x}) t^a] \Omega(\mathbf{x}) .$$

1.5 Color Glass Condensate

The MV model allows one to make a number of phenomenological calculations at tree level, e.g. of the Deep Inelastic Scattering structure functions [73, 74] of a nucleon or nucleus or the density of energy released at early times in heavy ion collisions [21]. However, complications arise when one tries to use it beyond tree level. It was soon realized that the $\delta(x^-)$ factor in the color current leads to singularities in these calculations: in order to obtain finite results in loop calculations, it is necessary to assume a less singular x^- dependence:

$$\delta(x^-) \rho_a(\mathbf{x}_\perp) \rightarrow \rho_a(x^-, \mathbf{x}_\perp) , \quad (1.18)$$

where now the x^- dependence (absorbed into the definition of ρ_a because there is no reason to assume that the x^- and \mathbf{x}_\perp dependences factorize) is still peaked around $x^- = 0$ but not singular.

The second problem in loop corrections with the MV model is that they lead to logarithms of the cutoff Λ^+ that separates the fast static sources from the slow gauge fields [75]. This issue is in fact related to that of the x^- dependence of the color sources. It has been shown that the logarithms of Λ^+ can be absorbed into a redefinition of the sources, that consist in adding layers of new sources that slightly enlarge the support in x^- of ρ_a . This modification amounts to turn the distribution $W[\rho_a]$ into a Λ^+ -dependent distribution,

$$W[\rho_a] \rightarrow W_{\Lambda^+}[\rho_a] , \quad (1.19)$$

that obeys an evolution equation of the form [76–83]

$$\frac{\partial W_{\Lambda^+}}{\partial \ln(\Lambda^+)} = \mathcal{H} W_{\Lambda^+} , \quad (1.20)$$

where \mathcal{H} is an operator that contains first and second derivatives with respect to ρ_a . This evolution equation for W_{Λ^+} is known as the *JIMWLK equation*¹⁰. By letting W_{Λ^+} evolve according to this equation, observables become independent of the cutoff Λ^+ . Eq. (1.20) can therefore be seen as a renormalization group equation, that ensures the consistency of the MV effective description by making observables independent of its cutoff. One starts with some initial distribution $W_{\Lambda_0^+}$ at a scale Λ_0^+ , and eq. (1.20) describes how this distribution evolves as the cutoff decreases. As $\Lambda^+ \rightarrow 0$, one integrates out progressively all the quantum fluctuations (at leading logarithmic accuracy) into the distribution W_{Λ^+} . With this extension of W into a cutoff dependent distribution, the Gaussian distribution in eq. (1.15) should now be seen as a model for the initial condition of eq. (1.20).

Let us add that the functional evolution equation (1.20) can also be formulated as an infinite hierarchy of evolution equations for correlators of Wilson lines [84]. These equations are nested because the evolution equation for a n -point function depends on the value of some p -point function with $p > n$. In particular, the first equation of the hierarchy, for the evolution of a 2-point function, depends on a 4-point function. In the limit of a large number of colors and of large nuclei, it has been argued that this 4-point function can be written as the product of two 2-point functions. This assumption leads to a closed, non-linear, equation for the 2-point function [85, 86], now known as the Balitsky-Kovchegov equation.

¹⁰JIMWLK = Jalilian-Marian, Iancu, McLerran, Weigert, Leonidov, Kovner.

Because this equation is much simpler than the JIMWLK equation¹¹, it has been used in many phenomenological applications where evolution to small x was important.

The *Color Glass Condensate* is the name under which this effective theory (i.e. the separation of degrees of freedom proposed in the MV model, plus the JIMWLK evolution equation) is known¹². The word *glass* refers to the fact that the degrees of freedom described by the color density ρ_a evolve on a time scale much larger than the typical time-scale of collision processes, and also refers to the similarity between the averaging procedure in eq. (1.17) and spin glasses. The word *condensate* is due to the fact that gluons reach their largest possible occupation number, of order $1/\alpha_s$, in the saturated regime. Gluon saturation can be seen as a repulsive interaction that prevents all the gluons from collapsing on the zero transverse momentum state; because of this repulsion newly radiated gluons are forced to occupy momentum modes near $k_\perp \sim Q_s(x)$.

Originally, the JIMWLK equation was proven for the expectation value of gauge invariant operators in the wave function of a single nucleus, e.g. Deep Inelastic Scattering structure functions. One of the main goals in the rest of this manuscript is to show that in collisions of two saturated projectiles, like heavy ion collisions, one can also factorize the leading logarithms by applying the JIMWLK equation to the distributions $W[\rho_a]$ of *each projectile*. This result indicates the universality of these distributions, and establishes a connection between measurements done in DIS experiments and inclusive observables in heavy ion collisions, in the non-linear saturated regime. We will see in the part II how the JIMWLK equation arises in the context of heavy ion collisions.

¹¹By noticing that the JIMWLK equation is a Fokker-Planck equation in a functional space, one can reformulate it as a Langevin equation [87]. This formulation paves the way for a numerical study of the JIMWLK equation on the lattice [88]. This numerical study of the JIMWLK equation has shown that the Balitsky-Kovchegov equation is indeed a rather good approximation, at least as far as 2-point correlators are concerned. Recently, this direct numerical approach has started to find its way into more phenomenological applications [89, 90].

¹²See [91–93] for extensive reviews of the theoretical and phenomenological aspects of the Color Glass Condensate.

Chapter 2

Particle production from strong classical sources



he Color Glass Condensate effective theory is a Yang-Mills theory coupled to an external time-dependent color source. A crucial property in the saturation regime is that this source is *strong*, reflecting the fact that the gluon occupation number in a saturated hadron is of order α_s^{-1} . Thus the source should be thought of being of order g^{-1} . The strength of the source implies that calculating observables in this effective theory is a non-perturbative problem, even if the coupling constant g is weak. Indeed, even at leading order, infinitely many diagrams contribute to any given observable. However, as we shall see, the situation is manageable because the sum of this infinite series of diagrams usually has a compact expression in terms of classical solutions of Yang-Mills equations.

In this chapter, based on [2, 3], we discuss in detail the main features of quantum field theories coupled to a strong external source. The questions we focus on here are fairly general, and the answers are valid for any sensible quantum field theory – the only crucial requirement being unitarity. Therefore, in order to avoid the additional complexity (both notational and in the handling of the gauge freedom) of gauge theories, we will use a simpler example in this chapter, consisting of a scalar field theory. We will of course go back to QCD in the second part of this manuscript, when we address the problem of particle production in heavy ion collisions.

The first section of the chapter explains the power counting in such a theory, which is an essential step in classifying the relevant contributions to a given observable. In the rest of the chapter, we study several questions related to the distribution of the produced particles at $t \rightarrow +\infty$. First, we define a generating functional that encodes all the relevant information about the final state. We show also that its first derivative is the sum of two sets of connected diagrams in the Schwinger-Keldysh formalism. At leading order, they can be expressed in terms of solutions of the classical equations of motion of the theory, albeit with complicated boundary conditions. From this generating functional, we proceed to the study of moments of the distribution of produced particles, and show that at leading order they can all be written in terms of classical fields with simple retarded boundary conditions. In order to stress the special role played by inclusive observables, we discuss briefly in the last section the technical complications that arise when one considers exclusive observables.

Finally, we extend our study of inclusive quantities by computing the corrections they receive at next-to-leading order (NLO). As we shall see when we turn to the Color Glass Condensate and heavy ion collisions, the main goal of computing these quantities at NLO is to extract the large logarithms of the collision energy that they contain, and to resum these logarithms.

2.1 Power counting

Let us consider a scalar field theory coupled to a source j , whose Lagrangian is

$$\mathcal{L} \equiv \frac{1}{2}(\partial_\mu \phi)(\partial^\mu \phi) - \mathcal{U}(\phi) + j\phi. \quad (2.1)$$

The potential $\mathcal{U}(\phi)$ encodes the self-interactions of the field ϕ . The points we discuss in this chapter do not depend on the details of $\mathcal{U}(\phi)$, but when we draw examples of diagrams we usually assume cubic or quartic interactions for simplicity. For convenience in the subsequent power counting, we write the terms in this potential as¹

$$g\phi^3, \quad g^2\phi^4, \quad g^3\phi^5 \dots \quad (2.2)$$

We assume that all the coupling constants have the same order of magnitude in case there are several interaction terms in $\mathcal{U}(\phi)$, so that a unique parameter g appears in the power counting.

The Feynman rules for this theory are the usual ones, where the time-ordered propagator in momentum space reads²

$$G_F^0(p) = \frac{i}{p^2 + i\epsilon}, \quad (2.3)$$

and where the contribution of a 4-particle vertex is $-ig^2$. In momentum space, a source j attached to the end of a propagator of momentum p contributes a factor $i\tilde{j}(p)$ (where \tilde{j} is the Fourier transform of j).

The source $j(x)$ is a given function of space-time, fixed once for all (we do not consider the question of averaging over an ensemble of such j 's in this chapter). To make things interesting, we assume that $j(x)$ is *large*. By large, we mean that j is proportional to the inverse coupling g^{-1} – we call this situation the *dense* regime. In contrast, the situation where the external source j is small – typically of order g – is called the *dilute* regime. As one can see in the figure 2.1, there is a crucial difference between the dense and the dilute regimes when one studies particle production: in the dense regime, any vertex connected to a source j does not contribute to the overall order of magnitude of the diagram, since the factor g brought by the vertex is compensated by the g^{-1} from the source it is attached to.

Let us make this point more precise. Consider a simply connected diagram (see figure 2.2), with n_e external legs, n_i internal lines, n_l independent loops, n_j sources, and $n_v^{(3)}$

¹Only the dependence on the coupling constant is written here. In general, these interaction terms must have additional dimensional factors. For instance, in four space-time dimensions, the interactions terms should be of the form $g^{n-2}Q^{4-n}\phi^n$, where Q is some quantity or operator that has the dimension of a mass. In four dimensions, only the ϕ^4 interaction term has a dimensionless coupling constant. Terms with $n > 4$ are non-renormalizable interactions, and Q is the scale at which they become relevant.

²Throughout this document, the propagators are normalized with an i in the numerator, so that in coordinate space $\square_x G_F^0(x, y) = -i\delta(x - y)$.

Figure 2.1: In these graphs, each circular dot represents one power of the external source j . Left: typical graph contributing in the dilute limit $j \sim g$. Right: typical graph in the dense case $j \sim g^{-1}$.

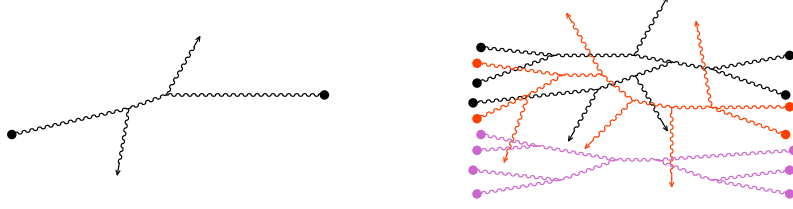
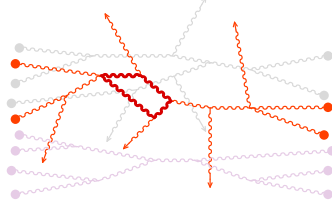


Figure 2.2: Connected subdiagram of a generic graph in the dense regime. In this example, $n_E = 5$, $n_I = 11$, $n_J = 4$, $n_L = 1$, $n_V^{(3)} = 5$ and $n_V^{(4)} = 2$.



cubic vertices, $n_V^{(4)}$ quartic vertices, etc... These parameters are not all independent. First, the number of propagator endpoints should match the available sites to which they can be attached. This leads to a first identity,

$$n_E + 2n_I = n_J + 3n_V^{(3)} + 4n_V^{(4)} + 5n_V^{(5)} + \dots \quad (2.4)$$

A second identity expresses the number of independent loops in terms of the other parameters,

$$n_L = n_I - (n_V^{(3)} + n_V^{(4)} + n_V^{(5)} + \dots) - n_J + 1. \quad (2.5)$$

It is obtained by recalling that the number of independent loops is the number of momenta flowing in the diagram that are not constrained by energy momentum conservation or by the choice of the external momenta that enter in the diagram. Each vertex provides a constraint among the momenta running on the n_I internal lines since the sum of the momenta arriving at a vertex must be zero. Similarly, each source provides a constraint, for the same reason. The final $+1$ is due to the fact that one of these constraints has to be a linear combination of the others, because of the global momentum conservation in the diagram.

Thanks to these two relations, the order of a diagram can be written as

$$j^{n_J} g^{n_V^{(3)} + 2n_V^{(4)} + 3n_V^{(5)} + \dots} = g^{-2} g^{n_E} g^{2n_L} (gj)^{n_J}. \quad (2.6)$$

First, we see that the final result does not depend on the number of vertices and on the number of internal lines; only the number of external legs, the number of independent loops and the

number of sources appear in the result. Moreover, because we have assumed strong sources, the factor $(gj)^{n_j}$ in the right hand side is of order unity and can be ignored in the power counting. In this case, the order of a diagram does not depend on its number of sources, and an infinite number of diagrams –with fixed n_E and n_L but arbitrary n_j – contribute at each order.

Note also that the previous power counting formula only applies to simply connected graphs. For graphs that are made of several disconnected subgraphs, the formula should be applied separately on each subgraph.

It is also interesting to discuss the order in the Planck constant \hbar of a given diagram. Recall that \hbar has the dimension of an action, so that the relevant quantity is the dimensionless ratio

$$\frac{S}{\hbar} = \int d^4x \left[-\frac{1}{2} \phi \frac{\square_x}{\hbar} \phi - \frac{1}{\hbar} \mathcal{U}(\phi) + \frac{j}{\hbar} \phi \right]. \quad (2.7)$$

One can thus apply the following mnemonic rules in order to compute the order in \hbar of a given diagram,

- i. a propagator has an \hbar in the numerator,
- ii. each vertex has a \hbar^{-1} ,
- iii. each source has a \hbar^{-1} .

Therefore, the order in \hbar of a generic connected diagram is given by

$$\hbar^{n_E + n_L - n_J - n_V^{(3)} - n_V^{(4)} - n_V^{(5)} - \dots} = \hbar^{n_E + n_L - 1}. \quad (2.8)$$

We see that the order in \hbar increases as the number of loops, the number of external legs n_E being held fixed. A particularly important case, that we shall encounter frequently later on, is that of 1-point functions, i.e. $n_E = 1$. At tree level ($n_L = 0$), this object is of order \hbar^0 , and is thus *classical*. As we will see, 1-point functions at tree level are in fact solutions of the classical equation of motion for the field, in accordance with the \hbar^0 power counting.

2.2 Generic features of the particle distribution

2.2.1 Exclusive and inclusive observables

Our main goal is to study particle production in a field theory whose Lagrangian is given by eq. (2.1), having in mind applications to heavy ion collisions described in the Color Glass Condensate framework. However, before exposing the tools that allow such a study, let us discuss in this section some generic aspects of the distribution of the produced particles. We limit ourselves here to those features that can be assessed without any detailed calculation, e.g. that follow simply from power counting arguments or unitarity considerations.

The initial state will always be assumed to be empty³, i.e. to be the state $|0_{\text{in}}\rangle$. Particle production is encoded in the transition amplitudes

$$\langle \mathbf{p}_1 \cdots \mathbf{p}_{n_{\text{out}}} | 0_{\text{in}} \rangle, \quad (2.9)$$

³Here, *empty* means that the only objects present in the initial state are those described by the external source j . In applications to heavy ion collisions, the two colliding nuclei will be encoded in such source terms. In this context, *empty* will therefore mean that only the two nuclei are present in the initial state.

that connect the in- vacuum state to a final state populated with n on-shell particles of momenta \mathbf{p}_1 to \mathbf{p}_n . Any observable related to particle production in this field theory can be expressed in terms of these amplitudes. For instance, the differential probability of producing exactly n particles is given by⁴

$$\frac{dP_n}{d^3\mathbf{p}_1 \cdots d^3\mathbf{p}_n} = \frac{1}{n!} \frac{1}{(2\pi)^3 2p_1} \cdots \frac{1}{(2\pi)^3 2p_n} |\langle \mathbf{p}_1 \cdots \mathbf{p}_{n\text{out}} | 0_{\text{in}} \rangle|^2, \quad (2.10)$$

where $\mathbf{p} \equiv |\mathbf{p}|$. More important in practical applications are inclusive observables. The simplest one is the *inclusive single particle spectrum*, defined by

$$\frac{dN_1}{d^3\mathbf{p}} \equiv \sum_{n=0}^{\infty} (n+1) \int d^3\mathbf{p}_1 \cdots d^3\mathbf{p}_n \frac{dP_{n+1}}{d^3\mathbf{p} d^3\mathbf{p}_1 \cdots d^3\mathbf{p}_n}. \quad (2.11)$$

Experimentally, this observable is obtained by the following procedure: for each event, make an histogram of the number of produced particles according to their momentum. Then, count the number of particles in the bin of momentum \mathbf{p} , and finally average this number over many events. Such a quantity is said *inclusive* because in its definition one particle is singled out, and all the other particles that may have been produced are integrated out.

2.2.2 Vacuum-vacuum diagrams

It is very handy to formulate the discussion of particle production from external sources in terms of the *vacuum-vacuum diagrams*. Vacuum-vacuum diagrams are simply Feynman diagrams that have no external legs (i.e. for which $n_e = 0$). They are contributions to the vacuum-to-vacuum transition amplitude $\langle 0_{\text{out}} | 0_{\text{in}} \rangle$, hence their name. The vacuum-vacuum diagrams also show up as disconnected factors in the perturbative expansion of any amplitude with external legs.

When one considers a field theory in the vacuum (i.e. with no external source j), the vacuum-vacuum diagrams are usually discarded. Indeed, it is easy to show that their sum is a pure phase, that appears as a prefactor in every transition amplitude but has no effect on transition probabilities. Physically, this is due to the fact that when $j = 0$, the in- vacuum must evolve into the out- vacuum with probability unity (since in an unitary theory with $j = 0$, particles cannot appear spontaneously from the vacuum).

The situation is very different in a theory in which the quantum fields are coupled to some external source j . Let us assume that this source is such⁵ that at least one transition from the in- vacuum to a populated state is non-zero:

$$\exists \alpha \neq 0, \quad \langle \alpha_{\text{out}} | 0_{\text{in}} \rangle \neq 0. \quad (2.12)$$

From unitarity, we know that

$$|\langle 0_{\text{out}} | 0_{\text{in}} \rangle|^2 + \sum_{\alpha \neq 0} |\langle \alpha_{\text{out}} | 0_{\text{in}} \rangle|^2 = 1, \quad (2.13)$$

⁴Throughout this document, the states are normalized so that $\langle \mathbf{p} | \mathbf{q} \rangle = 2p(2\pi)^3 \delta(\mathbf{p} - \mathbf{q})$.

⁵For instance if $j(x)$ has time-like Fourier modes, particles can be produced by a single source. In the color glass condensate, the kinematical properties of the sources are such that one needs at least two sources to produce a particle. In some cases, particles cannot be produced by any finite number of sources, but can be produced by some non-perturbative mechanisms (this is for instance what happens in the *Schwinger mechanism*).

where we have isolated the vacuum from the populated states in the sum over the final states. Thus, we conclude that

$$|\langle 0_{\text{out}} | 0_{\text{in}} \rangle|^2 < 1, \quad (2.14)$$

which means that the sum of the vacuum-vacuum diagrams is not a pure phase. Consequently, they cannot be discarded because they have a non trivial effect on the transition probabilities.

The sum of the vacuum-vacuum diagrams, $\langle 0_{\text{out}} | 0_{\text{in}} \rangle$, contains both simply connected and multiply connected diagrams. However, it is well known that the complete sum is the exponential of the sum of the simply connected diagrams. Hence, we can write

$$\langle 0_{\text{out}} | 0_{\text{in}} \rangle \equiv e^{i\mathcal{V}[j]}, \quad (2.15)$$

where $i\mathcal{V}[j]$ is the sum of all the simply connected vacuum-vacuum diagrams (it is a functional of the external source j). The prefactor i has been included for convenience. The diagrammatic expansion of $i\mathcal{V}[j]$ starts as follows

$$i\mathcal{V}[j] = \text{---} + \frac{1}{6} \text{---} + \frac{1}{8} \text{---} + \frac{1}{8} \text{---} + \dots \quad (2.16)$$

in a theory with cubic interactions. We have represented only tree diagrams in the right hand side, but of course $i\mathcal{V}[j]$ contains diagrams at any loop order. The rational number preceding each diagram is its symmetry factor. Note that the condition of eq. (2.14), that must be fulfilled in order to produce particles from the sources, can be rewritten as

$$e^{-2\text{Im } \mathcal{V}[j]} < 1, \quad (2.17)$$

which requires that $\text{Im } \mathcal{V}[j] \neq 0$. This can only happen in a field theory coupled to an external source. If $j = 0$, all the vacuum-vacuum diagrams are purely real and this condition cannot be satisfied.

If we write eq. (2.6) in the specific case $n_e = 0$ of connected vacuum-vacuum diagrams, we get

$$g^{-2} g^{2n_L} (gj)^{n_I} \sim g^{-2} g^{2n_L}. \quad (2.18)$$

(The right hand side is valid in the regime of strong sources, where $gj \sim 1$.) Thus, we see that all the tree connected vacuum-vacuum diagrams are of order g^{-2} , all the 1-loop ones are of order g^0 , etc...

This has several consequences. First, the argument of the exponential in eq. (2.15) is of order $g^{-2} \gg 1$, which means that the vacuum-to-vacuum transition amplitude is very different from unity (we already knew that its modulus is smaller than one, we now know that it is exponentially small). Also, since the argument of the exponential is of order g^{-2} , this implies that any quantity in which $\langle 0_{\text{out}} | 0_{\text{in}} \rangle$ appears as a prefactor is bound to have a pathological perturbative expansion⁶, since expanding the exponential generates arbitrarily high powers of g^{-2} . We will see that this problem affects the expression of the probabilities P_n , but that the inclusive quantities are free of this pathology.

The second consequence of the above power counting is that all the tree diagrams contribute at the same order in $i\mathcal{V}[j]$, which means that even the calculation of its leading order requires the resummation of an infinite series of diagrams.

⁶The function $f(z) \equiv \exp(-1/z)$ does not have a Taylor expansion around $z = 0$. Note however that quantities that have this problem may have a generalized expansion of the form $\exp(-A) * B$, where A and B have well defined perturbative series.

2.2.3 Cutting rules

Let us first discuss the *cutting rules* [94, 95] for vacuum-vacuum graphs in theories with external sources. These rules, for instance, can be employed to compute the imaginary part of $\mathcal{V}[j]$, which plays a crucial role in the study of the distribution of the produced particles.

One starts by decomposing the free Feynman (i.e. time-ordered) propagator in two pieces according to the time-ordering of the endpoints⁷

$$G_F^0(x, y) \equiv \theta(x^0 - y^0) G_{-+}^0(x, y) + \theta(y^0 - x^0) G_{+-}^0(x, y) . \quad (2.19)$$

This equation defines the functions G_{-+}^0 and G_{+-}^0 . The notations for these objects have been chosen in order to emphasize the analogy with the Schwinger-Keldysh formalism (see [96, 97], and our brief summary in appendix A). Pursuing this analogy, the Feynman propagator G_F^0 will be denoted G_{++}^0 . We introduce also the anti-time-ordered propagator G_{--}^0 defined as

$$G_{--}^0(x, y) \equiv \theta(x^0 - y^0) G_{+-}^0(x, y) + \theta(y^0 - x^0) G_{-+}^0(x, y) . \quad (2.20)$$

Note that the four propagators so defined are not independent, but obey the identity

$$G_{++}^0 + G_{--}^0 = G_{-+}^0 + G_{+-}^0 . \quad (2.21)$$

In addition to these four propagators, we will introduce two kinds of vertices, of type $+$ or $-$. The vertex of type $+$ is the ordinary vertex and gives a factor $-ig$ in Feynman diagrams. The vertex of type $-$ is the opposite of the $+$ vertex, and its Feynman rule is $+ig$. Likewise, for insertions of the source j , insertions of type $+$ appear with the factor $+ij(x)$ while insertions of type $-$ appear instead with $-ij(x)$. The motivation for introducing these additional vertices and sources will become clear shortly.

For each Feynman diagram iV (containing only “ $+$ ” vertices and sources) contributing to the sum of connected vacuum-vacuum diagrams, define a corresponding set of diagrams $iV_{\{\epsilon_i\}}$ by assigning the type ϵ_i to the vertex or source i of the original diagram (and connecting a vertex or source of type ϵ to a vertex or source of type ϵ' with the propagator $G_{\epsilon\epsilon'}^0$). Each ϵ_i can be either of the “ $+$ ” or “ $-$ ” type. Clearly the original Feynman diagram under consideration is nothing but $iV_{\{+\dots+\}}$. This generalized set of diagrams has 2^n terms if the original diagram had n vertices and sources. These diagrams obey the so-called *largest time equation* [95, 98]. If one considers these diagrams before the times at the vertices and sources have been integrated out, and if one assumes that the vertex or source with the largest time is numbered i , it is easy to prove that

$$iV_{\{\dots\epsilon_i\dots\}} + iV_{\{\dots-\epsilon_i\dots\}} = 0 , \quad (2.22)$$

where the dots denote the exact same configuration of ϵ ’s in both terms for the vertices and sources that do not carry the largest time. This equation leads immediately to a constraint,

$$\sum_{\{\epsilon_i = \pm\}} iV_{\{\epsilon_i\}} = 0 , \quad (2.23)$$

where the sum is extended to the 2^n possible configurations of the ϵ ’s in the Feynman diagram of interest.

⁷The superscript 0 indicates free propagators.

Consider now the probability P_2 for producing two particles from the vacuum. There is an obvious contribution to this probability that is obtained simply by squaring the b_1/g^2 piece of the probability for producing a single particle. This term corresponds to the case where the two particles are produced independently from one another. But two particles can also be produced correlated to each other. This *correlated* contribution to P_2 must come from a 2-particle cut through simply connected vacuum-vacuum diagrams. Let us represent this quantity as b_2/g^2 . Diagrammatically, b_2/g^2 is a series whose first terms are

$$\frac{b_2}{g^2} = \begin{array}{c} \text{diagram 1} + \frac{1}{6} \text{diagram 2} + \frac{1}{6} \text{diagram 3} + \frac{1}{6} \text{diagram 4} + \frac{1}{6} \text{diagram 5} + \frac{1}{6} \text{diagram 6} + \frac{1}{6} \text{diagram 7} \\ + \dots \end{array} \quad (2.31)$$

The net probability, from correlated and uncorrelated production, of two particles can therefore be represented as

$$P_2 = e^{-a/g^2} \left[\frac{1}{2!} \frac{b_1^2}{g^4} + \frac{b_2}{g^2} \right] \quad (2.32)$$

The prefactor $1/2!$ in front of the first term is a symmetry factor which is required because the two particles in the final state are indistinguishable.

Let us further discuss the case of three particle production before proceeding to the general case. One (*uncorrelated*) term will be the cube of b_1/g^2 (with a symmetry factor $1/3!$). A combination $b_1 b_2/g^4$ will also appear, corresponding to the case where two of the particles are produced in the same subdiagram, and the third is produced independently. Finally, there is a *fully correlated* three particle production probability corresponding to the three particles produced in the same simply connected diagram. We shall represent this contribution by b_3/g^2 . More precisely, b_3/g^2 is the sum of all 3-particle cuts in a/g^2 . Diagrammatically, some of the simplest terms in b_3/g^2 are

$$\frac{b_3}{g^2} = \begin{array}{c} \frac{1}{8} \text{diagram 1} + \frac{1}{8} \text{diagram 2} + \frac{1}{8} \text{diagram 3} \\ + \dots \end{array} \quad (2.33)$$

(Only a few terms have been represented at this order, due to the large number of possible permutations of cuts across the various legs.) The probability of producing three particles from the vacuum is then given by

$$P_3 = e^{-a/g^2} \left[\frac{1}{3!} \frac{b_1^3}{g^6} + \frac{b_1 b_2}{g^4} + \frac{b_3}{g^2} \right] \quad (2.34)$$

The previous examples can be generalized to obtain an expression for the production of n particles –for any n – that reads

$$P_n = e^{-a/g^2} \sum_{p=1}^n \frac{1}{p!} \sum_{r_1 + \dots + r_p = n} \frac{b_{r_1} \dots b_{r_p}}{g^{2p}} \quad (2.35)$$

In this formula, p is the number of simply connected subdiagrams producing the n particles, and b_r/g^2 denotes the contribution to the probability of the sum of all r -particle cuts through the connected vacuum-vacuum diagrams. This formula gives the probability of producing n

particles to all orders in the coupling g . (Recall also that, in addition to the factors of g^2 that appear explicitly in the formula, the quantities α, b_r are themselves series in g^{2n} where, further, the coefficients of the series are functions of $g_j \sim 1$). It should be noted that this formula has in fact little to do with quantum field theory: any probability distribution for a discrete quantity can be written in this form that expresses how a set of n identical objects can be decomposed into p independent clusters. Similar formulas can be found in [99, 100].

2.2.5 Unitarity

In our framework, unitarity implies that the sum of the probabilities P_n is unity:

$$\sum_{n=0}^{\infty} P_n = 1 . \quad (2.36)$$

From eq. (2.35), it is a simple matter of algebra to show that the l.h.s. above is given by

$$\sum_{n=0}^{\infty} P_n = \exp \left[-\frac{\alpha}{g^2} + \frac{1}{g^2} \sum_{r=1}^{\infty} b_r \right] . \quad (2.37)$$

Unitarity therefore requires that

$$\alpha = \sum_{r=1}^{\infty} b_r . \quad (2.38)$$

This relationship between α and the b_r 's is in fact an identity following directly from their respective definitions. Indeed, recall that (see eq. (2.28)) α/g^2 is the sum of all the possible cuts of simply connected vacuum-vacuum diagrams. On the other hand, b_r/g^2 was defined as the subset of connected vacuum-vacuum diagrams with r -particle cuts. (Recall that these are cuts that intercept r propagators.) The sum of these over all values of r is therefore equal to α/g^2 by definition.

2.2.6 Moments of the distribution

Moments of the distribution of probabilities P_n are easily computed from the generating function

$$G(x) \equiv \sum_{n=0}^{\infty} P_n e^{nx} , \quad (2.39)$$

such that $\langle N^p \rangle = G^{(p)}(0)$. Using eq. (2.35), this generating function can be evaluated in closed form, and one obtains

$$G(x) = e^{-\alpha/g^2} \exp \left[\frac{1}{g^2} \sum_{r=1}^{\infty} b_r e^{rx} \right] = \exp \left[\frac{1}{g^2} \sum_{r=1}^{\infty} b_r (e^{rx} - 1) \right] . \quad (2.40)$$

The mean of the distribution of multiplicities, $\langle N \rangle \equiv \sum_n n P_n$, is

$$\langle N \rangle = G'(0) = \frac{1}{g^2} \sum_{r=1}^{\infty} r b_r . \quad (2.41)$$

The average multiplicity is therefore given by the sum of all r -particle cuts through the connected vacuum-vacuum diagrams, weighted by the number r of particles on the cut. The second derivative of $G(x)$ at $x = 0$ is simply

$$G''(0) = \langle N^2 \rangle. \quad (2.42)$$

The variance of the distribution, $\langle N^2 \rangle - \langle N \rangle^2$, can instead be obtained directly from the second derivative of

$$g(x) \equiv \ln G(x) = \frac{1}{g^2} \sum_{r=1}^{\infty} b_r (e^{rx} - 1) \quad (2.43)$$

at $x = 0$. Thus,

$$\langle N^2 \rangle - \langle N \rangle^2 = g''(0) = \frac{1}{g^2} \sum_{r=1}^{\infty} r^2 b_r. \quad (2.44)$$

More generally, the connected part of the moment of order p reads

$$\langle N^p \rangle_{\text{connected}} = g^{(p)}(0) = \frac{1}{g^2} \sum_{r=1}^{\infty} r^p b_r. \quad (2.45)$$

One sees that if $b_r \neq 0$ for at least one $r > 1$, the variance and the mean are not equal and the distribution is not a Poisson distribution. The converse is true: it is trivial to check that eq. (2.35) is a Poisson distribution if $b_1 \neq 0$ and $b_r = 0$ for all $r > 1$. Indeed, in this case, eq. (2.35) becomes

$$P_n = e^{-b_1/g^2} \frac{1}{n!} \left(\frac{b_1}{g^2} \right)^n. \quad (2.46)$$

2.2.7 Clustering properties

Eq. (2.35) also provides informations about the clustering properties of the distribution of produced particles. Here, we call a *cluster* of size r a set of r correlated particles – i.e. r particles which are produced in the same simply connected graph.

Given the definition of b_r/g^2 as the sum of all the simply connected cut vacuum graphs that have exactly r cut lines, it is clear that the r on-shell particles corresponding to the cut lines form a cluster (since they belong to the same connected graph). Therefore, eq. (2.35) can be seen as a sum over all the possible cluster decompositions of a set of n particles. In this formula, p is the number of clusters (ranging from 1 to n), and for a given p one sums over all the partitions of n particles into p clusters of respective sizes r_1, \dots, r_p ($n = r_1 + \dots + r_p$).

From this interpretation, one can derive a number of results regarding the distribution of clusters in the final state. In order to do this, one needs the probability of having m_1 clusters of size 1, m_2 clusters of size 2, etc. It is given by

$$P(\{m_r\}) = e^{-a/g^2} \frac{1}{(\sum_{r=1}^{\infty} m_r)!} \prod_{r=1}^{\infty} \left(\frac{b_r}{g^2} \right)^{m_r}. \quad (2.47)$$

From this formula, one can first rederive the probability distribution of the particle number n by writing P_n as

$$P_n = \sum_{\{\mathbf{m}_r\} \mid \sum_r r \mathbf{m}_r = n} P(\{\mathbf{m}_r\}) . \quad (2.48)$$

Naturally, one recovers eq. (2.35).

The next quantity one can obtain is the probability distribution for the number p of clusters in an event:

$$P(p) = \sum_{\{\mathbf{m}_r\} \mid \sum_r \mathbf{m}_r = p} P(\{\mathbf{m}_r\}) = \frac{(\sum_r b_r/g^2)^p}{p!} e^{-a/g^2} . \quad (2.49)$$

Since $a = \sum_r b_r$, we see that the number of clusters follows a Poisson distribution of average $\langle p \rangle = \sum_r b_r/g^2$. The fact that this distribution is a Poisson distribution was obvious from the start, since by definition there are no correlations between clusters (each cluster is a separate disconnected graph). One can also compute the average number of clusters of size r in an event:

$$\langle \mathbf{m}_r \rangle = \sum_{\{\mathbf{m}_s\}} P(\{\mathbf{m}_s\}) \mathbf{m}_r = \frac{b_r}{g^2} , \quad (2.50)$$

which provides another interpretation for the meaning of the quantity b_r/g^2 . In particular, for a Poisson distribution the only clusters are 1-particle clusters, i.e. the only non-zero $\langle \mathbf{m}_r \rangle$ is $\langle \mathbf{m}_1 \rangle$. Thus, we recover the fact that for a Poisson distribution, the only non-zero b_r is b_1 .

As one sees, all the properties of the distribution of clusters are encoded in the b_r 's. Given the b_r 's, one can obtain the multiplicity distribution via eq. (2.35) but it is also possible to do the reverse, by noting for instance that

$$\frac{b_r}{g^2} = \oint_{\gamma} \frac{dz}{2\pi i} z^{-r} \ln \sum_{n=0}^{\infty} P_n z^n , \quad (2.51)$$

where the integration is done in the complex z -plane over any closed curve γ that circles once around the origin $z = 0$ in the counter-clockwise direction.

2.3 Generating functional

2.3.1 Definition of the generating functional

Any quantity that can be expressed in terms of the squares of the amplitudes defined in eq. (2.9) can be derived from the following *generating functional*¹¹,

$$\mathcal{F}[z(\mathbf{p})] \equiv \sum_{n=0}^{\infty} \frac{1}{n!} \int \frac{d^3 \mathbf{p}_1}{(2\pi)^3 2p_1} \cdots \frac{d^3 \mathbf{p}_n}{(2\pi)^3 2p_n} z(\mathbf{p}_1) \cdots z(\mathbf{p}_n) \left| \langle \mathbf{p}_1 \cdots \mathbf{p}_n \text{ out} | 0_{\text{in}} \rangle \right|^2 , \quad (2.52)$$

¹¹This generating functional is a generalization of the generating function introduced in eq. (2.39). Indeed, one obtains $G(x)$ by evaluating $\mathcal{F}[z(\mathbf{p})]$ for a constant $z(\mathbf{p})$ equal to e^x : $G(x) = \mathcal{F}[z(\mathbf{p})] \equiv e^x$. The main purpose of introducing a generating functional that depends on a momentum-dependent argument (as opposed to a constant one) is that this more general object allows one to keep track of the momentum of the produced particles.

where $z(\mathbf{p})$ is an arbitrary test function over the 1-particle phase-space. In particular, the differential probabilities and the single particle inclusive spectrum are obtained as functional derivatives of $\mathcal{F}[z(\mathbf{p})]$:

$$\begin{aligned} \frac{dP_n}{d^3\mathbf{p}_1 \cdots d^3\mathbf{p}_n} &= \frac{1}{n!} \frac{\delta^n \mathcal{F}[z(\mathbf{p})]}{\delta z(\mathbf{p}_1) \cdots \delta z(\mathbf{p}_n)} \Big|_{z(\mathbf{p})=0} , \\ \frac{dN_1}{d^3\mathbf{p}} &= \frac{\delta \mathcal{F}[z(\mathbf{p})]}{\delta z(\mathbf{p})} \Big|_{z(\mathbf{p})=1} . \end{aligned} \quad (2.53)$$

As one can see on these two example, observables in which the final state is fully specified correspond to derivatives evaluated at $z(\mathbf{p}) = 0$, while inclusive observables –in which most of the final state is simply integrated out– correspond to derivatives evaluated at $z(\mathbf{p}) = 1$. This is in fact a general property. For instance, the inclusive 2-particle spectrum is

$$\frac{dN_2}{d^3\mathbf{p} d^3\mathbf{q}} = \frac{\delta^2 \mathcal{F}[z(\mathbf{p})]}{\delta z(\mathbf{p}) \delta z(\mathbf{q})} \Big|_{z(\mathbf{p})=1} , \quad (2.54)$$

and this formula has an obvious generalization to the case of the inclusive n -particle spectrum.

2.3.2 Importance of unitarity

As we shall see, inclusive observables are much simpler to calculate than the exclusive ones. To a large extent, this simplification is due to unitarity. The simplest consequence of unitarity is

$$\mathcal{F}[z(\mathbf{p}) = 1] = 1 . \quad (2.55)$$

To check this identity, one should start from the definition of the generating functional in eq. (2.52), to see that

$$\mathcal{F}[z(\mathbf{p}) = 1] = \sum_{n=0}^{\infty} P_n , \quad (2.56)$$

where P_n is the total probability of producing exactly n particles. The sum of these probabilities must be equal to one in a unitary theory. Had one evaluated $\mathcal{F}[z(\mathbf{p})]$ at $z(\mathbf{p}) = 0$ instead, one would have obtained $\mathcal{F}[z(\mathbf{p}) = 0] = P_0$, which is a very complicated object. These considerations show that it is much simpler to study the generating functional near the point $z(\mathbf{p}) = 1$ than near the point $z(\mathbf{p}) = 0$. In terms of a diagrams, the identity (2.55) corresponds to an exact cancellation among an infinite set of diagrams when one evaluates $\mathcal{F}[z(\mathbf{p})]$ at $z(\mathbf{p}) = 1$.

2.3.3 Diagrammatic interpretation of $\mathcal{F}[z(\mathbf{p})]$

The reason why we discussed at length vacuum-vacuum diagrams in the previous subsection is that they play an important role in organizing the calculation of other quantities. The key observation here is that the sum of the vacuum-vacuum diagrams is nothing but the generating functional for time-ordered Green's functions. More precisely, one has

$$\langle 0_{\text{out}} | T \phi(x_1) \cdots \phi(x_n) | 0_{\text{in}} \rangle = \frac{\delta}{i\delta\eta(x_1)} \cdots \frac{\delta}{i\delta\eta(x_n)} e^{i\mathcal{V}[j+\eta]} \Big|_{\eta=0} . \quad (2.57)$$

In order to see this, one should compare the eq. (A.10) for the generating functional $Z[\eta]$ of time-ordered Green's functions (in the appendix A) with the following formula¹² for the sum of the vacuum-vacuum diagrams :

$$e^{i\mathcal{V}[j]} \equiv \langle 0_{\text{out}} | 0_{\text{in}} \rangle = \langle 0_{\text{in}} | T \exp i \int_{-\infty}^{+\infty} d^4x [\mathcal{L}_{\text{int}}(\phi_{\text{in}}(x))] | 0_{\text{in}} \rangle . \quad (2.58)$$

Therefore, we obviously have

$$Z[\eta] = e^{i\mathcal{V}[j+\eta]} , \quad (2.59)$$

which implies eq. (2.57).

Then, it is easy to obtain a formal but useful formula for $\mathcal{F}[z(\mathbf{p})]$. Start from the Lehmann–Symanzik–Zimmermann [101] reduction formula for the transition amplitude to a final state with n particles,

$$\begin{aligned} \langle \mathbf{p}_1 \cdots \mathbf{p}_{n,\text{out}} | 0_{\text{in}} \rangle &= i^n \int d^4x_1 \cdots d^4x_n e^{i(\mathbf{p}_1 \cdot \mathbf{x}_1 + \cdots + \mathbf{p}_n \cdot \mathbf{x}_n)} \\ &\quad \times \square_{x_1} \cdots \square_{x_n} \langle 0_{\text{out}} | T \phi(x_1) \cdots \phi(x_n) | 0_{\text{in}} \rangle . \end{aligned} \quad (2.60)$$

By plugging eq. (2.57) in this reduction formula and squaring the result, we can write the squared amplitude as

$$|\langle \mathbf{p}_1 \cdots \mathbf{p}_{n,\text{out}} | 0_{\text{in}} \rangle|^2 = \mathcal{C}_{\mathbf{p}_1} \cdots \mathcal{C}_{\mathbf{p}_n} e^{i\mathcal{V}[j+\eta_+]} e^{-i\mathcal{V}^*[j+\eta_-]} \Big|_{\eta_{\pm}=0} , \quad (2.61)$$

where the operator $\mathcal{C}_{\mathbf{p}}$ is defined by

$$\mathcal{C}_{\mathbf{p}} \equiv \int d^4x d^4y e^{i\mathbf{p} \cdot (\mathbf{x}-\mathbf{y})} \square_x \square_y \frac{\delta^2}{\delta \eta_+(x) \delta \eta_-(y)} . \quad (2.62)$$

In the right hand side of eq. (2.61), the factors $\exp(i\mathcal{V})$ and $\exp(-i\mathcal{V}^*)$ come respectively from the amplitude and its complex conjugate. Note that it is essential to keep their arguments distinct—hence the separate η_+ and η_- —so that the two derivatives in the operators $\mathcal{C}_{\mathbf{p}}$ act on different factors. One should set η_{\pm} to zero only after all the derivatives have been evaluated. The final step is to substitute eq. (2.61) into the definition (2.52) of $\mathcal{F}[z(\mathbf{p})]$. One obtains immediately

$$\mathcal{F}[z(\mathbf{p})] = \exp \left[\int \frac{d^3\mathbf{p}}{(2\pi)^3 2p} z(\mathbf{p}) \mathcal{C}_{\mathbf{p}} \right] e^{i\mathcal{V}[j+\eta_+]} e^{-i\mathcal{V}^*[j+\eta_-]} \Big|_{\eta_{\pm}=0} . \quad (2.63)$$

We will use extensively this formula in order to derive expressions for various observables.

Let us now turn to the diagrammatic interpretation of $\mathcal{F}[z(\mathbf{p})]$, which can be inferred from eq. (2.63). In order to do that, we need the eq. (A.22) established in the appendix A.3. Indeed, the last two exponentials are respectively $Z[\eta_+]$ and $Z^*[\eta_-]$ (thanks to eq. (2.59)), and it is easy to check that the operator in the first exponential is identical to the first exponential of eq. (A.22) except for the additional factor $z(\mathbf{p})$, since

$$G_{+-}^0(x, y) = \int \frac{d^3\mathbf{p}}{(2\pi)^3 2p} e^{i\mathbf{p} \cdot (\mathbf{x}-\mathbf{y})} . \quad (2.64)$$

¹²Here, the interaction term of the Lagrangian \mathcal{L}_{int} comprises both the self-interactions of the fields, and their coupling to the external source, i.e. $\mathcal{L}_{\text{int}} = -\mathcal{U}(\phi) + j\phi$.

Therefore, eq. (2.63), before we set the sources η_{\pm} to zero, is the generating functional for correlators in a *z-modified* Schwinger-Keldysh formalism¹³ in which every off-diagonal free propagator (G_{+-}^0 and G_{-+}^0) is multiplied by $z(\mathbf{p})$ in momentum space. Because we are going to reuse this object later, let us denote

$$e^{i\mathcal{W}[\eta_{\pm}, j]} \equiv \exp \left[\int \frac{d^3 \mathbf{p}}{(2\pi)^3 2p} z(\mathbf{p}) \mathcal{C}_{\mathbf{p}} \right] e^{i\mathcal{V}[j+\eta_+]} e^{-i\mathcal{V}^*[j+\eta_-]} . \quad (2.65)$$

Since we must set η_{\pm} to zero in order to obtain $\mathcal{F}[z(\mathbf{p})]$ according to eq. (2.63), we see that $\mathcal{F}[z(\mathbf{p})]$ is the sum of all the vacuum-vacuum diagrams¹⁴ in the *z-modified* Schwinger-Keldysh formalism.

2.3.4 First derivative of $\mathcal{F}[z(\mathbf{p})]$

General formula

There is no simple expression for the generating functional $\mathcal{F}[z(\mathbf{p})]$ itself, but it turns out that it is much easier to find a formula for its first derivative $\delta\mathcal{F}[z(\mathbf{p})]/\delta z(\mathbf{p})$. Using eq. (2.63) and the explicit form of the operator $\mathcal{C}_{\mathbf{p}}$, we can write this derivative as

$$\begin{aligned} \frac{\delta\mathcal{F}[z(\mathbf{p})]}{\delta z(\mathbf{p})} &= \frac{1}{(2\pi)^3 2p} \int d^4 x d^4 y e^{i\mathbf{p} \cdot (\mathbf{x}-\mathbf{y})} e^{i\mathcal{W}[\eta_{\pm}, j]} \square_x \square_y \\ &\quad \times \left[\frac{\delta i\mathcal{W}[\eta_{\pm}, j]}{\delta \eta_+(x)} \frac{\delta i\mathcal{W}[\eta_{\pm}, j]}{\delta \eta_-(y)} + \frac{\delta^2 i\mathcal{W}[\eta_{\pm}, j]}{\delta \eta_+(x) \delta \eta_-(y)} \right]_{\eta_{\pm}=0} . \end{aligned} \quad (2.66)$$

Since when evaluated at $\eta_{\pm} = 0$ the exponential in the first line is nothing but the generating functional $\mathcal{F}[z(\mathbf{p})]$ itself, we can also write

$$\begin{aligned} \frac{\delta \ln \mathcal{F}[z(\mathbf{p})]}{\delta z(\mathbf{p})} &= \frac{1}{(2\pi)^3 2p} \int d^4 x d^4 y e^{i\mathbf{p} \cdot (\mathbf{x}-\mathbf{y})} \square_x \square_y \\ &\quad \times [\varphi_+(x) \varphi_-(y) + \mathcal{G}_{+-}(x, y)] . \end{aligned} \quad (2.67)$$

where we have introduced the following objects :

$$\begin{aligned} \varphi_{\pm}(x) &\equiv \left. \frac{\delta i\mathcal{W}[\eta_{\pm}, j]}{\delta \eta_{\pm}(x)} \right|_{\eta_{\pm}=0} , \\ \mathcal{G}_{+-}(x, y) &\equiv \left. \frac{\delta^2 i\mathcal{W}[\eta_{\pm}, j]}{\delta \eta_+(x) \delta \eta_-(y)} \right|_{\eta_{\pm}=0} . \end{aligned} \quad (2.68)$$

Note that these objects depend on the external source j and on the function $z(\mathbf{p})$, although we have not written this dependence explicitly in order to keep the notations compact. From this definition, and the fact that $\exp(i\mathcal{W})$ is the generating functional for Green's functions in the *z-modified* Schwinger-Keldysh formalism, we see that $\varphi_{\pm}(x)$ and $\mathcal{G}_{+-}(x, y)$ are respectively

¹³See the appendix A for a reminder on the Schwinger-Keldysh formalism.

¹⁴It is a general result that the generating functional for correlators, when evaluated at $\eta = 0$, is equal to the sum of the vacuum-vacuum diagrams in the theory under consideration.

connected¹⁵ 1- and 2-point Green's functions in this formalism. Diagrammatically, eq. (2.67) can be represented as follows:

$$\frac{\delta \ln \mathcal{F}[z(\mathbf{p})]}{\delta z(\mathbf{p})} = \begin{array}{c} \text{diagram 1} \end{array} + \begin{array}{c} \text{diagram 2} \end{array}, \quad (2.69)$$

where the shaded blobs represent the functions φ_{\pm} and \mathcal{G}_{+-} that have been amputated of their external legs (by the $\square_{x,y}$ operators), and where the crossed line that appears in the diagrams carries the on-shell momentum \mathbf{p} .

Leading order

The order of magnitude of these objects is easily obtained from our general results for the power counting of connected graphs :

$$\begin{aligned} \varphi_{\pm} &\sim \mathcal{O}(g^{-1}), \\ \mathcal{G}_{+-} &\sim \mathcal{O}(1). \end{aligned} \quad (2.70)$$

Therefore, the first derivative of $\ln \mathcal{F}[z(\mathbf{p})]$ starts at the order g^{-2} . Moreover, at this order, only the first term in $\varphi_+(x)\varphi_-(y)$ contributes. The term in \mathcal{G}_{+-} starts contributing only at the next-to-leading order. A further simplification at leading order is that it is sufficient to keep tree level contributions to the 1-point functions φ_{\pm} . Thanks to their tree structure, it is possible to write recursive integral equations that sum all the diagrams contributing to φ_{\pm} at leading order :

$$\begin{aligned} \varphi_+(x) &= i \int d^4y G_{++}^0(x,y) [j(y) - U'(\varphi_+(y))] \\ &\quad - i \int d^4y \overline{G}_{+-}^0(x,y) [j(y) - U'(\varphi_-(y))], \\ \varphi_-(x) &= i \int d^4y \overline{G}_{-+}^0(x,y) [j(y) - U'(\varphi_+(y))] \\ &\quad - i \int d^4y G_{--}^0(x,y) [j(y) - U'(\varphi_-(y))]. \end{aligned} \quad (2.71)$$

In these equations, G_{++}^0 and G_{--}^0 are the diagonal components of the free propagator in the Schwinger-Keldysh formalism, and $\overline{G}_{+-}^0, \overline{G}_{-+}^0$ are its non-diagonal components, appropriately modified by the function $z(\mathbf{p})$. In momentum space, they read:

$$\begin{aligned} \overline{G}_{+-}^0(p) &= 2\pi z(\mathbf{p}) \theta(-p^0) \delta(p^2), \\ \overline{G}_{-+}^0(p) &= 2\pi z(\mathbf{p}) \theta(+p^0) \delta(p^2). \end{aligned} \quad (2.72)$$

In the appendix B.5.2, we show that the solutions φ_{\pm} of coupled integral equations such as eqs. (2.71) are solutions of the classical equation of motion,

$$\square_x \varphi_{\pm}(x) + U'(\varphi_{\pm}(x)) = j(x), \quad (2.73)$$

¹⁵They are connected because they are obtained by differentiating the logarithm of the generating functional.

with the following boundary conditions

$$\begin{aligned} f_+^{(+)}(-\infty, \mathbf{p}) &= f_-^{(-)}(-\infty, \mathbf{p}) = 0, \\ f_+^{(-)}(+\infty, \mathbf{p}) &= z(\mathbf{p}) f_-^{(-)}(+\infty, \mathbf{p}), \\ f_-^{(+)}(+\infty, \mathbf{p}) &= z(\mathbf{p}) f_+^{(+)}(+\infty, \mathbf{p}). \end{aligned} \quad (2.74)$$

Here, the boundary conditions have been written in terms of the coefficients of the Fourier decomposition of the fields φ_{\pm} ,

$$\varphi_{\epsilon}(\mathbf{y}) \equiv \int \frac{d^3 \mathbf{p}}{(2\pi)^3 2p} \left[f_{\epsilon}^{(+)}(\mathbf{y}^0, \mathbf{p}) e^{-i\mathbf{p} \cdot \mathbf{y}} + f_{\epsilon}^{(-)}(\mathbf{y}^0, \mathbf{p}) e^{+i\mathbf{p} \cdot \mathbf{y}} \right]. \quad (2.75)$$

By plugging the Fourier representation of φ_{\pm} in the general formula (2.67) (and setting $\mathcal{G}_{+-} = 0$ at this order), we get a very simple formula for the first derivative of $\ln \mathcal{F}[z(\mathbf{p})]$ at leading order:

$$\left. \frac{\delta \ln \mathcal{F}[z(\mathbf{p})]}{\delta z(\mathbf{p})} \right|_{\text{LO}} = \frac{1}{(2\pi)^3 2p} f_+^{(+)}(+\infty, \mathbf{p}) f_-^{(-)}(+\infty, \mathbf{p}). \quad (2.76)$$

One can note that the dependence on the function $z(\mathbf{p})$ enters in the fields φ_{\pm} only via the boundary conditions they satisfy, since the equation of motion itself does not contain $z(\mathbf{p})$ explicitly. The second remark is that it is in general extremely difficult to solve a non-linear partial differential equation with boundary conditions imposed both at $x^0 = -\infty$ and at $x^0 = +\infty$. Therefore, one should not hope to be able to find solutions of this problem (either analytically or numerically). Nevertheless, this result for the first derivative of the generating functional $\mathcal{F}[z(\mathbf{p})]$ is very useful as an intermediate tool for deriving other results, as will be shown in the rest of this chapter.

2.4 Inclusive moments at leading order

2.4.1 Single inclusive spectrum

Let us now show how to obtain inclusive moments (for now, at leading order) from eq. (2.76). The simplest one is the single inclusive spectrum,

$$\frac{dN_1}{d^3 \mathbf{p}} = \left. \frac{\delta \mathcal{F}[z(\mathbf{p})]}{\delta z(\mathbf{p})} \right|_{z(\mathbf{p})=1}. \quad (2.77)$$

At leading order, it is simply obtained by evaluating eq. (2.76) at the special point $z(\mathbf{p}) = 1$, since $\mathcal{F}[z(\mathbf{p}) = 1] = 1$. This means that one must solve the classical equation of motion with boundary conditions (2.74) in which one sets $z(\mathbf{p}) = 1$. As explained in appendix B.5.2, setting $z(\mathbf{p}) = 1$ in these boundary conditions simplifies them considerably: when $z(\mathbf{p}) = 1$ the two fields φ_+ and φ_- are identical,

$$\varphi_+(x) = \varphi_-(x) \equiv \varphi(x), \quad (2.78)$$

and obey the simple retarded boundary condition

$$\lim_{x^0 \rightarrow -\infty} \varphi(x^0, \mathbf{x}) = 0, \quad \lim_{x^0 \rightarrow -\infty} \partial^0 \varphi(x^0, \mathbf{x}) = 0. \quad (2.79)$$

Thus, the prescription for computing the single inclusive spectrum at leading order is the following:

- i. Solve the classical equation of motion with a null initial condition in the remote past,
- ii. At $x^0 \rightarrow +\infty$, compute the coefficients ¹⁶ $f^{(\pm)}(+\infty, \mathbf{p})$ of the Fourier decomposition of this classical field,
- iii. the single inclusive spectrum is then obtained as:

$$\left. \frac{dN_1}{d^3\mathbf{p}} \right|_{\text{Lo}} = \frac{1}{(2\pi)^3 2p} \left| f^{(+)}(+\infty, \mathbf{p}) \right|^2. \quad (2.80)$$

In eq. (2.80), we used the fact that the retarded classical field ϕ is purely real ¹⁷. Therefore, its positive and negative energy Fourier coefficients are mutual complex conjugates:

$$f^{(-)}(+\infty, \mathbf{p}) = \left[f^{(+)}(+\infty, \mathbf{p}) \right]^*. \quad (2.81)$$

This ensures that the spectrum is a positive definite real number.

2.4.2 Multi-particle inclusive spectra

The n -particle inclusive spectrum is also obtained from derivatives of the generating functional $\mathcal{F}[z(\mathbf{p})]$ evaluated at $z(\mathbf{p}) = 1$,

$$\frac{dN_n}{d^3\mathbf{p}_1 \cdots d^3\mathbf{p}_n} = \left. \frac{\delta^n \mathcal{F}[z(\mathbf{p})]}{\delta z(\mathbf{p}_1) \cdots \delta z(\mathbf{p}_n)} \right|_{z(\mathbf{p})=1}. \quad (2.82)$$

Note that the n -gluon spectrum defined in this way gives the expectation value of $N(N-1) \cdots (N-n+1)$ when integrated over the momenta \mathbf{p}_1 to \mathbf{p}_n :

$$\int d^3\mathbf{p}_1 \cdots d^3\mathbf{p}_n \frac{dN_n}{d^3\mathbf{p}_1 \cdots d^3\mathbf{p}_n} = \sum_{N=n}^{\infty} N(N-1) \cdots (N-n+1) P_N, \quad (2.83)$$

where P_N is the total probability of producing exactly N particles. Since we already have an expression for the first derivative of $\ln \mathcal{F}[z(\mathbf{p})]$, it is simpler to rewrite eq. (2.82) as follows

$$\frac{dN_n}{d^3\mathbf{p}_1 \cdots d^3\mathbf{p}_n} = \left. \frac{\delta^n e^{\ln \mathcal{F}[z(\mathbf{p})]}}{\delta z(\mathbf{p}_1) \cdots \delta z(\mathbf{p}_n)} \right|_{z(\mathbf{p})=1}. \quad (2.84)$$

By performing explicitly the derivatives, we obtain :

$$\begin{aligned} \frac{dN_n}{d^3\mathbf{p}_1 \cdots d^3\mathbf{p}_n} &= \prod_{i=1}^n \left[\frac{\delta \ln \mathcal{F}}{\delta z(\mathbf{p}_i)} \right]_{z(\mathbf{p})=1} \\ &+ \sum_{i < j} \left[\frac{\delta^2 \ln \mathcal{F}}{\delta z(\mathbf{p}_i) \delta z(\mathbf{p}_j)} \right]_{z(\mathbf{p})=1} \prod_{k \neq i, j} \left[\frac{\delta \ln \mathcal{F}}{\delta z(\mathbf{p}_k)} \right]_{z(\mathbf{p})=1} \\ &+ \cdots \end{aligned} \quad (2.85)$$

The terms we have not written explicitly have increasingly high order derivatives (but less and less factors), up to an n -th derivative in a single factor. However, we do not need these

¹⁶Since the fields ϕ_+ and ϕ_- are equal, there is no need to have a subscript \pm for these coefficients.

¹⁷Its initial condition is real, and its equation of motion involves only real quantities.

terms. Indeed, we already know that at leading order $\ln \mathcal{F}$ is of order g^{-2} since it is a sum of simply connected vacuum-vacuum diagrams. Therefore, in the right hand side of this equation, the first term is of order g^{-2n} , the second term is of order $g^{-2(n-1)}$, etc... The leading contribution is thus the first term, and all the subsequent terms are subleading¹⁸. We see that, at leading order, the n -particle inclusive spectrum is simply the product of n single particle spectra:

$$\left. \frac{dN_n}{d^3\mathbf{p}_1 \cdots d^3\mathbf{p}_n} \right|_{\text{Lo}} = \prod_{i=1}^n \left. \frac{dN_1}{d^3\mathbf{p}_i} \right|_{\text{Lo}}. \quad (2.86)$$

Any deviation from this factorized result has to be a subleading effect¹⁹. Note also that at this order, there is no difference between the factorial moments $\langle N(N-1) \cdots (N-n+1) \rangle$ and the ordinary moments $\langle N^n \rangle$.

2.5 Exclusive quantities at leading order

Let us now consider exclusive quantities. This discussion will be very short, and its purpose is only to illustrate the fact that the calculation of exclusive quantities is considerably more difficult than that of inclusive quantities.

Let us consider as an example the calculation of the differential probability of producing exactly one particle. It is obtained from $\mathcal{F}[z(\mathbf{p})]$ by the formula

$$\frac{dP_1}{d^3\mathbf{p}} = \left. \frac{\delta \mathcal{F}[z(\mathbf{p})]}{\delta z(\mathbf{p})} \right|_{z(\mathbf{p})=0} = \underbrace{\mathcal{F}[z(\mathbf{p})=0]}_{P_0} \left. \frac{\delta \ln \mathcal{F}[z(\mathbf{p})]}{\delta z(\mathbf{p})} \right|_{z(\mathbf{p})=0}. \quad (2.87)$$

We can see two major differences compared to the inclusive quantities studied in the previous section :

- i. The derivative of $\ln \mathcal{F}[z(\mathbf{p})]$ must be evaluated at the point $z(\mathbf{p}) = 0$. At leading order, it can still be expressed in terms of the Fourier coefficients of a pair of solutions of the classical equation of motion, via eq. (2.76). However, because now we must set $z(\mathbf{p}) = 0$ in the boundary conditions (2.74) for these classical fields, they are not retarded fields anymore²⁰, and it is much more difficult to calculate them.
- ii. The quantity $\mathcal{F}[z(\mathbf{p})=0]$ appears as a prefactor in front of all the exclusive quantities. This prefactor is nothing but the probability P_0 for not producing anything, i.e. the vacuum *survival probability*. Calculating P_0 directly is a very difficult task. However, if one was able to calculate the second factor for all the probabilities P_1, P_2, \dots , one could then obtain P_0 from the unitarity condition $\sum_{n=0}^{\infty} P_n = 1$.

These difficulties, observed here on the example of $dP_1/d^3\mathbf{p}$, are in fact generic to all exclusive quantities. They have so far prevented any progress in the evaluation of these quantities. Note however that this is to a large extent an academic problem, since exclusive quantities

¹⁸We will need the second term later when we study the next-to-leading order corrections.

¹⁹As we will see in the following chapters, some of these subleading corrections are enhanced by large logarithms of the energy, and can thus be quantitatively comparable to the leading order contribution.

²⁰It is precisely because in exclusive observables the final state is constrained that the boundary conditions for the fields cannot be purely retarded.

—where one specifies in minute detail the final state— are not very interesting for the phenomenology of processes in which the final state has typically a very large number of particles, parametrically of order g^{-2} . Indeed, in this context, the probability of occurrence of a given fully specified final state is exponentially suppressed, like e^{-c/g^2} .

2.6 Next-to-Leading Order corrections

2.6.1 Preliminary remarks

In order to save some work, it is useful to determine precisely what one really needs to calculate in order to obtain the inclusive spectra at NLO. This can be done easily by going back to eq. (2.85). The first line of the right hand side, evaluated at leading order, gives the leading order contribution to the n -particle inclusive spectrum. NLO contributions come in two places:

- i. Via an NLO correction to one of the factors $\delta \ln \mathcal{F}/\delta z(\mathbf{p}_i)$ in the first line,
- ii. In the second line, with all the factors it contains evaluated at leading order. Thus we also need the LO contribution to the second derivative $\delta^2 \ln \mathcal{F}/\delta z(\mathbf{p})\delta z(\mathbf{q})$.

The first type of NLO correction just amounts to calculating the single inclusive spectrum at NLO. The second type of NLO correction is somewhat different, and occurs only in the 2- and more particle inclusive spectra.

2.6.2 Single inclusive spectrum

The single particle inclusive spectrum is given by the first derivative of the generating functional $\mathcal{F}[z(\mathbf{p})]$, for which a general formula was given in eq. (2.67). We must now evaluate this formula at NLO, i.e. at the order g^0 . Therefore, we need to calculate two quantities:

- i. The 1-loop corrections β_{\pm} to the 1-point functions φ_{\pm} ,
- ii. The 2-point function \mathcal{G}_{+-} at tree level.

Since we are not going to calculate further derivatives²¹ with respect to $z(\mathbf{p})$, it is sufficient to evaluate these quantities at the point $z(\mathbf{p}) = 1$ — which will simplify considerably the calculations. In particular, by setting $z(\mathbf{p}) = 1$, we need not distinguish the two fields φ_{\pm} since they are both equal to the retarded classical field φ with a null initial condition at $x^0 = -\infty$. In terms of these two objects, the NLO correction to the single inclusive spectrum reads²²

$$\left. \frac{dN_1}{d^3\mathbf{p}} \right|_{\text{NLO}} = \frac{1}{(2\pi)^3 2p} \int d^4x d^4y e^{ip \cdot (x-y)} \square_x \square_y \times \left[\varphi(x) \beta_-(y) + \beta_+(x) \varphi(y) + \mathcal{G}_{+-}(x, y) \right], \quad (2.88)$$

²¹The second derivative $\delta^2 \ln \mathcal{F}/\delta z(\mathbf{p})\delta z(\mathbf{q})$ —that we need in the calculation of the 2-particle spectrum— will only be needed at leading order. We will obtain it from eq. (2.76), which is valid at LO for any $z(\mathbf{p})$.

²²The last term, proportional to $\mathcal{G}_{+-}(x, y)$, can be shown to contain the contribution due to the production of pairs of particle by the Schwinger mechanism [102].

to be compared with its leading order expression

$$\left. \frac{dN_1}{d^3\mathbf{p}} \right|_{\text{LO}} = \frac{1}{(2\pi)^3 2p} \int d^4x d^4y e^{ip \cdot (x-y)} \square_x \square_y \varphi(x) \varphi(y) . \quad (2.89)$$

Let us start with β_{\pm} . These quantities are the 1-loop corrections to 1-point simply connected Green's functions. To the propagators that constitute the loop, one can attach any number of fields φ : in other words, they are nothing but the Schwinger-Keldysh propagators in the presence of a background field φ . For a generic interaction potential, it is easy to write $\beta_{\pm}(x)$ as follows:

$$\beta_{\epsilon}(x) = -\frac{i}{2} \sum_{\epsilon'=\pm} \int d^4z \epsilon' \mathcal{G}_{\epsilon\epsilon'}(x, z) \mathcal{U}'''(\varphi(z)) \mathcal{G}_{\epsilon'\epsilon'}(z, z) . \quad (2.90)$$

In this formula, the $1/2$ is a symmetry factor, the factor ϵ' in the integrand takes into account the fact that vertices of type $-$ have an opposite sign in the Schwinger-Keldysh formalism, and the factor $-i\mathcal{U}'''(\varphi(z))$ is the general form of the 3-particle vertex in the presence of an external field (for an arbitrary interaction potential \mathcal{U}).

Thus, we have reduced the calculation of β_{\pm} to that of the 2-point functions $\mathcal{G}_{\pm\pm}$ at tree level. These four propagators are defined recursively by the following equations :

$$\mathcal{G}_{\epsilon\epsilon'}(x, y) = G_{\epsilon\epsilon'}^0(x, y) - i \sum_{\eta=\pm} \eta \int d^4z G_{\epsilon\eta}^0(x, z) \mathcal{U}''(\varphi(z)) \mathcal{G}_{\eta\epsilon'}(z, y) . \quad (2.91)$$

Here, $-i\mathcal{U}''(\varphi(z))$ is the general form for the insertion of a background field on a propagator in a theory with potential $\mathcal{U}(\varphi)$. From these equations²³, it is easy to derive the following equations :

$$\begin{aligned} [\square_x + \mathcal{U}''(\varphi(x))] \mathcal{G}_{+-}(x, y) &= [\square_y + \mathcal{U}''(\varphi(y))] \mathcal{G}_{+-}(x, y) = 0 , \\ [\square_x + \mathcal{U}''(\varphi(x))] \mathcal{G}_{-+}(x, y) &= [\square_y + \mathcal{U}''(\varphi(y))] \mathcal{G}_{-+}(x, y) = 0 . \end{aligned} \quad (2.92)$$

In addition to these equations of motion, these propagators must become equal to their free counterparts G_{+-}^0 and G_{-+}^0 when $x^0, y^0 \rightarrow -\infty$. Once \mathcal{G}_{+-} and \mathcal{G}_{-+} have been determined, it is possible to obtain \mathcal{G}_{++} and \mathcal{G}_{--} by the following expressions,

$$\begin{aligned} \mathcal{G}_{++}(x, y) &= \theta(x^0 - y^0) \mathcal{G}_{-+}(x, y) + \theta(y^0 - x^0) \mathcal{G}_{+-}(x, y) , \\ \mathcal{G}_{--}(x, y) &= \theta(x^0 - y^0) \mathcal{G}_{+-}(x, y) + \theta(y^0 - x^0) \mathcal{G}_{-+}(x, y) , \end{aligned} \quad (2.93)$$

which follow from the definition of the various components of the Schwinger-Keldysh propagators.

The above conditions determine \mathcal{G}_{+-} and \mathcal{G}_{-+} uniquely. In order to find these propagators, it is convenient to start from the following representation of their free counterparts :

$$\begin{aligned} G_{+-}^0(x, y) &= \int \frac{d^3\mathbf{p}}{(2\pi)^3 2p} a_{\mathbf{p}}^*(x) a_{\mathbf{p}}(y) , \\ G_{-+}^0(x, y) &= \int \frac{d^3\mathbf{p}}{(2\pi)^3 2p} a_{\mathbf{p}}(x) a_{\mathbf{p}}^*(y) , \end{aligned} \quad (2.94)$$

²³For a more explicit method of solving these equations, see the appendix A.4.

where

$$\square_x a_{\mathbf{p}}(x) = 0, \quad \lim_{x^0 \rightarrow -\infty} a_{\mathbf{p}}(x) = e^{-i\mathbf{p} \cdot x}. \quad (2.95)$$

It is trivial to generalize this representation of the off-diagonal propagators to the case of a non zero background field. One can write :

$$\begin{aligned} \mathcal{G}_{+-}(x, y) &= \int \frac{d^3 \mathbf{p}}{(2\pi)^3 2p} a_{\mathbf{p}}^*(x) a_{\mathbf{p}}(y), \\ \mathcal{G}_{-+}(x, y) &= \int \frac{d^3 \mathbf{p}}{(2\pi)^3 2p} a_{\mathbf{p}}(x) a_{\mathbf{p}}^*(y), \end{aligned} \quad (2.96)$$

with

$$[\square_x + U''(\varphi(x))] a_{\mathbf{p}}(x) = 0, \quad \lim_{x^0 \rightarrow -\infty} a_{\mathbf{p}}(x) = e^{-i\mathbf{p} \cdot x}. \quad (2.97)$$

By construction, these expressions of \mathcal{G}_{+-} and \mathcal{G}_{-+} obey the appropriate equations of motion, and go to the correct limit in the remote past. Thus, the problem of finding the Schwinger-Keldysh propagators in a background field has been reduced to solving the equation of motion of a small fluctuation on top of the background field, with retarded boundary conditions.

2.6.3 Surgery of retarded graphs

At this point, we have all the building blocks in order to obtain the single inclusive spectrum at NLO. One can go further and obtain a formal relationship between the LO and NLO inclusive spectra, that will be very useful when we discuss factorization in heavy ion collisions.

The general idea of the following manipulations is that retarded fields evolve causally. Therefore, it is possible to split their time evolution in two parts, separated by a certain surface Σ on which we assume that all the fields or field fluctuations are known. The final formula of this section will show that all the relevant dynamics above the surface Σ is already contained in the LO inclusive spectrum. As discussed in the appendix B, the surface Σ must be locally space-like (or at least light-like), i.e. such that specifying the fields and canonical momenta on Σ uniquely determines the fields above Σ . Thanks to eq. (B.16), one can write the small fluctuation $a_{\mathbf{k}}$ as

$$a_{\mathbf{k}}(x) = \int_{\Sigma} d^3 \mathbf{S}_{\mathbf{u}} [a_{\mathbf{k}} \cdot \mathbb{T}_{\mathbf{u}}] \varphi(x), \quad (2.98)$$

where the operator $a_{\mathbf{k}} \cdot \mathbb{T}_{\mathbf{u}}$ is defined by

$$a_{\mathbf{k}} \cdot \mathbb{T}_{\mathbf{u}} = a_{\mathbf{k}}(\mathbf{u}) \frac{\delta}{\beta(\mathbf{u})} + (\mathbf{n} \cdot \partial a_{\mathbf{k}}(\mathbf{u})) \frac{\delta}{\delta(\mathbf{n} \cdot \partial \varphi(\mathbf{u}))}. \quad (2.99)$$

(\mathbf{n}^{μ} is a unit vector normal to the surface Σ at the point \mathbf{u} , and $d^3 \mathbf{S}_{\mathbf{u}}$ is the measure on Σ .) In this formula, one must consider the classical field $\varphi(x)$ as a functional of its initial value on the surface Σ .

Thus, the propagator $\mathcal{G}_{+-}(x, y)$ that enters in the NLO inclusive spectrum can be written as

$$\mathcal{G}_{+-}(x, y) = \int \frac{d^3\mathbf{k}}{(2\pi)^3 2k} \int_{\Sigma} d^3\mathbf{S}_u d^3\mathbf{S}_v \left[[a_{\mathbf{k}}^* \cdot \mathbb{T}_u] \varphi(x) \right] \left[[a_{\mathbf{k}} \cdot \mathbb{T}_v] \varphi(y) \right]. \quad (2.100)$$

The important point for the applicability of this formula is that the points x and y are both located above the surface Σ . This is indeed the case since the single inclusive spectrum involves only fields in the limit $x^0 \rightarrow +\infty$. (This can be seen for instance in eq. (2.80), which contains only the Fourier coefficients of the classical field at $x^0 \rightarrow +\infty$.) Moreover, in the case of this observable, the times x^0 and y^0 can be taken equal, which allows one to interchange²⁴ $a_{\mathbf{k}}$ and $a_{\mathbf{k}}^*$ and to symmetrize the formula

$$\begin{aligned} \mathcal{G}_{+-}(x, y) = & \frac{1}{2} \int \frac{d^3\mathbf{k}}{(2\pi)^3 2k} \int_{\Sigma} d^3\mathbf{S}_u d^3\mathbf{S}_v \left\{ \left[[a_{\mathbf{k}}^* \cdot \mathbb{T}_u] \varphi(x) \right] \left[[a_{\mathbf{k}} \cdot \mathbb{T}_v] \varphi(y) \right] \right. \\ & \left. + \left[[a_{\mathbf{k}} \cdot \mathbb{T}_v] \varphi(x) \right] \left[[a_{\mathbf{k}}^* \cdot \mathbb{T}_u] \varphi(y) \right] \right\}. \quad (2.101) \end{aligned}$$

As we shall see now, a similar expression can be obtained for the quantities β_{\pm} that also enter in the NLO inclusive spectrum. Let us start from eq. (2.90). From eqs. (2.93), we see that the propagators \mathcal{G}_{++} and \mathcal{G}_{--} are equal when the two endpoints are evaluated at equal times²⁵. Therefore, we can write

$$\beta_{\epsilon}(x) = -\frac{i}{2} \int \frac{d^3\mathbf{k}}{(2\pi)^3 2k} d^4z \underbrace{\left[\mathcal{G}_{\epsilon+}(x, z) - \mathcal{G}_{\epsilon-}(x, z) \right]}_{\mathcal{G}_R(x, z)} \mathcal{U}'''(\varphi(z)) a_{\mathbf{k}}^*(z) a_{\mathbf{k}}(z), \quad (2.102)$$

where \mathcal{G}_R is the retarded propagator in the presence of the background field φ . This equation shows that the two field fluctuations β_+ and β_- are equal. Therefore, we will simply denote them by β in the following. Moreover, it is easy to see that

$$\begin{aligned} [\square_x + \mathcal{U}''(\varphi(x))] \beta(x) &= -\frac{1}{2} \mathcal{U}'''(\varphi(x)) \int \frac{d^3\mathbf{k}}{(2\pi)^3 2k} a_{\mathbf{k}}^*(x) a_{\mathbf{k}}(x), \\ \lim_{x^0 \rightarrow -\infty} \beta(x) &= 0. \end{aligned} \quad (2.103)$$

This formula means that $\beta(x)$ is a small fluctuation propagating on top of φ , that vanishes in the remote past, with a 1-loop tadpole acting as a source. One can then write a Green's formula (see the appendix B for the derivation) for the solution of this partial differential equation, with a boundary condition set on the surface Σ :

$$\begin{aligned} \beta(x) = & \underbrace{-\frac{i}{2} \int \frac{d^3\mathbf{k}}{(2\pi)^3 2k} \int_{\Omega} d^4y \mathcal{G}_R(x, y) \mathcal{U}'''(\varphi(y)) a_{\mathbf{k}}^*(y) a_{\mathbf{k}}(y)}_{\beta_1(x)} \\ & + \underbrace{i \int_{\Sigma} d^3\mathbf{S}_u \mathcal{G}_R(x, u) (\mathbf{n} \cdot \vec{\partial}_u - \mathbf{n} \cdot \overleftarrow{\partial}_u) \beta(u)}_{\beta_2(x)}, \end{aligned} \quad (2.104)$$

²⁴The propagators $\mathcal{G}_{+-}(x, y)$ and $\mathcal{G}_{-+}(x, y)$ are equal at equal times (see the section C.3).

²⁵It seems that there is an ambiguity due to the fact that one needs the value of $\theta(0)$ in order to evaluate these propagators at equal times. However, this is not the case since \mathcal{G}_{+-} and \mathcal{G}_{-+} are equal at equal times.

where Ω is the region of space-time above the surface Σ . This formula gives the value of β at the point x (above the surface Σ) if we know it at any point $u \in \Sigma$. Thanks to eq. (B.19), the second term in the right hand side can be written directly as

$$\beta_2(x) = \int_{\Sigma} d^3 \mathbf{S}_u [\beta \cdot \mathbb{T}_u] \varphi(x). \quad (2.105)$$

Let us now write the first term, $\beta_1(x)$, in a similar way. The first step is to write the interactions with the background field more explicitly,

$$\begin{aligned} \beta_1(x) = & -i \int_{\Omega} d^4 y G_r^0(x, y) \left[U''(\varphi(y)) \beta_1(y) \right. \\ & \left. + \frac{1}{2} U'''(\varphi(y)) \int \frac{d^3 \mathbf{k}}{(2\pi)^3 2k} a_{\mathbf{k}}^*(y) a_{\mathbf{k}}(y) \right]. \end{aligned} \quad (2.106)$$

Consider now the quantity

$$\xi(x) \equiv \frac{1}{2} \int \frac{d^3 \mathbf{k}}{(2\pi)^3 2k} \int_{\Sigma} d^3 \mathbf{S}_u d^3 \mathbf{S}_v [a_{\mathbf{k}}^* \cdot \mathbb{T}_u] [a_{\mathbf{k}} \cdot \mathbb{T}_v] \varphi(x). \quad (2.107)$$

Our goal is to show that $\beta_1(x) = \xi(x)$. First, by using the fundamental relation (2.98), this can be rewritten as

$$\xi(x) = \frac{1}{2} \int \frac{d^3 \mathbf{k}}{(2\pi)^3 2k} \int_{\Sigma} d^3 \mathbf{S}_u [a_{\mathbf{k}}^* \cdot \mathbb{T}_u] a_{\mathbf{k}}(x). \quad (2.108)$$

Next, replace in this equation the fluctuation $a_{\mathbf{k}}(x)$ by its representation in terms of the Green's formula (B.12):

$$\xi(x) = -\frac{i}{2} \int \frac{d^3 \mathbf{k}}{(2\pi)^3 2k} \int_{\Sigma} d^3 \mathbf{S}_u [a_{\mathbf{k}}^* \cdot \mathbb{T}_u] \int_{\Omega} d^4 y G_r^0(x, y) U''(\varphi(y)) a_{\mathbf{k}}(y), \quad (2.109)$$

where we have dropped the boundary term from this Green's formula since the action of \mathbb{T}_u on it gives zero (this boundary term does not depend on the value of φ on Σ). Finally, we can expand the action of \mathbb{T}_u , by exploiting the fact that it is a first order differential operator. We get

$$\begin{aligned} \xi(x) = & -\frac{i}{2} \int \frac{d^3 \mathbf{k}}{(2\pi)^3 2k} \int_{\Sigma} d^3 \mathbf{S}_u \int_{\Omega} d^4 y G_r^0(x, y) \left\{ U''(\varphi(y)) [a_{\mathbf{k}}^* \cdot \mathbb{T}_u] a_{\mathbf{k}}(y) \right. \\ & \left. + U'''(\varphi(y)) [a_{\mathbf{k}}^* \cdot \mathbb{T}_u] \varphi(y) a_{\mathbf{k}}(y) \right\} \\ = & -i \int_{\Omega} d^4 y G_r^0(x, y) \left[U''(\varphi(y)) \xi(y) \right. \\ & \left. + U'''(\varphi(y)) \frac{1}{2} \int \frac{d^3 \mathbf{k}}{(2\pi)^3 2k} a_{\mathbf{k}}^*(y) a_{\mathbf{k}}(y) \right]. \end{aligned} \quad (2.110)$$

The second equation is identical to the equation (2.106) that determines $\beta_1(x)$. Therefore, we have $\beta_1(x) = \xi(x)$, as announced.

By combining the results for $\beta_1(x)$ and $\beta_2(x)$, we finally obtain

$$\beta(x) = \left[\frac{1}{2} \int \frac{d^3 \mathbf{k}}{(2\pi)^3 2k} \int_{\Sigma} d^3 \mathbf{S}_u d^3 \mathbf{S}_v [\mathbf{a}_k^* \cdot \mathbb{T}_u] [\mathbf{a}_k \cdot \mathbb{T}_v] + \int_{\Sigma} d^3 \mathbf{S}_u [\beta \cdot \mathbb{T}_u] \right] \varphi(x). \quad (2.111)$$

By inserting this expression, as well as eq. (2.101), in eq. (2.88), we can write the single inclusive spectrum at NLO as follows

$$\left. \frac{dN_1}{d^3 \mathbf{p}} \right|_{\text{NLO}} = \left[\frac{1}{2} \int \frac{d^3 \mathbf{k}}{(2\pi)^3 2k} \int_{\Sigma} d^3 \mathbf{S}_u d^3 \mathbf{S}_v [\mathbf{a}_k^* \cdot \mathbb{T}_u] [\mathbf{a}_k \cdot \mathbb{T}_v] + \int_{\Sigma} d^3 \mathbf{S}_u [\beta \cdot \mathbb{T}_u] \right] \left. \frac{dN_1}{d^3 \mathbf{p}} \right|_{\text{LO}}. \quad (2.112)$$

This is the central result of this chapter, and it will play a crucial role in the discussion of factorization in heavy ion collisions. Some remarks should be made about this formula:

- i. In this formula, the LO inclusive spectrum that appears in the right hand side must be considered as a functional of the classical field on the surface Σ ,
- ii. The LO and NLO spectra cannot be obtained in closed analytical form, because they contain the classical field φ – retarded solution of a non-linear partial differential equation that cannot be solved analytically in general,
- iii. In practical applications such as heavy ion collisions, the dynamics of φ is simple below the forward light-cone (i.e. at any point in space-time before the collision), and complicated above the light-cone,
- iv. Therefore, one can choose the surface Σ in such a way that the small field fluctuations \mathbf{a}_k and β are calculable analytically on Σ ,
- v. By doing this, the non-perturbative non-linear dynamics appears only in the factor $[dN_1/d^3 \mathbf{p}]_{\text{LO}}$, while the operator in the square bracket can be calculated analytically,
- vi. One can already foresee structural similarities between the operator between the square brackets and the JIMWLK Hamiltonian, that both contain terms with one and two functional derivatives. In the second part of this manuscript, our goal will be to show that in the collision of two nuclei, the logarithms of energy arise from this operator, with coefficients that are precisely the JIMWLK Hamiltonians of the projectiles.

2.6.4 Higher inclusive moments

Let us now turn to higher inclusive moments. Our goal is to prove that eq. (2.112) is also valid in this more general case. The starting point is the general formula (2.85) for the n -particle inclusive spectrum. This formula is valid to all orders. At leading order, the n -particle

spectrum is simply given by eq. (2.86) as the product of n 1-particle spectra. At next-to-leading order, eq. (2.85) leads to:

$$\begin{aligned} \left. \frac{dN_n}{d^3\mathbf{p}_1 \cdots d^3\mathbf{p}_n} \right|_{\text{NLO}} &= \sum_{i=1}^n \left. \frac{dN_1}{d^3\mathbf{p}_i} \right|_{\text{NLO}} \prod_{j \neq i} \left. \frac{dN_1}{d^3\mathbf{p}_j} \right|_{\text{LO}} \\ &+ \sum_{i < j} \left[\frac{\delta^2 \ln \mathcal{F}}{\delta z(\mathbf{p}_i) \delta z(\mathbf{p}_j)} \right]_{z(\mathbf{p})=1} \prod_{k \neq i,j} \left. \frac{dN_1}{d^3\mathbf{p}_k} \right|_{\text{LO}}. \end{aligned} \quad (2.113)$$

Therefore, the only new quantity that we need to evaluate is the second derivative of $\ln \mathcal{F}[z(\mathbf{p})]$. It is sufficient to evaluate it at leading order ($\mathcal{O}(g^{-2})$), i.e. at tree level. From eq. (2.76), we get

$$\begin{aligned} \left. \frac{\delta^2 \ln \mathcal{F}[z(\mathbf{p})]}{\delta z(\mathbf{p}) \delta z(\mathbf{q})} \right|_{\text{LO}} &= \frac{1}{(2\pi)^3 2p} \left[\frac{\delta f_+^{(+)}(+\infty, \mathbf{p})}{\delta z(\mathbf{q})} f_-^{(-)}(+\infty, \mathbf{p}) \right. \\ &\quad \left. + f_+^{(+)}(+\infty, \mathbf{p}) \frac{\delta f_-^{(-)}(+\infty, \mathbf{p})}{\delta z(\mathbf{q})} \right]. \end{aligned} \quad (2.114)$$

From eq. (2.75), it is obvious that the derivatives with respect to $z(\mathbf{q})$ of the Fourier coefficients $f_{\pm}^{(\pm)}$ are the Fourier coefficients of

$$b_{\pm\mathbf{q}}(x) \equiv \frac{\delta \varphi_{\pm}(x)}{\delta z(\mathbf{q})}. \quad (2.115)$$

By differentiating the equation of motion of $\varphi_{\pm}(x)$ with respect to $z(\mathbf{q})$, we find the equation of motion of $b_{\pm\mathbf{q}}(x)$,

$$\left[\square_x + \mathcal{U}''(\varphi_{\pm}(x)) \right] b_{\pm\mathbf{q}}(x) = 0, \quad (2.116)$$

and we see that $b_{\pm\mathbf{q}}(x)$ is a small field fluctuation propagating on top of the classical field φ_{\pm} . In order to fully determine $b_{\pm\mathbf{q}}(x)$, we also need to know its boundary conditions. These can be obtained by differentiating the boundary conditions of $\varphi_{\pm}(x)$ with respect to $z(\mathbf{q})$. If we denote $b_{\pm\mathbf{q}}^{(\pm)}(x^0, \mathbf{p})$ the Fourier coefficients of $b_{\pm\mathbf{q}}(x)$, we have the following boundary conditions:

$$\begin{aligned} b_{+\mathbf{q}}^{(+)}(-\infty, \mathbf{p}) &= b_{-\mathbf{q}}^{(-)}(-\infty, \mathbf{p}) = 0, \\ b_{+\mathbf{q}}^{(-)}(+\infty, \mathbf{p}) &= z(\mathbf{p}) b_{-\mathbf{q}}^{(-)}(+\infty, \mathbf{p}) + \delta(\mathbf{p} - \mathbf{q}) f_-^{(-)}(+\infty, \mathbf{p}), \\ b_{-\mathbf{q}}^{(+)}(+\infty, \mathbf{p}) &= z(\mathbf{p}) b_{+\mathbf{q}}^{(+)}(+\infty, \mathbf{p}) + \delta(\mathbf{p} - \mathbf{q}) f_+^{(+)}(+\infty, \mathbf{p}). \end{aligned} \quad (2.117)$$

Although the equation of motion (2.116) has no source term, the non homogeneous terms in the boundary conditions ensure that the small fluctuations $b_{\pm\mathbf{q}}(x)$ are non-zero.

At this point, since we are not going to take further derivatives, it is safe to set $z(\mathbf{p}) = 1$. This simplifies things a bit since $\varphi_+ = \varphi_-$ when $z(\mathbf{p}) = 1$. Therefore, we need not distinguish between $f_+^{(\pm)}$ and $f_-^{(\pm)}$, and we can simplify the notation for these Fourier coefficients

into $f^{(\pm)}$ (which are the Fourier coefficients of the classical field φ with null retarded boundary conditions). After this simplification, the boundary conditions for the small fluctuations become

$$\begin{aligned} b_{+q}^{(+)}(-\infty, \mathbf{p}) &= b_{-q}^{(-)}(-\infty, \mathbf{p}) = 0, \\ b_{+q}^{(-)}(+\infty, \mathbf{p}) &= b_{-q}^{(-)}(+\infty, \mathbf{p}) + \delta(\mathbf{p} - \mathbf{q}) f^{(-)}(+\infty, \mathbf{p}), \\ b_{-q}^{(+)}(+\infty, \mathbf{p}) &= b_{+q}^{(+)}(+\infty, \mathbf{p}) + \delta(\mathbf{p} - \mathbf{q}) f^{(+)}(+\infty, \mathbf{p}). \end{aligned} \quad (2.118)$$

The difficulty with these boundary conditions is that they are neither retarded nor advanced. However, since the equation of motion for the fluctuations $b_{\pm q}(x)$ is linear, we can write $b_{\pm q}(x)$ as a superposition of solutions of the same equation, but with retarded boundary conditions. A basis of such solutions has been introduced already in eq. (2.97). From the boundary conditions at $x^0 = -\infty$, we can write

$$\begin{aligned} b_{+q}(x) &= \int \frac{d^3 \mathbf{k}}{(2\pi)^3 2k} \beta_{+q}^{\mathbf{k}} a_{\mathbf{k}}^*(x) \\ b_{-q}(x) &= \int \frac{d^3 \mathbf{k}}{(2\pi)^3 2k} \beta_{-q}^{\mathbf{k}} a_{\mathbf{k}}(x). \end{aligned} \quad (2.119)$$

(Indeed, the first of eqs. (2.118) tells us that $b_{+q}(x)$ has no positive energy component and $b_{-q}(x)$ no negative energy component when $x^0 \rightarrow -\infty$, while $a_{\mathbf{k}}(x)$ is a positive energy plane wave in this limit.) In order to use this representation in order to solve the eqs. (2.118), we need to decompose the fluctuation $a_{\mathbf{k}}(x)$ in Fourier modes:

$$a_{\mathbf{k}}(x) \equiv \int \frac{d^3 \mathbf{p}}{(2\pi)^3 2p} \left[a_{\mathbf{k}}^{(+)}(x^0, \mathbf{p}) e^{-i\mathbf{p} \cdot \mathbf{x}} + a_{\mathbf{k}}^{(-)}(x^0, \mathbf{p}) e^{+i\mathbf{p} \cdot \mathbf{x}} \right]. \quad (2.120)$$

Then, one can rewrite the second and third boundary conditions in eqs. (2.118) as

$$\begin{aligned} \int \frac{d^3 \mathbf{k}}{(2\pi)^3 2k} \left[\beta_{-q}^{\mathbf{k}} a_{\mathbf{k}}^{(+)}(\mathbf{p}) - \beta_{+q}^{\mathbf{k}} a_{\mathbf{k}}^{* (+)}(\mathbf{p}) \right] &= \delta(\mathbf{p} - \mathbf{q}) f^{(+)}(\mathbf{p}), \\ \int \frac{d^3 \mathbf{k}}{(2\pi)^3 2k} \left[\beta_{+q}^{\mathbf{k}} a_{\mathbf{k}}^{* (-)}(\mathbf{p}) - \beta_{-q}^{\mathbf{k}} a_{\mathbf{k}}^{(-)}(\mathbf{p}) \right] &= \delta(\mathbf{p} - \mathbf{q}) f^{(-)}(\mathbf{p}), \end{aligned} \quad (2.121)$$

where we have not written the time argument in the Fourier coefficients since it is $x^0 = +\infty$ everywhere. Since $f^{(-)}(\mathbf{p}) = [f^{(+)}(\mathbf{p})]^*$, we see that the solution obeys

$$\beta_{-q}^{\mathbf{k}} = \left[\beta_{+q}^{\mathbf{k}} \right]^*, \quad (2.122)$$

which implies that $b_{-q}(x) = [b_{+q}(x)]^*$. Eqs. (2.121) thus reduce to a single equation. Moreover, one can see it as a system of linear equations for the coefficients $\beta_{\pm q}^{\mathbf{k}}$. It turns out that this linear system can be solved in closed form²⁶, in terms of the Fourier coefficients $a_{\mathbf{k}}^{(\pm)}(\mathbf{p})$, thanks to the equation (C.14) derived in appendix C. One can check that the following formulas solve eqs. (2.121),

$$\begin{aligned} \beta_{+q}^{\mathbf{k}} &= \frac{1}{(2\pi)^3 2q} \left[a_{\mathbf{k}}^{(-)}(\mathbf{q}) f^{(+)}(\mathbf{q}) + a_{\mathbf{k}}^{(+)}(\mathbf{q}) f^{(-)}(\mathbf{q}) \right], \\ \beta_{-q}^{\mathbf{k}} &= \frac{1}{(2\pi)^3 2q} \left[a_{\mathbf{k}}^{* (-)}(\mathbf{q}) f^{(+)}(\mathbf{q}) + a_{\mathbf{k}}^{* (+)}(\mathbf{q}) f^{(-)}(\mathbf{q}) \right]. \end{aligned} \quad (2.123)$$

²⁶Even though the Fourier coefficients $a_{\mathbf{k}}^{(\pm)}(\mathbf{p})$ are not known analytically, the fact that small field fluctuations evolve unitarily is sufficient to invert the system of eqs. (2.121).

These formulas completely determine the coefficients in the decompositions (2.119) in terms of the Fourier coefficients of the retarded classical field φ , and of the retarded small field fluctuations a_k, a_k^* .

Inserting this result back into the formula for $\delta^2 \ln \mathcal{F}[z]/\delta z(\mathbf{p})\delta z(\mathbf{q})$, we can write it as:

$$\begin{aligned} \left. \frac{\delta^2 \ln \mathcal{F}[z]}{\delta z(\mathbf{p})\delta z(\mathbf{q})} \right|_{\substack{\text{LO} \\ z \equiv 1}} &= \frac{1}{2} \frac{1}{(2\pi)^6 4pq} \int \frac{d^3 \mathbf{k}}{(2\pi)^3 2k} \\ &\times \left\{ \left(a_k^{*(-)}(\mathbf{p}) a_k^{(-)}(\mathbf{q}) + a_k^{(-)}(\mathbf{p}) a_k^{*(-)}(\mathbf{q}) \right) f^{(+)}(\mathbf{p}) f^{(+)}(\mathbf{q}) \right. \\ &+ \left(a_k^{*(+)}(\mathbf{p}) a_k^{(+)}(\mathbf{q}) + a_k^{(+)}(\mathbf{p}) a_k^{*(+)}(\mathbf{q}) \right) f^{(-)}(\mathbf{p}) f^{(-)}(\mathbf{q}) \\ &+ \left(a_k^{*(-)}(\mathbf{p}) a_k^{(+)}(\mathbf{q}) + a_k^{(-)}(\mathbf{p}) a_k^{*(+)}(\mathbf{q}) \right) f^{(+)}(\mathbf{p}) f^{(-)}(\mathbf{q}) \\ &+ \left. \left(a_k^{*(+)}(\mathbf{p}) a_k^{(-)}(\mathbf{q}) + a_k^{(+)}(\mathbf{p}) a_k^{*(-)}(\mathbf{q}) \right) f^{(-)}(\mathbf{p}) f^{(+)}(\mathbf{q}) \right\} \\ &- \frac{1}{(2\pi)^3 2p} \delta(\mathbf{p} - \mathbf{q}) \left| f^{(+)}(\mathbf{p}) \right|^2. \end{aligned} \quad (2.124)$$

Thus, we have managed to express this quantity entirely in terms of the Fourier coefficients of the retarded classical field and of retarded small field fluctuations. This will play a crucial role later in the proof of factorization for the multigluon inclusive spectra. Moreover, this formula is explicitly symmetric under the exchange of the momenta \mathbf{p} and \mathbf{q} , as expected for a second derivative. Note also the last term, equal to $\delta(\mathbf{p} - \mathbf{q})$ times the single inclusive gluon spectrum. It arises because we have chosen to define the 2-gluon spectrum so that its integral over \mathbf{p} and \mathbf{q} gives the average value of $N(N-1)$ instead of N^2 – this term leads to the $-N$ in this integral.

A final step in obtaining a useful expression for the NLO correction to the multiparticle inclusive spectrum is to rewrite everything in terms of the operators \mathbb{T}_u introduced for the NLO corrections to the single inclusive spectrum. Let us recall eq. (2.98), from which we deduce the following relations for the Fourier coefficients at $x^0 = +\infty$,

$$\begin{aligned} a_k^{(\epsilon)}(\mathbf{p}) &= \int_{\Sigma} d^3 \mathbf{S}_u \left[a_k \cdot \mathbb{T}_u \right] f^{(\epsilon)}(\mathbf{p}), \\ a_k^{*(\epsilon)}(\mathbf{p}) &= \int_{\Sigma} d^3 \mathbf{S}_u \left[a_k^* \cdot \mathbb{T}_u \right] f^{(\epsilon)}(\mathbf{p}). \end{aligned} \quad (2.125)$$

Inserting these identities into eq. (2.124), we see that we can write it in a very compact fashion

$$\left. \frac{\delta^2 \ln \mathcal{F}[z]}{\delta z(\mathbf{p})\delta z(\mathbf{q})} \right|_{\substack{\text{LO} \\ z \equiv 1}} = \left[\mathcal{T}_2 \right]_{\text{connected}} \left. \frac{dN_1}{d^3 \mathbf{p}} \right|_{\text{LO}} \left. \frac{dN_1}{d^3 \mathbf{q}} \right|_{\text{LO}} - \delta(\mathbf{p} - \mathbf{q}) \left. \frac{dN_1}{d^3 \mathbf{p}} \right|_{\text{LO}}, \quad (2.126)$$

where the operator \mathcal{T}_2 is the quadratic part of the operator that appears in eq. (2.112),

$$\mathcal{T}_2 \equiv \frac{1}{2} \int \frac{d^3 \mathbf{k}}{(2\pi)^3 2k} \int_{\Sigma} d^3 \mathbf{S}_u d^3 \mathbf{S}_v \left[a_k^* \cdot \mathbb{T}_u \right] \left[a_k \cdot \mathbb{T}_v \right], \quad (2.127)$$

and where the subscript *connected* indicates that the two factors $\mathbb{T}_{u,v}$ cannot act on the same factor $dN_1/d^3\mathbf{p}$ or $dN_1/d^3\mathbf{q}$. More explicitly,

$$\left[\mathbb{T}_u \mathbb{T}_v\right]_{\text{connected}} AB \equiv [\mathbb{T}_u A][\mathbb{T}_v B] + [\mathbb{T}_v A][\mathbb{T}_u B]. \quad (2.128)$$

Now, it is trivial to insert this result—as well as eq. (2.112)—into eq. (2.113), in order to obtain the following formula for the n -particle inclusive spectrum at NLO,

$$\begin{aligned} \left.\frac{dN_n}{d^3\mathbf{p}_1 \cdots d^3\mathbf{p}_n}\right|_{\text{NLO}} &= \left[\frac{1}{2} \int \frac{d^3\mathbf{k}}{(2\pi)^3 2k} \int_{\Sigma} d^3\mathbf{S}_u d^3\mathbf{S}_v [\mathbf{a}_k^* \cdot \mathbb{T}_u][\mathbf{a}_k \cdot \mathbb{T}_v] \right. \\ &\quad \left. + \int_{\Sigma} d^3\mathbf{S}_u [\beta \cdot \mathbb{T}_u] \right] \prod_i \left.\frac{dN_1}{d^3\mathbf{p}_i}\right|_{\text{LO}} \\ &\quad - \sum_{i < j} \delta(\mathbf{p}_i - \mathbf{p}_j) \left.\frac{dN_1}{d^3\mathbf{p}_i}\right|_{\text{LO}} \prod_{k \neq i,j} \left.\frac{dN_1}{d^3\mathbf{p}_k}\right|_{\text{LO}}. \end{aligned} \quad (2.129)$$

This is the generalization of eq. (2.112) to the case of the n -particle spectrum. We see that, except for the last term whose origin is due to our choice of normalizing the n -particle spectrum so that its integral is the average of $N(N-1) \cdots (N-n+1)$, the NLO contribution is obtained by acting on the LO result with the same operator as in the case of the single particle spectrum. This goes a long way in the direction of proving factorization for all the inclusive multiparticle spectra. Thanks to this formula, the proof of factorization that we shall develop for the single particle spectrum can be generalized without further effort to the case of multiparticle spectra.

To close this chapter, it is important to stress again the importance of considering inclusive observables in order to obtain relations such as (2.112) and (2.129). Indeed, these formulas explicitly factorize the NLO corrections into an object that depends on space-time points below the surface Σ and an object that depend on points above Σ . This was made possible because all the expressions we had to manipulate could be expressed in terms of fields and field fluctuations that obeyed retarded boundary conditions. In turn, this is true only for quantities that are defined in an inclusive manner.

Part II

Initial State Factorization in Heavy Ion Collisions

Introduction



In the first part of this manuscript, we have derived the necessary tools and results in order to study particle production in a quantum field theory coupled to strong external sources. All the derivations have been done in the simpler case of a scalar field theory, but their generalization to a gauge theory is straightforward. In this second part, we apply these results to heavy ion collisions described by the Color Glass Condensate effective theory.

In chapter 3, we show that NLO corrections to observables contain logarithms of the cutoff that separates the sources from the fields in the color glass condensate framework. However, it turns out that these logarithms are universal properties of the incoming nuclei, that can be factorized into the probability distribution of sources for each projectile. We discuss thoroughly this factorization in the case of the inclusive gluon spectrum in heavy ion collisions. We also show how this result can be extended to the calculation of the expectation value of the energy-momentum tensor, which is a more interesting quantity in practical applications, since it is the initial condition for the subsequent hydrodynamical evolution of the system. Then we extend the proof of factorization to correlations between multiple gluons, or between the values of the energy momentum tensor at different spatial points.

Then, we discuss in chapter 4 some applications of these results to the phenomenology of heavy ion collisions at high energy, and compare these predictions to experimental results from the Relativistic Heavy Ion Collider (RHIC). In particular, we show that the color glass condensate description of heavy ion collisions may explain rather naturally some striking correlations that have been observed at RHIC.

Chapter 3

Inclusive gluon spectra at Leading Log accuracy



This chapter is devoted to the calculation of the single inclusive gluon spectrum produced in the collision of two high energy nuclei. We will start with its evaluation at leading order, in order to prove that it can be obtained from retarded classical solutions of the Yang-Mills equations. Then, we resum the leading logarithmic corrections that arise in higher orders, and show that they can all be *factorized* into distributions that describe the gluon content of the incoming projectiles. Moreover, we recover for these distributions the JIMWLK renormalization group equation, originally derived in the context of deep inelastic scattering. This result is therefore a first hint of the universality of the distributions that appear in the calculation of this quantity.

Strictly speaking, the gluon spectrum is not a good observable. Indeed, the number of produced gluons is not stable against soft and collinear splittings, and therefore cannot be defined properly. In the study of hadronic collisions, this issue is related to hadronization and is solved by introducing fragmentation functions, that describe how partons become hadrons and resum the logarithms associated with this process. However, it is not clear whether a similar treatment can be generalized to obtain single hadron spectra in heavy ion collisions, due to the very dense environment in which the produced gluons evolve.

A better point of view in heavy ions collisions is to consider the Color Glass Condensate calculation as an initial condition for the subsequent evolution, usually treated via hydrodynamical equations. With this in mind, a much better quantity to calculate is the spatial distribution of the energy-momentum tensor, at some fixed initial time. Moreover, since this quantity measures the distribution of energy and momentum in the system, it is insensitive to soft and collinear emissions, and therefore can be calculated unambiguously in QCD. As we shall see later in the chapter, the calculation of the energy-momentum tensor and its factorization can be achieved by the same techniques, previously developed for the single gluon spectrum.

3.1 Gluon spectrum at Leading Order

3.1.1 Generalities

The single inclusive gluon spectrum is defined in the same way as for scalar fields. One can first define a generating functional $\mathcal{F}[z]$ by

$$\mathcal{F}[z] \equiv \sum_{n=0}^{\infty} \frac{1}{n!} \int \frac{d^3 \mathbf{p}_1}{(2\pi)^3 2p_1} \cdots \frac{d^3 \mathbf{p}_n}{(2\pi)^3 2p_n} z(\mathbf{p}_1) \cdots z(\mathbf{p}_n) |\langle \mathbf{p}_1 \cdots \mathbf{p}_{n,\text{out}} | 0_{\text{in}} \rangle|^2, \quad (3.1)$$

where $z(\mathbf{p})$ is some arbitrary function over the 1-gluon phase space. The only difference with the scalar case here is that the produced gluons carry polarizations λ_i and colors α_i . The squared transition amplitude that appears in the right hand side of this formula must be summed over the polarizations and colors of the produced gluons. Note that only the two physical (transverse) polarizations must be included in this sum. This implies the following change in the operator $\mathcal{C}_{\mathbf{p}}$ defined in eq. (2.62). It now reads¹

$$\mathcal{C}_{\mathbf{p}} \equiv \sum_{\lambda, \alpha} \int d^4 x d^4 y e^{i\mathbf{p} \cdot (\mathbf{x} - \mathbf{y})} \square_{\mathbf{x}} \square_{\mathbf{y}} \epsilon_{\lambda}^{\mu}(\mathbf{p}) \epsilon_{\lambda}^{\nu*}(\mathbf{p}) \frac{\delta^2}{\delta \eta_{+}^{\mu\alpha}(x) \delta \eta_{-}^{\nu\alpha}(y)}. \quad (3.2)$$

In this definition, $\epsilon_{\lambda}^{\mu}(\mathbf{p})$ is the polarization vector for a gluon of momentum \mathbf{p} and polarization λ . Note also that the currents η_{\pm} must now carry both a Lorentz and a color index in order to be coupled to the gauge fields.

Assuming that the above generating functional is known, the single inclusive gluon spectrum is obtained from the first derivative of $\mathcal{F}[z]$ evaluated at $z \equiv 1$:

$$\frac{dN_1}{d^3 \mathbf{p}} = \left. \frac{\delta \mathcal{F}[z]}{\delta z(\mathbf{p})} \right|_{z(\mathbf{p})=1}. \quad (3.3)$$

Then, all the steps of the derivation in the scalar case can be reproduced in the case of gauge fields. At leading order, i.e. $\mathcal{O}(g^{-2})$, one finds that the inclusive gluon spectrum can be expressed as

$$\left. \frac{dN_1}{d^3 \mathbf{p}} \right|_{\text{LO}} = \frac{1}{(2\pi)^3 2p} \sum_{\lambda, \alpha} \int d^4 x d^4 y e^{i\mathbf{p} \cdot (\mathbf{x} - \mathbf{y})} \square_{\mathbf{x}} \square_{\mathbf{y}} \epsilon_{\lambda}^{\mu}(\mathbf{p}) \epsilon_{\lambda}^{\nu*}(\mathbf{p}) \mathcal{A}_{\mu\alpha}(x) \mathcal{A}_{\nu\alpha}(y), \quad (3.4)$$

where the color field $\mathcal{A}_{\mu}(x)$ obeys the classical Yang-Mills equations,

$$[\mathcal{D}_{\mu}, \mathcal{F}^{\mu\nu}] = J^{\nu}, \quad (3.5)$$

where $\mathcal{F}^{\mu\nu}$ is the field strength,

$$\mathcal{F}^{\mu\nu} \equiv \partial^{\mu} \mathcal{A}^{\nu} - \partial^{\nu} \mathcal{A}^{\mu} + ig [\mathcal{A}^{\mu}, \mathcal{A}^{\nu}], \quad (3.6)$$

and with a null retarded boundary condition

$$\lim_{x^0 \rightarrow -\infty} \mathcal{A}^{\mu}(x) = 0, \quad \lim_{x^0 \rightarrow -\infty} \partial_{x^0} \mathcal{A}^{\mu}(x) = 0. \quad (3.7)$$

¹Since we sum over the polarizations of the produced gluons, the generating functional defined here is not suitable for the calculation of polarized observables.

Although eq. (3.4) apparently involves an integration of the gauge field over the entire space-time, it is easy to show that one needs in fact only its asymptotic behavior at $x^0 \rightarrow +\infty$. In order to see this, note first the identity

$$\int d^3\mathbf{x} e^{i\mathbf{p}\cdot\mathbf{x}} \square_x \mathcal{A}_\mu(x) = \partial_x^0 \int d^3\mathbf{x} e^{i\mathbf{p}\cdot\mathbf{x}} (\partial_x^0 - i\mathbf{p}) \mathcal{A}_\mu(x) . \quad (3.8)$$

In other words, the integrand for the dx^0 integral in eq. (3.4) is a total time derivative. Therefore, the integral depends only on the behavior of the gauge field at infinite time. Moreover, given the boundary condition (3.7) obeyed by the gauge field, the boundary at $x^0 = -\infty$ does not contribute, and one is left with a formula that involves only $x^0, y^0 = +\infty$:

$$\left. \frac{dN_1}{d^3\mathbf{p}} \right|_{\text{LO}} = \lim_{t \rightarrow +\infty} \frac{1}{(2\pi)^3 2p} \sum_{\lambda, \alpha} \int d^3\mathbf{x} d^3\mathbf{y} e^{-i\mathbf{p}\cdot(\mathbf{x}-\mathbf{y})} (\partial_x^0 - i\mathbf{p})(\partial_y^0 + i\mathbf{p}) \\ \times \epsilon_\lambda^\mu(\mathbf{p}) \epsilon_\lambda^{*\nu}(\mathbf{p}) \mathcal{A}_{\mu\alpha}(t, \mathbf{x}) \mathcal{A}_{\nu\alpha}(t, \mathbf{y}) . \quad (3.9)$$

3.1.2 Covariant current conservation

In non abelian gauge theories, where the gauge fields themselves carry a charge, there is an additional constraint that must be obeyed by the external current J^ν :

$$[\mathcal{D}_\mu, J^\mu] = 0 . \quad (3.10)$$

This is the generalization to QCD of the usual current conservation law. It is usually named *covariant current conservation*, since it involves a covariant derivative instead of an ordinary derivative. The physical meaning of this difference is that the color flux encoded in the current J^μ can have its color altered by a gauge field. Eq. (3.10) quantifies the color precession of the current due to the background gauge field. Therefore, the Yang-Mills equations and the covariant current conservation constraint must be solved simultaneously, with the external current J^ν specified only in the remote past, where the gauge field vanishes thanks to the boundary condition (3.7).

There are some gauges in which the constraint due to covariant current conservation becomes trivial. Consider for instance the color current J^ν created by a projectile moving at the speed of light in the $+z$ direction. Its only non zero component is J^+ . Therefore, in the *light-cone gauge* $\mathcal{A}^- = 0$, eq. (3.10) simply becomes

$$\partial_\mu J^\mu = 0 , \quad (3.11)$$

i.e. the ordinary current conservation. The covariant current conservation constraint thus decouples from the Yang-Mills equations, and can be solved once for all. In the case of the collision of two fast projectiles, moving respectively in the $+z$ and $-z$ directions, the current has the following form before the collision:

$$J^\mu(x) = \delta^{\mu+} \rho_1(x^-, \mathbf{x}_\perp) + \delta^{\mu-} \rho_2(x^+, \mathbf{x}_\perp) . \quad (3.12)$$

ρ_1 is taken independent of x^+ and ρ_2 independent of x^- so that the projectiles are invariant along their trajectory (in other words, if they did not collide, nothing would happen at all). The \mathbf{x}_\perp dependence of these sources reflect both the transverse size of the colliding nuclei and the impact parameter of the collision. In contrast, we keep an x^- dependence for ρ_1 and an x^+ dependence for ρ_2 . However, due to the Lorentz contraction factor that applies to

these fast moving color charges, these color charge densities are non zero only if $x^- \approx 0$ or $x^+ \approx 0$ respectively:

$$\rho_1(x^-, \mathbf{x}_\perp) \sim \delta(x^-) \quad , \quad \rho_2(x^+, \mathbf{x}_\perp) \sim \delta(x^+) \quad . \quad (3.13)$$

Note also that this form of the current satisfies the abelian current conservation law $\partial_\mu J^\mu = 0$. The peculiarity of eq. (3.12) is that it has a $+$ component whose support is restricted to the $x^- = 0$ hyperplane, and a $-$ component whose support is the $x^+ = 0$ hyperplane. Therefore, the gauge condition [103, 104]

$$x^+ \mathcal{A}^- + x^- \mathcal{A}^+ = 0 \quad , \quad (3.14)$$

known as the *Fock-Schwinger gauge*, renders the covariant current conservation law equivalent to the abelian one. Indeed, a gauge field that satisfies eq. (3.14) has $\mathcal{A}^- = 0$ on the $x^- = 0$ hyperplane and $\mathcal{A}^+ = 0$ on the $x^+ = 0$ hyperplane. This is the reason why the Fock-Schwinger gauge is often used in the study of high energy hadronic collisions in the CGC framework.

3.1.3 Initial conditions on the forward light-cone

Given the sources $\rho_{1,2}$ that describe the configuration of color charges in the two colliding projectiles, eqs. (3.5), (3.7) and (3.4) completely determine the corresponding inclusive 1-gluon spectrum at leading order. The main difficulty resides in the fact that one cannot solve analytically the Yang-Mills equations².

Therefore, one has to use numerical methods [20–26] in order to obtain this solution. This is straightforward, since the boundary conditions that specify the classical solution of interest are retarded boundary conditions. However, one cannot start the numerical resolution at $x^0 = -\infty$, because the sources $\rho_{1,2}$ contain $\delta(x^\pm)$ singularities that cannot be handled by a computer. Since these singularities lie on the light-cones $x^\pm = 0$, it is preferable to start the numerical resolution on a surface $\tau = \text{const}$ just above the two light-cones, in order to completely avoid the singularities in the numerical algorithm.

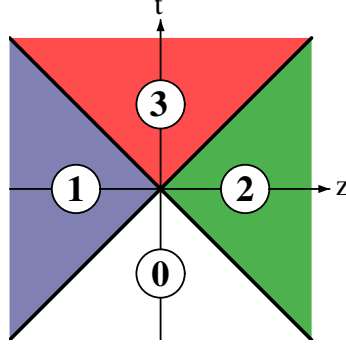
Fortunately, it turns out that it is possible to find an analytical solution to the Yang-Mills equations with these boundary conditions and external sources, on the surface $\tau = 0^+$ [104] (The $+$ superscript indicates that this surface is above the light-cones, at some infinitesimal positive proper time). Then, the numerical solution is started from this analytical solution on the light-cone.

In order to obtain this initial condition, it is useful to divide the space-time into four distinct regions, as illustrated in the figure 3.1. The two diagonal lines represent the trajectories of the two nuclei. Therefore, any point located below these two lines (region 0) is a point where none of the projectiles has passed yet. Since the initial condition for the gauge field in the remote past is $\mathcal{A}^\mu = 0$, the value of \mathcal{A}^μ remains zero throughout the entire region 0.

Finding the solution in the domains 1 and 2 is also rather easy, thanks to causality. In these regions, one of the projectiles has passed, but the second projectile has not yet arrived.

²Several analytical approximations have been developed. An expansion in the sources $\rho_{1,2}$ has been developed in [105], where the radiated field was evaluated at the lowest order. [106] assumes the cancellation of a certain set of graphs in light-cone gauge in order to obtain a closed result. However, this cancellation is only established if one of the two sources is weak. In [107], the solution of the classical Yang-Mills equations was organized as an expansion in commutators of Wilson lines, while in [108] the solution was expanded in powers of the proper time τ . More recently, in [109], it was argued that one can choose the gauge in a way that minimizes the final state interactions and thus where the solution at $\tau = 0^+$ is already a good approximation of the late time solution.

Figure 3.1: Division of space-time in four regions for the solution of Yang-Mills equations.



Therefore, one only needs to solve the Yang-Mills equations with a single source. Let us do this explicitly for the region 1. The relevant Yang-Mills equation is

$$[\mathcal{D}_\mu, \mathcal{F}_1^{\mu\nu}] = \delta^{\nu+} \delta(x^-) \rho_1(\mathbf{x}_\perp) . \quad (3.15)$$

(The subscript 1 indicates that this is the solution of Yang-Mills equations in the presence of the source ρ_1 only.) In order to solve this equation, it is useful to go temporarily to the *Lorenz gauge*, where the gauge field obeys the condition

$$\partial_\mu \tilde{\mathcal{A}}_1^\mu = 0 . \quad (3.16)$$

(A tilde distinguishes quantities expressed in the Lorenz gauge.) When this condition is satisfied, one can rewrite the Yang-Mills equations as

$$\square \tilde{\mathcal{A}}_1^\nu = \delta^{\nu+} \tilde{\rho}_1(x^-, \mathbf{x}_\perp) + ig[\tilde{\mathcal{A}}_{1\mu}, \tilde{\mathcal{F}}_1^{\mu\nu} + \partial^\mu \tilde{\mathcal{A}}_1^\nu] . \quad (3.17)$$

Written in this form, it is clear that one can solve this equation iteratively in successive powers of the source $\tilde{\rho}_1$. Indeed, the gauge field $\tilde{\mathcal{A}}_1^\mu$ and field strength $\tilde{\mathcal{F}}_1^{\mu\nu}$ are both at least of order one in $\tilde{\rho}_1$. Therefore, the commutator that appears in the right hand side is of order two and can be dropped in the first iteration. One gets

$$\tilde{\mathcal{A}}_1^{(1)\nu}(x) = -\delta^{\nu+} \frac{1}{\nabla_\perp^2} \tilde{\rho}_1(x^-, \mathbf{x}_\perp) , \quad (3.18)$$

where the superscript (1) indicates that this is the first order in an expansion in powers of the source $\tilde{\rho}_1$. The object $\delta^{\nu+}$ is defined by

$$\begin{aligned} \delta^{\nu+} &= 1 & \text{if } \nu = + , \\ \delta^{\nu+} &= 0 & \text{if } \nu = -, i . \end{aligned} \quad (3.19)$$

It is important to note that this field has no $-$ component, and therefore has no effect on the covariant conservation constraint. Therefore, the current $\delta^{\nu+} \tilde{\rho}_1(x^-, \mathbf{x}_\perp)$ is not modified by the radiated field at this order. One can then proceed to calculate the second order contribution to the gauge field. But it is easy to see that the only possible source for such terms –the commutator in the right hand side of eq. (3.17)– vanishes. Therefore,

$$\tilde{\mathcal{A}}_1^{(2)\nu}(x) = 0 . \quad (3.20)$$

By induction, one sees that in fact all the contributions of higher order in $\tilde{\rho}_1$ to $\tilde{\mathcal{A}}_1^\nu(x)$ are zero. Therefore, the full solution of eq. (3.17) reads

$$\tilde{\mathcal{A}}_1^\nu(x) = -\delta^{\nu+} \frac{1}{\nabla_\perp^2} \tilde{\rho}_1(x^-, \mathbf{x}_\perp) . \quad (3.21)$$

We must now find the gauge rotation that transforms this solution into the Fock-Schwinger gauge solution. Let us write

$$\mathcal{A}_1^\mu = \Omega_1^\dagger \tilde{\mathcal{A}}_1^\mu \Omega_1 + \frac{i}{g} \Omega_1^\dagger \partial^\mu \Omega_1 , \quad (3.22)$$

where Ω_1 is an element of $SU(3)$. A trivial way to satisfy the Fock-Schwinger gauge condition is to have both $\mathcal{A}_1^+ = \mathcal{A}_1^- = 0$. It is possible to have $\mathcal{A}_1^- = 0$ simply by taking an Ω_1 that does not depend on x^+ . In order to have also $\mathcal{A}_1^+ = 0$, the matrix Ω_1 must obey

$$\partial^+ \Omega_1 = ig \tilde{\mathcal{A}}_1^+ \Omega_1 , \quad (3.23)$$

which can be solved by³

$$\Omega_1(x^-, \mathbf{x}_\perp) = T_- \exp ig \int_{-\infty}^{x^-} dz^- \tilde{\mathcal{A}}_1^+(z^-, \mathbf{x}_\perp) . \quad (3.24)$$

(In this equation T_- denotes an ordering of the exponential in the x^- direction, such that the fields with the largest x^- always appear on the left of the expression.) Therefore, we now know all the components of the gauge field \mathcal{A}_1^μ in the Fock-Schwinger gauge, in the region 1 [110]:

$$\begin{aligned} \mathcal{A}_1^\pm &= 0 , \\ \mathcal{A}_1^i &= \frac{i}{g} \Omega_1^\dagger \partial^i \Omega_1 . \end{aligned} \quad (3.25)$$

This solution of Yang-Mills equations is a pure gauge in the transverse plane, since it obeys

$$\mathcal{F}_1^{ij} = 0 . \quad (3.26)$$

In fact, the gauge field is also obviously a pure gauge in region 0 –albeit a different one–, and the field strength is non zero at the discontinuity between these two pure gauges, i.e. on the surface $x^- = 0$.

Note also that this formula determines \mathcal{A}_1^μ explicitly in terms of the color source $\tilde{\rho}_1$ in the Lorenz gauge. Only implicit relations between \mathcal{A}_1^μ and the color source ρ_1 in the Fock-Schwinger gauge can be obtained. This is not an important limitation in practice.

It is trivial to mimic this derivation for the region 2, where the only relevant source is ρ_2 . One finds that for this region, the gauge field in the Fock-Schwinger gauge is given by:

$$\begin{aligned} \mathcal{A}_2^\pm &= 0 , \\ \mathcal{A}_2^i &= \frac{i}{g} \Omega_2^\dagger \partial^i \Omega_2 , \end{aligned} \quad (3.27)$$

³This solution is not unique. A more general solution is $\Omega_1'(x^-, \mathbf{x}_\perp) \equiv \Omega_1(x^-, \mathbf{x}_\perp) \Theta(\mathbf{x}_\perp)$, which leads to the following gauge fields:

$$\mathcal{A}'^\pm = 0 , \quad \mathcal{A}'^i = \Theta^\dagger \Omega_1^\dagger (\partial^i \Omega_1) \Theta + \frac{i}{g} \Theta^\dagger \partial^i \Theta .$$

This residual arbitrariness is due to the fact that the Fock-Schwinger gauge condition imposed on the gauge field does not determine it uniquely. We use the choice $\Theta \equiv 1$.

with

$$\begin{aligned}\Omega_2(x) &= T_+ \exp ig \int_{-\infty}^{x^+} dz^+ \tilde{\mathcal{A}}_2^-(z^+, \mathbf{x}_\perp), \\ \tilde{\mathcal{A}}_2^\gamma(x) &= -\delta^{\gamma-} \frac{1}{\nabla_\perp^2} \tilde{\rho}_2(x^+, \mathbf{x}_\perp).\end{aligned}\quad (3.28)$$

The final step is to find the gauge field in region 3, at least on the surface $\tau = 0^+$, so that one can solve the Yang-Mills equations numerically at later times. Let us make the following ansatz for the solution above the forward light-cone:

$$\mathcal{A}^i(x) = \mathcal{A}_3^i(\tau, \mathbf{x}_\perp), \quad \mathcal{A}^+(x) = x^+ \gamma(\tau, \mathbf{x}_\perp), \quad \mathcal{A}^-(x) = -x^- \gamma(\tau, \mathbf{x}_\perp). \quad (3.29)$$

This ansatz automatically obeys $x^+ \mathcal{A}^- + x^- \mathcal{A}^+ = 0$, and $\gamma(x)$ is an unknown function that we must determine from the Yang-Mills equation. Moreover, we have used the boost invariance of the problem in the longitudinal direction, which implies that the function $\gamma(x)$ cannot depend on the rapidity $\eta \equiv \ln(x^+/x^-)/2$ (the prefactors x^\pm in \mathcal{A}^\pm ensure that \mathcal{A}^μ transforms like a 4-vector under longitudinal boosts). Similarly, the transverse components \mathcal{A}^i of the gauge field cannot depend on η . Therefore, the gauge field takes the following form over the entire space-time,

$$\begin{aligned}\mathcal{A}^+(x) &= \theta(x^+) \theta(x^-) x^+ \gamma(\tau, \mathbf{x}_\perp), \\ \mathcal{A}^-(x) &= -\theta(x^+) \theta(x^-) x^- \gamma(\tau, \mathbf{x}_\perp), \\ \mathcal{A}^i(x) &= \theta(-x^+) \theta(-x^-) \mathcal{A}_1^i(x) + \theta(x^+) \theta(-x^-) \mathcal{A}_2^i(x) \\ &\quad + \theta(x^+) \theta(x^-) \mathcal{A}_3^i(\tau, \mathbf{x}_\perp).\end{aligned}\quad (3.30)$$

Consider now the equation $[\mathcal{D}_\mu, \mathcal{F}^{\mu i}] = 0$. The left hand side of this equation can potentially contain a singularity $\delta(x^+) \delta(x^-)$, while the right hand side is zero. This singularity disappears provided that we have

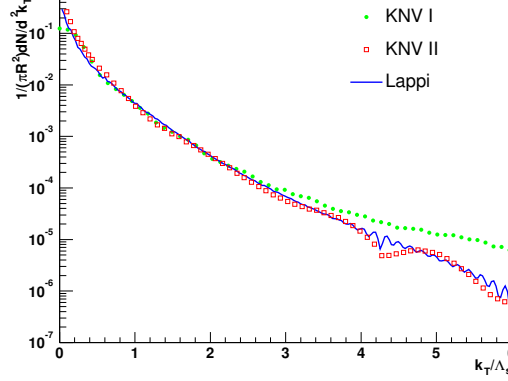
$$\mathcal{A}_3^i(\tau = 0^+, \mathbf{x}_\perp) = \mathcal{A}_1^i(x) + \mathcal{A}_2^i(x). \quad (3.31)$$

This is the initial condition for \mathcal{A}_3^i in the forward light-cone. Similarly, by matching the $\delta(x^\pm)$ singularities in the left and right hand sides of the equation $[\mathcal{D}_\mu, \mathcal{F}^{\mu\pm}] = J^\pm$, one obtains the following conditions for the initial value of the function γ :

$$\begin{aligned}\gamma(\tau = 0^+, \mathbf{x}_\perp) &= \frac{ig}{2} [\mathcal{A}_1^i(x), \mathcal{A}_2^i(x)], \\ \partial_\tau \gamma(\tau = 0^+, \mathbf{x}_\perp) &= 0.\end{aligned}\quad (3.32)$$

Note that in eqs. (3.31) and (3.32), the fields $\mathcal{A}_{1,2}^i(x)$ depend only on the transverse coordinate \mathbf{x}_\perp . Indeed, since the sources ρ_1 and ρ_2 are proportional to delta functions in x^- and x^+ respectively, the fields \mathcal{A}_1^i and \mathcal{A}_2^i are proportional to theta functions $\theta(x^-)$ and $\theta(x^+)$ respectively. Therefore, when evaluated just above the forward light-cone, these theta functions are equal to one, and the fields depend only on \mathbf{x}_\perp .

Figure 3.2: Single gluon spectrum at Leading Order (the MV model is assumed for the distribution of color sources $\rho_{1,2}$). From [25].



3.1.4 Phenomenological implications

The equations (3.31) and (3.32) completely determine the evolution of the gauge field in the Fock-Schwinger gauge at $\tau > 0$. However, no analytic solution is known at the moment, and this evolution has to be computed numerically.

In numerical evaluations of the gluon yield, one does a Monte-Carlo sampling of the distributions⁴ of color sources $\rho_{1,2}$ (or equivalently distributions for the Wilson lines $\Omega_{1,2}$). Then, for each configuration $\rho_{1,2}$ of the sources, one evaluates the fields \mathcal{A}^i and γ at $\tau = 0^+$, thanks to eqs. (3.31) and (3.32). The next (and most time consuming) step is to solve the Yang-Mills equations numerically in the forward light-cone, until one reaches a time of the order of a few times Q_s^{-1} . The final step is to perform the Fourier decomposition of the gauge field at this late time, in order to obtain the gluon spectrum with eq. (3.9).

Such computations have been performed in [20–26, 111–113], in which various quantities relevant to heavy ion collisions have been calculated, such as the gluon multiplicity discussed above or the transverse energy released in the collision (see also [93] for a review). In these calculations, these two quantities are usually parameterized as

$$\begin{aligned} \frac{dN}{d\eta} &= f_N \frac{(g^2\mu)^2 S_\perp}{g^2} \\ \frac{d\text{perp}}{d\eta} &= f_E \frac{(g^2\mu)^2 S_\perp}{g^2}, \end{aligned} \quad (3.33)$$

where $f_N \approx 0.25$ and $f_E \approx 0.3$ are non-perturbative numerical prefactors determined numerically, S_\perp is the transverse area of the interacting region, and μ a parameter of the MV model that characterizes the density of color charges. μ is related to the saturation momentum Q_s , and the precise relationship between the two can be obtained by a computation of Wilson line correlators in the MV model [114]:

$$Q_s^2 \approx 0.57 g^2 \mu. \quad (3.34)$$

⁴A popular choice is to use the color source distribution of the McLerran-Venugopalan model [70–72]. It is expected to provide a good description of a large nucleus at moderately small values of $x \sim 10^{-2}$.

The best numerical estimates of the saturation momentum for average central collisions of Gold nuclei at RHIC energy is $Q_s \approx 1.2$ GeV, which corresponds to an MV parameter $g^2\mu \approx 2.1$ GeV. Using this value in eq. (3.33), one gets the estimate

$$\frac{dN}{d\eta} \approx 1100 \quad (3.35)$$

for the number of gluons released per unit rapidity in these collisions. This number is in good agreement with the measured total hadronic multiplicity.

3.2 Leading logarithms in the single gluon spectrum

3.2.1 Introduction

Although it leads to a reasonable phenomenology, the calculation of the gluon spectrum at leading order has some important shortcomings. Its main limitation is that it gives a spectrum which is rapidity independent. A non trivial rapidity dependence arises only from higher order corrections. As we shall see in this section, there is a special subset of these higher order corrections –called the leading logarithmic corrections– that can be resummed simply by letting the distributions for the sources $\rho_{1,2}$ evolve with rapidity according to the JIMWLK⁵ equation.

In other words, all these logarithms of the collision energy can be assigned to one of the projectiles, and can be hidden into a redefinition of the distributions $W[\rho_{1,2}]$. This renormalization of the distributions $W[\rho_{1,2}]$ turns them into rapidity dependent objects. Moreover, it will become apparent in the next sections that these logarithms are in fact universal: the same evolved distributions also resum the leading logarithms that arise in other observables, such as the expectation value of the energy-momentum tensor, or the inclusive multi-gluon correlations.

After presenting a general argument based on causality that explains qualitatively why these logarithms are universal and can be factorized, we reproduce in the case of a gauge theory the calculation of the NLO corrections to the inclusive single gluon spectrum. The next step will be to extract the large logarithms contained in these corrections, and to show that they can be expressed in a very compact way in terms of the JIMWLK Hamiltonian. Finally, one uses the hermiticity of this Hamiltonian in order to show that its action can be shifted onto the distributions $W[\rho_{1,2}]$.

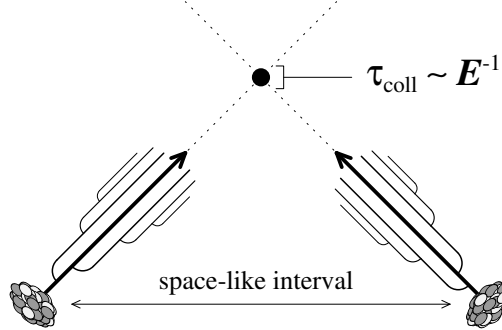
3.2.2 Causality argument

Before going into the technical details of the factorization of the leading energy logarithms, let us describe a qualitative argument that explains the relationship between factorization and causality, illustrated in the figure 3.3.

- i. First, the duration of a collision between two projectiles at the energy E decreases with the collision energy as E^{-1} . Indeed, this is the energy scaling of the time it takes for the two projectiles to go through one another.

⁵Jalilian-Marian, Iancu, McLerran, Weigert, Leonidov and Kovner.

Figure 3.3: *Causal aspects of a high energy collision.*



- ii. Next, one should note that the logarithms of the collision energy that we want to resum are due to radiation in the initial state: one gets such a logarithm if an incoming parton radiates a secondary parton that has a much lower longitudinal momentum (the logarithm comes from the integration over the longitudinal momentum of the radiated parton).
- iii. The final point in the argument is that the two projectiles are not in causal contact before they actually collide. Therefore, anything that happens inside one of the projectiles before the collision must be independent of the second projectile, and also of the observable that is going to be measured after the collision. Therefore, all the logarithms that occur in the evolution of the projectiles before the collision must be universal, and factorizable into the distributions that describe the incoming projectiles.

Although this argument is very qualitative and hides all the technical intricacies of gauge theories, it is based on very robust principles such as causality that are valid in any sensible quantum field theory. It therefore suggests that the factorization of the initial state logarithms is a very general property of high energy collisions, regardless of the details of the theory under consideration.

Although it is very general, note however that this argument does not tell us the precise nature of the *distributions* into which one can factorize these logarithms. It only tells us that, for a given type of logarithms, these distributions must be universal. But the amount of detail with which one must describe the projectiles may depend on the nature of the observable one wishes to calculate. In particular, one expects that exclusive observables need much more detailed information about the incoming projectiles than inclusive observables. In practice, this may mean that one needs more general distributions⁶ in order to calculate exclusive observables⁷. Nevertheless, one should expect from this causality argument that the leading logarithms coming from initial state radiation in exclusive observables can also be factorized

⁶The distributions $W[p_{1,2}]$ that enter into the calculation of the inclusive gluon spectrum and other inclusive quantities can be interpreted as probability distributions, i.e. as the diagonal elements of the density matrices that describe the projectiles. It is reasonable to expect that more complicated observables require to know the non diagonal elements of these density matrices as well (see [115] for a work that hints at this possibility).

⁷Of course, one could also calculate inclusive observables with these more general distributions. Any information they contain that is not necessary in order to calculate an inclusive observable could easily be *integrated out* (since the observable under study does not depend on it), reducing these distributions to simpler distributions that contain only the amount of details necessary to compute these inclusive observables.

into these more general distributions – although a complete theory of exclusive processes is still missing in the Color Glass Condensate framework.

3.2.3 NLO corrections to the gluon spectrum

Let us now turn to a rigorous proof of the factorizability of the leading logarithms of the collision energy, in the case of the single inclusive gluon spectrum. The starting point is the gluon spectrum at leading order, whose calculation has been detailed in the first section of this chapter.

Before studying the Next to Leading Order corrections, it is important to remember that there are cutoffs Λ^\pm that separate the fast and the slow partons: the gluon modes $k^+ > \Lambda^+$ are described by the sources ρ_1 , those with $k^- > \Lambda^-$ by the sources ρ_2 , and the rest is contained in the gauge field A^μ . Although these cutoffs do not show up explicitly at leading order, they become crucial at NLO. Indeed, one should use these cutoffs in loop integrations, in order to avoid double counting of the modes already included in the sources $\rho_{1,2}$. In practice, we shall integrate out the field modes in a small layer just below the cutoff, $\Lambda'^\pm < k^\pm < \Lambda^\pm$, and in the next subsection we will show that the corresponding logarithmic contribution can be absorbed into a redefinition of the distributions of the sources.

The calculation of the NLO corrections to the gluon spectrum is very similar to what we have presented in the section 2.6 for scalar fields. In particular, the final result in eq. (2.112) is formally identical in the case of gluon production, provided the definition of the operator \mathbb{T}_u is slightly modified. Therefore, we are not going to reproduce here all the derivation, but we limit ourselves to a discussion of the differences.

First of all, eq. (2.88) should be generalized to the case of gluons into

$$\left. \frac{dN_1}{d^3\mathbf{p}} \right|_{\text{NLO}} = \frac{1}{(2\pi)^3 2p} \sum_{\lambda, \alpha} \int d^4x d^4y e^{ip \cdot (x-y)} \square_x \square_y \epsilon_\lambda^\mu(\mathbf{p}) \epsilon_\lambda^{\nu*}(\mathbf{p}) \times \left[\mathcal{A}_{\mu\alpha}(x) \beta_{\nu\alpha}(y) + \beta_{\mu\alpha}(x) \mathcal{A}_{\nu\alpha}(y) + \mathcal{G}_{\mu\alpha\nu\alpha}^{+-}(x, y) \right]. \quad (3.36)$$

$\beta_{\mu\alpha}(x)$ is a 1-loop correction to the classical field $\mathcal{A}_{\mu\alpha}(x)$. Here, we have used the experience gained in the section 2.6 in order to anticipate the fact that we need not distinguish the + and – Schwinger-Keldysh indices attached to the end-point for this quantity. $\mathcal{G}_{\mu\alpha\nu\alpha}^{+-}(x, y)$ is the +- component of the Schwinger-Keldysh propagator at tree level, in which the color indices at the end-points are identical. Note that the objects $\beta_{\mu\alpha}$ and $\mathcal{G}_{\mu\alpha\nu\alpha}^{+-}$ must be determined in the same gauge as the one used to compute the gluon spectrum at leading order, i.e. in the Fock-Schwinger gauge.

The next step is to express these quantities in terms of a basis of small fluctuations that propagate over the classical field \mathcal{A}_μ . In order to do this, it is convenient to chose small fluctuations that obey simple retarded boundary conditions:

$$\left[\square_x g^{\mu\nu} - \partial_x^\mu \partial_x^\nu - \frac{\partial^2 \mathcal{U}(\mathcal{A})}{\partial \mathcal{A}_\mu(x) \partial \mathcal{A}_\nu(x)} \right] a_{\pm k \lambda \alpha}^\nu(x) = 0, \quad \lim_{x^0 \rightarrow -\infty} a_{\pm k \lambda \alpha}^\nu(x) = \epsilon_\lambda^\nu(\mathbf{k}) T^\alpha e^{\pm i \mathbf{k} \cdot \mathbf{x}}. \quad (3.37)$$

In words, the $a_{\pm k \lambda \alpha}^\nu(x)$ are small field fluctuations that have a definite momentum \mathbf{k} , color α and polarization λ in the remote past. Each of them can have a positive or negative energy

when $x^0 \rightarrow -\infty$. In the equation of motion for these fluctuations, $U(\mathcal{A})$ is the interaction potential of the Yang-Mills theory – it contains all the terms of the potential that have a degree of three or higher in the gauge field (note that the color indices have not been written in this equation of motion – only the color label of the initial condition has been written explicitly).

Then, it is possible to mimic the definition of the operator $\mathbb{T}_{\mathbf{u}}$ in order to write, for any small fluctuation $a^\mu(x)$,

$$a^{\mu a}(x) = \int_{\Sigma} d^3 \mathbf{S}_{\mathbf{u}} [\mathbf{a} \cdot \mathbb{T}_{\mathbf{u}}] \mathcal{A}^{\mu a}(x). \quad (3.38)$$

In this identity, Σ is some locally space-like surface in \mathbb{R}^4 and $\mathbb{T}_{\mathbf{u}}$ is defined as the generator for shifts of the initial conditions on the surface Σ . More precisely, if $\mathcal{B}^\mu[\mathcal{A}]$ is the boundary term in the Green's formula that expresses the classical field $\mathcal{A}^\mu(x)$ in terms of its initial condition on the surface Σ , then

$$\mathcal{B}^\mu[\mathbf{a}] = \int_{\Sigma} d^3 \mathbf{S}_{\mathbf{u}} [\mathbf{a} \cdot \mathbb{T}_{\mathbf{u}}] \mathcal{B}^\mu[\mathcal{A}]. \quad (3.39)$$

This definition is identical to the case of a scalar field theory. However, the details are a bit more involved. First, in a gauge theory, it is crucial that the classical field \mathcal{A}^μ and the small fluctuation a^μ be expressed in the same gauge. Moreover, the precise form of the operator $\mathbb{T}_{\mathbf{u}}$ should be derived from the boundary term in the Green's formula, that depends on the gauge condition and on the surface Σ . This study is carried out in detail in the case of the light-cone gauge $\mathcal{A}^+ = 0$ in the appendix D.

At this point, it is immediate to reproduce the derivation of eqs. (2.101) and (2.111), in order to obtain

$$\begin{aligned} \mathcal{G}_{\mu a \nu a}^{+-}(x, y) &= \frac{1}{2} \sum_{\lambda, b} \int \frac{d^3 \mathbf{k}}{(2\pi)^3 2k} \int_{\Sigma} d^3 \mathbf{S}_{\mathbf{u}} d^3 \mathbf{S}_{\mathbf{v}} \\ &\quad \times \left\{ \left[[\mathbf{a}_{-\mathbf{k}\lambda b} \cdot \mathbb{T}_{\mathbf{u}}] \mathcal{A}_{\mu a}(x) \right] \left[[\mathbf{a}_{+\mathbf{k}\lambda b} \cdot \mathbb{T}_{\mathbf{v}}] \mathcal{A}_{\nu a}(y) \right] \right. \\ &\quad \left. + \left[[\mathbf{a}_{+\mathbf{k}\lambda b} \cdot \mathbb{T}_{\mathbf{v}}] \mathcal{A}_{\mu a}(x) \right] \left[[\mathbf{a}_{-\mathbf{k}\lambda b} \cdot \mathbb{T}_{\mathbf{u}}] \mathcal{A}_{\nu a}(y) \right] \right\} \end{aligned} \quad (3.40)$$

and

$$\begin{aligned} \beta_{\mu a}(x) &= \left[\frac{1}{2} \sum_{\lambda, b} \int \frac{d^3 \mathbf{k}}{(2\pi)^3 2k} \int_{\Sigma} d^3 \mathbf{S}_{\mathbf{u}} d^3 \mathbf{S}_{\mathbf{v}} [\mathbf{a}_{-\mathbf{k}\lambda b} \cdot \mathbb{T}_{\mathbf{u}}] [\mathbf{a}_{+\mathbf{k}\lambda b} \cdot \mathbb{T}_{\mathbf{v}}] \right. \\ &\quad \left. + \int_{\Sigma} d^3 \mathbf{S}_{\mathbf{u}} [\boldsymbol{\beta} \cdot \mathbb{T}_{\mathbf{u}}] \right] \mathcal{A}_{\mu a}(x). \end{aligned} \quad (3.41)$$

From these two identities, one obtains for the gluon spectrum at NLO a formula which is formally identical to eq. (2.112),

$$\begin{aligned} \frac{dN_1}{d^3 \mathbf{p}} \Big|_{\text{NLO}} &= \left[\frac{1}{2} \sum_{\lambda, a} \int \frac{d^3 \mathbf{k}}{(2\pi)^3 2k} \int_{\Sigma} d^3 \mathbf{S}_{\mathbf{u}} d^3 \mathbf{S}_{\mathbf{v}} [\mathbf{a}_{-\mathbf{k}\lambda a} \cdot \mathbb{T}_{\mathbf{u}}] [\mathbf{a}_{+\mathbf{k}\lambda a} \cdot \mathbb{T}_{\mathbf{v}}] \right. \\ &\quad \left. + \int_{\Sigma} d^3 \mathbf{S}_{\mathbf{u}} [\boldsymbol{\beta} \cdot \mathbb{T}_{\mathbf{u}}] \right] \frac{dN_1}{d^3 \mathbf{p}} \Big|_{\text{LO}}. \end{aligned} \quad (3.42)$$

All the differences that exist between scalar field theory and Yang-Mills theory are hidden in the shift operator $\mathbb{T}_{\mathbf{u}}$, and in the form of the fluctuations $\alpha_{\pm\mathbf{k}\lambda\alpha}^{\nu}$ and β^{ν} on the initial surface Σ . To a large extent, this formula relies only on the fact that the inclusive gluon spectrum is expressible in terms of fields and field fluctuations with retarded boundary conditions, and on the causal structure of these retarded objects. For this reason, it is also valid in any gauge. In particular, although we have emphasized the Fock-Schwinger gauge in the previous section –because it is the gauge employed in numerical solutions of the Yang-Mills equations inside the forward light-cone–, eq. (3.42) is not restricted to this particular gauge (in fact, no explicit mention of the gauge choice needs to be made in its derivation). The detailed form of the operator $\mathbb{T}_{\mathbf{u}}$, as well as the fluctuations $\alpha_{\pm\mathbf{k}\lambda\alpha}^{\mu}$ and β^{μ} , depend on the gauge condition – but all these details are transparent at the level of eq. (3.42). Naturally, for this formula to make sense, the quantity $dN_1/d^3\mathbf{p}|_{\text{lo}}$ in the right hand side must be a functional of the gauge fields on Σ in the same gauge.

3.2.4 Choice of the gauge and initial surface

Two loop integrations are contained in eq. (3.42). One appears explicitly in the term that contains two operators $\mathbb{T}_{\mathbf{u},\mathbf{v}}$. The second momentum integral is hidden in the value of the fluctuation β^{μ} on the surface Σ . As we shall see now, these integrals are logarithmically divergent, when either k^+ or k^- go to infinity. Fortunately, since we are working in the CGC effective theory, we should not integrate over field modes that have an arbitrarily high longitudinal momentum, because these modes are already included in the sources $\rho_{1,2}$. Therefore, the above mentioned integrals are finite, but display an unphysical logarithmic sensitivity to the cutoff scales Λ^{\pm} . Our task in this subsection is to calculate these logarithms, and to show that they can be resummed via a renormalization of the distributions $W[\rho_{1,2}]$ for the hard sources.

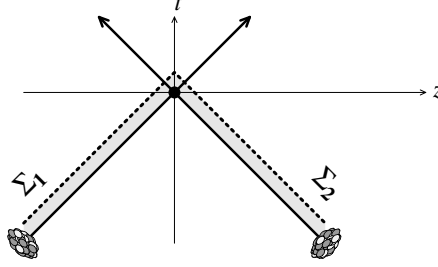
In order to calculate these logarithms explicitly, we need expressions for the fluctuations $\alpha_{\pm\lambda\alpha}^{\mu}$ and β^{μ} on the surface Σ . This is where the choice of Σ becomes important. Let us recall that eq. (3.42) is valid for any locally space-like surface Σ . Thus, we are free to choose it in a way that simplifies the calculations and exhibits the physics we are interested in. Since computations inside the forward light-cone are not feasible analytically, we should choose a surface Σ contained entirely below the forward light-cone, i.e. a surface located *before* the collision of the two projectiles. However, since we are interested in the evolution inside the incoming projectiles, the surface should be located above the backward light-cone. It turns out that the simplest choice is a surface Σ that runs just above the backward light-cone, as illustrated in figure 3.4. The two half planes Σ_1 and Σ_2 that constitute this surface are defined by the equations:

$$\begin{aligned} (\Sigma_1) \quad & x^- = \epsilon, \quad x^+ \leq \epsilon, \\ (\Sigma_2) \quad & x^+ = \epsilon, \quad x^- \leq \epsilon. \end{aligned} \tag{3.43}$$

The value of the small parameter ϵ should be such that the color sources are located below the surface Σ . It may seem that this choice of Σ somewhat disobeys our requirement that Σ be entirely below the forward light-cone. However, the tip of the wedge (the part of Σ located above the forward light-cone) is too small to produce any logarithmic contribution.

Although all the numerical studies of the Yang-Mills equations in the forward light-cone are performed in the Fock-Schwinger gauge –whose advantages are to treat the two nuclei symmetrically and to render trivial the constraint of covariant current conservation–, this

Figure 3.4: Choice of the surface Σ in eq. (3.42).



gauge condition is not well suited to the present problem. This is readily seen by calculating the free propagator in this gauge[116, 117], which is made very complicated by the explicit space-time dependence of the gauge condition. Fortunately, as explained after eq. (3.42), the relationship that exists between the gluon spectrum at LO and at NLO is valid in any gauge.

Since the JIMWLK equation has been originally derived in light-cone gauge, it is convenient for us to also use this gauge, since this will facilitate the interpretation of our results. There is however a complication in our case: since there are two projectiles, there are also two different light-cone gauges one may chose. In order not to break the symmetry of the problem, one can use the fact that the two branches of the surface Σ are not causally connected, and use different light-cone gauges on each branch. We thus make the following gauge choices:

$$\begin{aligned} (\Sigma_1) \quad & A^+ = 0, \\ (\Sigma_2) \quad & A^- = 0. \end{aligned} \tag{3.44}$$

This means that, depending on whether they are evaluated on the branch Σ_1 or Σ_2 of the surface Σ , the fluctuations $\alpha_{\pm\lambda\alpha}^\mu$ and β^μ must be obtained either in the $A^+ = 0$ or in the $A^- = 0$ light-cone gauge.

According to the appendix D, when the initial surface is defined by $x^- = \epsilon$ and the gauge condition is $A^+ = 0$, the operator \mathbb{T}_u is given by:

$$\begin{aligned} \alpha \cdot \mathbb{T}_u = & \partial^- (\Omega_{1ab}(u) a^{ib}(u)) \frac{\delta}{\delta(\partial^- \mathcal{A}_\Omega^{ia}(u))} \\ & + \Omega_{1ab}(u) a^{-b}(u) \frac{\delta}{\delta(\mathcal{A}_\Omega^{-a}(u))} \\ & + \partial_\mu (\Omega_{1ab}(u) a^{\mu b}(u)) \frac{\delta}{\delta(\partial_\nu \mathcal{A}_\Omega^{\nu a}(u))}, \end{aligned} \tag{3.45}$$

where Ω_1 is the Wilson line that we have already encountered in eq. (3.24). The field \mathcal{A}_Ω^μ that appears in the functional derivatives is obtained by a residual gauge transformation of the field \mathcal{A}^μ ,

$$\mathcal{A}_\Omega^\mu \equiv \Omega_1 \left(\mathcal{A}^\mu + \frac{i}{g} \partial^\mu \right) \Omega_1^\dagger, \tag{3.46}$$

which has the virtue of eliminating the pure gauge field above the boundary Σ while preserving $\mathcal{A}_\Omega^\pm = 0$. (The same transformation must be performed on the branch Σ_2 , that involves instead the Wilson line Ω_2 .) Thanks to this formula, we see that for each fluctuation $\alpha \in \{\beta, \alpha_{\pm k\lambda\alpha}\}$, we need to calculate the following quantities on the branch Σ_1 :

$$\partial^-(\Omega_{1ab}(u)\alpha^{ib}(u)), \quad \Omega_{1ab}(u)\alpha^{-b}(u), \quad \partial_\mu(\Omega_{1ab}(u)\alpha^{\mu b}(u)). \quad (3.47)$$

As we shall see shortly, only the third of these quantities is necessary in the calculation of the logarithmic divergences.

3.2.5 Field fluctuations on the initial surface

Let us now calculate the quantities listed in eq. (3.47) on the branch Σ_1 , in the case of the fluctuations $\alpha_{\pm k\lambda\alpha}^\mu(x)$. In the remote past, they start as plane waves:

$$\lim_{x^0 \rightarrow -\infty} \alpha_{\pm k\lambda\alpha}^\mu(x) = \epsilon_\lambda^\mu(k) T^a e^{\pm i k \cdot x}, \quad (3.48)$$

and they propagate unmodified in the region 0 (see the figure 3.1), since the classical background field is zero in this region. When crossing the light-cone in order to reach the branch Σ_1 of the surface Σ , we face a difficulty since the $-$ component of the incoming fluctuation induces a correction to the J^+ current that lives on the light-cone, because of covariant current conservation. However, this is easily circumvented by going temporarily into a gauge where the $-$ component of the fluctuation is zero [1]. In this gauge, where we denote the fields and field fluctuations with a tilde, the modification of the fluctuation when crossing the region $0 \leq x^- \leq \epsilon$ is calculated in the appendix C. But before, let us write explicitly the gauge transformation that relates the two gauges:

$$\mathcal{A}^\mu + \alpha^\mu = \Omega^\dagger (\tilde{\mathcal{A}}^\mu + \tilde{\alpha}^\mu) \Omega + \frac{i}{g} \Omega^\dagger \partial^\mu \Omega. \quad (3.49)$$

Note that we already know the gauge transformation that relates the classical fields \mathcal{A}^μ and $\tilde{\mathcal{A}}^\mu$ in these two gauges, since it is precisely the transformation of eq. (3.22) with the Ω_1 given in eq. (3.24). Since the fluctuation we are adding on top of the classical field is a small perturbation, we can write the transformation Ω of eq. (3.49) as a small correction to Ω_1 :

$$\Omega \equiv (1 + i g \omega) \Omega_1, \quad (3.50)$$

where ω is an $SU(3)$ element with components of order one. Subtracting from eq. (3.49) the gauge transformation of the classical part of the gauge field, and keeping only terms of relative order g , we find the following gauge transformation for the fluctuations:

$$\alpha^\mu = \Omega_1^\dagger (\tilde{\alpha}^\mu - i g [\omega, \tilde{\mathcal{A}}^\mu] - \partial^\mu \omega) \Omega_1. \quad (3.51)$$

In order to determine ω , we need to request that $\alpha^+ = 0$, which leads to

$$\partial^+ \omega + i g [\omega, \tilde{\mathcal{A}}^+] = \tilde{\alpha}^+, \quad (3.52)$$

the solution of which can be written as

$$\omega(x) = \Omega_1(x^-, \mathbf{x}_\perp) f(x^+, \mathbf{x}_\perp) + \int_{-\infty}^{x^-} dz^- \bar{\Omega}_1(x^-, z^-, \mathbf{x}_\perp) \tilde{\alpha}^+(x^+, z^-, \mathbf{x}_\perp). \quad (3.53)$$

In this equation, $f(x^+, x_\perp)$ can be any function independent of x^- , and $\overline{\Omega}_1(x^-, z^-, x_\perp)$ is a Wilson line along the $-$ direction, where one integrates only between z^- and x^- :

$$\overline{\Omega}_1(x^-, z^-, x_\perp) \equiv T_- \exp \left[ig \int_{z^-}^{x^-} dy^- \tilde{\mathcal{A}}^+(y^-, x_\perp) \right]. \quad (3.54)$$

The arbitrariness in the choice of the function f means that there is a residual gauge freedom after one has enforced the gauge condition $a^+ = 0$.

A crucial point in the derivation is how this residual gauge freedom is fixed. In our calculation of the NLO corrections, the small field fluctuations entered in the formula (2.96) for the propagator \mathcal{G}_{+-} . This way of writing this propagator is valid only if the initial value of the fluctuations $a_{\pm k\lambda a}$ are plane waves with on-shell momenta, as one can easily check on the corresponding free propagator. Thus, eq. (3.53) must lead to a plane wave for the fluctuation in light-cone gauge if $x^- < 0$. The simplest way to achieve this is to take a plane wave for the fluctuation \tilde{a}^μ in the original gauge and to set the function f to zero⁸. Therefore, the requirement that eq. (2.96) be valid leaves no room for a residual gauge freedom.

We only need to know ω on the branch Σ_1 of the surface Σ , i.e. at $x^- = \epsilon$. Because the components of Ω_1 and of \tilde{a}^μ are of order one, it is legitimate to neglect the values of z^- in the range between 0 and ϵ in the integration in eq. (3.53). Moreover, for $z^- < 0$ and $x^- = \epsilon$, the incomplete Wilson line $\overline{\Omega}_1$ is equal to the complete one Ω_1 . Thus we can factor it out of the integration,

$$\omega(x^+, x^- = \epsilon, x_\perp) = \Omega_1(\epsilon, x_\perp) \int_{-\infty}^0 dz^- \tilde{a}^+(x^+, z^-, x_\perp). \quad (3.55)$$

Once ω has been determined, the $-$ and i components of the fluctuation in light-cone gauge are given by

$$\begin{aligned} a^- &= \Omega_1^\dagger (-\partial^- \omega) \Omega_1, \\ a^i &= \Omega_1^\dagger (\tilde{a}^i - \partial^i \omega) \Omega_1. \end{aligned} \quad (3.56)$$

As we will see later, the logarithmic divergences we are interested in come from the integration over the longitudinal momentum k^+ , when $k^+ \rightarrow +\infty$. However, the first two quantities listed in eq. (3.47) carry a $-$ index, which implies that they scale like $k^- \sim k_\perp^2/k^+ \rightarrow 0$ in this limit. This is the reason why they do not contribute to the divergence. Let us therefore focus on the third combination⁹

$$\begin{aligned} \partial_\mu (\Omega_1 a^\mu \Omega_1^\dagger) &= \partial_\mu (\tilde{a}^\mu - ig[\omega, \tilde{\mathcal{A}}^\mu] - \partial^\mu \omega) \\ &= -\partial^+ \partial^- \omega - \partial^i (\tilde{a}^i - \partial^i \omega). \end{aligned} \quad (3.57)$$

(In the second line, we have used eq. (3.52) as well as $\tilde{a}^- = 0$.) Using again eq. (3.52) to replace $\partial^+ \omega$, and the fact that $\tilde{\mathcal{A}}^+ = 0$ at $x^- = \epsilon$, we get

$$\partial_\mu (\Omega_1 a^\mu \Omega_1^\dagger) = \nabla_\perp^2 \omega - \partial^- \tilde{a}^+ - \partial^i \tilde{a}^i. \quad (3.58)$$

⁸This choice is still not unique. There are other combinations of choices for the initial value of \tilde{a}^μ and for the function f that also give a plane wave for a^μ . But our choice is the most natural.

⁹Here, we use the relation $(\Omega_1 a \Omega_1^\dagger)_c = \Omega_{1cb} a^b$ in order to adopt a matricial notation. The validity of this identity follows from the definition of the adjoint representation. In the left hand side of the identity, a is the SU(3) matrix $a \equiv a^b T^b$. This matricial notation is more convenient here given eqs. (3.56) for the fluctuations.

Let us now consider specifically the fluctuations $\alpha_{\pm k\lambda a}$. In the gauge $\tilde{a}^- = 0$, their expression below the light cone (i.e. for $x^- < 0$) reads

$$\tilde{a}_{\pm k\lambda a}^\mu(x) = \tilde{\epsilon}_\lambda^\mu(\mathbf{k}) T^a e^{\pm i\mathbf{k}\cdot\mathbf{x}}, \quad (3.59)$$

with the following polarization vectors:

$$\begin{aligned} \tilde{\epsilon}_\lambda^-(\mathbf{k}) &= 0, \\ \sum_{\lambda=1,2} \tilde{\epsilon}_\lambda^i(\mathbf{k}) \tilde{\epsilon}_\lambda^j(\mathbf{k}) &= \delta^{ij}, \\ \tilde{\epsilon}_\lambda^+(\mathbf{k}) &= \frac{\mathbf{k}_\perp \cdot \tilde{\epsilon}_{\lambda\perp}(\mathbf{k})}{k^-}. \end{aligned} \quad (3.60)$$

The formulas that govern the light-cone crossing in this gauge [1] are derived in the appendix C. Using this result, one obtains the following expressions¹⁰ for these fluctuations just above the light-cone, at $x^- = \epsilon$:

$$\begin{aligned} \tilde{a}_{\pm k\lambda a}^{+b}(x) &= \left[\Omega_{1ba}(\epsilon, \mathbf{x}_\perp) \tilde{\epsilon}_\lambda^+(\mathbf{k}) \pm (\partial^i \Omega_{1ba}(\epsilon, \mathbf{x}_\perp)) \frac{1}{ik^-} \tilde{\epsilon}_\lambda^i(\mathbf{k}) \right] e^{\pm i\mathbf{k}\cdot\mathbf{x}}, \\ \tilde{a}_{\pm k\lambda a}^{ib}(x) &= \Omega_{1ba}(\epsilon, \mathbf{x}_\perp) \tilde{\epsilon}_\lambda^i(\mathbf{k}) e^{\pm i\mathbf{k}\cdot\mathbf{x}}. \end{aligned} \quad (3.61)$$

Note that for these fluctuations, one has

$$\partial^- \tilde{a}_{\pm k\lambda a}^+ = \partial^i \tilde{a}_{\pm k\lambda a}^i. \quad (3.62)$$

(It is in fact a general property of the $\tilde{a}^- = 0$ gauge that $\partial^+(\partial_\mu \tilde{a}^\mu) = 0$.) Therefore, we have

$$\partial_\mu (\Omega_1 a_{\pm k\lambda a}^\mu \Omega_1^\dagger) = \partial^i (\partial^i \omega - 2\tilde{a}_{\pm k\lambda a}^i). \quad (3.63)$$

Substituting eq. (3.60) into eq. (3.55), one gets the value of ω on the hyperplane $x^- = \epsilon$,

$$\omega_b(x^+, \epsilon, \mathbf{x}_\perp) = \mp 2i \Omega_{1ba}(\epsilon, \mathbf{x}_\perp) \frac{k^j}{k_\perp^2} \tilde{\epsilon}_\lambda^j(\mathbf{k}) e^{\pm i\mathbf{k}\cdot\mathbf{x}}. \quad (3.64)$$

Therefore,

$$\partial_\mu (\Omega_{1bc} a_{\pm k\lambda a}^{\mu c} \Omega_1^\dagger) = \partial_\mu (\Omega_1 a_{\pm k\lambda a}^\mu \Omega_1^\dagger)_b = -2\partial^i \left[e^{\pm i\mathbf{k}\cdot\mathbf{x}} \alpha_{\pm k a}^{ib} \tilde{\epsilon}_\lambda^i(\mathbf{k}) \right], \quad (3.65)$$

where we denote

$$\alpha_{\pm k a}^{ib} \equiv \left(\delta^{il} - \frac{k^i k^l}{k_\perp^2} \right) \Omega_{1ba}(\epsilon, \mathbf{x}_\perp) \pm i \frac{k^l}{k_\perp^2} \partial^i \Omega_{1ba}(\epsilon, \mathbf{x}_\perp). \quad (3.66)$$

¹⁰In the notation $\tilde{a}_{\pm k\lambda a}^{\mu b}(x)$, the color index a is the initial color of the fluctuation (i.e. when $x^0 \rightarrow -\infty$), while b is its color index at the point x .

3.2.6 Origin of the logarithmic divergences

In eq. (3.42), let us consider first the term which is bilinear in the operator \mathbb{T}_u (*real correction*). As we will see later, the term in $\beta \cdot \mathbb{T}_u$ (*virtual correction*) can be derived easily from it. For a fixed momentum \mathbf{k} , this term is in fact finite, and the divergences arise from the integration over this on-shell momentum. More precisely, the dangerous integral is the k^+ integral. Indeed, the momentum k^μ being on-shell, one has an integral

$$\int_0^{+\infty} \frac{dk^+}{k^+}, \quad (3.67)$$

which can potentially diverge at both ends. Note that wherever k^- appears in the integrand, it should be replaced by its on-shell value,

$$k^- = \frac{\mathbf{k}_\perp^2}{2k^+}. \quad (3.68)$$

By inspecting the integrand in eq. (3.42), we see that it contains the following exponential factor

$$\exp\left(i \frac{\mathbf{k}_\perp^2 (v^+ - u^+)}{2k^+}\right). \quad (3.69)$$

Among the exponential factors, this is the only one that depends on k^+ . Indeed, the term in $k^+(v^- - u^-)$ does not appear thanks to our choice of the surface Σ , since on its branch Σ_1 we have $u^- = v^- = \epsilon$. Moreover, given the structure of the previous exponential, it is clear that the integral is convergent at the limit $k^+ \rightarrow 0$, since the fast oscillations of the exponential cancel out any potential logarithmic divergence. However, no such cancellation happens at the other end, since the exponential goes to 1. Whether one gets a divergence or not depends on the other k^+ -dependent factors in the integrand: in order to get a divergence, these factors should not go to zero when $k^+ \rightarrow +\infty$.

It is straightforward to see that the combinations $\Omega_1 \alpha^-$ and $\partial^-(\Omega_1 \alpha^i)$ contain an extra power of k^- , i.e. of $1/k^+$. If any of these terms is kept in the k^+ integral in eq. (3.42), one gets a finite result. Thus, as previously announced, the only divergence arises when we have the term in $\partial_\mu(\Omega_1 \alpha^\mu)$ in front of both \mathbb{T} 's.

Naturally, in the Color Glass Condensate effective theory, the k^+ integral is not really divergent, since there is an upper cutoff Λ^+ that separates the modes that are described as color sources ($k^+ > \Lambda^+$) from those that are described as color fields ($k^+ < \Lambda^+$). Moreover, in view of the forthcoming discussion of the CGC renormalization group, it will be useful to consider only a small slice of field modes, located just below the cutoff,

$$\Lambda'^+ < k^+ < \Lambda^+. \quad (3.70)$$

We will show that the leading contribution coming from this slice of field modes can be absorbed into a redefinition of the color sources, thus leading to a new CGC effective theory with a lower cutoff and a renormalized distribution of sources.

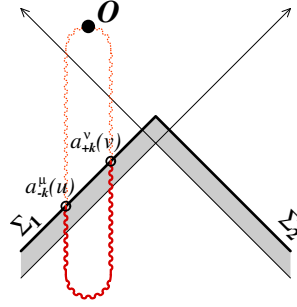
3.2.7 Real corrections

The relevant part of the bilinear term in eq. (3.42) is

$$\begin{aligned} & \frac{1}{8\pi} \ln \left(\frac{\Lambda^+}{\Lambda'^+} \right) \int \frac{d^2 \mathbf{k}_\perp}{(2\pi)^2} \int d^2 \mathbf{u}_\perp d^2 \mathbf{v}_\perp \\ & \times \sum_{\lambda, \alpha} \partial_\mu^u \left(\Omega_{1bd}(\epsilon, \mathbf{u}_\perp) a_{+k\lambda\alpha}^{\mu d}(u) \right) \partial_\nu^v \left(\Omega_{1ce}(\epsilon, \mathbf{v}_\perp) a_{-k\lambda\alpha}^{\mu e}(v) \right) \\ & \times \int_{-\infty}^{\epsilon} du^+ dv^+ \frac{\delta}{\delta \partial_\mu \mathcal{A}_\Omega^{\mu b}(u)} \frac{\delta}{\delta \partial_\nu \mathcal{A}_\Omega^{\mu c}(v)} . \end{aligned} \quad (3.71)$$

Note that this is only the contribution one gets when the two points u and v are both on the branch Σ_1 of Σ , as illustrated in the figure 3.5. When they are both on the branch Σ_2 , it is

Figure 3.5: One-loop correction to the expectation value of an observable \mathcal{O} where the points u and v are located on the same branch of the surface Σ .



easy to guess the answer by symmetry, and when they are on different branches we will show that there is no logarithmic contribution at all.

In order to simplify the notations, let us use the shorthand $\vartheta_1(u^+, \mathbf{u}_\perp) \equiv \partial_\mu \mathcal{A}_{\Omega_1}^\mu(u)$. The quantity on which the functional derivatives with respect to ϑ_1 are acting depends on the value of the classical field (in the LC gauge) on the surface Σ . This initial classical field has no $+$ or $-$ component, and its i component does not depend on the u^+ coordinate along the branch Σ_1 of Σ . Therefore, the observable depends only on the u^+ -independent mode of ϑ_1 ,

$$\vartheta_1(\mathbf{u}_\perp) \equiv \frac{1}{L} \int_{-L+\epsilon}^{\epsilon} du^+ \vartheta_1(u^+, \mathbf{u}_\perp) , \quad (3.72)$$

where L is the length of the u^+ interval¹¹. Thus, one can replace derivatives with respect to $\vartheta_1(u^+, \mathbf{u}_\perp)$ by derivatives with respect to $\vartheta_1(\mathbf{u}_\perp)$,

$$\frac{\delta}{\delta \vartheta_1(u^+, \mathbf{u}_\perp)} F[\vartheta_1(\mathbf{u}_\perp)] = \frac{1}{L} \frac{\delta}{\delta \vartheta_1(\mathbf{u}_\perp)} F[\vartheta_1(\mathbf{u}_\perp)] . \quad (3.73)$$

Moreover, since this derivative is obviously independent of u^+ , the subsequent integration with respect to u^+ simply produces a factor L , so that we have

$$\int_{-L+\epsilon}^{\epsilon} du^+ \frac{\delta}{\delta \vartheta_1(u^+, \mathbf{u}_\perp)} F[\vartheta_1(\mathbf{u}_\perp)] = \frac{\delta}{\delta \vartheta_1(\mathbf{u}_\perp)} F[\vartheta_1(\mathbf{u}_\perp)] . \quad (3.74)$$

¹¹Since the u^+ interval is semi-infinite, it is better to consider $u^+ \in [-L + \epsilon, \epsilon]$ in all the intermediate steps, and to take $L \rightarrow +\infty$ at the end. All the L dependence disappears in this limit.

We are now free to take the limit $L \rightarrow +\infty$, since the right hand side does not depend on L .

The quantity $\vartheta_1(\mathbf{u}_\perp)$ can be expressed in terms of the gauge field $\mathcal{A}_{\Omega_1}^i$,

$$\vartheta_{1b}(\mathbf{u}_\perp) = -\partial^i \mathcal{A}_{\Omega_1}^{ib}(\epsilon, \mathbf{u}_\perp), \quad (3.75)$$

where $\mathcal{A}_{\Omega_1}^i$ is related to \mathcal{A}_1^i by eq. (3.46). Recalling the expression of \mathcal{A}_1^i in terms of the Lorenz gauge field $\tilde{\mathcal{A}}_1^+$,

$$\begin{aligned} \mathcal{A}_1^i(\epsilon, \mathbf{u}_\perp) &= \frac{i}{g} \Omega_1^\dagger(\epsilon, \mathbf{u}_\perp) \partial^i \Omega_1(\epsilon, \mathbf{u}_\perp) \\ &= -\int_{-\infty}^{\epsilon} dz^- \Omega_1^\dagger(z^-, \mathbf{u}_\perp) \left(\partial^i \tilde{\mathcal{A}}_1^+(z^-, \mathbf{u}_\perp) \right) \Omega_1(z^-, \mathbf{u}_\perp), \end{aligned} \quad (3.76)$$

it is easy to relate¹² variations of $\vartheta_1(\mathbf{u}_\perp)$ to variations of $\tilde{\mathcal{A}}_1^+(z^-, \mathbf{u}_\perp)$ in the z^- -bin neighboring the endpoint $z^- = \epsilon$:

$$\delta \vartheta_1(\mathbf{u}_\perp) = \nabla_\perp^2 dz^- \delta \tilde{\mathcal{A}}_1^+(\epsilon, \mathbf{u}_\perp). \quad (3.77)$$

In this relation, dz^- is the width of the bin of z^- in which the variation of $\tilde{\mathcal{A}}_1^+$ occurs¹³. A variation $\delta \tilde{\mathcal{A}}_1^+(\epsilon, \mathbf{u}_\perp)$ in the slice $[\epsilon - dz^-, \epsilon]$ also amounts to multiplying the Wilson line Ω_1 on the left by the factor $1 + ig dz^- \delta \tilde{\mathcal{A}}_1^+(\epsilon, \mathbf{u}_\perp)$. If we introduce the left Lie derivative¹⁴ $\nabla_{\mathbf{x}_\perp}^a$, we can thus write

$$\frac{\delta}{\delta \vartheta_1^a(\mathbf{u}_\perp)} = \int d^2 \mathbf{x}_\perp G(\mathbf{u}_\perp - \mathbf{x}_\perp) \nabla_{\mathbf{x}_\perp}^a, \quad (3.78)$$

where $G(\mathbf{u}_\perp - \mathbf{x}_\perp)$ is a Green's function of the two-dimensional Laplacian operator:

$$\nabla_\perp^2 G(\mathbf{u}_\perp - \mathbf{x}_\perp) = \delta(\mathbf{u}_\perp - \mathbf{x}_\perp). \quad (3.79)$$

(Some useful properties of this Green's function are derived in the appendix E.) We can now rewrite the operator in eq. (3.71) as

$$\frac{1}{2} \ln \left(\frac{\Lambda^+}{\Lambda'^+} \right) \int d^2 \mathbf{x}_\perp d^2 \mathbf{y}_\perp \eta^{bc}(\mathbf{x}_\perp, \mathbf{y}_\perp) \nabla_{\mathbf{x}_\perp}^b \nabla_{\mathbf{y}_\perp}^c, \quad (3.80)$$

where we have defined

$$\begin{aligned} \eta^{bc}(\mathbf{x}_\perp, \mathbf{y}_\perp) &\equiv \frac{1}{4\pi} \int \frac{d^2 \mathbf{k}_\perp}{(2\pi)^2} \int d^2 \mathbf{u}_\perp d^2 \mathbf{v}_\perp G(\mathbf{x}_\perp - \mathbf{u}_\perp) G(\mathbf{y}_\perp - \mathbf{v}_\perp) \\ &\quad \times \sum_{\lambda, \alpha} \partial_\mu^u \left(\Omega_{1bd}(\epsilon, \mathbf{u}_\perp) a_{+\mathbf{k}\lambda\alpha}^{ud}(u) \right) \partial_\nu^v \left(\Omega_{1ce}(\epsilon, \mathbf{v}_\perp) a_{-\mathbf{k}\lambda\alpha}^{ve}(v) \right). \end{aligned} \quad (3.81)$$

¹²In doing this, it is important to keep the transformation from \mathcal{A}_1^i to $\mathcal{A}_{\Omega_1}^i$ fixed. (Otherwise, one would always get $\delta \vartheta_1(\mathbf{u}_\perp) = 0$). This transformation was introduced in order to eliminate the background field \mathcal{A}_1^i above the surface Σ (by using the residual gauge freedom of the light-cone gauge), and the exact same transformation must be applied to perturbations over the background field.

¹³Indeed, since \mathcal{A}_1^i depends on the integral of $\tilde{\mathcal{A}}_1^+$ over z^- , changing $\tilde{\mathcal{A}}_1^+$ at a single point has no effect on the value of \mathcal{A}_1^i .

¹⁴This derivative is defined in such a way that

$$\nabla_{\mathbf{x}_\perp}^a \Omega(\mathbf{y}_\perp) = ig \delta(\mathbf{x}_\perp - \mathbf{y}_\perp) t^a \Omega(\mathbf{y}_\perp), \quad \nabla_{\mathbf{x}_\perp}^a \Omega^\dagger(\mathbf{y}_\perp) = -ig \delta(\mathbf{x}_\perp - \mathbf{y}_\perp) \Omega^\dagger(\mathbf{y}_\perp) t^a.$$

Thanks to eq. (3.65), this quantity can be rewritten as follows

$$\begin{aligned} \eta^{bc}(\mathbf{x}_\perp, \mathbf{y}_\perp) &\equiv \frac{1}{4\pi^3} \int \frac{d^2\mathbf{k}_\perp}{(2\pi)^2} \int d^2\mathbf{u}_\perp d^2\mathbf{v}_\perp \sum_a \alpha_{-k_a}^{ilb}(\mathbf{u}_\perp) \alpha_{+k_a}^{jlc}(\mathbf{v}_\perp) \\ &\times e^{i\mathbf{k}_\perp \cdot (\mathbf{u}_\perp - \mathbf{v}_\perp)} \frac{\mathbf{u}_\perp^i - \mathbf{x}_\perp^i}{(\mathbf{u}_\perp - \mathbf{x}_\perp)^2} \frac{\mathbf{v}_\perp^j - \mathbf{y}_\perp^j}{(\mathbf{v}_\perp - \mathbf{y}_\perp)^2}. \end{aligned} \quad (3.82)$$

In order to obtain this formula, we have integrated by parts in order to shift the action of the derivatives ∂_u^i and ∂_v^j onto the propagators $G(\mathbf{u}_\perp - \mathbf{x}_\perp)$ and $G(\mathbf{v}_\perp - \mathbf{y}_\perp)$ respectively (explicit formulas for the derivatives of the 2-dimensional propagator can be found in the appendix E). Moreover, the sum over the two physical polarization states has already been performed in this formula, using eqs. (3.60).

From the explicit formula (3.66) for the coefficients $\alpha_{\pm k_a}^{ilc}$ that appear in this expression, it is easy to express $\eta^{bc}(\mathbf{x}_\perp, \mathbf{y}_\perp)$ in terms of the Wilson line Ω_1 . Note that $\alpha_{\pm k_a}^{ilc}$ is the sum of two terms that are mutually orthogonal, since one is parallel to k^i while the other is orthogonal to k^i . We obtain a first contribution to η^{bc} by keeping only the first term of each α in eq. (3.82),

$$\begin{aligned} \eta_{\perp\perp}^{bc}(\mathbf{x}_\perp, \mathbf{y}_\perp) &= -\frac{1}{8\pi^4} \int d^2\mathbf{u}_\perp d^2\mathbf{v}_\perp \frac{\mathbf{x}_\perp^i - \mathbf{u}_\perp^i}{(\mathbf{x}_\perp - \mathbf{u}_\perp)^2} \frac{\mathbf{y}_\perp^j - \mathbf{v}_\perp^j}{(\mathbf{y}_\perp - \mathbf{v}_\perp)^2} \\ &\times \Delta^{ij}(\mathbf{u}_\perp - \mathbf{v}_\perp) \left[\Omega_1(\epsilon, \mathbf{u}_\perp) \Omega_1^\dagger(\epsilon, \mathbf{v}_\perp) - 1 \right]_{bc}, \end{aligned} \quad (3.83)$$

where the function $\Delta^{ij}(\mathbf{u}_\perp - \mathbf{v}_\perp)$ is defined in eq. (E.11) in the appendix E. If we keep the second term in each of the α 's, we get

$$\begin{aligned} \eta_{\parallel\parallel}^{bc}(\mathbf{x}_\perp, \mathbf{y}_\perp) &= \frac{1}{\pi} \int \frac{d^2\mathbf{u}_\perp}{(2\pi)^2} \frac{(\mathbf{x}_\perp - \mathbf{u}_\perp) \cdot (\mathbf{y}_\perp - \mathbf{u}_\perp)}{(\mathbf{x}_\perp - \mathbf{u}_\perp)^2 (\mathbf{y}_\perp - \mathbf{u}_\perp)^2} \\ &\times \left[1 + \Omega_1(\epsilon, \mathbf{x}_\perp) \Omega_1^\dagger(\epsilon, \mathbf{y}_\perp) \right. \\ &\quad \left. - \Omega_1(\epsilon, \mathbf{x}_\perp) \Omega_1^\dagger(\epsilon, \mathbf{u}_\perp) - \Omega_1(\epsilon, \mathbf{u}_\perp) \Omega_1^\dagger(\epsilon, \mathbf{y}_\perp) \right]_{bc} \\ &+ \frac{1}{8\pi^4} \int d^2\mathbf{u}_\perp d^2\mathbf{v}_\perp \frac{\mathbf{x}_\perp^i - \mathbf{u}_\perp^i}{(\mathbf{x}_\perp - \mathbf{u}_\perp)^2} \frac{\mathbf{y}_\perp^j - \mathbf{v}_\perp^j}{(\mathbf{y}_\perp - \mathbf{v}_\perp)^2} \\ &\times \Delta^{ij}(\mathbf{u}_\perp - \mathbf{v}_\perp) \left[\Omega_1(\epsilon, \mathbf{u}_\perp) \Omega_1^\dagger(\epsilon, \mathbf{v}_\perp) - 1 \right]_{bc}. \end{aligned} \quad (3.84)$$

Thanks to the orthogonality between the first and second terms in α , the mixed terms are zero:

$$\eta_{\perp\parallel}^{bc}(\mathbf{x}_\perp, \mathbf{y}_\perp) = \eta_{\parallel\perp}^{bc}(\mathbf{x}_\perp, \mathbf{y}_\perp) = 0. \quad (3.85)$$

We see that when we add up all the contributions to $\eta^{bc}(\mathbf{x}_\perp, \mathbf{y}_\perp)$, the terms containing Δ^{ij} cancel out, leaving only

$$\begin{aligned} \eta^{bc}(\mathbf{x}_\perp, \mathbf{y}_\perp) &= \frac{1}{\pi} \int \frac{d^2\mathbf{u}_\perp}{(2\pi)^2} \frac{(\mathbf{x}_\perp - \mathbf{u}_\perp) \cdot (\mathbf{y}_\perp - \mathbf{u}_\perp)}{(\mathbf{x}_\perp - \mathbf{u}_\perp)^2 (\mathbf{y}_\perp - \mathbf{u}_\perp)^2} \\ &\times \left[1 + \Omega_1(\epsilon, \mathbf{x}_\perp) \Omega_1^\dagger(\epsilon, \mathbf{y}_\perp) - \Omega_1(\epsilon, \mathbf{x}_\perp) \Omega_1^\dagger(\epsilon, \mathbf{u}_\perp) - \Omega_1(\epsilon, \mathbf{u}_\perp) \Omega_1^\dagger(\epsilon, \mathbf{y}_\perp) \right]_{bc}. \end{aligned} \quad (3.86)$$

It is interesting to note that the integrand in this formula can be factorized as follows:

$$\begin{aligned}\eta^{bc}(\mathbf{x}_\perp, \mathbf{y}_\perp) &= \frac{1}{\pi} \int d^2 \mathbf{u}_\perp \mathbf{J}(\mathbf{x}_\perp, \mathbf{u}_\perp) \cdot \mathbf{J}^\dagger(\mathbf{y}_\perp, \mathbf{u}_\perp) \\ \mathbf{J}_{ba}^i(\mathbf{x}_\perp, \mathbf{u}_\perp) &\equiv \frac{1}{2\pi} \frac{(\mathbf{x}_\perp - \mathbf{u}_\perp)^i}{(\mathbf{x}_\perp - \mathbf{u}_\perp)^2} [\Omega(\mathbf{x}_\perp) - \Omega(\mathbf{u}_\perp)]_{ba} .\end{aligned}\quad (3.87)$$

(The first of these two equations has an implicit sum over the indices i and a .) Eqs. (3.80) and (3.86) provide an explicit result for the contribution of the term bilinear in \mathbb{T} , when both \mathbf{u} and \mathbf{v} are on the branch Σ_1 of the surface Σ . If they are both on the branch Σ_2 , one obtains a large logarithm in the \mathbf{k} integration when $k^- \rightarrow +\infty$, and it is easy to guess the result by symmetry:

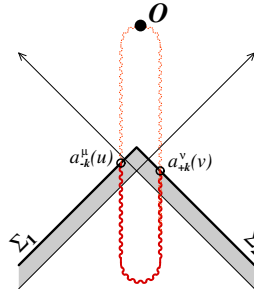
$$\frac{1}{2} \ln \left(\frac{\Lambda^-}{\Lambda'^-} \right) \int d^2 \mathbf{x}_\perp d^2 \mathbf{y}_\perp \eta^{bc}(\mathbf{x}_\perp, \mathbf{y}_\perp) \nabla_{\mathbf{x}_\perp}^b \nabla_{\mathbf{x}_\perp}^c , \quad (3.88)$$

with Lie derivatives that act now on Ω_2 and

$$\begin{aligned}\eta^{bc}(\mathbf{x}_\perp, \mathbf{y}_\perp) &= \frac{1}{\pi} \int \frac{d^2 \mathbf{u}_\perp}{(2\pi)^2} \frac{(\mathbf{x}_\perp - \mathbf{u}_\perp) \cdot (\mathbf{y}_\perp - \mathbf{u}_\perp)}{(\mathbf{x}_\perp - \mathbf{u}_\perp)^2 (\mathbf{y}_\perp - \mathbf{u}_\perp)^2} \\ &\times \left[1 + \Omega_2(\epsilon, \mathbf{x}_\perp) \Omega_2^\dagger(\epsilon, \mathbf{y}_\perp) - \Omega_2(\epsilon, \mathbf{x}_\perp) \Omega_2^\dagger(\epsilon, \mathbf{u}_\perp) - \Omega_2(\epsilon, \mathbf{u}_\perp) \Omega_2^\dagger(\epsilon, \mathbf{y}_\perp) \right]_{bc} .\end{aligned}\quad (3.89)$$

The only remaining case to consider is when the points \mathbf{u} and \mathbf{v} belong to different branches of the surface Σ , as illustrated in the figure 3.6. In this case, neither $u^+ - v^+$ nor $u^- - v^-$ vanishes. Therefore, the exponential factors in the integrand oscillate both when $k^+ \rightarrow +\infty$ and when $k^- \rightarrow +\infty$, preventing the occurrence of any divergence in these limits.

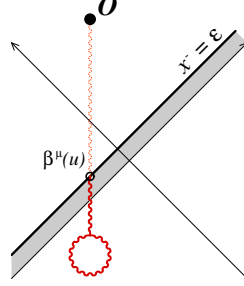
Figure 3.6: One-loop configuration where the points \mathbf{u} and \mathbf{v} are located on different branches of the surface Σ .



There is also a potential complication with the tip of the wedge in the figure 3.6. Indeed, if the points \mathbf{u} or \mathbf{v} are located in the part of Σ that sits above the forward light-cone, then our calculations are not correct because the background classical field that one should use is the radiated field resulting from the collision. However, we need not bother with this complication in the limit $\epsilon \rightarrow 0$, since the terms coming from the tip of the wedge vanish like ϵ or ϵ^2 (depending on whether only one or both of \mathbf{u}, \mathbf{v} are located there).

3.2.8 Virtual corrections

Figure 3.7: Linear term in $\beta \cdot \mathbb{T}_u$ in eq. (3.42).



We must now calculate the term in $\beta \cdot \mathbb{T}_u$ in eq. (3.42), illustrated in the figure 3.7. By mimicking the evaluation of the real contribution, we can first write, when the point u is on the branch Σ_1 of Σ ,

$$\begin{aligned} \int_{-\infty}^{\epsilon} du^+ d^2 u_{\perp} [\beta \cdot \mathbb{T}_u] &= \\ &= \int d^2 x_{\perp} \underbrace{\int d^2 u_{\perp} G(u_{\perp} - x_{\perp}) \partial_{\mu}^u (\Omega_{1bd}(\epsilon, u_{\perp}) \beta_d^{\mu}(u))}_{\ln \left(\frac{\Lambda^+}{\Lambda'^+} \right) v^b(x_{\perp})} \nabla_{x_{\perp}}^b. \end{aligned} \quad (3.90)$$

In writing this equation, we have anticipated that a logarithm of Λ^+/Λ'^+ arises from the k^+ integral hidden in $\beta_d^{\mu}(u)$, and we denote by $v^b(x_{\perp})$ its prefactor.

In principle, one could calculate directly the function $v^b(x_{\perp})$, by extracting the logarithmic divergences in the k^+ integral (hidden in the source term in the equation of motion for β^{μ}). However, it is much simpler to try to relate $v^b(x_{\perp})$ to the previously obtained function $\eta^{bc}(x_{\perp}, y_{\perp})$. This relation will save us a fair amount of calculations, and by doing this we will get for free the additional result that the renormalization group evolution is unitary. The starting point for doing this is the Green's formula for $\beta^{\mu}(u)$, that expresses it in terms of its value on the hypersurface defined by $v^- = 0$,

$$\begin{aligned} \beta^{\mu}(u) &= -i \int_{v^- > 0} d^4 v G_{0_R}^{\mu\nu}(u, v) \left[\frac{\partial^2 \mathcal{U}(\mathcal{A})}{\partial \mathcal{A}^{\nu}(v) \partial \mathcal{A}^{\rho}(v)} \beta^{\rho}(v) \right. \\ &\quad \left. + \frac{1}{2} \frac{\partial^3 \mathcal{U}(\mathcal{A})}{\partial \mathcal{A}^{\nu}(v) \partial \mathcal{A}^{\rho}(v) \partial \mathcal{A}^{\sigma}(v)} \mathcal{G}_{++}^{\rho\sigma}(v, v) \right]. \end{aligned} \quad (3.91)$$

In this formula, $G_{0_R}^{\mu\nu}$ is the free retarded propagator for a gauge field in light-cone gauge, and $\mathcal{G}_{++}^{\rho\sigma}$ is the $++$ component of the Schwinger-Keldysh propagator, dressed by the background classical field. Note that there is no boundary term in this Green's formula, thanks to our choice of the surface $v^- = 0$ for the boundary. Indeed, the fluctuation β^{μ} is identically zero

at $v^- \leq 0$. The propagator $\mathcal{G}_{++}^{\rho\sigma}$ can be expressed in terms of the fluctuations $\alpha_{\pm k\lambda\alpha}$ thanks to eqs. (2.93) and (2.96). Consider now the Green's formula that expresses the fluctuation $\alpha_{+k\lambda\alpha}(x)$ in terms of its value on the surface $y^- = 0$,

$$\alpha_{+k\lambda\alpha}^\mu(x) = -i \int_{y^- > 0} d^4y \, G_{0_R}^{\mu\nu}(x, y) \frac{\partial^2 \mathcal{U}(\mathcal{A})}{\partial \mathcal{A}^\nu(v) \partial \mathcal{A}^\rho(v)} \alpha_{+k\lambda\alpha}^\rho(y) + \mathcal{B}^\mu[\alpha_{+k\lambda\alpha}]. \quad (3.92)$$

It is not necessary here to make the boundary term more explicit (its detailed form in light-cone gauge can be found in the appendix D). In this formula, both the fluctuation $\alpha_{+k\lambda\alpha}$ and the second derivative of the gauge potential depend on the background classical field. Let us introduce an operator $\alpha \cdot \mathcal{T}_v$ that substitutes a power of the background field \mathcal{A} by a power of the fluctuation α at the point v^μ . This operator is somewhat similar to the operator $\alpha \cdot \mathbb{T}_v$, except that it acts in the bulk, while the latter performs this substitution only in the boundary term. Now, define

$$\zeta^\mu(u) \equiv \frac{1}{2} \sum_{\lambda, \alpha} \int \frac{d^3k}{(2\pi)^3 2k} \int_{v^- > 0} d^4v \, [\alpha_{-k\lambda\alpha} \cdot \mathcal{T}_v] \alpha_{+k\lambda\alpha}^\mu(u). \quad (3.93)$$

By using the above Green's formula for $\alpha_{+k\lambda\alpha}^\mu$, we obtain

$$\begin{aligned} \zeta^\mu(u) = & -i \int_{v^- > 0} d^4v \, G_{0_R}^{\mu\nu}(u, v) \left[\frac{\partial^2 \mathcal{U}(\mathcal{A})}{\partial \mathcal{A}^\nu(v) \partial \mathcal{A}^\rho(v)} \zeta^\rho(v) \right. \\ & \left. + \frac{1}{2} \frac{\partial^3 \mathcal{U}(\mathcal{A})}{\partial \mathcal{A}^\nu(v) \partial \mathcal{A}^\rho(v) \partial \sigma(v)} \mathcal{G}_{++}^{\rho\sigma}(v, v) \right]. \end{aligned} \quad (3.94)$$

Thus, we see that ζ^μ and β^μ are equal, which proves that

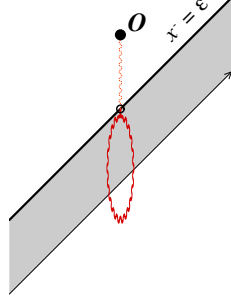
$$\beta^\mu(u) = \frac{1}{2} \sum_{\lambda, \alpha} \int \frac{d^3k}{(2\pi)^3 2k} \int_{v^- > 0} d^4v \, [\alpha_{-k\lambda\alpha} \cdot \mathcal{T}_v] \alpha_{+k\lambda\alpha}^\mu(u). \quad (3.95)$$

Inserting this identity into the equation (3.90) that defines $v^b(x_\perp)$, we get

$$\begin{aligned} \ln\left(\frac{\Lambda^+}{p^+}\right) v^b(x_\perp) = & \frac{1}{2} \sum_{\lambda, \alpha} \int \frac{d^3k}{(2\pi)^3 2k} \int_{v^- > 0} d^4v \, [\alpha_{-k\lambda\alpha} \cdot \mathcal{T}_v] \\ & \times \int d^2u_\perp \, G(u_\perp - x_\perp) \partial_\mu^u \left(\Omega_{1bd}(\epsilon, u_\perp) \alpha_{+k\lambda\alpha}^{\mu d}(u) \right). \end{aligned} \quad (3.96)$$

Note that in this equation, the k^+ integration is confined to the slice $\Lambda'^+ \leq k^+ \leq \Lambda^+$. Moreover, this equation is only valid for the logarithmic part of this integral, but not for the finite terms. Therefore, in order to obtain $v^b(x_\perp)$, we must identify the logarithms in the right hand side of this equation. In order to get a logarithm from the integration over k^+ , we need to tame the oscillations that arise from the factor $\exp(ik^+(u^- - v^-))$. This is only the case if v^- is very close to the endpoint $u^- = \epsilon$ (due to the retarded propagator in eq. (3.91), v^- cannot be larger than u^-). Thus, the diagrammatic representation in the figure 3.7 is a bit misleading: the vertex where the loop is attached must lie very close to the surface Σ in order to pick up the terms enhanced by a logarithm. A more faithful graphical representation is that of the figure 3.8.

Figure 3.8: Log enhanced part of the term $\beta \cdot \mathbb{T}_u$ in eq. (3.42).



The final step in the calculation of v^b is to note that if one integrates the *bulk* operator $a \cdot \mathcal{T}_v$ over v^- in a very small slice near Σ , one gets the *boundary* operator $a \cdot \mathbb{T}_v$. More precisely,

$$\lim_{\delta x^- \rightarrow 0} \int_{\epsilon - \delta x^-}^{\epsilon} dv^- [a \cdot \mathcal{T}_v] = a \cdot \mathbb{T}_v . \quad (3.97)$$

Using this identity, as well as the relation between the operator \mathbb{T}_v and the derivative with respect to $\tilde{\mathcal{A}}_1^+$, we obtain

$$\begin{aligned} \int_{v^- > 0} d^4 v [a_{-k\lambda a} \cdot \mathcal{T}_v] &\stackrel{\text{LLog}}{=} \int d^2 \mathbf{y}_\perp \int d^2 \mathbf{v}_\perp G(\mathbf{y}_\perp - \mathbf{v}_\perp) \\ &\times \partial_v^v \left(\Omega_{1ce}(\epsilon, \mathbf{v}_\perp) a_{-k\lambda a}^v(v) \right) \nabla_{\mathbf{y}_\perp}^c . \end{aligned} \quad (3.98)$$

(This identity is only valid for the logarithmic terms, as emphasized by the *LLog* subscript below the equality sign; indeed it is only for these terms that the v^- integral is restricted to an infinitesimal slice near $v^- = \epsilon$, so that we can use eq. (3.97).) Once inserted in eq. (3.96), this leads to

$$\begin{aligned} \ln \left(\frac{\Lambda^+}{\Lambda'^+} \right) v^b(\mathbf{x}_\perp) &= \frac{1}{2} \int d^2 \mathbf{y}_\perp \sum_{\lambda, a} \int \frac{d^3 \mathbf{k}}{(2\pi)^3 2k} \\ &\times \int d^2 \mathbf{v}_\perp G(\mathbf{y}_\perp - \mathbf{v}_\perp) \partial_v^v \left(\Omega_{1ce}(\epsilon, \mathbf{v}_\perp) a_{-k\lambda a}^v(v) \right) \\ &\times \nabla_{\mathbf{y}_\perp}^c \int d^2 \mathbf{u}_\perp G(\mathbf{x}_\perp - \mathbf{u}_\perp) \partial_\mu^u \left(\Omega_{1bd}(\epsilon, \mathbf{u}_\perp) a_{+k\lambda a}^{\mu d}(u) \right) . \end{aligned} \quad (3.99)$$

If we consider the underlined terms alone and recall eq. (3.81), we recognize

$$\ln \left(\frac{\Lambda^+}{\Lambda'^+} \right) \eta^{bc}(\mathbf{x}_\perp, \mathbf{y}_\perp) . \quad (3.100)$$

The final step in our derivation is to notice that since $\nabla_{\mathbf{y}_\perp}^c$ shares a color index with Ω_1 , we have the identity [81, 83, 118]

$$\nabla_{\mathbf{y}_\perp}^c \partial_v^v \left(\Omega_{1ce}(\epsilon, \mathbf{v}_\perp) a_{-k\lambda a}^v(v) \right) = 0 , \quad (3.101)$$

because of the antisymmetry of the adjoint generators of $SU(3)$. We can therefore move the operator $\nabla_{\mathbf{y}_\perp}^c$ immediately after the measure $d^2\mathbf{y}_\perp$ to obtain

$$\mathbf{v}^b(\mathbf{x}_\perp) = \frac{1}{2} \int d^2\mathbf{y}_\perp \nabla_{\mathbf{y}_\perp}^c \eta^{bc}(\mathbf{x}_\perp, \mathbf{y}_\perp), \quad (3.102)$$

which expresses \mathbf{v}^b in terms of the coefficient η^{bc} (the latter being known explicitly in terms of the Wilson line Ω_1). Let us finally recall that this is the contribution that one gets when the operator $\beta \cdot \mathbb{T}_u$ is taken on the branch Σ_1 of Σ . We must add the contribution from the branch Σ_2 , which is obtained by replacing the $\ln(\Lambda^+/\Lambda'^+)$ by $\ln(\Lambda^-/\Lambda'^-)$, and the field $\tilde{\mathcal{A}}_1^+$ and Wilson line Ω_1 by $\tilde{\mathcal{A}}_2^+$ and Ω_2 respectively.

Let us now combine the results from eqs. (3.86), (3.89) and (3.102). We see that the logarithmic part of the single gluon spectrum at NLO can be written as

$$\left. \frac{dN_1}{d^3\mathbf{p}} \right|_{\text{NLO}} \Big|_{\Lambda'^\pm < \mathbf{k}^\pm < \Lambda^\pm} \stackrel{\text{LLog}}{=} \left[\ln\left(\frac{\Lambda^+}{\Lambda'^+}\right) \mathcal{H}_1 + \ln\left(\frac{\Lambda^-}{\Lambda'^-}\right) \mathcal{H}_2 \right] \left. \frac{dN_1}{d^3\mathbf{p}} \right|_{\text{LO}}, \quad (3.103)$$

where the operator \mathcal{H}_1 , known as the *JIMWLK Hamiltonian* [76–83], is defined by

$$\mathcal{H}_1 \equiv \frac{1}{2} \int d^2\mathbf{x}_\perp d^2\mathbf{y}_\perp \nabla_{\mathbf{y}_\perp}^c \eta^{bc}(\mathbf{x}_\perp, \mathbf{y}_\perp) \nabla_{\mathbf{x}_\perp}^b, \quad (3.104)$$

and \mathcal{H}_2 by the same definition with $\tilde{\mathcal{A}}_2^-$ instead of $\tilde{\mathcal{A}}_1^+$. We have made use of eq. (3.102) in order to write this operator as a total derivative. This property is crucial, because it ensures that it is a self-adjoint operator. The inequality under the equal sign in eq. (3.103) is a reminder of the fact that this formula gives only the logarithmic NLO terms that arise from a slice of field modes located just below the cutoff of the CGC effective theory. Modes that have a longitudinal momentum smaller than Λ'^\pm are not included in this result. Note also that, although the coupling constant g does not appear explicitly in the JIMWLK Hamiltonian, it gives nevertheless a correction of relative order g^2 . This is due to the presence of two functional derivatives with respect to fields of order $\mathcal{A} \sim g^{-1}$.

3.2.9 Renormalization group evolution

Eq. (3.103) gives the logarithmic NLO contributions to the single gluon spectrum from the slice of field modes $\Lambda'^\pm < \mathbf{k}^\pm < \Lambda^\pm$. This formula is valid for a given configuration of the sources $\tilde{\rho}_{1,2}$ (in Lorenz gauge) describing the projectiles. Since the JIMWLK Hamiltonian in eq. (3.104) contains derivatives with respect to the fields $\tilde{\mathcal{A}}_{1,2}^\pm$, i.e. with respect to the sources near the cutoffs Λ^\pm , this formula suggests that these NLO corrections can be taken into account simply by adding a layer of slower sources just below the cutoff. Let us see in more detail how this works.

In the CGC with cutoffs Λ^\pm , the sources $\tilde{\rho}_{1,2}(\mathbf{x}^\mp, \mathbf{x}_\perp)$ are defined over the range $0 < \mathbf{x}^\mp < 1/\Lambda^\pm$, and their distribution is given by a pair of functionals $W_{\Lambda^\pm}[\tilde{\rho}_{1,2}(\mathbf{x}^\mp, \mathbf{x}_\perp)]$. The expectation value for the single gluon spectrum, including both the leading order and the slice $\Lambda'^\pm < \mathbf{k}^\pm < \Lambda^\pm$ from the next-to-leading order, can be written in this effective theory as

$$\begin{aligned} \left\langle \frac{dN_1}{d^3\mathbf{p}} \right\rangle_{\text{LO} + [\Lambda'^\pm, \Lambda^\pm]}^{\Lambda^\pm} &= \int [D\tilde{\rho}_1(\mathbf{x}^-, \mathbf{x}_\perp) D\tilde{\rho}_2(\mathbf{x}^+, \mathbf{x}_\perp)] \\ &\quad \times W_{\Lambda^+}[\tilde{\rho}_1(\mathbf{x}^-, \mathbf{x}_\perp)] W_{\Lambda^-}[\tilde{\rho}_2(\mathbf{x}^+, \mathbf{x}_\perp)] \\ &\quad \times \left[1 + \ln\left(\frac{\Lambda^+}{\Lambda'^+}\right) \mathcal{H}_1 + \ln\left(\frac{\Lambda^-}{\Lambda'^-}\right) \mathcal{H}_2 \right] \left. \frac{dN_1}{d^3\mathbf{p}} \right|_{\text{LO}}. \end{aligned} \quad (3.105)$$

(The superscript Λ^\pm in the left hand side is a reminder of the fact that the calculation is done in an effective theory where all the modes above Λ^\pm are treated as sources.) At this point, two properties are crucial. First, we can use the fact that the operators $\mathcal{H}_{1,2}$ are self-adjoint in order to integrate by parts. Secondly, if the slice of modes that we integrate out in the NLO correction is small enough, then we can write

$$1 + \ln \left(\frac{\Lambda^+}{\Lambda'^+} \right) \mathcal{H}_1 + \ln \left(\frac{\Lambda^-}{\Lambda'^-} \right) \mathcal{H}_2 = \left[1 + \ln \left(\frac{\Lambda^+}{\Lambda'^+} \right) \mathcal{H}_1 \right] \left[1 + \ln \left(\frac{\Lambda^-}{\Lambda'^-} \right) \mathcal{H}_2 \right], \quad (3.106)$$

up to terms of order α_s^2 . Let us now extend the sources $\tilde{\rho}_{1,2}$ into sources $\tilde{\rho}'_{1,2}$ that are defined over the range $0 < x^\mp < 1/\Lambda'^\pm$, by the following relations:

- i. The sources $\tilde{\rho}'_{1,2}$ and $\tilde{\rho}_{1,2}$ coincide over the common part of their domain of definition: if $x^\mp < 1/\Lambda^\pm$, then $\tilde{\rho}'_{1,2}(x^\mp, \mathbf{x}_\perp) = \tilde{\rho}_{1,2}(x^\mp, \mathbf{x}_\perp)$,
- ii. The value of the sources in the range $1/\Lambda^\pm < x^\mp < 1/\Lambda'^\pm$ is stochastic, with a probability distribution given by

$$W'_{\Lambda'^\pm}[\tilde{\rho}'_{1,2}(x^\mp, \mathbf{x}_\perp)] \equiv \left[1 + \ln \left(\frac{\Lambda^\pm}{\Lambda'^\pm} \right) \mathcal{H}_{1,2} \right] W_{\Lambda^\pm}[\tilde{\rho}_{1,2}(x^\mp, \mathbf{x}_\perp)]. \quad (3.107)$$

By doing this, we are changing the original CGC effective theory into another effective theory, whose cutoffs are now at the scales Λ'^\pm , and the field modes that we have integrated out in this process are now described as classical sources. Note also that the probability for $\tilde{\rho}'_{1,2}$ in the new slice depends on the value it takes in all the previous slices, since the Hamiltonians $\mathcal{H}_{1,2}$ contain the Wilson lines $\Omega_{1,2}$. Thus we have proven the following identity:

$$\left\langle \frac{dN_1}{d^3\mathbf{p}} \right\rangle_{\text{LO} + [\Lambda'^\pm, \Lambda^\pm]}^{\Lambda^\pm} = \left\langle \frac{dN_1}{d^3\mathbf{p}} \right\rangle_{\text{LO}}^{\Lambda'^\pm}. \quad (3.108)$$

In words, this equation means that in order to include at leading log accuracy the NLO contributions that arise from the slice $\Lambda'^\pm < k^\pm < \Lambda^\pm$, it is sufficient to perform the calculation at LO and to use a CGC effective theory with lower cutoffs, where the source distributions in the new effective theory are defined by eq. (3.107).

What has been done here for one slice of quantum modes can be repeated indefinitely, until all the modes have been integrated out down to $k^\pm \rightarrow 0$. One should consider a sequence of increasingly smaller cutoffs:

$$\dots \Lambda_n^\pm < \dots < \Lambda_1^\pm < \Lambda_0^\pm. \quad (3.109)$$

Λ_0^\pm are the cutoff scales of the original CGC effective theory, and they must be taken close to the fragmentation region of the two projectiles. Then, one uses the result of eq. (3.108) repeatedly in order to integrate out the leading contribution from the loop corrections in the successive slices $\Lambda_{i+1}^\pm < k^\pm < \Lambda_i^\pm$. At the end of this resummation, one obtains the complete leading log answer for the single gluon spectrum, that we can write as:

$$\begin{aligned} \left\langle \frac{dN_1}{d^3\mathbf{p}} \right\rangle_{\text{LLog}} &= \int [D\tilde{\rho}_1(x^-, \mathbf{x}_\perp) D\tilde{\rho}_2(x^+, \mathbf{x}_\perp)] \\ &\quad \times W[\tilde{\rho}_1(x^-, \mathbf{x}_\perp)] W[\tilde{\rho}_2(x^+, \mathbf{x}_\perp)] \left. \frac{dN_1}{d^3\mathbf{p}} \right|_{\text{LO}}. \end{aligned} \quad (3.110)$$

In this formula, $W[\tilde{\rho}_{1,2}(x^\mp, \mathbf{x}_\perp)]$ are the limiting distributions obtained by repeating infinitely many steps such as (3.107), until $\Lambda^\pm \rightarrow 0$. This is a central result of this chapter; it shows that all the leading logarithms that arise from loop corrections can be absorbed into the distributions $W[\tilde{\rho}_{1,2}]$ that represent the distribution of sources in the projectiles.

At this stage, we have not said a word about the universality of these distributions, i.e. about whether they are intrinsic properties of the projectiles, regardless of the observable one is measuring. A first indication of their universality is the fact that the JIMWLK evolution equation (3.107) that drives the evolution of these distributions as one lowers the cutoff was first encountered in the context of inclusive deep inelastic scattering off a nucleus. Moreover, in the next sections, we will see that the same distributions enter in the formula for the multi-gluon inclusive spectra.

Let us end with a note concerning how far one must carry the evolution of the distributions $W[\tilde{\rho}_{1,2}(x^\mp, \mathbf{x}_\perp)]$ in practice. The single gluon spectrum contains a Fourier transform of the classical fields, with the momentum p^μ . Thus, it is sensitive to sources in the region $0 < x^\mp < 1/p^\pm$. Sources at higher values of x^\mp –or equivalently that carry a longitudinal momentum smaller than p^\pm – are irrelevant in this observable. Therefore, it is sufficient to evolve the distributions $W_{\Lambda^\pm}[\tilde{\rho}_{1,2}]$ down to scales $\Lambda^\pm \sim p^\pm$. One can of course evolve them further down in longitudinal momentum, but the slower sources one adds to the distribution by doing this do not contribute to the production of a gluon of longitudinal momentum p^\pm .

3.2.10 Iteration of the JIMWLK kernel

Eq. (3.107) is the form of the JIMWLK equation for a small change in the cutoffs $\Lambda^\pm \rightarrow \Lambda'^\pm$ of the effective theory. Naturally, it can be written in differential form as follows¹⁵

$$\frac{\partial W_{\Lambda^\pm}}{\partial \ln(\Lambda^\pm)} = -\mathcal{H}_{1,2}(\Lambda^\pm) W_{\Lambda^\pm} . \quad (3.111)$$

Here, we have included an argument Λ^\pm in the Hamiltonian itself, to recall that it depends on Wilson lines $\Omega_{1,2}$ that integrate sources down to the scale Λ^\pm and that the derivatives it contains are with respect to sources near the cutoff. This is important, because it means that the Hamiltonians at different values of the cutoff do not commute. Therefore, when we formally solve eq. (3.111), we must write the solution as an ordered exponential:

$$W_{\Lambda^\pm} = \underbrace{T_\pm \exp \left[- \int_{\Lambda_0^\pm}^{\Lambda^\pm} \frac{d\kappa^\pm}{\kappa^\pm} \mathcal{H}_{1,2}(\kappa^\pm) \right]}_{\mathcal{U}_{1,2}(\Lambda^\pm, \Lambda_0^\pm)} W_{\Lambda_0^\pm} , \quad (3.112)$$

where Λ_0^\pm is the scale where the initial condition is given. T_\pm is an ordering such that products of Hamiltonians are ordered from left to right in order of increasing cutoffs¹⁶. As is the case with other evolution equations in QCD (such as DGLAP, BFKL), the initial condition $W_{\Lambda_0^\pm}$ is a priori non-perturbative.

¹⁵This equation is often written in terms of the rapidity interval $Y \equiv \ln(\Lambda_0^\pm/\Lambda^\pm)$ between the initial value of the cutoff and its current value. It has the same form as eq. (3.111), except for the minus sign.

¹⁶I.e. Hamiltonians with a lower cutoff must appear on the left of the product.

By inserting eq. (3.112) (with $\Lambda^\pm \rightarrow 0$) into eq. (3.110), and by integrating by parts, we get

$$\begin{aligned} \left\langle \frac{dN_1}{d^3\mathbf{p}} \right\rangle_{\text{LLog}} &= \int [D\tilde{\rho}_1(x^-, \mathbf{x}_\perp) D\tilde{\rho}_2(x^+, \mathbf{x}_\perp)] \\ &\quad \times W_{\Lambda_0^+}[\tilde{\rho}_1(x^-, \mathbf{x}_\perp)] W_{\Lambda_0^-}[\tilde{\rho}_2(x^+, \mathbf{x}_\perp)] \\ &\quad \times \mathcal{U}_1^\dagger(0, \Lambda_0^+) \mathcal{U}_2^\dagger(0, \Lambda_0^-) \left. \frac{dN_1}{d^3\mathbf{p}} \right|_{\text{LO}}. \end{aligned} \quad (3.113)$$

Although too formal to be of any use in phenomenological applications, this equation sheds some light on the structure of the leading logarithms that arise in higher loop corrections. Note first that the Hermitian conjugate of the evolution operator $\mathcal{U}_{1,2}$ is simply obtained by reversing the ordering, since the Hamiltonian $\mathcal{H}_{1,2}$ is Hermitian:

$$\mathcal{U}_{1,2}^\dagger(\Lambda^\pm, \Lambda_0^\pm) = \bar{\mathcal{T}}_\pm \exp \left[- \int_{\Lambda_0^\pm}^{\Lambda^\pm} \frac{d\kappa^\pm}{\kappa^\pm} \mathcal{H}_{1,2}(\kappa^\pm) \right]. \quad (3.114)$$

($\bar{\mathcal{T}}_\pm$ denotes the opposite ordering to \mathcal{T}_\pm .) Thus, in $\mathcal{U}_{1,2}^\dagger$, Hamiltonians with the largest value of the cutoff appear on the left. Moreover, an essential property of the JIMWLK Hamiltonian at the scale Λ^+ is that it contains derivatives with respect to the sources at the scale Λ^+ , and has prefactors that depends on all the sources that have longitudinal momenta $k^+ \geq \Lambda^+$. Thus, in a combination of the form

$$\mathcal{H}_1(\kappa_1^+) \mathcal{H}_1(\kappa_2^+) \mathcal{O} \quad (3.115)$$

with $\kappa_1^+ > \kappa_2^+$, the derivatives in the leftmost Hamiltonian ($\mathcal{H}_1(\kappa_1^+)$) can act both on the observable \mathcal{O} and on the Hamiltonian $\mathcal{H}_1(\kappa_2^+)$. This possibility has a simple diagrammatic interpretation. Consider the leading logs of Λ^+ at 2-loop in eq. (3.113). This amounts to expanding the evolution operator \mathcal{U}_1^\dagger to second order in the JIMWLK Hamiltonian. Because of the κ^+ ordering in \mathcal{U}_1 , these 2-loop terms are of the form

$$\mathcal{O}_{2\text{-loop}} \stackrel{\text{LLog}}{=} \int_{\Lambda_0^+}^{\Lambda^+} \frac{d\kappa_1^+}{\kappa_1^+} \int_{\kappa_1^+}^{\Lambda^+} \frac{d\kappa_2^+}{\kappa_2^+} \mathcal{H}(\kappa_1^+) \mathcal{H}(\kappa_2^+) \mathcal{O}_{\text{LO}}. \quad (3.116)$$

The terms where the derivatives in $\mathcal{H}(\kappa_1^+)$ do not act on $\mathcal{H}(\kappa_2^+)$ correspond to the diagrams of figure 3.9. If we look only at what happens below the line $x^- = \epsilon$, these contributions are just disconnected products of terms we had already at 1-loop. The analysis we performed of the logarithmic contributions at one loop extends trivially to these terms and it is easy to see that they have two powers of the logarithms.

In addition, eq. (3.116) also contains terms in which at least one of the derivatives in $\mathcal{H}(\kappa_1^+)$ acts on $\mathcal{H}(\kappa_2^+)$. This corresponds to topologies of the type displayed in figure 3.10. Such terms, that have a gluon vertex inside the region where the sources live, have a large logarithm for the same reason that the tadpole has a logarithm in the 1-loop terms. Thus one can see that it is crucial to properly order the powers of the Hamiltonian \mathcal{H} in longitudinal momentum in order not to lose these terms.

Note also that there are some two loops topologies that never appear in eq. (3.116), such as those of the figure 3.11. The contributions in this figure are radiative corrections to the coefficients of the operators $\mathbb{T}_{u,v}$ in eq. (3.42). In other words, these terms generate corrections of order α_s to the coefficients in the JIMWLK equation, and do not have double logs of Λ^+ . This explains why they are not generated by the leading log formula in eq. (3.116).

Figure 3.9: Two-loop contributions made of products of pieces already encountered at 1-loop. Although we do not make this distinction in the figure, one of the factors is attached at a slightly smaller value of x^- , because the two Hamiltonians in eq. (3.116) are at different longitudinal momentum scales.

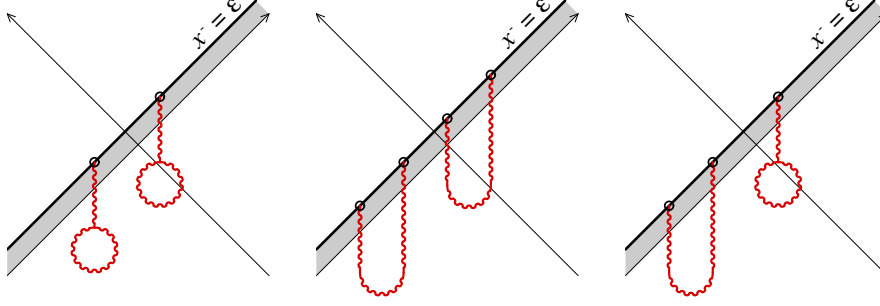


Figure 3.10: Example of term obtained when the derivatives in $\mathcal{H}(\kappa_1^+)$ can act on the coefficients of $\mathcal{H}(\kappa_2^+)$. Here, one of the derivatives in $\mathcal{H}(\kappa_1^+)$ acts on the function $\eta^{bc}(\mathbf{x}_\perp, \mathbf{y}_\perp)$ of $\mathcal{H}(\kappa_2^+)$ and the second derivative in $\mathcal{H}(\kappa_1^+)$ acts directly on \mathcal{O}_{LO} .

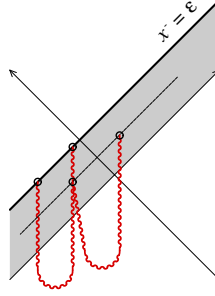
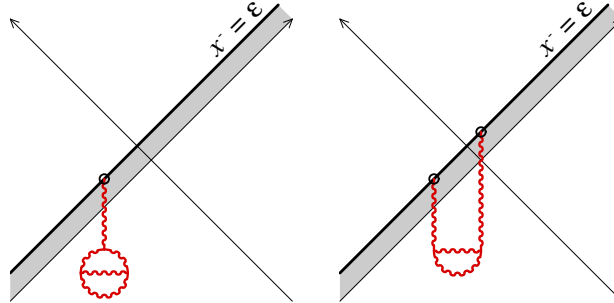


Figure 3.11: Two-loop corrections to the observable \mathcal{O} that do not appear at leading log.



3.2.11 The dense-dilute limit

It is interesting to study the limit of the single inclusive gluon spectrum at leading log accuracy, given in eq. (3.110), when one of the two colliding projectiles is dilute. Let us assume for instance that the source $\tilde{\rho}_1$ is that of a dilute projectile, i.e. that it is of order g (instead of g^{-1}). In this case, it turns out that the classical Yang-Mills equation can be solved analytically [18, 119] and that a closed expression for the gluon spectrum in the integrand of eq. (3.110) can be obtained:

$$\begin{aligned} \left. \frac{dN_1}{d^3\mathbf{p}} \right|_{\text{LO}} &= \frac{\alpha_s}{p} \int \frac{d^2\mathbf{k}_\perp}{(2\pi)^2} \frac{d^2\delta_\perp}{(2\pi)^2} e^{i\delta_\perp \cdot \mathbf{b}} \frac{(\mathbf{p}_\perp - \mathbf{k}_\perp)^2}{\mathbf{p}_\perp^2 \mathbf{k}_\perp^2} \\ &\times \frac{\text{tr} \left[\Omega_2(\mathbf{p}_\perp - \mathbf{k}_\perp + \frac{\delta_\perp}{2}) \Omega_2^\dagger(\mathbf{p}_\perp - \mathbf{k}_\perp - \frac{\delta_\perp}{2}) \right]}{N_c^2 - 1} \\ &\times \tilde{\rho}_{1a}(\mathbf{k}_\perp + \frac{\delta_\perp}{2}) \tilde{\rho}_{1a}^\dagger(\mathbf{k}_\perp - \frac{\delta_\perp}{2}), \end{aligned} \quad (3.117)$$

where $\tilde{\rho}_1$ is the color source of the dilute projectile, and Ω_2 the Wilson line constructed from the source of the dense projectile (both are Fourier transformed in this formula). Here, the formula has been written here for a collision at impact parameter \mathbf{b} . For *mean bias* collisions, one would integrate over \mathbf{b} , which would eliminate the integral over the skewness δ_\perp .

Because $\tilde{\rho}_1$ is weak, one can also truncate the JIMWLK Hamiltonian \mathcal{H}_1 to the lowest order in $\tilde{\rho}_1$, which is quadratic order. In this approximation, it is well known that the evolution of the correlators $\langle \tilde{\rho}_1 \tilde{\rho}_1 \rangle$ simplifies into the BFKL evolution¹⁷.

Therefore, the leading log result for the single gluon spectrum in collisions of dense-dilute projectiles is fairly simple: the dilute projectile is entirely described by an unintegrated gluon distribution that evolves according to the BFKL equation, while the dense projectile is described by a correlator of two Wilson lines that evolves according to the JIMWLK equation. Note that the JIMWLK evolution of $\text{tr}(\Omega_2 \Omega_2^\dagger)$ mixes with that of more complicated operators that contain more than two Wilson lines. It is only in the Balitsky-Kovchegov approximation that it evolves via a closed equation [84–86].

3.3 Logarithms in the energy-momentum tensor

So far in this chapter, we have used the example of the single inclusive gluon spectrum in order to illustrate the factorization of large logarithms of the longitudinal momentum. However, the number of produced gluons is not an infrared and collinear safe quantity. At NLO, it contains divergences due to the splitting of a gluon in two gluons in the final state. Because gluons are massless, this splitting can be either collinear or can produce a very soft gluon, both situations leading to a divergent contribution. Naturally, hadrons and not gluons are the observed final particles. In proton-proton collisions, it is well known that one should convolute the gluon spectrum with a gluon-to-hadron fragmentation function, and that all the above divergences can be absorbed into a renormalization of these fragmentation function.

In heavy ion collisions, it is unclear whether this approach remains effective due to the complicated final state dynamics. And even if one could still use the concept of fragmentation function, it is most likely incorrect to convolute them with the CGC-predicted gluon

¹⁷Up to some prefactors, the correlator $\langle \tilde{\rho}_1 \tilde{\rho}_1 \rangle$ is in fact an unintegrated gluon distribution.

spectrum. Indeed, the CGC calculation enables one to describe the dynamics of the collision up to a proper time equal to a few times Q_s^{-1} . Beyond such a time, additional effects that are not encompassed in the CGC description –such as two body collisions [120]– start affecting the evolution of the system. On the other hand, the infrared and collinear divergences that are resummed into the fragmentation functions correspond to very late stages of the evolution of the system. Therefore, there is most likely a gap between the stage at which the CGC applies and the stage at which fragmentation functions become relevant, and one should not convolute directly one with the other.

On the other hand, the CGC is thought to be an appropriate framework in order to determine the initial conditions for an hydrodynamical description of the final state evolution. In this context, the initial information one needs is the energy-momentum tensor at a certain proper time τ_0 , as a function of the spatial rapidity $\eta = \ln(x^+/x^-)/2$ and of the transverse position \mathbf{x}_\perp . The advantages of this point of view are two-fold. Firstly, by choosing an initial time τ_0 of the order of a few times Q_s^{-1} , one does not need to use the CGC beyond its range of applicability. And secondly, since the quantity of interest is now the energy-momentum tensor, which encodes the flow of energy and momentum in the system, one avoids the collinear and infrared singularities due to gluon splittings in the final state. Indeed, since these splittings conserve the energy and momentum, they have no effect on any observable that only measures energy and momentum – as opposed to an observable that counts the number of gluons, like the gluon spectrum. In this section, we will argue that the factorization theorem that we proved earlier for the inclusive gluon spectrum also applies to the expectation value of the energy-momentum tensor.

The energy-momentum tensor is a local composite operator, whose expression in a Yang-Mills theory is given by

$$T^{\mu\nu} = \frac{1}{4} g^{\mu\nu} F^{\lambda\sigma} F_{\lambda\sigma} - F^{\mu\lambda} F^\nu{}_\lambda, \quad (3.118)$$

where $F^{\mu\nu}$ is the field strength. Note that this formula does not contain any contribution due to quarks. While present in QCD, the quarks are suppressed by a power of α_s in the CGC framework (for the collision of two saturated projectiles), and therefore they do not contribute until the next-to-leading order.

At leading order, the expectation value of the energy momentum tensor for a given configuration of the color sources $\tilde{\rho}_{1,2}$ is simply obtained by substituting the operator $F^{\mu\nu}$ by the classical value of the field strength $\mathcal{F}^{\mu\nu}$ (i.e. the field strength obtained from the classical solution of Yang-Mills equations):

$$T_{\text{LO}}^{\mu\nu} = \frac{1}{4} g^{\mu\nu} \mathcal{F}^{\lambda\sigma} \mathcal{F}_{\lambda\sigma} - \mathcal{F}^{\mu\lambda} \mathcal{F}^\nu{}_\lambda. \quad (3.119)$$

For this quantity, the power counting indicates that

$$T_{\text{LO}}^{\mu\nu} \sim \frac{Q_s^4}{g^2}. \quad (3.120)$$

Before turning to the next-to-leading order corrections, let us make an important comment on the evaluation of $T_{\text{LO}}^{\mu\nu}$. Strictly speaking, one is evaluating the *out* energy momentum tensor in the *in* vacuum state, i.e.

$$\langle 0_{\text{in}} | T_{\text{out}}^{\mu\nu} | 0_{\text{in}} \rangle. \quad (3.121)$$

Because this matrix element has the *in* vacuum on both sides¹⁸, the appropriate diagrammatic rules for its perturbative expansion are those of the Schwinger-Keldysh formalism. In particular, one must sum over the \pm indices at each vertex of a given diagram. Similarly to the case of the inclusive gluon spectrum, this sum implies that the boundary condition for the classical field that enters in $\mathcal{F}^{\mu\nu}$ must be a null retarded boundary condition,

$$\lim_{x^0 \rightarrow -\infty} \mathcal{A}^\mu(x) = 0, \quad (3.122)$$

as was also the case for the inclusive gluon spectrum.

At Next to Leading Order, there are two types of corrections. One of them consists in replacing one instance of the classical field $\mathcal{A}^\mu(x)$ in $T_{\text{LO}}^{\mu\nu}(x)$ by the 1-loop correction $\beta^\mu(x)$ already encountered in the study of the 1-loop corrections to the gluon spectrum. The second kind of NLO correction consists in replacing a pair of classical fields $\mathcal{A}^\mu(x)\mathcal{A}^\nu(x)$ by the propagator $\mathcal{G}^{\mu\nu}(x, x)$. At this point, one can reproduce all the manipulations performed in section 3.2.3. Likewise, one obtains the following relationship between the expectation value of the energy-momentum tensor at LO and NLO,

$$\begin{aligned} T_{\text{NLO}}^{\mu\nu}(x) = & \left[\frac{1}{2} \sum_{\lambda, \alpha} \int \frac{d^3 \mathbf{k}}{(2\pi)^3 2k} \int_{\Sigma} d^3 \mathbf{S}_u d^3 \mathbf{S}_v [\mathbf{a}_{-\mathbf{k}\lambda\alpha} \cdot \mathbb{T}_u] [\mathbf{a}_{+\mathbf{k}\lambda\alpha} \cdot \mathbb{T}_v] \right. \\ & \left. + \int_{\Sigma} d^3 \mathbf{S}_u [\beta \cdot \mathbb{T}_u] \right] T_{\text{LO}}^{\mu\nu}(x), \end{aligned} \quad (3.123)$$

identical to what we had in the case of the inclusive gluon spectrum. Therefore, all the subsequent analysis of the large logarithms of the cutoffs Λ^\pm remains valid, since we have shown that these logarithms arise from the coefficients in front of the operators $\mathbb{T}_{u,v}$. In other words, the results of the sections 3.2.7 and 3.2.8 can be summarized by the formula

$$\begin{aligned} & \frac{1}{2} \sum_{\lambda, \alpha} \int \frac{d^3 \mathbf{k}}{(2\pi)^3 2k} \int_{\Sigma} d^3 \mathbf{S}_u d^3 \mathbf{S}_v [\mathbf{a}_{-\mathbf{k}\lambda\alpha} \cdot \mathbb{T}_u] [\mathbf{a}_{+\mathbf{k}\lambda\alpha} \cdot \mathbb{T}_v] \\ & + \int_{\Sigma} d^3 \mathbf{S}_u [\beta \cdot \mathbb{T}_u] \stackrel{\text{LLog}}{=} \ln \left(\frac{\Lambda^+}{\Lambda'^+} \right) \mathcal{H}_1(\Lambda^+) + \ln \left(\frac{\Lambda^-}{\Lambda'^-} \right) \mathcal{H}_2(\Lambda^-), \end{aligned} \quad (3.124)$$

which tells us what logarithms arise when we integrate out one small layer of quantum modes just below the cutoffs Λ^\pm . Obviously, thanks to this formula, the structure of the leading logarithms of Λ^\pm is universal for all the quantities for which eq. (3.123) is valid. When this relationship between LO and NLO is valid, the coefficients of the logarithms are given by the JIMWLK Hamiltonians of the projectiles, and as a consequence it is possible to factorize these logarithms in the distributions $W[\tilde{\rho}_{1,2}]$ of color sources for these projectiles.

Applied to the expectation value of the energy momentum tensor, this factorization formula reads

$$\begin{aligned} \langle T^{\mu\nu}(\tau, \eta, \mathbf{x}_\perp) \rangle_{\text{LLog}} = & \int [D\tilde{\rho}_1(x^-, \mathbf{x}_\perp) D\tilde{\rho}_2(x^+, \mathbf{x}_\perp)] \\ & \times W[\tilde{\rho}_1(x^-, \mathbf{x}_\perp)] W[\tilde{\rho}_2(x^+, \mathbf{x}_\perp)] T_{\text{LO}}^{\mu\nu}(\tau, \eta, \mathbf{x}_\perp). \end{aligned} \quad (3.125)$$

¹⁸As opposed to S-matrix elements, that have the *in* vacuum on one side and the *out* vacuum on the other side.

Here also, the $W[\tilde{\rho}_{1,2}(\mathbf{x}^\mp, \mathbf{x}_\perp)]$ are the limiting distributions obtained by evolving the distributions of color sources of the two projectiles down to $\Lambda^\pm \rightarrow 0$. In practice, it is sufficient to evolve them to a sufficiently low cutoff so that all the sources *faster than the local comoving frame* are included in the distributions. Evolving to smaller values of the cutoff has no impact on the final result since the inclusion of these slower color sources do not affect the deposition of energy or momentum at the rapidity η .

3.4 Multigluon correlations at Leading Log accuracy

3.4.1 Introduction

Let us now extend the discussion of the factorization of the leading logarithms of the collision energy to the case of multi-gluon inclusive spectra. The proof follows closely what we have already done for the case of the single inclusive spectrum, and its starting point is again a formula that formally expresses the NLO corrections in terms of the LO result.

However, a delicate aspect of the discussion is the case of correlations between gluons with a wide rapidity separation between them. Indeed, if this rapidity interval is $\alpha_s^{-1} \lesssim \Delta Y$, then the probability of radiating additional gluons in the interval ΔY is of order unity. This radiation leads to corrections that behave like powers of $\alpha_s \Delta Y$, and therefore should be included on the same footing as the leading logarithms of the collision energy. We will see that these terms are also resummed via the JIMWLK evolution of the distributions of color sources of the two projectiles. This observation will lead us to the following striking result: in the collision of two saturated projectiles, all the correlations among the produced gluons are, at leading logarithmic accuracy, correlations that pre-exist in the wavefunctions of the projectiles. Any correlation built up during the collision itself or via final state interactions is a next-to-leading-log effect (i.e. of relative order α_s , but without any enhancement by a large logarithm or rapidity interval).

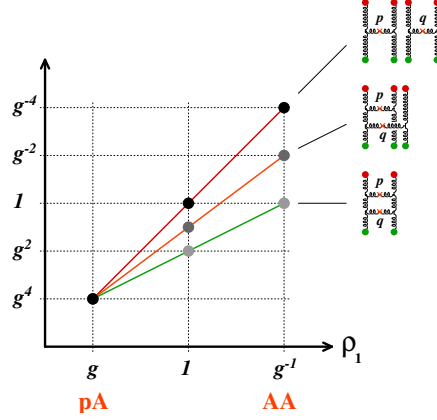
3.4.2 Expressions at LO and NLO

As we have seen in chapter 2, at Leading Order, the n -gluon inclusive spectrum in a fixed configuration of sources $\tilde{\rho}_{1,2}$ is simply the product of n single inclusive spectra:

$$\left. \frac{dN_n}{d^3\mathbf{p}_1 \cdots d^3\mathbf{p}_n} \right|_{\text{LO}} = \prod_{i=1}^n \left. \frac{dN_1}{d^3\mathbf{p}_i} \right|_{\text{LO}}. \quad (3.126)$$

This result is extremely simple, but to be valid it is crucial that both sources $\tilde{\rho}_1$ and $\tilde{\rho}_2$ are strong. If one or both of the sources become weak (i.e. if the number of color sources in at least one of the projectiles is of order unity), this formula must be completed by some additional contributions of the same order. This phenomenon is illustrated in the figure 3.12, where we show how the order of magnitude of three contributions to the 2-gluon spectrum evolve as we decrease the magnitude of the source $\tilde{\rho}_1$ (the source $\tilde{\rho}_2$ is fixed to a value of order g^{-1}). We see on this plot that the case where one collides a dense projectile on a dilute one (as would be the case in some kinematical range in proton-nucleus collisions) is the most complicated situation, since the three diagrams have the same order of magnitude and all contribute at leading order. Although this is not the subject of this manuscript, let us note here that the importance of these extra terms in the calculation of multi-gluon spectra is

Figure 3.12: Evolution of three contributions to the 2-gluon spectrum as one evolves from dense to dilute-dense collisions (i.e. when $\bar{\rho}_1$ goes from g^{-1} to g , while $\bar{\rho}_2$ is fixed and of order g^{-1}).



possibly related to the *pomeron splittings* that also play a role in the discussion of pomeron loops (see [121–127] for partial attempts to derive an effective theory that includes these effects) in the dilute regime.

Each of the factors in the right hand side of eq. (3.126) is obtained from the classical solution of Yang-Mills equations, with null retarded boundary conditions. It is also important to realize that at this order, the multi-gluon spectrum is totally independent of the rapidities of the measured gluons: it does not depend on the position of these rapidities with respect to the rapidities of the two projectiles, nor does it depend on the position of these rapidities relative to one another.

In order to discuss the factorization of large logarithms, we also need the next-to-leading order formula for the multi-gluon spectrum. This formula was derived in the case of a scalar theory in eq. (2.129). As we have seen earlier in this chapter, going from scalar fields to gluons does not change the general structure of such a formula, and one needs only to properly track the color and polarization indices of the fluctuations β_a^μ and $a_{\pm p\lambda a}^\mu$. The other difference between a scalar theory and QCD lies in the detailed form of the operator $a \cdot \mathbb{T}_u$. Therefore, without further discussion, we can directly write the following formula for the NLO correction to the n -gluon inclusive spectrum

$$\begin{aligned} \left. \frac{dN_n}{d^3\mathbf{p}_1 \cdots d^3\mathbf{p}_n} \right|_{\text{NLO}} = & \left[\frac{1}{2} \sum_{\lambda a} \int \frac{d^3\mathbf{k}}{(2\pi)^3 2k} \int_{\Sigma} d^3\mathbf{S}_u d^3\mathbf{S}_v [a_{-k\lambda a} \cdot \mathbb{T}_u] [a_{k\lambda a} \cdot \mathbb{T}_v] \right. \\ & \left. + \int_{\Sigma} d^3\mathbf{S}_u [\beta \cdot \mathbb{T}_u] \right] \prod_i \left. \frac{dN_1}{d^3\mathbf{p}_i} \right|_{\text{LO}} \\ & - \sum_{i < j} \delta(\mathbf{p}_i - \mathbf{p}_j) \left. \frac{dN_1}{d^3\mathbf{p}_i} \right|_{\text{LO}} \prod_{k \neq i, j} \left. \frac{dN_1}{d^3\mathbf{p}_k} \right|_{\text{LO}}. \end{aligned} \quad (3.127)$$

In this identity, the fluctuations β_a^μ and $a_{\pm p\lambda a}^\mu$ are the same as those already introduced in the previous section.

3.4.3 Leading logarithms and factorization

Our next task is to extract the logarithms in this expression. For the terms on the first two lines, this is best done by using the eq. (3.124) derived in the previous section. This formula tells us that the operator enclosed in the square brackets contains logarithms, and indicates that when one integrates out only a small slice of longitudinal momentum modes, just below the cutoffs Λ^\pm , the coefficients in front of these logarithms are nothing but the JIMWLK Hamiltonians of the projectiles at the scales Λ^\pm . The term in the third line is even simpler: since it is a mere product of single inclusive gluon spectra at leading order, it does not contain any logarithm. This term is therefore a NLO correction but not a leading logarithmic correction.

From now on, we can reproduce the reasoning that led us in the previous section to the renormalization group evolution for the single gluon spectrum. We start at cutoff scales Λ_0^\pm , with distributions of sources $W_{\Lambda_0^\pm}[\tilde{\rho}_{1,2}]$. Then, we integrate out the quantum fluctuations whose longitudinal momentum lies in a small slice just below these cutoffs. Thanks to eqs. (3.127) and (3.124), the leading logarithmic part of these quantum corrections can be included simply by modifying the distributions $W_{\Lambda_0^\pm}[\tilde{\rho}_{1,2}]$ according to the JIMWLK equation. One must repeat this process until $\Lambda^\pm \rightarrow 0$, or at least until one has incorporated in these distributions all the color sources that have longitudinal momentum larger than that of the slowest of the gluons $\mathbf{p}_1, \dots, \mathbf{p}_n$. Finally, we end up with the following factorized formula for the inclusive n-gluon spectrum, at leading log accuracy:

$$\left\langle \frac{dN_n}{d^3\mathbf{p}_1 \cdots d^3\mathbf{p}_n} \right\rangle_{\text{LLog}} = \int [D\tilde{\rho}_1(x^-, \mathbf{x}_\perp) D\tilde{\rho}_2(x^+, \mathbf{x}_\perp)] \times W[\tilde{\rho}_1(x^-, \mathbf{x}_\perp)] W[\tilde{\rho}_2(x^+, \mathbf{x}_\perp)] \prod_i \left. \frac{dN_1}{d^3\mathbf{p}_i} \right|_{\text{LO}}. \quad (3.128)$$

As one can see, this formula provides a very simple generalization of our previous result for the single inclusive gluon spectrum. It possesses a very striking property: since the product of LO 1-gluon spectra in the integrand is independent of rapidity, all the rapidity dependence of the n-gluon spectrum is contained in the evolved distributions of the sources $\tilde{\rho}_{1,2}$. In other words, all the rapidity correlations among the gluons produced in the collision are correlations that pre-exist in the wavefunctions of the incoming projectiles. This simple result is valid only for the collision of two densely occupied projectiles, and only at leading logarithmic accuracy. New correlations that cannot be factorized into the distributions W arise if one of the projectiles is dilute or if one considers next-to-leading-log terms. Note also that the dependence on the rapidity differences $y_i - y_j$ between the measured gluons are no different – they are also completely determined by the JIMWLK evolution of the two distributions W . This formula provides another example of the universality of the distributions $W[\tilde{\rho}]$ and of the JIMWLK evolution equation.

It is interesting to see in more detail how the rapidity dependence (or equivalently their x^\pm dependence) of the distributions of sources is transferred into the rapidity dependence of the multi-gluon spectrum. The factor $(dN_1/d^3\mathbf{p})_{\text{LO}}$ depends on the color sources $\tilde{\rho}_{1,2}(x^\mp, \mathbf{x}_\perp)$ for $0 \leq x^\mp \leq 1/p^\pm$ respectively. More precisely, the relevant quantity is the integrated color charge in the strip $0 \leq x^\mp \leq 1/p^\pm$, since the factor $(dN_1/d^3\mathbf{p})_{\text{LO}}$ depends on the color sources only via Wilson lines along the x^- or x^+ axis respectively. Therefore, if one sees the functions $\tilde{\rho}_{1,2}(x^\mp, \mathbf{x}_\perp)$ as *trajectories* with x^\mp playing the role of the time, the n factors in the integrand of eq. (3.128) are sensitive to the integrated color charge along different portions of these trajectories: the larger p^\pm and the smaller the relevant extent in x^\mp is.

This also means that if $p_i^\pm \approx p_j^\pm$, then the gluons i and j are strongly correlated since the corresponding factors in the integrand of eq. (3.128) see very similar integrated color charges. On the contrary, two gluons with a wide separation in rapidity are less correlated, since the corresponding factors do not probe the same integrated charge. The further separated in rapidity they are and the weaker is the correlation, since the portions of $\tilde{\rho}_{1,2}$ -trajectories they are sensitive to differ more and more (or equivalently overlap less and less).

3.4.4 Generating functional

All our results on the multigluon inclusive spectra at leading logarithmic accuracy can be summarized in a simple generating functional. Indeed, the inclusive spectra are the functional derivatives of the following generating functional at the point $z(\mathbf{p}) \equiv 1$,

$$\begin{aligned} \mathcal{F}[z(\mathbf{p})] &= \sum_{n=0}^{\infty} \frac{1}{n!} \int \left[\prod_{i=1}^n d^3 \mathbf{p}_i (z(\mathbf{p}_i) - 1) \right] \left\langle \frac{dN_n}{d^3 \mathbf{p}_1 \cdots d^3 \mathbf{p}_n} \right\rangle_{\text{LL, log}} \\ &= \int [D\tilde{\rho}_1(\mathbf{x}^-, \mathbf{x}_\perp) D\tilde{\rho}_2(\mathbf{x}^+, \mathbf{x}_\perp)] W[\tilde{\rho}_1(\mathbf{x}^-, \mathbf{x}_\perp)] W[\tilde{\rho}_2(\mathbf{x}^+, \mathbf{x}_\perp)] \\ &\quad \times \exp \left[\int d^3 \mathbf{p} (z(\mathbf{p}) - 1) \left. \frac{dN_1}{d^3 \mathbf{p}} \right|_{\text{LO}} \right]. \end{aligned} \quad (3.129)$$

An interesting feature of this generating functional is that the integrand is the exponential of a linear functional of $z(\mathbf{p})$, i.e. the generating functional of a Poisson distribution. The logarithm of a generating functional tells us about the clustering properties of the produced particles: if this logarithm contains a term z^q , then there are clusters of q correlated particles. Therefore, the fact that the logarithm of the integrand is of degree 1 indicates that the only gluon clusters that exist in a given configuration of the sources $\tilde{\rho}_{1,2}$ are clusters of size 1. In other words, gluons are produced independently of one another.

The situation is changed by the average over the configurations of $\tilde{\rho}_{1,2}$, and $\ln \mathcal{F}[z]$ contains terms z^q of arbitrary orders. Thus, the distribution of particles has some non-trivial clustering, but it comes entirely from the correlations that pre-exist in the distributions of color sources of the projectiles – not from the production mechanism itself. This is of course due to the fact that the gluons are produced uncorrelated at leading order, and that the leading log part of higher order corrections –that bring correlations– can be absorbed into the distributions W thanks to factorization.

3.4.5 Multi-point correlations of the energy-momentum tensor

If one sees the Color Glass Condensate as a framework to obtain initial conditions for the hydrodynamical evolution of the matter produced in heavy ion collisions, then one must calculate the value of the energy-momentum tensor on some surface of constant proper time τ . In the section 3.3, we have derived a formula (see eq. (3.125)) for the expectation value of the energy-momentum tensor at a given point (η, \mathbf{x}_\perp) , at leading logarithmic accuracy. This result is sufficient if one wishes to perform a hydrodynamical simulation with an *event averaged* initial condition.

However, this is insufficient in order to study fluctuations. Indeed, since the equations of hydrodynamics are non-linear, solving them for an average initial condition does not lead

to the same result as solving them for an ensemble of initial conditions and performing the average at the end of the hydrodynamical evolution. The latter procedure is the correct one if one wants to study the effects of fluctuations. Therefore, it is necessary to obtain multi-point correlators of the energy-momentum tensor on a surface of fixed τ :

$$\langle T^{\mu_1 \nu_1}(\tau, \eta_1, \mathbf{x}_{1\perp}) \cdots T^{\mu_n \nu_n}(\tau, \eta_n, \mathbf{x}_{n\perp}) \rangle . \quad (3.130)$$

At leading order, in a fixed configuration of the sources $\tilde{\rho}_{1,2}$, this correlator is of order $(Q_s^4/g^2)^n$ and is simply the product of the LO values of $T^{\mu\nu}$ at the n points under consideration:

$$[T^{\mu_1 \nu_1}(\tau, \eta_1, \mathbf{x}_{1\perp}) \cdots T^{\mu_n \nu_n}(\tau, \eta_n, \mathbf{x}_{n\perp})]_{\text{LO}} = \prod_{i=1}^n T_{\text{LO}}^{\mu_i \nu_i}(\tau, \eta_i, \mathbf{x}_{i\perp}) . \quad (3.131)$$

The right hand side of this formula is a product of n disconnected terms, each of them corresponding to one power of the energy-momentum tensor at LO. At Next to Leading Order, there are two types of corrections. Firstly, one can pick up the NLO correction to one of the n factors in the right hand side of the previous formula, while keeping the LO value for the $n - 1$ remaining factors. The second type of correction is made of a gluon connecting two points i and j . When both types of corrections are combined, one gets a simple generalization of eq. (3.123) to the case of n points¹⁹:

$$\begin{aligned} [T^{\mu_1 \nu_1}(\mathbf{x}_1) \cdots T^{\mu_n \nu_n}(\mathbf{x}_n)]_{\text{NLO}} &= \\ &= \left[\frac{1}{2} \sum_{\lambda, a} \int \frac{d^3 \mathbf{k}}{(2\pi)^3 2k} \int_{\Sigma} d^3 \mathbf{S}_u d^3 \mathbf{S}_v [\mathbf{a}_{-k\lambda a} \cdot \mathbb{T}_u] [\mathbf{a}_{+k\lambda a} \cdot \mathbb{T}_v] \right. \\ &\quad \left. + \int_{\Sigma} d^3 \mathbf{S}_u [\boldsymbol{\beta} \cdot \mathbb{T}_u] \right] T_{\text{LO}}^{\mu_1 \nu_1}(\mathbf{x}_1) \cdots T_{\text{LO}}^{\mu_n \nu_n}(\mathbf{x}_n) . \end{aligned} \quad (3.132)$$

The relationship between the LO and NLO contributions to the n -point correlation of the energy-momentum tensor is formally identical to that for the expectation value of $T^{\mu\nu}$ at a single point. Therefore, by using eq. (3.124), we immediately see that the resummation of the leading logarithms of the longitudinal momentum leads to the following factorized formula :

$$\begin{aligned} \langle T^{\mu_1 \nu_1}(\tau, \eta_1, \mathbf{x}_{1\perp}) \cdots T^{\mu_n \nu_n}(\tau, \eta_n, \mathbf{x}_{n\perp}) \rangle_{\text{LLog}} &= \\ &= \int [D\tilde{\rho}_1(x^-, \mathbf{x}_\perp) D\tilde{\rho}_2(x^+, \mathbf{x}_\perp)] W[\tilde{\rho}_1(x^-, \mathbf{x}_\perp)] W[\tilde{\rho}_2(x^+, \mathbf{x}_\perp)] \\ &\quad \times T_{\text{LO}}^{\mu_1 \nu_1}(\tau, \eta_1, \mathbf{x}_{1\perp}) \cdots T_{\text{LO}}^{\mu_n \nu_n}(\tau, \eta_n, \mathbf{x}_{n\perp}) . \end{aligned} \quad (3.133)$$

3.4.6 Generating heavy ion collision events

The formula (3.133) suggests a straightforward procedure in order to build a generator for initial conditions for hydrodynamics. Note that the initial classical color field $\mathcal{A}^\mu(\tau_0, \eta, \mathbf{x}_\perp)$

¹⁹Let us mention here a subtlety in the proof of this formula. A technical step in the derivation requires that all the components of the dressed Schwinger-Keldysh propagators be equal when the endpoints are the points where the value of the energy momentum tensor are needed, e.g. $\mathcal{G}_{++}(\mathbf{x}_i, \mathbf{x}_j) = \mathcal{G}_{+-}(\mathbf{x}_i, \mathbf{x}_j)$. This is equivalent to a vanishing retarded propagator between these pairs of points, which is true in the case of interest to us because there is no causal connection between pairs of points located on the same proper time surface. However, eq. (3.132) would not work for the calculation of a commutator such as $[T^{\mu\nu}(x), T^{\rho\sigma}(y)]$, since this object is non-zero only for time-like intervals. See the section 6.4.3 for an example of computation of a correlator at a time-like separation.

depends on the color charge distributions $\tilde{\rho}_{1,2}$ only via Wilson lines $\Omega_{1,2}$ that integrate all the sources that move faster than the comoving frame at the rapidity η . Thus, if the label 1 denotes the sources moving in the $+z$ direction and the label 2 those moving in the $-z$ direction, Ω_1 integrates $\tilde{\rho}_1$ from the rapidity $y = \eta$ to the beam rapidity of the projectile 1, and Ω_2 integrates $\tilde{\rho}_2$ from the (negative) beam rapidity of the projectile 2 to the rapidity $y = \eta$. For this reason, it is convenient to replace the functional integrations over the sources $\tilde{\rho}_{1,2}$ in eq. (3.133) by functional integrations over the Wilson lines themselves. In order to do this, one needs the formulation of the JIMWLK equation that uses Wilson lines and group Lie derivatives instead of the $\tilde{\rho}$'s themselves [87, 128].

With this in mind, the algorithm for generating such events can be sketched as follows:

- i. Solve the JIMWLK equations in order to obtain the probability distributions for the Wilson lines $\Omega_{1,2}$.
- ii. Pick two Wilson lines $\Omega_{1,2}(\eta, \mathbf{x}_\perp)$ according to these probability distributions.
- iii. Solve the classical Yang-Mills equations with initial conditions built with these Wilson lines. The classical solution must be evolved up to the time at which one wishes to calculate the initial condition for hydrodynamics – typically $\tau \sim Q_s^{-1}$.
- iv. At a proper time of the order of Q_s^{-1} , compute the energy momentum tensor $T^{\mu\nu}$ from the classical field \mathcal{A}^μ .
- v. Repeat steps ii-iv in order to perform the functional integration over $\Omega_{1,2}$ by a Monte-Carlo sampling.

The step i –solving the JIMWLK equation– amounts to obtaining an ensemble of Wilson lines $\{\Omega_{1,2}(\eta, \mathbf{x}_\perp)\}$, given an ensemble of Wilson lines $\{\Omega_{1,2}(\eta_0, \mathbf{x}_\perp)\}$ at a rapidity close to the fragmentation region of the projectiles. This can be done by interpreting the JIMWLK equation as a diffusion equation on the space of mappings from \mathbb{R}^2 to the gauge group $SU(N)$, the rapidity η playing the role of the *time* in this diffusion process [87]. From this formulation, it is possible to turn the JIMWLK equation into a Langevin equation for individual configurations $\Omega_{1,2}(\eta, \mathbf{x}_\perp)$ of the Wilson lines. Thus, each element $\Omega_{1,2}(\eta_0, \mathbf{x}_\perp)$ of the initial ensemble is the starting point of a random walk, and it is sufficient to look at where these points have moved at a *time* η in order to obtain the ensemble of configurations evolved at a different rapidity. This method of solving the JIMWLK equation has been implemented by Rummukainen and Weigert in [88]. The approach of [88] has recently been repeated independently in [89] and [90], and solving the JIMWLK equation is now becoming routinely doable in applications to phenomenology.

Chapter 4

RHIC phenomenology



e now explore some of the consequences of the factorization results obtained in the previous chapter, when applied to the description of high energy heavy ion collisions. We consider only observables that are sensitive to the physics at early stages of the evolution after the collision, and which are the least affected by the evolution at later stages.

Let us try to characterize these observables. The color glass condensate can only make predictions regarding the evolution of the matter produced in heavy ion collisions up to a proper time of the order of $\tau \sim Q_s^{-1}$. Beyond this time, one must use another description –e.g. some flavor of kinetic theory or of hydrodynamics– which is beyond the scope of the CGC. Moreover, it is expected that the system evolves towards a state close to local thermal equilibrium, which means that it loses memory of the details of its initial stages, except for a few quantities preserved by conservation laws. Therefore, many observables are unsuitable for the purpose of testing the predictions of the color glass condensate, since they are irremediably lost in the thermalization process.

After a general discussion of the structure of the classical chromo- electric and magnetic fields at early times, we will focus on two observables for which the CGC can make predictions. The first one is the 2-particle correlation function, especially in the situation where the two particles are separated by a large rapidity interval. Indeed, in this configuration, a simple causality argument indicates that the correlation must have been created at early times – making the observation of these long range rapidity correlations a very good probe of the color glass condensate.

The second observable we shall consider is the multiplicity distribution in heavy ion collisions. It has been observed experimentally that the multiplicity is well described by a negative binomial distribution, and we will show that this type of distribution is obtained quite naturally in the CGC framework.

4.1 Glasma and color flux tubes

From the initial conditions for the classical color field on the forward light-cone, given in eqs. (3.31) and (3.32) of section 3.1.3, one can calculate the initial value of the chromo-electric and chromo-magnetic fields [129]. One finds that the transverse components of both

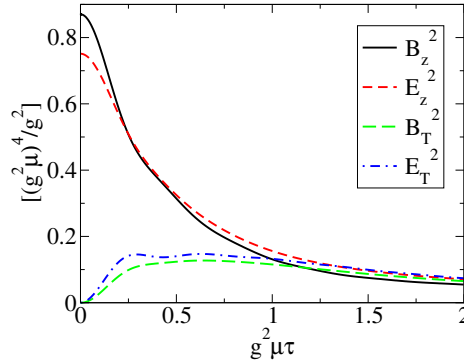
fields are zero at $\tau = 0^+$, while their longitudinal components are non-zero:

$$\begin{aligned} \mathbf{E}^i &= \mathbf{B}^i = 0, \\ \mathbf{E}^z &= ig[\mathcal{A}_1^i(x), \mathcal{A}_2^i(x)], \\ \mathbf{B}^z &= ig\epsilon^{ij}[\mathcal{A}_1^i(x), \mathcal{A}_2^j(x)], \end{aligned} \quad (4.1)$$

where ϵ^{ij} is the totally antisymmetric tensor in two dimensions, normalized to $\epsilon^{12} = 1$. One sees that the non-zero components of these fields are proportional to commutators, and would therefore be zero in an abelian gauge theory like QED. Indeed, it is well known in QED that the gauge field inside the forward light-cone is simply the superposition of the two pure gauge fields \mathcal{A}_1^i and \mathcal{A}_2^i and is a pure gauge field itself – therefore, in QED the gauge field in the forward light-cone does not carry any field strength and the corresponding components of the electric and magnetic field are all zero. Physically, this means that no photon can be produced¹ when two abelian Weizäcker-Williams fields cross each other in the collision process. In contrast, this is perfectly possible in QCD since gluons carry a color charge.

In order to go beyond $\tau = 0^+$, one must solve the Yang-Mills equations numerically. The results are shown in the figure 4.1. This numerical simulation confirms that all the trans-

Figure 4.1: Classical field components at early times. From [129].

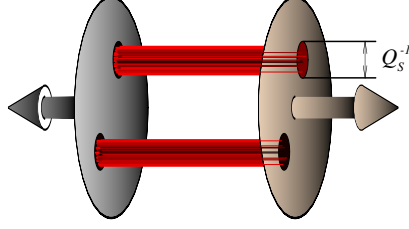


verse components vanish at $\tau = 0^+$, and shows that it takes a time of the order of Q_s^{-1} (the parameter $g^2 \mu$ in the figure is equivalent to Q_s , up to a factor of order one) for all the components to reach values that are of comparable magnitude. Therefore, during most of the period where the color glass condensate description is relevant, the chromo-electric and magnetic fields are predominantly longitudinal. Another crucial property of these early time fields is that they do not depend on the rapidity² η . Thus, one can picture this situation as illustrated in the figure 4.2, where one has longitudinal *color flux tubes* – i.e. field configurations where all the field lines are parallel to the collision axis. What determines the diameter of these tubes is the correlation length of the color charges $\tilde{\rho}_{1,2}$ in the transverse plane. It has

¹Naturally, this is only true at this order of the expansion in the coupling constant. At higher orders, photons can be emitted via a fermion loop.

²This property of invariance under boosts in the longitudinal direction is broken by the leading log quantum corrections whose resummation has been discussed in the previous chapter. In particular, after one has resummed the leading logarithmic corrections, the fields depend on the rapidity at which they are measured. However, this rapidity dependence is significant only for rapidity variations of the order of $\Delta\eta \sim \alpha_s^{-1}$ or larger.

Figure 4.2: Topology of the field lines shortly after the collision.



been shown [130] that in the CGC, the quantum evolution leads to a screening of these color charges at distances $r \geq Q_s^{-1}$. This is thus the effective diameter of the flux tubes. Such a configuration of chromo-electric and magnetic color fields has been named *glasma* in [129], a contraction of the words *glass* and *plasma*, justified by its position as an intermediate stage between the color glass condensate that describes the wavefunctions of the incoming nuclei, and the quark-gluon plasma that is formed later on.

It is also interesting to look in detail at the components of the energy-momentum tensor, whose expression at leading order is

$$T_{\text{lo}}^{\mu\nu} = \frac{1}{4} g^{\mu\nu} \mathcal{F}^{\lambda\sigma} \mathcal{F}_{\lambda\sigma} - \mathcal{F}^{\mu\lambda} \mathcal{F}^{\nu}_{\lambda} . \quad (4.2)$$

By an explicit calculation [129], one can obtain analytically its value at the initial time $\tau = 0^+$,

$$T_{\text{lo}}^{\mu\nu} = \frac{\mathbf{E}_z^2 + \mathbf{B}_z^2}{2} \times \text{diag}(1, 1, 1, -1) . \quad (4.3)$$

Naturally, this tensor is traceless, as expected for the energy-momentum tensor in QCD in a classical approximation³. A remarkable feature of this tensor is that it has a negative longitudinal pressure, and is therefore quite far from the situation one would need to have an ideal fluid – where all the components of the pressure would be equal and positive.

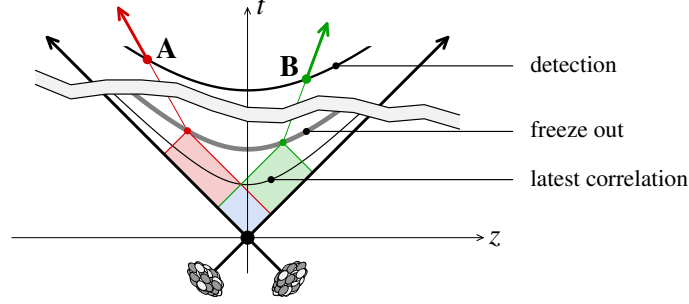
Note finally that this picture of color flux tubes has many similarities with the old string description of hadronic collisions (see for instance [131–134]). Two things are new however compared to these old models: one has here a perturbative QCD-based description of the dynamics of the collision, and there is also a chromo-magnetic field of the same magnitude as the chromo-electric field (string models only have the electric component of the field). Another essential difference is the diameter of a string in these models (typically, $r \sim \Lambda_{\text{QCD}}^{-1}$, since the underlying dynamics was thought to be non-perturbative and related to confinement), which is much larger than the diameter of a flux tube in the CGC ($r \sim Q_s^{-1}$, where $Q_s \gg \Lambda_{\text{QCD}}$). To pursue the analogy further, one can also notice that the negative longitudinal pressure in the glasma fields can be identified to a string tension, the parameter that characterizes the energy per unit length of the hadronic strings. Moreover, in hadronic string models, the string breaks via the production of $q\bar{q}$ pairs by the Schwinger mechanism. One can prove [102] that in the CGC approach, the 1-loop corrections to the gluon spectrum contain the Schwinger contribution to the production of gluon pairs.

³The Yang-Mills Lagrangian has an exact scale invariance. This implies that the energy-momentum tensor constructed from solutions of the classical equation of motion is traceless. This property may be broken by quark masses and by running coupling corrections – both of which are effects that come into play at higher orders.

4.2 Long range rapidity correlations

4.2.1 Rapidity correlations and early stages of the collision

Figure 4.3: Causal relationship between a pair of particles separated by a large rapidity interval.



In the introduction of this chapter, we have stated that correlations between particles can only be produced at early times if the rapidity separation between the particles is large. This is illustrated in the figure 4.3. There, a pair of particles A and B are detected with respective momentum rapidities y_A and y_B . In heavy ion collisions, there is a *freeze out* time $\tau_{f.o.}$ after which the particle density is too small to allow interactions. Therefore, between this freeze out time and the time of their detection, the particles A and B simply propagate on straight lines at constant velocity. Any event that had an influence on these particles must be located inside a cone whose tip is the position of the particle on the freeze out surface, and whose opening angle is determined by the speed of light. This cone plays the role of an *event horizon* for the particle under consideration: any event located outside of this cone is not visible to an observer comoving with the particle. Any event that induces a correlation between the particles A and B must lie within the intersection of the event horizons of the two particles. From the figure 4.3, it is straightforward to see that there exists a maximal time for this intersection. Simple geometry tells us that this maximal time⁴ is

$$\tau_{\max} = \tau_{f.o.} e^{-|y_A - y_B|/2}. \quad (4.4)$$

Note that one assumes in this argument that particles with a momentum rapidity y come from a point of spatial rapidity $\eta = y$ on the freeze-out surface. This is a good approximation for a nearly boost invariant flow of the particles, since the local thermal motion blurs the correspondence between η and y at most by an amount of order unity.

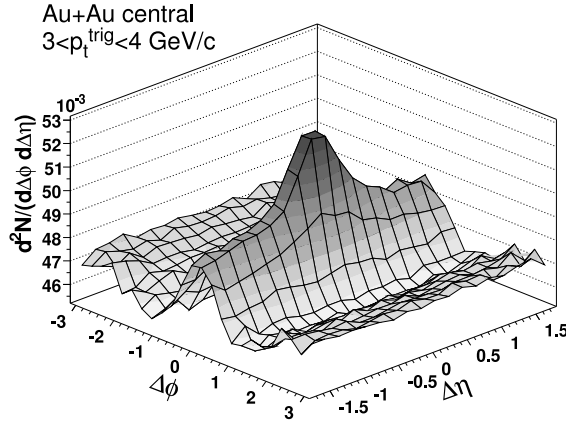
A reasonable estimate of the freeze out time for heavy ion collisions at RHIC energy is $\tau_{f.o.} \sim 10$ fm/c. Therefore, if a correlation is observed between particles separated in rapidity by $|y_A - y_B| = 4$, it must have been produced by an event that occurred at a time $\tau \leq 1.4$ fm/c. For a separation $|y_A - y_B| = 6$, this limit would become $\tau \leq 0.5$ fm/c. One sees the great potential that these correlations have in telling us something about the earliest

⁴Note that processes taking place *before* the collision –i.e. in the evolution of the wavefunctions of the projectiles– can also be responsible for this kind of correlation, since they lie also inside the intersection of the two event horizons.

stages of the evolution after and/or before the collision⁵: because the rapidity interval enters in an exponential in the above bound, the maximal time for the creation of the correlation decreases extremely fast as one increases the rapidity interval.

4.2.2 RHIC data

Figure 4.4: 2-hadron correlations measured by the STAR experiment. From [135].



Two-hadron correlations in heavy ion collisions have been studied in detail by three RHIC collaborations: STAR [135–138], PHENIX [139] and PHOBOS [140]. A common observation in central collisions is the existence of long range rapidity correlations –that span at least four units of rapidity– in conjunction with a fairly narrow correlation in azimuthal angle (see the figure 4.4). This striking feature of the 2-hadron correlation function has been named the *ridge*. The same measurement, when done in proton-proton collisions, shows only a narrow peak centered at $\Delta\eta = \Delta\phi = 0$. Moreover, this peak is symmetrical in all directions, unlike the elongated structure seen in nucleus-nucleus collisions. A similar ridge has also been seen by the CMS collaboration [141] in proton-proton collisions at LHC energy. There, the correlation is much weaker than in nucleus-nucleus collisions, and requires that one triggers on high multiplicity events in order to be seen.

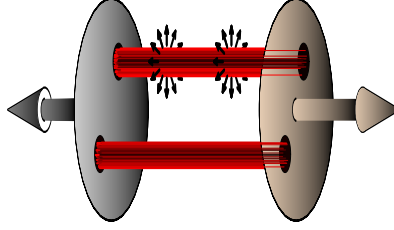
Note that there are two ways of performing this measurement: triggered or untriggered. In the triggered measurement, one first selects a hadron that fulfills some criterion (usually that its transverse momentum exceeds a given value), and then one looks at the distribution of the other hadrons relative to the first one. In the untriggered measurement, one considers all the pairs of hadrons in a given event. The ridge is observed in both measurements, but the triggered correlation function displays in addition to the ridge a narrow central peak similar to the one observed in proton-proton collisions. This narrow peak is interpreted as an effect of jet fragmentation, and will not be discussed further here.

⁵This is analogous to the way angular correlations observed in the Cosmic Microwave Background (CMB) provide us with information about what occurred at the time of inflation in the expansion of the early universe: this is possible because points that appear far apart on the sky today have not been in causal contact since the inflationary epoch.

4.2.3 Qualitative explanation

First of all, as explained earlier, the measured long range correlation in rapidity can only be explained by features that existed at very early times. This makes the color glass condensate the most suitable place to look for an explanation of this structure.

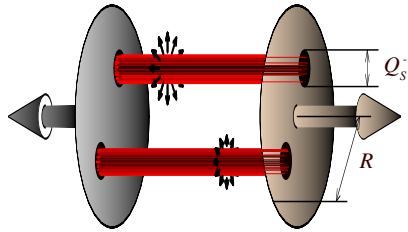
Figure 4.5: Correlation between particles emitted at various rapidities in a single flux tube.



A crucial property of the glasma color fields is their independence with respect to rapidity (at leading order). This translates into a correlation between particles produced at all rapidities. Consider for the sake of the argument a single flux tube (see the figure 4.5). This flux tube is characterized by a certain chromo-electrical field \mathbf{E} and magnetic field \mathbf{B} , which have the same value at all rapidities. Locally, the mechanism of particle production from classical fields depends only on the value of these fields, which means that particles are emitted in this tube with the same intensity at all rapidities, hence the correlation.

It is also easy to understand by the same qualitative argument how the strength of the correlation varies with the centrality of the collision. For this, one needs to realize that there is no correlation between the particles emitted from distinct flux tubes (see the figure 4.6). This is because the color fields in two distinct tubes are not correlated – simply because our definition of the diameter of a single flux tube is precisely based on the color correlation length in the transverse plane. Therefore, a given pair of particles exhibits a correlation only

Figure 4.6: Particles emitted from separate flux tubes are not correlated.



if they come from the same flux tube. The total number of pairs in a given event scales like the square of the transverse area S_{\perp} ,

$$N_{\text{all pairs}} \propto S_{\perp}^2, \quad (4.5)$$

while the number of pairs coming from the same flux tube is the total transverse area (the first particle in the pair can be produced anywhere) multiplied by the typical area of one flux tube

(since the second particle has to be in the same tube as the first one), i.e. Q_s^{-2} ,

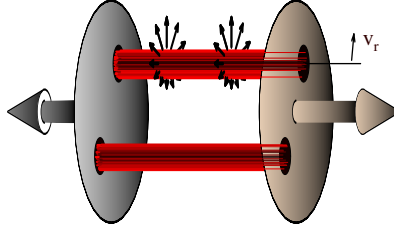
$$N_{\text{same tube}} \propto S_{\perp} Q_s^{-2}. \quad (4.6)$$

Therefore, the CGC prediction for the strength of the 2-particle correlation normalized by the square of the particle yield is

$$\text{Correlation} \propto \frac{1}{S_{\perp} Q_s^2}. \quad (4.7)$$

At this point, we have a natural explanation for the existence of a long range rapidity correlation, and an estimate for its strength. However, as one can see in the figure 4.5, one would naively expect this correlation to be flat in the azimuthal angle difference $\Delta\phi$. Indeed, on the average, flux tubes emit particles isotropically in ϕ . Therefore, there should not be a preferred direction of emission of one particle in the pair relative to the second particle. The

Figure 4.7: Collimation in azimuthal angle due to radial flow.



collimation in $\Delta\phi$ of the 2-particle correlation has a natural explanation from the evolution of the system at later stages⁶. It is important to recall the existence of a non-zero transverse pressure gradient in the system, whose effect is to push the matter outwards – a phenomenon known as *radial flow*. The fact that the matter is flowing radially outwards is what collimates the correlation in $\Delta\phi$, as illustrated in the figure 4.7. Indeed, the spectra of particles emitted at two rapidities from the same tube are both collimated in the same manner (here, we assume that the radial flow velocity v_r depends only weakly on the rapidity). Therefore, after the radial flow has developed, there is a greater probability to find two particles emitted from the same tube with nearby azimuthal angles.

4.2.4 Semi-quantitative description

After having seen that the color glass condensate framework offers a natural explanation for the ridge structure observed in 2-particle correlations in high energy heavy ion collisions, let us now turn to a semi-quantitative calculation of the effect. The main result of the section 3.4 tells us that the 2-particle inclusive spectrum, at leading logarithmic accuracy, reads (see eq. (3.128), applied here for $n = 2$):

$$\left\langle \frac{dN_2}{d^3\mathbf{p} d^3\mathbf{q}} \right\rangle_{\text{LLog}} = \int [D\tilde{\rho}_1 D\tilde{\rho}_2] W[\tilde{\rho}_1] W[\tilde{\rho}_2] \left. \frac{dN_1}{d^3\mathbf{p}} \right|_{\text{LO}} \times \left. \frac{dN_1}{d^3\mathbf{q}} \right|_{\text{LO}}. \quad (4.8)$$

⁶Note that this is not in contradiction with the causality argument developed earlier in the chapter. Only the correlation in rapidity needs to be produced by some very early time process. The correlation in azimuth can be created at any time.

Note that the interesting quantity to discuss the ridge is not the 2-gluon spectrum itself, but the correlated part defined as

$$C(\mathbf{p}, \mathbf{q}) \equiv \left\langle \frac{dN_2}{d^3\mathbf{p}d^3\mathbf{q}} \right\rangle_{\text{LLo}} - \left\langle \frac{dN_1}{d^3\mathbf{p}} \right\rangle_{\text{LLo}} \left\langle \frac{dN_1}{d^3\mathbf{q}} \right\rangle_{\text{LLo}}. \quad (4.9)$$

At this point, the only way to pursue the calculation without making further approximations is numerical [142]. This involves solving the JIMWLK equation in order to obtain the distributions $W[\tilde{\rho}_{1,2}]$ and solving the Yang-Mills equations for fixed sources $\tilde{\rho}_{1,2}$ – both of which are quite challenging in practice (in [142], only the latter was done exactly – the distributions W were taken from the MV model rather than from solving the JIMWLK equation).

It is however possible to perform a simple approximate analytical calculation in order to assess semi-quantitatively the effects that lead to the ridge. For this, let us assume that $|\mathbf{p}|, |\mathbf{q}| \gg Q_s$. In this regime, non-linearities in the solution of the Yang-Mills equations become small and it has a simple analytical form in terms of $\tilde{\rho}_{1,2}$. In addition, to avoid the complications associated with solving the JIMWLK equation, we simply disregard the effects of quantum evolution and use the McLerran-Venugopalan Gaussian model for the distributions of $\tilde{\rho}_{1,2}$. In this large momentum approximation, the Fourier transform of the classical gauge field is

$$\mathcal{A}_a^\mu(\mathbf{p}) = \frac{igf^{abc}}{p^2} \int \frac{d^3\mathbf{k}_\perp}{(2\pi)^2} L^\mu(\mathbf{p}, \mathbf{k}_\perp) \frac{\tilde{\rho}_{1b}(\mathbf{k}_\perp)}{\mathbf{k}_\perp^2} \frac{\tilde{\rho}_{2c}(\mathbf{p}_\perp - \mathbf{k}_\perp)}{(\mathbf{p}_\perp - \mathbf{k}_\perp)^2}, \quad (4.10)$$

where L^μ denotes the so called Lipatov effective vertex. Here, we won't need the components of this 4-vector – the only properties we will use are

$$\begin{aligned} L^\mu(\mathbf{p}, \mathbf{k}_\perp) &= L^\mu(\mathbf{p}, \mathbf{p}_\perp - \mathbf{k}_\perp), \\ L^\mu(\mathbf{p}, \mathbf{k}_\perp) L_\mu(\mathbf{p}, \mathbf{k}_\perp) &= -4 \frac{\mathbf{k}_\perp^2 (\mathbf{p}_\perp - \mathbf{k}_\perp)^2}{\mathbf{p}_\perp^2}. \end{aligned} \quad (4.11)$$

When inserted in the formula for the single particle spectrum, and after summing over the polarization and color of the produced gluon, this result leads to

$$\begin{aligned} \left. \frac{dN_1}{d^3\mathbf{p}} \right|_{\text{Lo}} &= -g^2 f^{abc} f^{ade} \int \frac{d^2\mathbf{k}_\perp}{(2\pi)^2} \frac{d^2\mathbf{l}_\perp}{(2\pi)^2} L^\mu(\mathbf{p}, \mathbf{k}_\perp) L_\mu(\mathbf{p}, \mathbf{l}_\perp) \\ &\quad \times \frac{\tilde{\rho}_{1b}(\mathbf{k}_\perp)}{\mathbf{k}_\perp^2} \frac{\tilde{\rho}_{2c}(\mathbf{p}_\perp - \mathbf{k}_\perp)}{(\mathbf{p}_\perp - \mathbf{k}_\perp)^2} \frac{\tilde{\rho}_{1d}(\mathbf{l}_\perp)}{\mathbf{l}_\perp^2} \frac{\tilde{\rho}_{2e}(\mathbf{p}_\perp - \mathbf{l}_\perp)}{(\mathbf{p}_\perp - \mathbf{l}_\perp)^2} \end{aligned} \quad (4.12)$$

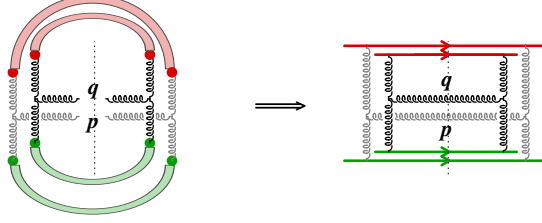
for a fixed configuration of the color sources $\tilde{\rho}_{1,2}$.

The next step is to insert this formula into eq. (4.8) and to perform an average over the sources $\tilde{\rho}_{1,2}$, using the Gaussian distribution of the MV model (see eq. (1.15)) as a simplifying assumption. In the MV model, the average of a functional of $\tilde{\rho}_{1,2}$ amounts to perform all the possible pairwise contractions, with the following elementary building block

$$\langle \tilde{\rho}_{1a}(\mathbf{k}_\perp) \tilde{\rho}_{1b}(\mathbf{l}_\perp) \rangle = (2\pi)^2 \delta(\mathbf{k}_\perp + \mathbf{l}_\perp) \delta_{ab} g^4 \mu^2, \quad (4.13)$$

where μ^2 is the only parameter in the Gaussian distribution. The saturation scale Q_s is related to μ^2 by $Q_s^2 \sim g^4 \mu^2$.

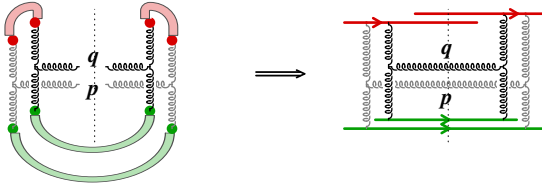
Figure 4.8: *Trivial color connection.* This type of connection between the sources leads to a non correlated contribution to the 2-gluon spectrum.



In eq. (4.8), we must perform Gaussian averages of an expression that contains four powers of $\tilde{\rho}_1$ and four powers of $\tilde{\rho}_2$. Since this requires to make all the possible pairwise links among four factors (both for $\tilde{\rho}_1$ and $\tilde{\rho}_2$), there are three possibilities for $\tilde{\rho}_1$ and three possibilities for $\tilde{\rho}_2$, hence 9 terms in total. One of these terms is trivial, illustrated in the figure 4.8, since it is a disconnected contribution that has no correlation between the two produced gluons. This term therefore does not contribute to $C(\mathbf{p}, \mathbf{q})$.

Of the remaining 8 terms, four give identical leading contributions in the region where $|\mathbf{p}_\perp|, |\mathbf{q}_\perp| \gg Q_s$. Two of these terms, as shown in figure 4.9, have a topology such that a single source in the amplitude is attached to the two produced gluons⁷. Note that the sources on opposite sides of the cut may be localized at different transverse positions. The other

Figure 4.9: Two gluons are emitted from the same source line in the amplitude and likewise in the complex conjugate amplitude. This emission however occurs at different spatial positions for the sources, which are localized in a transverse area of size Q_s^{-1} . There is an identical contribution with $\tilde{\rho}_1 \leftrightarrow \tilde{\rho}_2$.



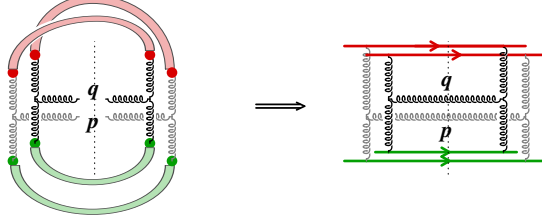
two terms with leading contributions have the structure of an interference graph depicted in figure 4.10. Of the four remaining terms, two are suppressed respectively by additional powers of p_\perp^{-1} or q_\perp^{-1} and two give δ -function contributions for $\mathbf{p}_\perp = \pm \mathbf{q}_\perp$. The delta function terms are also suppressed relative to the terms we keep at large p_\perp and q_\perp .⁸

An explicit calculation of the four leading contributions gives the following result for the

⁷One may characterize this contribution as *single diffractive*, however this denomination is misleading here since we are computing an inclusive spectrum and therefore the unmeasured gluons produced along with the two tagged ones most likely prevent the appearance of a gap between the projectile and the measured gluon.

⁸Moreover, they would give a contribution not localized in the transverse coordinate, so that they would give a flat background once flow effects are included.

Figure 4.10: *Interference contribution in which the transverse positions of the participating sources are exchanged in the complex conjugate amplitude for $\tilde{\rho}_2$ while they are the same for $\tilde{\rho}_1$. There is an identical contribution for $\tilde{\rho}_1 \leftrightarrow \tilde{\rho}_2$.*



2-gluon correlation in the Color Glass Condensate approach:

$$C(\mathbf{p}, \mathbf{q}) = \frac{S_{\perp}}{(2\pi)^6} \frac{(g^2\mu)^8}{g^4 Q_s^2} \frac{\pi N_c^2 (N_c^2 - 1)}{|\mathbf{p}||\mathbf{q}| p_{\perp}^4 q_{\perp}^4}, \quad (4.14)$$

where S_{\perp} is the transverse area of the interacting region (i.e. simply $S_{\perp} = \pi R^2$ for a central collision of identical nuclei). The Q_s^2 in the denominator arose from the regulation of an integral that diverges in the infrared, for which a cutoff at the scale Q_s was introduced by hand⁹. As a consequence, the numerical prefactor in $C(\mathbf{p}, \mathbf{q})$ is somewhat uncertain. Note also that the factors $|\mathbf{p}||\mathbf{q}|$ in the denominators are there due to our choice of using $d^3\mathbf{p}$ as the 1-particle measure instead of $dy_p d^2\mathbf{p}_{\perp}$ ($|\mathbf{p}|$ is the Jacobian that converts one measure into the other). The relation of $g^2\mu$ to Q_s can be quantified numerically by computing Wilson line correlators in the nuclear wavefunction. A careful comparison [114] (see also [143]) gives $Q_s \approx 0.57 g^2\mu$. It is instructive to express the result in eq. (4.14) in terms of the inclusive single gluon spectrum. This is given by the Gunion-Bertsch formula [144], and has been computed previously in the CGC framework [103–105, 145] to have the form

$$\left\langle \frac{dN_1}{d^3\mathbf{p}} \right\rangle = \frac{S_{\perp}}{4\pi^4} \frac{(g^2\mu)^4}{g^2} \frac{N_c(N_c^2 - 1)}{|\mathbf{p}| p_{\perp}^4} \ln \left(\frac{p_{\perp}}{Q_s} \right). \quad (4.15)$$

Therefore, up to logarithms that we do not control in eq. (4.14), we can write:

$$C(\mathbf{p}, \mathbf{q}) = \frac{\kappa}{S_{\perp} Q_s^2} \left\langle \frac{dN_1}{d^3\mathbf{p}} \right\rangle \left\langle \frac{dN_1}{d^3\mathbf{q}} \right\rangle, \quad (4.16)$$

with a numerical constant $\kappa \sim 4$. The quantity which is measured experimentally [146] (and displayed in the figure 4.4) is

$$\frac{\Delta\rho}{\sqrt{\rho_{\text{ref}}}} \equiv C(\mathbf{p}, \mathbf{q}) \frac{\left\langle \frac{dN_1}{dy} \right\rangle}{\left\langle \frac{dN_1}{d^3\mathbf{p}} \right\rangle \left\langle \frac{dN_1}{d^3\mathbf{q}} \right\rangle}. \quad (4.17)$$

Parametrically, one can write

$$\left\langle \frac{dN_1}{dy} \right\rangle = \frac{\kappa'}{\alpha_s} S_{\perp} Q_s^2, \quad (4.18)$$

⁹In the McLerran-Venugopalan model, the only natural infrared cutoff is at the scale set by the nucleon size, i.e. at Λ_{QCD} . However, it has been shown [130] that quantum evolution leads to color screening at transverse distances of the order of Q_s^{-1} . We have implemented this feature of the CGC by hand here.

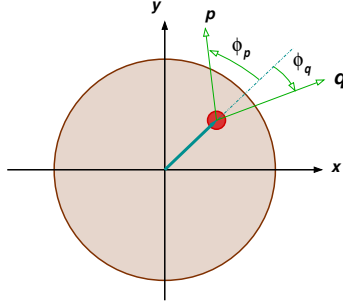
with $\kappa' \sim 0.075$ for an $SU(3)$ gauge theory. Therefore, one gets

$$\frac{\Delta\rho}{\sqrt{\rho_{\text{ref}}}} = \frac{K_N}{\alpha_s}, \quad (4.19)$$

with $K_N \approx \kappa\kappa' \approx 0.3$. Note however that our computation was performed for large momenta $p_\perp, q_\perp \gg Q_s$ while we are interested in the $p_\perp, q_\perp \lesssim Q_s$ region. While we expect the structure of eq. (4.19) to be quite robust, as mentioned earlier, we cannot trust the accuracy of this prefactor. We will therefore only assume it is a number of order unity to be determined by a more accurate numerical computation.

This relationship is basically a consequence of dimensionality: the correlations are due to a classical effect and there is only one dimensional scale which characterizes the Glasma. The expression in eq. (4.17) is very interesting because it is independent both of the rapidities¹⁰ y_p and y_q of the particles as well as of their azimuthal angles ϕ_p and ϕ_q respectively. It confirms our picture of flux tubes of transverse size Q_s^{-1} stretching between the two nuclei (as shown in figure 4.5) and emitting particles isotropically, with equal probability along their length. This is not the full picture though. In the high parton density environment created in central heavy ion collisions, the pressure created by interactions among those particles has a gradient that leads to collective radial flow. The particles emitted by the Glasma tubes will also experience this collective flow. As we shall now discuss, this collimates the relative azimuthal distribution of the pairs.

Figure 4.11: Notations for the azimuthal angles.



We define the particles azimuthal angles $\phi_{p,q}$ with respect to the radius of the point of emission (see the figure 4.11), and we denote $\zeta_{p,q} \equiv -\ln(\tan(\phi_{p,q}/2))$ the pseudo-rapidities of the particles in the radial direction. It is important to note that the two particles will experience the same radial boost since they are localized within Q_s^{-1} of each other in the transverse plane—indeed, they come from the same flux tube, and we assume that the radial flow velocity does not depend on rapidity. Expressing the angular distribution (which is independent of ϕ_p and ϕ_q) in terms of these variables, and boosting it in the direction of radial flow, one obtains¹¹

$$C(\mathbf{p}, \mathbf{q}) \propto \frac{1}{\cosh(\zeta_p) \cosh(\zeta_q)} \xrightarrow{\text{Boost}} \frac{1}{\cosh(\zeta_p - \zeta_B) \cosh(\zeta_q - \zeta_B)}. \quad (4.20)$$

¹⁰Quantum corrections, not considered here, will introduce a modest dependence on rapidity over scales $\Delta y \sim \alpha_s^{-1}$.

¹¹The hyperbolic cosines in the denominator come from the Jacobian of the change of variables $\phi \rightarrow \zeta$.

Here, ζ_B is the rapidity of the radial boost and is given by $\tanh(\zeta_B) \equiv v_r$, where v_r is the radial flow velocity. Defining $\Phi \equiv (\phi_p + \phi_q)/2$, $\Delta\phi \equiv \phi_p - \phi_q$, and re-expressing the boosted 2-gluon distribution in terms of Φ and $\Delta\phi$, one can re-write eq. (4.17) as

$$\frac{\Delta\rho}{\sqrt{\rho_{\text{ref}}}} = \frac{K_N}{\alpha_s} \frac{\cosh \zeta_p \cosh \zeta_q}{\cosh(\zeta_p - \zeta_B) \cosh(\zeta_q - \zeta_B)} . \quad (4.21)$$

Substituting $\cosh \zeta_p = 1/\sin \phi_p$ and $\sinh \zeta_p = \cos \phi_p / \sin \phi_p$, we finally obtain

$$\begin{aligned} \int_{-\pi}^{+\pi} \frac{d\Phi}{2\pi} \frac{\Delta\rho}{\sqrt{\rho_{\text{ref}}}} &= \\ &= \frac{K_N}{\alpha_s} \int_{-\pi}^{+\pi} \frac{d\Phi}{\left[\cosh \zeta_B - \cos(\Phi + \frac{\Delta\phi}{2}) \sinh \zeta_B \right] \left[\cosh \zeta_B - \cos(\Phi - \frac{\Delta\phi}{2}) \sinh \zeta_B \right]} . \end{aligned} \quad (4.22)$$

The integral over Φ leads to the following result for the 2-gluon correlation, averaged over the mean angle Φ

$$\left\langle \frac{\Delta\rho}{\sqrt{\rho_{\text{ref}}}} \right\rangle_{\Phi} = \frac{K_N}{\alpha_s} \frac{\cosh \zeta_B}{\cosh^2 \zeta_B - \sinh^2 \zeta_B \cos^2 \frac{\Delta\phi}{2}} . \quad (4.23)$$

In the particular cases of $\Delta\phi = 0$ or $\Delta\phi = \pi$, the results are

$$\begin{aligned} \frac{\Delta\rho}{\sqrt{\rho_{\text{ref}}}}(\Delta\phi = 0) &= \frac{K_N}{\alpha_s} \gamma_B \\ \frac{\Delta\rho}{\sqrt{\rho_{\text{ref}}}}(\Delta\phi = \pi) &= \frac{K_N}{\alpha_s} \frac{1}{\gamma_B} , \end{aligned} \quad (4.24)$$

where $\gamma_B \equiv \cosh \zeta_B$ is the γ -factor of the radial boost. Hence, the amplitude of the peak, relative to the pedestal, is given by

$$\mathcal{A} = \frac{K_N}{\alpha_s} (\gamma_B - \gamma_B^{-1}) . \quad (4.25)$$

Thus, we see clearly here that there is a collimation in $\Delta\phi$ of the 2-gluon correlation, caused by the radial flow.

From blast wave fits to the RHIC data, the PHENIX collaboration [147] has extracted the average transverse velocity $\langle v_r \rangle$ as a function of the number of participants in a heavy ion collision. To estimate the centrality dependence of the coupling¹², $\alpha_s(Q_s)$, we note that the square of the saturation momentum is $Q_s^2 \simeq 1\text{-}1.3 \text{ GeV}^2$ for central Au+Au collisions at full RHIC energy, decreasing like $N_{\text{part}}^{1/3}$ [148, 149] towards peripheral collisions¹³. The magnitude of \mathcal{A} in central collisions fixes $K_N \sim 0.1$, in the ballpark of our naive earlier estimate. The resulting $\mathcal{A}(N_{\text{part}})$ is compared to preliminary STAR data in the figure 4.12, which shows a fairly good agreement with RHIC data.

¹²We determine the running coupling from the one-loop QCD β -function with $\beta_0 = 11N_C - 2N_f = 27$, assuming $\Lambda_{\text{QCD}} \simeq 200 \text{ MeV}$.

¹³The dependence of Q_s^2 on centrality is in fact more complex (we refer to refs. [113, 150, 151]) but the simplified form $Q_s^2 \sim N_{\text{part}}^{1/3}$ is sufficient for the present purposes.

Figure 4.12: Evolution of the amplitude of the ridge (peak at $\Delta\phi = 0$ relative to pedestal at $\Delta\phi = \pi$) with the number of participants.

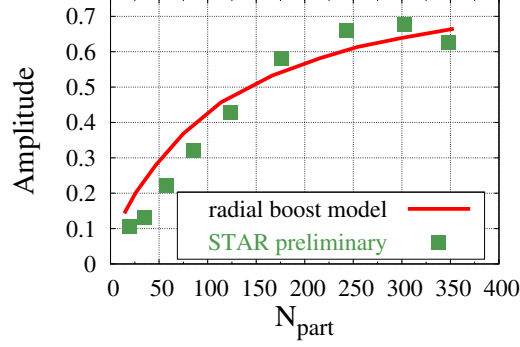
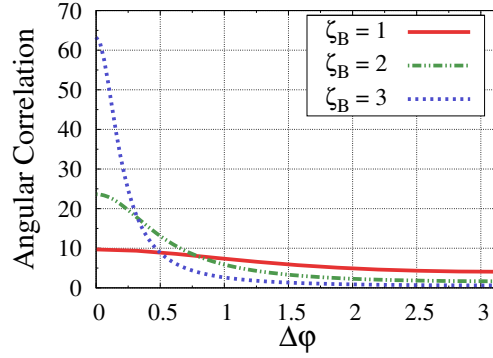


Figure 4.13: Angular correlation function for three different radial boost rapidities ζ_B .



The angular width of the correlation function is not reproduced very well by the simple radial boost model; the integral from eq. (4.22), without any prefactors, is shown as a function of $\Delta\phi$ in the figure 4.13. The width narrows to $\simeq 1$ radians only for boost rapidities $\zeta_B \simeq 2$, corresponding to large boost velocities $\langle v_r \rangle \geq 0.9$. To improve the agreement with the measured angular distributions one may also need to account for the absorption of high- p_\perp particles by the medium [152]. Let us also mention the work of [153], where a much better agreement is obtained via a more realistic modeling of the radial flow.

4.2.5 Rapidity dependence

So far, we have only evaluated the 2-gluon inclusive spectrum at leading order, where all the fields are independent of rapidity. This crude approximation leads to a correlation that is infinitely long ranged in rapidity. In order to get the rapidity dependence of the correlation function, one needs to take into account the rapidity evolution of the distributions $W[\bar{\rho}_{1,2}]$ when evaluating eq. (4.8).

In eq. (4.8), the sources $\tilde{\rho}_{1,2}$ are both dependent on the transverse position \mathbf{x}_\perp and on the rapidity y . However, the factors $dN_1/d^3\mathbf{p}$ and $dN_1/d^3\mathbf{q}$ under the integral depend on the color sources only locally in rapidity, i.e. near y_p and y_q respectively. Let us denote by $\tilde{\rho}_{1,2}^p(\mathbf{x}_\perp)$ and $\tilde{\rho}_{1,2}^q(\mathbf{x}_\perp)$ these sources (these sources are functions that depend solely on \mathbf{x}_\perp). Eq. (4.8) can be rewritten as

$$\left\langle \frac{dN_2}{d^3\mathbf{p}d^3\mathbf{q}} \right\rangle_{\text{LLog}} = \int [D\tilde{\rho}_1^p D\tilde{\rho}_1^q D\tilde{\rho}_2^p D\tilde{\rho}_2^q] Z_{y_p, y_q}[\tilde{\rho}_1^p, \tilde{\rho}_1^q] Z_{y_q, y_p}[\tilde{\rho}_2^q, \tilde{\rho}_2^p] \times \frac{dN_1[\tilde{\rho}_{1,2}^p]}{d^3\mathbf{p}} \Big|_{\text{LO}} \times \frac{dN_1[\tilde{\rho}_{1,2}^q]}{d^3\mathbf{q}} \Big|_{\text{LO}}, \quad (4.26)$$

where the double distribution $Z_{y_p, y_q}[\tilde{\rho}^p, \tilde{\rho}^q]$ is the combined probability to have the source $\tilde{\rho}^p(\mathbf{x}_\perp)$ at the rapidity y_p and the source $\tilde{\rho}^q(\mathbf{x}_\perp)$ at the rapidity y_q . We have written the arguments for the factors $dN_1/d^3\mathbf{p}$ and $dN_1/d^3\mathbf{q}$, to stress the fact that they depend only on the sources located near the rapidity of the produced gluon. The double distribution Z_{y_p, y_q} is related to the distribution $W[\tilde{\rho}]$ of eq. (4.8) via the formal relation:

$$Z_{y_p, y_q}[\tilde{\rho}^p, \tilde{\rho}^q] = \int [D\tilde{\rho}(y, \mathbf{x}_\perp)] W[\tilde{\rho}] \delta[\tilde{\rho}(y_p, \mathbf{x}_\perp) - \tilde{\rho}^p(\mathbf{x}_\perp)] \delta[\tilde{\rho}(y_q, \mathbf{x}_\perp) - \tilde{\rho}^q(\mathbf{x}_\perp)]. \quad (4.27)$$

In other words, $Z_{y_p, y_q}[\tilde{\rho}^p, \tilde{\rho}^q]$ is obtained by summing over all the rapidity dependent $\tilde{\rho}$'s, with the constraints that $\tilde{\rho}$ takes specific values $\tilde{\rho}^p$ and $\tilde{\rho}^q$ at the rapidities y_p and y_q . There are two limiting behaviors of the double distribution $Z_{y_p, y_q}[\tilde{\rho}^p, \tilde{\rho}^q]$, that correspond to completely correlated or completely decorrelated sources at the rapidities y_p and y_q .

$$\begin{aligned} Z_{y_p, y_q}[\tilde{\rho}^p, \tilde{\rho}^q] &= Z_{y_p}[\tilde{\rho}^p] \delta[\tilde{\rho}^p - \tilde{\rho}^q] && \text{(complete correlation)}, \\ Z_{y_p, y_q}[\tilde{\rho}^p, \tilde{\rho}^q] &= Z_{y_p}[\tilde{\rho}^p] Z_{y_q}[\tilde{\rho}^q] && \text{(complete decorrelation)}. \end{aligned} \quad (4.28)$$

The first case is what was implicitly assumed in the study of the ridge in the previous sections, where we neglected the evolution of the sources between the rapidities y_p and y_q . The second case is what happens if the evolution is very important between the rapidities y_p and y_q . In this case, the 2-gluon spectrum factorizes into the product of two single gluon spectra, and there will be no correlation between the two gluons. Our goal in this section is to quantitatively assess how one goes from the first to the second situation.

From eq. (4.27), it is easy to check that Z_{y_p, y_q} can be factored into a single distribution for $\tilde{\rho}^p$ and a *propagator* for the JIMWLK evolution from y_p to y_q (assuming $y_p < y_q$),

$$Z_{y_p, y_q}[\tilde{\rho}^p, \tilde{\rho}^q] = Z_{y_p}[\tilde{\rho}^p] G_{y_p, y_q}[\tilde{\rho}^p, \tilde{\rho}^q], \quad (4.29)$$

where

$$Z_{y_p}[\tilde{\rho}^p] = \int [D\tilde{\rho}(y, \mathbf{x}_\perp)] W[\tilde{\rho}] \delta[\tilde{\rho}(y_p, \mathbf{x}_\perp) - \tilde{\rho}^p(\mathbf{x}_\perp)], \quad (4.30)$$

and

$$\begin{aligned} \partial_{y_q} G_{y_p, y_q}[\tilde{\rho}^p, \tilde{\rho}^q] &= \mathcal{H}_{y_q} G_{y_p, y_q}[\tilde{\rho}^p, \tilde{\rho}^q], \\ \lim_{y_q \rightarrow (y_p)^+} G_{y_p, y_q}[\tilde{\rho}^p, \tilde{\rho}^q] &= \delta[\tilde{\rho}^p - \tilde{\rho}^q]. \end{aligned} \quad (4.31)$$

The propagator $G_{y_p, y_q}[\tilde{\rho}^p, \tilde{\rho}^q]$ can be used to relate the single source distributions at two rapidities, e.g.

$$Z_{y_q}[\tilde{\rho}^q] = \int [D\tilde{\rho}^p] Z_{y_p}[\tilde{\rho}^p] G_{y_p, y_q}[\tilde{\rho}^p, \tilde{\rho}^q] . \quad (4.32)$$

Arguably, determining $Z_{y_p}[\tilde{\rho}^p]$ and the propagator $G_{y_p, y_q}[\tilde{\rho}^p, \tilde{\rho}^q]$ is as difficult as solving the JIMWLK equation. However, this formulation is convenient in order to use the large N_c limit and replace the JIMWLK equation by the Balitsky-Kovchegov equation [84–86]. In this approximation, all the rapidity evolution is reduced to that of a 2-point function (the *dipole amplitude*), and higher-point functions are assumed to factorize as products of 2-point functions. Thus, the single distribution $Z_y[\tilde{\rho}^y]$ is a Gaussian in the BK limit,

$$Z_y[\tilde{\rho}^y] = \exp \left[-\frac{1}{2} \int d^2\mathbf{x}_\perp d^2\mathbf{y}_\perp \frac{\tilde{\rho}_a^y(\mathbf{x}_\perp) \tilde{\rho}_a^y(\mathbf{y}_\perp)}{\mu^2(y; \mathbf{x}_\perp - \mathbf{y}_\perp)} \right] , \quad (4.33)$$

where the function $\mu^2(y; \mathbf{x}_\perp - \mathbf{y}_\perp)$ determines the correlations between sources at different locations in the transverse plane, at a given rapidity (here we assume translation invariance in the transverse plane, in order to write it as a function of the difference $\mathbf{x}_\perp - \mathbf{y}_\perp$). Since the distributions $Z_{y_p, q}$ in eq. (4.32) are both Gaussians, the propagator G_{y_p, y_q} should itself be a Gaussian,

$$G_{y_p, y_q}[\tilde{\rho}^p, \tilde{\rho}^q] = \exp \left[-\frac{1}{2} \int d^2\mathbf{x}_\perp d^2\mathbf{y}_\perp \frac{\Delta\tilde{\rho}_a(\mathbf{x}_\perp) \Delta\tilde{\rho}_a(\mathbf{y}_\perp)}{\Delta\mu^2(\mathbf{x}_\perp - \mathbf{y}_\perp)} \right] , \quad (4.34)$$

where we denote

$$\begin{aligned} \Delta\tilde{\rho}(\mathbf{x}_\perp) &\equiv \tilde{\rho}^q(\mathbf{x}_\perp) - \tilde{\rho}^p(\mathbf{x}_\perp) \\ \Delta\mu^2(\mathbf{r}_\perp) &\equiv \mu^2(y_q, \mathbf{r}_\perp) - \mu^2(y_p, \mathbf{r}_\perp) . \end{aligned} \quad (4.35)$$

We can already see in the form of this propagator the effect of the rapidity evolution of the sources, namely the progressive spreading in $\tilde{\rho}^q - \tilde{\rho}^p$ as $y_q - y_p$ increases. This is reminiscent of the fact that the JIMWLK equation can be interpreted as a diffusion equation in $\tilde{\rho}$ -space, with the rapidity playing the role of a time variable.

Thus, in the BK approximation, all one needs to determine is the rapidity evolution of the function $\mu^2(y, \mathbf{r}_\perp)$ (there are in fact two such functions, one for each projectile). In more detail, the steps to perform in order to compute the rapidity evolution of the 2-gluon spectrum are the following:

- i. choose an initial condition for the dipole amplitude $T(y_0, \mathbf{r}_\perp)$ in a nucleus at a rapidity close to the fragmentation region, e.g. from the McLerran-Venugopalan model,
- ii. solve the BK equation,

$$\begin{aligned} \partial_y T(y, \mathbf{r}_\perp) &= \int d^2\mathbf{r}_{1\perp} \mathcal{K}(\mathbf{r}_\perp; \mathbf{r}_{1\perp}, \mathbf{r}_{2\perp}) \left[T(y, \mathbf{r}_{1\perp}) + T(y, \mathbf{r}_{2\perp}) \right. \\ &\quad \left. - T(y, \mathbf{r}_\perp) - T(y, \mathbf{r}_{1\perp}) T(y, \mathbf{r}_{2\perp}) \right] , \end{aligned} \quad (4.36)$$

where $\mathbf{r}_{2\perp} \equiv \mathbf{r}_\perp - \mathbf{r}_{1\perp}$ and where the kernel \mathcal{K} is given by

$$\mathcal{K}(\mathbf{r}_\perp; \mathbf{r}_{1\perp}, \mathbf{r}_{2\perp}) = \frac{\alpha_s N_c}{2\pi^2} \frac{\mathbf{r}_\perp^2}{\mathbf{r}_{1\perp}^2 \mathbf{r}_{2\perp}^2} \quad (4.37)$$

in the fixed coupling case and by

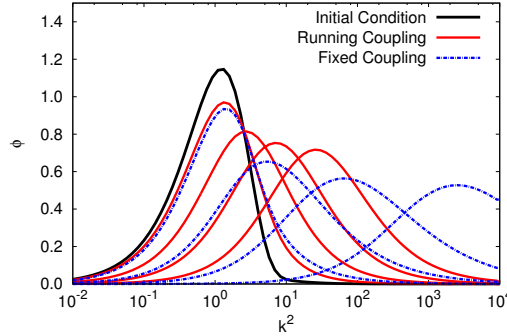
$$\begin{aligned} \mathcal{K}(\mathbf{r}_\perp; \mathbf{r}_{1\perp}, \mathbf{r}_{2\perp}) = & \frac{\alpha_s(\mathbf{r}_\perp^2) N_c}{2\pi^2} \left[\frac{\mathbf{r}_\perp^2}{\mathbf{r}_{1\perp}^2 \mathbf{r}_{2\perp}^2} \right. \\ & \left. + \frac{1}{\mathbf{r}_{1\perp}^2} \left(\frac{\alpha_s(\mathbf{r}_{1\perp}^2)}{\alpha_s(\mathbf{r}_{2\perp}^2)} - 1 \right) + \frac{1}{\mathbf{r}_{2\perp}^2} \left(\frac{\alpha_s(\mathbf{r}_{2\perp}^2)}{\alpha_s(\mathbf{r}_{1\perp}^2)} - 1 \right) \right] \end{aligned} \quad (4.38)$$

in the running coupling case (we adopt Balitsky's prescription¹⁴ here [160, 161]),

- iii. extract the function $\mu^2(y, \mathbf{r}_\perp)$ from the solution of the BK equation, compute the single distribution Z_y at the lowest of the two rapidities $y_{p,q}$ and the propagator G_{y_p, y_q} ,
- iv. insert these distributions in eqs. (4.29) and (4.26), and use eq. (4.12) for the single gluon spectrum. All the integrals that need to be performed are Gaussian integrals, and can be computed analytically.

Note that the steps **i,ii,iii** must be performed for each of the two projectiles in case they are not identical.

Figure 4.14: *Unintegrated gluon distribution in the adjoint representation at rapidities $Y = 0, 2, 6, 10, 15$ (from left to right) in the fixed coupling and running coupling cases (with Balitsky's prescription in the latter case).*

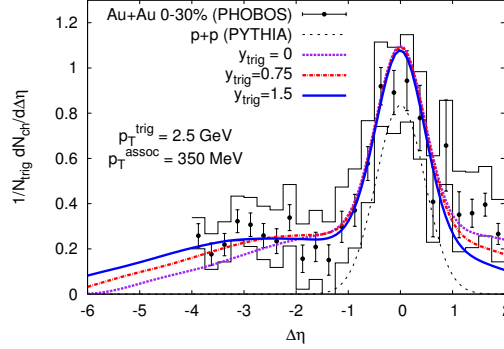


In the figure 4.14, we plot the result of solving the BK equation for a 2-point function closely related to the dipole amplitude, namely the unintegrated gluon distribution (i.e. the Fourier transform of the dipole amplitude, up to a prefactor). We see that it has a peak that shifts to higher momenta as the rapidity increases, which is a consequence of the increase of the saturation scale with rapidity. This increase is slower if one uses the running coupling BK equation instead of the fixed coupling one, and there is a lot of data from Deep Inelastic Scattering indicating that the former indeed provides a better description.

The rapidity dependence of the ridge obtained in this approach for RHIC energy is shown in the figure 4.15, and compared to a measurement by the PHOBOS collaboration [162] (that

¹⁴For other prescriptions, see [154, 155]. See also [156–159] for a discussion of numerical solutions of the BK equation using various prescriptions for the implementation of the running coupling.

Figure 4.15: Comparison with data from the PHOBOS collaboration [162]. The curves shown are the sum of our result for long range rapidity correlations in the PHOBOS acceptance and of the short range jet correlation obtained using PYTHIA.



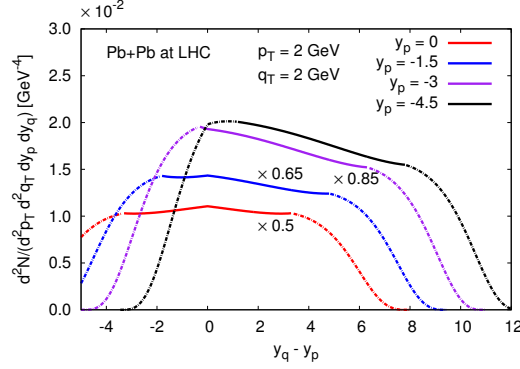
covers 6 units of rapidity). To our calculation, we have superimposed a short range contribution to the rapidity dependence of the correlation, due to jet fragmentation (dotted curve in the figure 4.15). This contribution is not contained in the present approach, and has been taken from the PYTHIA event generator. The Gaussian spreading of the propagator $G_{y_p, y_q}[\tilde{\rho}^p, \tilde{\rho}^q]$ due to the JIMWLK diffusion in $\tilde{\rho}$ -space leads to a decorrelation when the rapidity separation between the two tagged hadrons becomes large. However, this is a slow effect, that requires a rapidity interval parametrically of the order of α_s^{-1} to produce visible deviations from a flat correlation. Over the range of $\Delta\eta$ covered by the PHOBOS measurement, the predicted long range rapidity correlation is almost flat, in good agreement with the data outside of the region $|\Delta\eta| < 1$ dominated by jet fragmentation. In order to see deviations from this flat behavior, one would have to perform the measurement at a larger rapidity difference, which unfortunately is impossible at RHIC due to a limited acceptance. Also interesting but presumably equally beyond the reach of RHIC experiments is the fact that the correlation function is not mirror symmetric around $\Delta\eta = 0$, unless the trigger particle is taken at mid rapidity. The amount by which it is skewed when the trigger is not at mid rapidity is also a prediction of the BK equation. Finally, we close this section with the same calculation at LHC energy, whose results are displayed in the figure 4.16. Note that there, we have not superimposed the short range correlation due to jet fragmentation.

4.3 Multiplicity fluctuations

Another interesting observation [163–166] has been made in high energy hadronic or nuclear collisions, that has a natural explanation in the glasma flux tube picture: multiplicities of charged particles in high energy hadronic collisions are well described as a negative binomial distribution. Similarly, multiplicity fluctuations at RHIC have been found to agree with the negative binomial distribution by the PHENIX collaboration [167, 168].

Let us first recall here that a negative binomial distribution is a two-parameter distribution

Figure 4.16: Prediction for the 2-gluon correlation at LHC energy, for two gluons of transverse momenta $p_{\perp} = q_{\perp} = 2$ GeV, as a function of the rapidity separation $y_q - y_p$. The trigger gluon rapidity y_p varies from 0 to -4.5 . The dashed parts of the curves involve one or more gluon distribution at large $x > 0.01$, while for the solid portions all the distributions are probed at small $x < 0.01$. Some curves have been scaled by the indicated factor for clarity.



defined by the following probability law

$$P_n^{\text{NB}} = \frac{\Gamma(k+n)}{\Gamma(k)\Gamma(n+1)} \frac{\langle n \rangle^n k^k}{(\langle n \rangle + k)^{n+k}}, \quad (4.39)$$

where $\Gamma(n)$ is Euler's gamma function (for integer arguments $\Gamma(n) = (n-1)!$). With these notations, $\langle n \rangle$ is the mean of the distribution, $\langle n \rangle \equiv \sum_n n P_n$, and k is a parameter that controls how different the distribution is from a Poisson distribution. It is easy to check that one recovers a Poisson distribution in the limit $k \rightarrow +\infty$, while holding $\langle n \rangle$ fixed:

$$\lim_{k \rightarrow +\infty} P_n^{\text{NB}} = \frac{\langle n \rangle^n}{n!} e^{-\langle n \rangle}. \quad (4.40)$$

At any finite and positive k , P_n^{NB} is wider than the Poisson distribution of same average. For instance, its variance,

$$\sigma^2 \equiv \langle n^2 \rangle - \langle n \rangle^2 = \langle n \rangle + \frac{\langle n \rangle^2}{k}, \quad (4.41)$$

is larger than that of a Poisson distribution, namely $\langle n \rangle$. Another related difference between a negative binomial distribution and a Poisson distribution is how the tail behaves when $n \rightarrow \infty$ (at fixed $\langle n \rangle$ and k). In the Poissonian case, this behavior is dominated by the factorial $n!$ in the denominator, and thus the tail decreases faster than any exponential of n . In the case of the negative binomial distribution, the behavior of the tail is dominated by $(\langle n \rangle / (\langle n \rangle + k))^n$ (up to some corrections that are polynomial in n), and therefore decays much slower than the tail of the Poisson distribution.

A very useful object in calculations involving a negative binomial distribution is the generating function for the probability law,

$$F_{\text{NB}}(z) \equiv \sum_{n=0}^{+\infty} z^n P_n^{\text{NB}} = \frac{1}{(1 - \frac{\langle n \rangle}{k}(z-1))^k}. \quad (4.42)$$

Conversely, the generating function of a Poisson distribution is $F_P(z) = \exp(\langle n \rangle(z-1))$. The fact that the negative binomial distribution has a much wider tail than a Poisson distribution is linked to the fact that the radius of convergence of $F_{NB}(z)$ is finite, while that of $F_{Poisson}(z)$ is infinite.

Another way to characterize a negative binomial distribution, that we are going to use later here, is via its moments. Let us consider the *factorial cumulants*,

$$m_q \equiv \langle n(n-1) \cdots (n-q+1) \rangle_{\text{connected}} = \left. \frac{d^q \ln F_{NB}(z)}{dz^q} \right|_{z=1}, \quad (4.43)$$

where the subscript *connected* indicates that we subtract the disconnected contributions to the moment of order q , that depend only on the lower order moments. A simple calculation tells us that in the case of a negative binomial distribution, the moments m_q read

$$m_q = k(q-1)! \left[\frac{\langle n \rangle}{k} \right]^q. \quad (4.44)$$

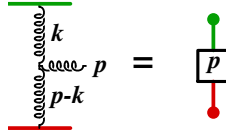
After these preliminaries, let us show how a negative binomial distribution emerges naturally in the glasma flux tube picture. In line with the approximations made in the calculation of the 2-gluon spectrum (see the previous section), let us focus on counting only particles with a transverse momentum \mathbf{p}_\perp larger than some cutoff $\Lambda \gg Q_s$. Since we chose the cutoff Λ to be larger than the saturation scale, it is legitimate to approximate the spectrum as in eq. (4.12) where we keep only the lowest order term in $\tilde{\rho}_{1,2}$. Using eq. (4.15) and integrating it in the range $|\mathbf{p}_\perp| \geq \Lambda$ leads immediately to the first moment

$$m_1 = \langle n \rangle = \frac{S_\perp \Delta Y}{4\pi^3} \frac{(g^2 \mu)^4}{g^2} \frac{N_c(N_c^2 - 1)}{\Lambda^2} \ln \left(\frac{\Lambda}{Q_s} \right), \quad (4.45)$$

where ΔY is the size of the rapidity interval in which we count the gluons (there is no rapidity dependence of the spectrum in the MV model, therefore we can factorize ΔY in front of the integral).

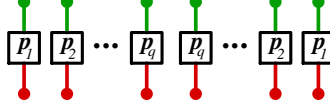
In order to obtain the moment m_q , we must now generalize the method of the previous section in order to perform the average over Gaussian distributions of sources of q factors such as eq. (4.12). In order to do so, we introduce in the figure 4.17 a convenient graphical representation for the one-gluon production amplitude, that emphasizes the sources $\tilde{\rho}_{1,2}$ that must be connected in the process of averaging over the sources. For each produced gluon,

Figure 4.17: Compact notation for the fundamental building block, the one-gluon production amplitude.



there are two such building blocks: one in the amplitude and one in its complex conjugate. Therefore, in the calculation of the moment m_q , there are $2q$ such blocks, as illustrated in the figure 4.18. The Gaussian average over the sources amounts to connecting pairwise the

Figure 4.18: *Diagrams that have to be contracted into a single connected graph.*



green dots among themselves, and the red dots among themselves. Note that since m_q is defined by subtracting the disconnected contributions, we must pair the $2q$ sources \tilde{p}_1 and the $2q$ sources \tilde{p}_2 in such a way that we get a simply connected graph at the end.

In addition, we should discard the terms that are suppressed by powers of Q_s^2/Λ^2 , since we have assumed that $\Lambda \gg Q_s$. In fact, this requirement selects a very special set of connections among the sources. In order to see this, compare the figures 4.19 and 4.20. In the

Figure 4.19: *Contraction contributing to the dominant correlation, building block of rainbow diagram.*

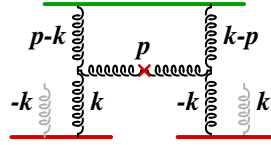


Figure 4.20: *Contraction contributing to a subdominant correlation, non-rainbow diagram.*

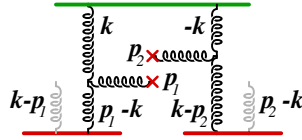


figure 4.19, we have connected the \tilde{p}_1 's from matching amplitudes and complex conjugate amplitudes. This constrains the momentum flow in the graph in such a way that there are four gluon propagators with the momentum k , two of which are compensated by the momentum dependence of the Lipatov vertices attached at the endpoint of these propagators. Thus, the integration over k_\perp is of the form

$$\int \frac{d^2 k_\perp}{k_\perp^4} \sim \frac{1}{Q_s^2} . \quad (4.46)$$

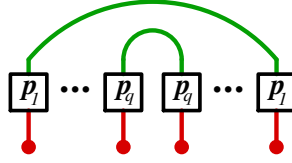
The infrared divergent integral over k_\perp is a sign that multigluon correlations are sensitive to the transverse size over which the color sources are correlated, i.e. Q_s^{-1} . This is why the glasma flux tubes are the relevant entity when discussing these correlations. On the other hand, in the figure 4.20, there are only two propagators carrying the same momentum, which

means that the integrals have at most a logarithmic sensitivity to the scale Q_s^{-1} . Overlooking these logarithms, the momentum integrals are typically of the form

$$\int \frac{d^2 \mathbf{k}_\perp}{(\mathbf{p}_{1\perp} - \mathbf{k}_\perp)^2 (\mathbf{p}_{2\perp} - \mathbf{k}_\perp)^2} \lesssim \frac{1}{\Lambda^2} \ll \frac{1}{Q_s^2}. \quad (4.47)$$

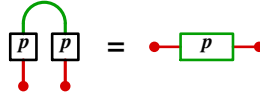
Thus, the source connection pictured in the figure 4.20 leads to a suppression by a factor Q_s^2/Λ^2 compared to the contribution of figure 4.19. In order to avoid this kind of suppression completely, one must connect all the $\tilde{\rho}_1$'s (or all the $\tilde{\rho}_2$) in a rainbow-like manner, as shown in the figure 4.21. Then, one needs to connect all the $\tilde{\rho}_2$'s pairwise. In order to do so, it is

Figure 4.21: *Rainbow diagram.*



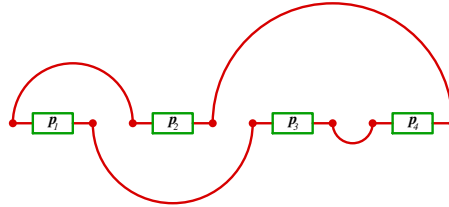
convenient to introduce an even more compact notation that hides the details of how the $\tilde{\rho}_1$'s are connected, as illustrated in the figure 4.22. We have q such objects, totaling $2q$ sources

Figure 4.22: *Dimer notation for rainbow-like links.*



$\tilde{\rho}_2$, and we must connect them pairwise in order to make a *simply connected* graph. The first end of the first dimer can be connected to $2q - 2$ other loose dimer ends. Let us assume it is connected to dimer r . The second end of dimer r has $2q - 4$ loose ends available – indeed, we cannot connect it to the first dimer as this would immediately create a disconnected subgraph. The only possibility is to make a loop by chaining all the dimers together, as shown in figure 4.23. There are $(2q - 2)(2q - 4) \cdots 2 = 2^{q-1} (q - 1)!$ possible ways of making such a loop.

Figure 4.23: *Connected diagram in the polymer notation introduced in Fig. 4.22*



Remembering that we can form the rainbow either with the $\tilde{\rho}_1$'s or with the $\tilde{\rho}_2$'s, we finally arrive at $2^q (q - 1)!$ topologies.

The color structure can be simplified in as follows. Let us denote the color indices of the sources $i = 1 \dots q$ contracted on the upper side of the diagram in the figure 4.21 by α_i (because of the rainbow structure of the connections on the upper side, we do not need separate indices for the sources in the complex conjugate amplitude), the color index of the gluon with \mathbf{p}_i by b_i and the color indices on the lower side of the diagram c_i (source connected to gluon \mathbf{p}_i in the amplitude) and c'_i (in the complex conjugate). Now the color structure is $f^{\alpha_1 b_1 c_1} f^{\alpha_1 b_1 c'_1} \dots f^{\alpha_q b_q c_q} f^{\alpha_q b_q c'_q} = (C_A)^q \delta^{c_1 c'_1} \dots \delta^{c_q c'_q}$. $C_A = N_c$ is the Casimir of the adjoint representation of $SU(N_c)$. The $\{c_i, c'_i\}$ indices must now be contracted pairwise into a single loop as in the figure 4.23, which yields a factor $\text{tr}(1_{\text{adj}}) = N_c^2 - 1$, making the total color factor $(N_c)^q (N_c^2 - 1)$.

Let us then turn to the structure of momentum flow in the diagram. Transverse momentum is conserved at the vertices and in the sources connections due to the expectation value in eq. (4.13). Altogether there are originally $4q$ transverse momentum integrals from the powers of the sources. There are $2q$ delta functions from the source correlators (4.13) and $2q$ momentum conservation delta functions from the three gluon vertices. Not all these delta functions are independent: two of them end up having the same argument, yielding one factor $(2\pi)^2 \delta(0)$ that we interpret as the transverse area S_\perp . Therefore, there is only one remaining transverse momentum integral. One can choose this remaining momentum to be the one circulating in all of the lower part of the diagram, which we shall denote by \mathbf{k}_\perp (this is the momentum that circulates along the loop in the figure 4.23). On the rainbow side of the diagram there is a squared propagator $1/(\mathbf{k}_\perp - \mathbf{p}_{i\perp})^4$ for all the sources $i = 1 \dots q$. On the non-rainbow side the transverse momentum in all the propagators is the same, giving a factor $1/\mathbf{k}_\perp^{4q}$. Half of these propagators are cancelled by the squares of the Lipatov vertices, which also contribute an inverse square of the external momentum. Combining the combinatorial factors from the source averages, the propagators, Lipatov vertices and factors from the invariant measure, we finally get

$$\left\langle \frac{dN_q}{dy_1 d^2\mathbf{p}_{1\perp} \dots dy_q d^2\mathbf{p}_{q\perp}} \right\rangle_{\text{conn.}} = 2^q (q-1)! \frac{(N_c)^q (N_c^2 - 1) S_\perp}{(\mathbf{p}_{1\perp})^2 \dots (\mathbf{p}_{q\perp})^2} \frac{1}{g^{2q}} \frac{2^q}{(2\pi)^{3q}} \times \int \frac{d^2\mathbf{k}_\perp}{(2\pi)^2} \left(\frac{g^4 \mu^2}{\mathbf{k}_\perp^2} \right)^q \frac{(g^4 \mu^2)^q}{(\mathbf{p}_{1\perp} - \mathbf{k}_\perp)^2 \dots (\mathbf{p}_{q\perp} - \mathbf{k}_\perp)^2} . \quad (4.48)$$

This general formula also reproduces the result of [103, 105, 145] for the single inclusive spectrum case $q = 1$; in this case the combinatorial factor in the square bracket must be taken to be 1 instead of 2 to avoid double counting the only contributing diagram.

The weak source result in eq. (4.48) is infrared divergent in the MV model (i.e. when $g^4 \mu^2$ is independent of momentum). Physically, this is modified by several effects. Even in the weak field limit, BK or BFKL evolution leads to an anomalous dimension $0 < \gamma < 1$ that changes this constant into

$$g^4 \mu^2(\mathbf{k}_\perp) \sim \mathbf{k}_\perp^{2(1-\gamma)} , \quad (4.49)$$

in the geometric scaling region $\mathbf{k}_\perp \gtrsim Q_s$. Moreover, deep inside the saturation regime it has been argued in [130] that the correlator effectively behaves as

$$g^4 \mu^2(\mathbf{k}_\perp) \sim \mathbf{k}_\perp^2 . \quad (4.50)$$

And ultimately, the infrared behavior of the multigluon spectrum is regulated by the nonlinear interactions that are not included in our present computation. This is seen explicitly and

analytically in the proton-nucleus case [18, 119, 169] and in numerical computations of the glasma fields in the fully nonlinear case [20, 23, 26]. Since the full nonlinear dynamics is known to regulate the infrared behavior in the case of the single gluon spectrum, we have strong reasons to expect that they will also do so in the case of multiple gluon production, at the same scale $k_\perp \lesssim Q_s$. An essential point in this argument is that the quantity appearing in eq. (4.48) is not a single color charge correlator divided by a large power k_\perp^{2q} , but the same combination $g^4 \mu^2 / k_\perp^2$ that appears in the single inclusive gluon spectrum raised to the power q .

The effect of saturation on the multigluon spectrum at $k_\perp \lesssim Q_s$ has a very intuitive interpretation in the glasma flux tube picture. The transverse size of a flux tube, Q_s^{-1} , is the correlation length of color charges in the transverse plane and we should not have contributions from longer distance scales. We effectively take this into account by regulating all the infrared divergences at the scale Q_s , and thus approximating the integral in eq. (4.48) by

$$\left(2\pi \kappa^{q-1} Q_s^{2(q-2)} \mathbf{p}_{1\perp}^2 \cdots \mathbf{p}_{q\perp}^2 \right)^{-1}. \quad (4.51)$$

Here κ is a constant of order one that depends on the details of how the infrared divergences are regulated at that scale. In our analytical calculation, we do not have control over the value of this coefficient.

We also use the corresponding approximation for the single inclusive spectrum,

$$\left\langle \frac{dN_1}{dy d^2 \mathbf{p}_\perp} \right\rangle \approx \frac{N_c(N_c^2 - 1)}{4\pi^4 g^2} \frac{S_\perp (g^2 \mu)^4}{\mathbf{p}_\perp^4}, \quad (4.52)$$

where we disregard the logarithm (see eq. (4.12)). We can now express our result for the connected part of the q -gluon spectrum as

$$\begin{aligned} \left\langle \frac{dN_q}{dy_1 d^2 \mathbf{p}_{1\perp} \cdots dy_q d^2 \mathbf{p}_{q\perp}} \right\rangle_{\text{conn.}} &= \\ &= (q-1)! \frac{(N_c^2 - 1) \kappa Q_s^2 S_\perp}{2\pi} \left(\frac{(g^2 \mu)^4}{g^2} \frac{1}{2\pi^3} \frac{N_c}{\kappa Q_s^2} \right)^q \frac{1}{(\mathbf{p}_{1\perp})^4 \cdots (\mathbf{p}_{q\perp})^4} \\ &= (q-1)! \frac{(N_c^2 - 1) \kappa Q_s^2 S_\perp}{2\pi} \frac{\prod_{i=1}^q \left\langle \frac{dN_1}{dy_i d^2 \mathbf{p}_{i\perp}} \right\rangle}{((N_c^2 - 1) \kappa Q_s^2 S_\perp / (2\pi))^q}. \end{aligned} \quad (4.53)$$

If we integrate this equation over the rapidities (in the range of size ΔY) and transverse momenta of the q gluons (from Λ to ∞), we obtain the following result for the factorial cumulant

$$m_q = (q-1)! k \left[\frac{\langle n \rangle}{k} \right]^q, \quad (4.54)$$

with

$$k = \kappa \frac{(N_c^2 - 1) Q_s^2 S_\perp}{2\pi}. \quad (4.55)$$

The exact constant factors, encoded in the coefficient κ , depend on the precise way the infrared divergences (logarithmic in the single inclusive spectrum, power law for the multigluon correlations) are regulated. These factors cannot be obtained exactly in an analytic calculation

to lowest order in the sources. However, the leading parametric dependences in the relevant variables α_s , Q_s , S_\perp and N_c can be expected to be the same to all orders in the sources. A possible additional (mild) q -dependence in κ would be a minor correction to the behavior of the probability distribution, mostly determined by the combinatorial factor $(q-1)!$.

Equations (4.54) and (4.55) are the main result of this section. One can see that these factorial cumulants are those that define a *negative binomial* distribution. It arises very naturally in the glasma based on the Gaussian combinatorics of the classical sources and the assumption of the fluctuations in the system being dominated by a correlation length Q_s^{-1} . It is important to stress the main difference between the moments in eq. (4.54) and what one would get for a Poisson distribution (i.e. in the absence of correlations among the produced particles): with a Poisson distribution, all the m_q 's for $q > 1$ are zero, while in eq. (4.54) they are growing factorially.

It is also easy to interpret this result as the superposition of k incoherent sources¹⁵, each of them emitting $\langle n \rangle/k$ gluons distributed according to the Bose-Einstein distribution. This is seen by noticing that the generating function for the negative binomial distribution is the k -th power of $(1 - \frac{\langle n \rangle}{k}(z-1))^{-1}$, which is the generating function for the Bose-Einstein distribution. In the glasma flux tube picture, these elementary sources emit gluons of one given color from one given flux tube, as one can see from their number given by eq. (4.55). Geometrically, the transverse area S_\perp is filled with $Q_s^2 S_\perp$ independent flux tubes of transverse area $\sim 1/Q_s^2$. Each of these tubes emits gluons in $N_c^2 - 1$ different colors. Our result shows that the probability distribution of gluons of a given color emitted from one flux tube is approximately a Bose-Einstein distribution.

Experimentally, the parameter k increases somewhat with ΔY , the size of the rapidity interval in which the particles are measured. The dependence is, however, very slow for large ΔY , pointing to the presence of a long range rapidity correlation in the system [170]. This is natural in the glasma picture, since flux tubes are coherent over large rapidity intervals. The number of flux tubes, which gives the parameter k of the negative binomial distribution, essentially depends only on the transverse area of the projectiles and on the saturation momentum.

The main difficulty in interpreting the experimental results arises from the geometrical fluctuations that result from averaging over different impact parameters in one finite centrality bin. To minimize this effect one should use as small centrality bins as possible. To the extent that this uncertainty allows us to compare results in gold-gold and $p\bar{p}$ collisions, the picture we present seems fairly consistent. For a fixed collision energy, we would expect a scaling $k \sim Q_s^2 S_\perp \sim N_{\text{part}}$. While keeping this caveat in mind, the results from UA5 [166] and E735 [171] ($k \approx 2 \dots 4$, $N_{\text{part}} = 2$) and PHENIX $k \approx 350$ for 0-5% most central collisions [167] or $k = 690$ when extrapolated to a zero centrality bin width [168], $N_{\text{part}} \approx 350$) seem consistent with this estimate.

From the fit of the parameter k in central gold-gold collisions by the PHENIX experiment [168] and the value $Q_s \approx 1.1$ GeV estimated from measurements of the charged multiplicity, one can use eq. (4.55) to obtain an estimate $\kappa \approx 0.2$ for the parameter that reflects our uncertainty in the infrared sector. This means that at RHIC energies the flux tube

¹⁵Explicitly, consider $n = n_1 + \dots + n_k$ where the n_i 's are k random variables independent of each other that have the same probability distribution p_{n_i} . The probability distribution of the random variable n is then $P_n = \sum_{n_1} \dots \sum_{n_k} \delta(n - \sum_{i=1}^k n_i) p_{n_1} \dots p_{n_k}$ and the generating function $\sum_n z^n P_n = \sum_{n_1} \dots \sum_{n_k} z^{n_1 + \dots + n_k} p_{n_1} \dots p_{n_k}$, which is the k -th power of the generating function for one of the variables n_i .

size, as measured from the multiplicity distribution, is not yet very clearly separated from the confinement scale. At LHC energies we can expect this separation to be better.

For increasing collision energy we would expect Q_s and therefore k to increase. The energies where the UA5 measurements are done are still in the transition region from a behavior of k decreasing with energy from lower \sqrt{s} , but we would expect k at the LHC to be clearly larger. The decreasing behavior at low energy follows because of the Poisson nature of low energy particle emission, and that for a Poisson distribution $k \rightarrow \infty$.

In other approaches, the negative binomial has been interpreted as resulting from a partial stimulated emission or cascade process [170]. A popular approach has been to interpret the observations in terms of a fluctuating number of strings [131], each producing particles typically with a Poisson distribution [172, 173] (see also [174, 175] for a more pQCD based approach). While the picture of flux tubes in the glasma has many similarities to ideas in string model phenomenology, they differ in the distribution of particles produced from a single flux tube: the probability distribution of gluons from a glasma flux tube is not a narrow Poissonian, but has instead a longer tail.

Part III

Final State Evolution, Thermalization?

Introduction



In the previous part of this manuscript, we have shown how the dependence of observables on the collision energy or on rapidity arises from universal distributions that describe the color charge content of the projectiles. Then we discussed a number of phenomenological consequences of this factorization, that can be evaluated based on the assumption that they are not much affected by the evolution of the system after the collision. However, it is also well known that some observables depend crucially on the final state evolution. One key example of these observables is the *elliptic flow*, that measures that momentum space anisotropy of the distribution of particles in collisions with a non-zero impact parameter. At the time of the collision, the locality of the particle production processes makes them insensitive to the geometry of the colliding region, and therefore there is no reason to expect any significant momentum anisotropy of the produced particles. The appearance of the elliptic flow can be explained by the evolution of the system after the collision, but seems to require that it expands like a fluid with a very small viscosity [57].

In the first section of chapter 4, we have seen that the classical color fields produced in the collision of two nuclei have chromo-magnetic field lines that are parallel to the collision axis at $\tau = 0$. Such a configuration of color fields, called the *Glasma*, has a negative longitudinal pressure, making the system less than ideal for the applicability of hydrodynamics. This observation raises an interesting question in the CGC description of heavy ion collisions: how does one go from highly coherent but anisotropic classical fields to a nearly perfect fluid? A natural question to ask is whether there are some important higher order contributions, not included in the classical solutions of Yang-Mills equations, that make the system behave closer to a perfect fluid.

In the chapter 5, we show that classical solutions of the Yang-Mills equations are subject to instabilities, that produce unphysical secular divergences in higher order corrections to observables. We modify our power counting rules in order to track these pathological terms, and we resum them into a manifestly finite expression that amounts to add Gaussian fluctuations to the initial conditions for the classical color field fluctuate at $\tau = 0^+$.

In the chapter 6, we study the effect of these Gaussian fluctuations in a simpler scalar field theory, in order to avoid some difficulties of the implementation in QCD. We demonstrate that these fluctuations, via a decoherence process, lead the pressure of the system of fields to relax in time towards the equilibrium value of the pressure. We also show that they significantly alter the energy density fluctuations in the system, making the system more thermal-like. Then, we investigate more thoroughly the properties of the system of fields when the Gaussian fluctuations are included, by computing its spectral density, the mass of its quasi-particles, its occupation number and entropy density. All these quantities point to the conclusion that, although the system has the equation of state of an ideal fluid, it has not yet reached local thermal equilibrium.

Chapter 5

Unstable modes, Resummation of the Secular Terms



At leading order (or leading log, if the initial state logarithms have been resummed), the CGC describes the matter produced in heavy ion collisions as a solution of classical Yang-Mills equations. The energy-momentum tensor of this classical field configuration is however very peculiar, because its longitudinal pressure is negative, making it unsuitable for an hydrodynamical description of its expansion. Moreover, the existence of a negative pressure suggests that the system of fields may in fact be unstable.

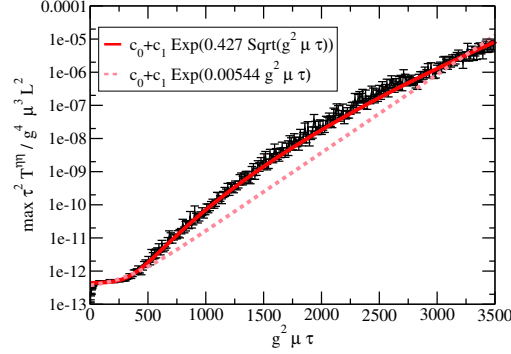
As we shall discuss in this chapter, this is indeed the case: the classical Yang-Mills equations suffer from an instability that makes their solutions extremely sensitive to their initial condition (see the section 5.1). In other words, subleading perturbations (in powers of g) to their initial condition grow exponentially in time and eventually become as large as the leading order classical field. The existence of these unstable modes implies that some NLO corrections to the energy-momentum tensor will have an unbounded growth as time increases (a phenomenon known as a *secular divergence*), and after some time they will become as large as the LO contribution.

Therefore, one should alter the power counting in order to resum these corrections. In the section 5.2, we present a resummation scheme that collects the fastest growing corrections at higher loop orders, and we show that this resummation can be reformulated as an average over a Gaussian ensemble of initial conditions at $\tau = 0^+$ for the classical Yang-Mills equations. In the next section, we discuss the time evolution of this ensemble of classical fields, and argue that it is controlled by a classical Liouville equation.

5.1 Unstable modes in Yang-Mills equations

As we have seen before, the classical solutions of the Yang-Mills equations that are relevant in the CGC description of heavy ion collisions at leading logarithmic accuracy are independent of the space-time rapidity η . An important question is whether these rapidity independent solutions are stable under small perturbations. In other words, what happens if one superimposes a small perturbation (possibly η -dependent) to their initial condition? In order to

Figure 5.1: Numerical simulation of the time evolution of rapidity dependent perturbations. From [176].



answer this question, one must now solve numerically the classical Yang-Mills equations in 3+1 dimensions, which has been done in [12, 31, 176, 177]. A result of this numerical simulation is shown in the figure 5.1. The horizontal axis is the proper time in units of the inverse saturation scale, and the vertical axis represents the largest Fourier η -mode of the longitudinal pressure, defined as

$$\max_{\nu \neq 0} \left[\int d\eta d^2 x_{\perp} e^{i\nu\eta} \tau^2 T^{\eta\eta} \right], \quad (5.1)$$

where we denote

$$\tau^2 T^{\eta\eta} \equiv \sinh^2(\eta) T^{00} + \cosh^2(\eta) T^{33}. \quad (5.2)$$

Note that with the leading order Glasma fields, $\tau^2 T^{\eta\eta}$ is independent of the rapidity η , and thus its only Fourier mode is the mode $\nu = 0$. Therefore, the maximum over the non-zero modes defined in eq. (5.1) is zero. We see in the figure 5.1 that it indeed starts at a very small value at $\tau = 0$, a consequence of the fact that the initial value of the perturbation is taken to be very small. Subsequently, this quantity grows exponentially in time¹, as $\exp(\sqrt{\text{const}} \times \tau)$, suggesting that the perturbation of the gauge field itself grows exponentially fast. This exponential growth of a seemingly negligible perturbation is the sign of an instability in the classical Yang-Mills equations, which should have been expected since it has been shown in [28, 29, 178] that they have positive Lyapunov exponents. Semi-analytic studies of small perturbations to solutions of the Yang-Mills equations have also confirmed the existence of unstable modes [179, 180].

A similar instability, known as the *Weibel instability* (or *filamentation instability*), has also been observed in the study of a quark-gluon plasma that has an anisotropic distribution of particles in momentum space. In this case, certain modes develop an imaginary Debye screening mass [40, 41], that signals the instability.

¹It is easy to understand at a qualitative level that the square root of time (as opposed to a linear dependence in time) inside the exponential is due to the expansion of the system. Indeed, one can see the unstable modes as having imaginary screening masses. In a system whose volume is proportional to time due to the longitudinal expansion, the square of the screening masses decreases as $1/\tau$ since it is proportional to the square of the classical field. Such a screening term in the equation of motion of a field leads to solutions that behave like Bessel I_n functions, whose leading behavior at late time contains an exponential of $\sqrt{\tau}$. See also [48].

Note that the quantity displayed in the figure 5.1 cannot grow indefinitely in time. Indeed, when the perturbation becomes comparable in size to the underlying Glasma field, the nonlinearities of the Yang-Mills equations should prevent the energy momentum tensor from growing any further. However, this observation leads to the hope that fluctuations that are not included in the Glasma leading order calculation may grow fast enough to make the longitudinal pressure become positive (recall that the Glasma classical field gives a negative value $\tau^2 T^{\eta\eta} = -\epsilon$). In the toy calculation of [176], the perturbations that led to this positive growing contribution to the longitudinal pressure have been introduced by hand. However, such perturbations are naturally generated by the quantum fluctuations in the system. In the CGC formalism, these should arise at higher orders via loop corrections. In the next section we show how to resum the loop contributions that give the fastest growing corrections due to this instability, we justify the averaging procedure used in [176], and argue about what the ensemble of initial conditions should be.

5.2 Resummation of the secular divergences

5.2.1 NLO correction

Let us first recall the one-loop result for the energy-momentum tensor. We have derived in the chapter 3 a formal expression for the NLO correction to the energy momentum tensor in a given configuration $\tilde{\rho}_{1,2}$ of the color sources that represent the fast partons in the two nuclei:

$$\begin{aligned} T_{\text{NLO}}^{\mu\nu}(x) = & \left[\frac{1}{2} \sum_{\lambda, \alpha} \int \frac{d^3 \mathbf{k}}{(2\pi)^3 2k} \int_{\Sigma} d^3 \mathbf{S}_u d^3 \mathbf{S}_v [\mathbf{a}_{-\mathbf{k}\lambda\alpha} \cdot \mathbb{T}_u] [\mathbf{a}_{+\mathbf{k}\lambda\alpha} \cdot \mathbb{T}_v] \right. \\ & \left. + \int_{\Sigma} d^3 \mathbf{S}_u [\beta \cdot \mathbb{T}_u] \right] T_{\text{LO}}^{\mu\nu}(x) , \end{aligned} \quad (5.3)$$

In this NLO correction, some of the terms that are independent of the rapidity η have logarithms of the cutoff of the CGC effective theory, and can be interpreted as being part of the wavefunctions of the incoming projectiles. We assume in the following that these leading logarithmic terms have already been absorbed in the distributions of the sources $\tilde{\rho}_{1,2}$ via the JIMWLK evolution equation.

In order to keep the subsequent formulas compact, we will use the notation²

$$\Gamma_2(\mathbf{u}, \mathbf{v}) \cdot \mathbb{T}_u \mathbb{T}_v \equiv \sum_{\lambda, \alpha} \int \frac{d^3 \mathbf{k}}{(2\pi)^3 2k} [\mathbf{a}_{-\mathbf{k}\lambda\alpha} \cdot \mathbb{T}_u] [\mathbf{a}_{+\mathbf{k}\lambda\alpha} \cdot \mathbb{T}_v] . \quad (5.4)$$

Although we do not introduce a new notation, from now on Γ_2 and β denote what is left in eq. (5.3) after one has isolated the leading logarithmic terms that are resummed via the JIMWLK evolution. In this chapter, we focus mostly on what happens for a fixed configuration $\tilde{\rho}_{1,2}$ of the sources that describe the incoming projectiles, since our goal is to argue whether thermalization and/or flow occurs in a given collision. In order to stress the fact that the energy-momentum tensor at leading order is a functional of the initial classical fields at $\tau = 0^+$, we may use the notation

$$T_{\text{LO}}^{\mu\nu}(x) \equiv T_{\text{LO}}^{\mu\nu}[\mathbb{A}_0[\tilde{\rho}_{1,2}]; x] , \quad (5.5)$$

²Since in Yang-Mills theory, the operator $\mathbf{a} \cdot \mathbb{T}_u$ is the sum of three terms (see eq. (3.45)), the quantity $\Gamma_2(\mathbf{u}, \mathbf{v})$ that we have introduced via this notation should therefore be thought of as being a 3×3 matrix.

\mathbb{A}_0 is the pair $(\mathcal{A}_0, \mathcal{E}_0)$ where \mathcal{A}_0 is the initial value of the gauge field and \mathcal{E}_0 the initial value of the corresponding canonical momentum³ (which is an electric field, hence the notation). \mathcal{A}_0 and \mathcal{E}_0 are themselves functions of $\tilde{\rho}_{1,2}$. \mathbf{x} is the space-time point at which the energy-momentum tensor is evaluated.

The numerical evidence shown in the figure 5.1 for the existence of instabilities in the classical solutions of Yang-Mills equations implies that the NLO correction to the energy-momentum tensor contains secular divergences: some of its components⁴ at least should diverge when $\tau \rightarrow \infty$. Therefore, a strict application of the g^2 expansion for the calculation of the energy-momentum tensor is bound to fail after a finite amount of time, after which the CGC predictions cannot be trusted unless the behavior of the perturbative expansion can be cured by a resummation.

5.2.2 Modified power counting rules

So far, our power counting has been limited to keeping track of the powers of the coupling constant g , coming either explicitly from the vertices in Feynman diagrams or implicitly via the sources $\tilde{\rho}_{1,2}$ that are parametrically of order g^{-1} in the saturated regime. We have in fact already departed from a strict application of this counting by resumming the higher order terms that come with a sufficiently high power of a logarithm of the cutoff Λ^\pm – the so-called leading logarithmic corrections. Now, the instabilities that introduce secular divergences in the NLO corrections to the energy-momentum tensor call for another improvement to this power counting. Ideally, we would like to resum all the terms that have secular divergences in higher loop corrections. In order to achieve that, we need now some power counting rules to determine which terms are important and which terms can be neglected.

At leading order (tree level), the energy momentum tensor is of order Q_s^4/g^2 . In the absence of any secular divergence, its NLO corrections should therefore be of order Q_s^4 . This can be recovered from eq. (5.3) by the following counting rules:

$$\Gamma_2(\mathbf{u}, \mathbf{v}) \sim a_{-\mathbf{k}\lambda\alpha}(\mathbf{u})a_{+\mathbf{k}\lambda\alpha}(\mathbf{v}) \sim \mathcal{O}(1) , \quad (5.6)$$

$$\beta(\mathbf{u}) \sim \mathcal{O}(g) , \quad (5.7)$$

$$\mathbb{T}_{\mathbf{u}} \sim \frac{\delta}{\delta\mathcal{A}_0} \sim \mathcal{O}(g) . \quad (5.8)$$

The existence of instabilities implies that we must alter our estimate of the order of magnitude of the operators $\mathbb{T}_{\mathbf{u}}$. Indeed, since $\mathbb{T}_{\mathbf{u}}\mathcal{A}(\tau, \mathbf{x})$ is the propagator of a small fluctuation over the background field between the initial surface Σ and the point (τ, \mathbf{x}) , it grows at the same pace as the unstable fluctuations. Thus, the counting rule for $\mathbb{T}_{\mathbf{u}}$ should be modified to read :

$$\mathbb{T}_{\mathbf{u}} \sim \mathcal{O}(ge^{\sqrt{\mu}\tau}) , \quad (5.9)$$

³Since the Yang-Mills equations contain second derivatives with respect to time, the initial condition must specify both the initial field \mathcal{A}_0 and its first time derivative \mathcal{E}_0 . Moreover, we have not written here the Lorentz indices of the gauge potential and electric field – \mathcal{A}_0 and \mathcal{E}_0 are themselves multicomponent objects.

⁴The conservation of the energy-momentum tensor, $\partial_\mu T^{\mu\nu} = 0$, which is valid order by order in g^2 , ensures that some combinations of its components are protected from any such divergences.

and the combination $\Gamma_2(\mathbf{u}, \mathbf{v}) \mathbb{T}_{\mathbf{u}} \mathbb{T}_{\mathbf{v}}$ that enters in eq. (5.3) leads to a relative correction of order $g^2 e^{2\sqrt{\mu}\tau}$ to the energy momentum tensor. At short times, this is indeed a correction suppressed by a factor g^2 –as expected for a 1-loop correction– but it is enhanced exponentially at later times due to the instability. When this corrective factor becomes of order unity, the loop expansion breaks down. This happens at a time

$$\tau_{\max} \sim \mu^{-1} \ln^2 \left(\frac{1}{g} \right). \quad (5.10)$$

When this time is reached, the 1-loop correction becomes as large as the leading order contribution, and one should in fact expect that an infinite series of higher loop corrections become equally important.

5.2.3 Dominant higher loop corrections

Our goal now is to collect from the higher orders all the terms that are leading at the time τ_{\max} . This comprises all the terms where the extra powers of g^2 are compensated by an equal number of factors such as $e^{2\sqrt{\mu}\tau}$.

A typical higher order correction to the energy momentum tensor can still be written in the form of eq. (5.3), but with a more general operator acting on $T_{\text{LO}}^{\mu\nu}(\mathbf{x})$:

$$\int_{\Sigma} d^3 \mathbf{S}_{\mathbf{u}_1} \cdots d^3 \mathbf{S}_{\mathbf{u}_n} \Gamma_n(\mathbf{u}_1, \dots, \mathbf{u}_n) \cdot \mathbb{T}_{\mathbf{u}_1} \cdots \mathbb{T}_{\mathbf{u}_n}, \quad (5.11)$$

where Γ_n is some n -point function (simply connected or not). If eq. (5.11) is a piece of a L -loop correction to the energy-momentum tensor, the order g^p and the number n of points of the function Γ_n are related by:

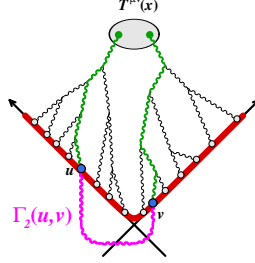
$$n + p = 2L. \quad (5.12)$$

In the figures 5.2 and 5.3, we illustrate this formula by some examples of 1-loop and 2-loop contributions. This formula also works if Γ_n contains tadpole contributions (such as β for instance) that are disconnected from the rest of the n -point function. Note that $p = 0$ is the smallest possible value for p . Taking into account the effect of the instabilities, the order of magnitude of a contribution obtained from eq. (5.11) is

$$g^p \left[g e^{\sqrt{\mu}\tau} \right]^n. \quad (5.13)$$

If we disregard the time-dependent factors in this formula, the naive power counting would indicate that this is a correction of order g^{2L} . However, at the time τ_{\max} it is in reality of order g^p . In other words, at the time τ_{\max} all the terms for which $p = 0$ are of the same order and leading, while all the terms for which $p > 0$ are suppressed. Therefore, it is natural to resum all the $p = 0$ terms, and to neglect all those with $p > 0$. This implies that the numbers n of points must be even, equal to $2L$. Moreover, if we restrict ourselves to terms of order $p = 0$ in Γ_{2L} , the only possibility is to construct Γ_{2L} as a product of L factors Γ_2 . In particular, tadpole contributions such as β are excluded in the $p = 0$ terms, since they contain at least one power of g . Any non-factorized contribution to Γ_{2L} requires extra powers of the coupling g , and therefore cannot contribute at the order $p = 0$.

Figure 5.2: Representation of the 1-loop contribution involving the function $\Gamma_2(\mathbf{u}, \mathbf{v})$. The thick red line is the Σ surface on which the initial value problem is set up. The open circles represent the initial data. The filled blue circles represent the two operators $\mathbb{T}_{\mathbf{u}, \mathbf{v}}$, and the U-shaped wavy line below the light-cone is the function $\Gamma_2(\mathbf{u}, \mathbf{v})$.



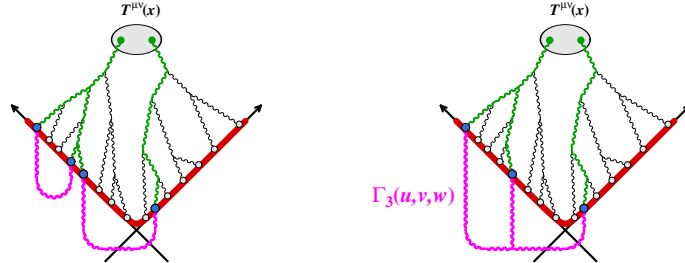
Therefore, the leading operator at L loops in eq. (5.11) is in fact the L-th power of the 2-point operator that appears at 1-loop, i.e.

$$\frac{1}{L!} \left[\frac{1}{2} \int_{\Sigma} d^3 \mathbf{S}_{\mathbf{u}} d^3 \mathbf{S}_{\mathbf{v}} \Gamma_2(\mathbf{u}, \mathbf{v}) \cdot \mathbb{T}_{\mathbf{u}} \mathbb{T}_{\mathbf{v}} \right]^L, \quad (5.14)$$

where the inverse factorial prefactor is a symmetry factor that prevents multiple countings. When we sum all these contributions from $L = 0$ (leading order) to $L = +\infty$, we obtain the exponential of the leading order result

$$\mathbb{T}_{\text{resummed}}^{\mu\nu}(x) = \exp \left[\frac{1}{2} \int_{\Sigma} d^3 \mathbf{S}_{\mathbf{u}} d^3 \mathbf{S}_{\mathbf{v}} \Gamma_2(\mathbf{u}, \mathbf{v}) \cdot \mathbb{T}_{\mathbf{u}} \mathbb{T}_{\mathbf{v}} \right] \mathbb{T}_{\text{LO}}^{\mu\nu}(x). \quad (5.15)$$

Figure 5.3: Representation of two examples of 2-loop contributions. The thick red line is the $\tau = 0^+$ surface on which the initial value problem is set up. The open circles represent the initial data. The filled blue circles represent operators $\mathbb{T}_{\mathbf{u}, \mathbf{v}}$. Left: contribution with a Γ_4 that factorizes into two Γ_2 's. Right: contribution with a Γ_3 .



5.2.4 Average over initial fluctuations

Eq. (5.15) provides an expression that resums all the leading contributions at the time $\tau = \tau_{\max}$. However, this is a very formal expression, and in this form it is not obvious that it leads to a result that is free of the secular divergences encountered at NLO. Moreover, this is not a formula that one can evaluate numerically since it contains functional derivatives with respect to the initial condition of the classical color field.

Fortunately, eq. (5.15) can be rewritten in a much more intuitive way. One should recall that the operator $\mathbb{T}_{\mathbf{u}}$ is the generator of shifts of the initial conditions at the point $\mathbf{u} \in \Sigma$ for the classical field \mathcal{A} . In other words, if $\mathbf{a}_0(\mathbf{u})$ is a perturbation of this initial condition, we can write:

$$\exp \left[\int_{\Sigma} d^3 \mathbf{S}_{\mathbf{u}} [\mathbf{a}_0 \cdot \mathbb{T}_{\mathbf{u}}] \right] \mathcal{F}[\mathbb{A}_0] = \mathcal{F}[\mathbb{A}_0 + \mathbf{a}_0] , \quad (5.16)$$

for any functional $\mathcal{F}[\mathbb{A}_0]$. ($\mathbb{A}_0 \equiv (\mathcal{A}_0, \mathcal{E}_0)$ is the collection of the initial classical fields \mathcal{A}_0 and their canonical momenta \mathcal{E}_0 – similarly, \mathbf{a}_0 combines the perturbation to the gauge fields and the perturbation to the electric fields). The second step is to note that⁵

$$\exp \left[\frac{1}{2} \int_{\Sigma} d^3 \mathbf{S}_{\mathbf{u}} d^3 \mathbf{S}_{\mathbf{v}} \Gamma_2(\mathbf{u}, \mathbf{v}) \cdot \mathbb{T}_{\mathbf{u}} \mathbb{T}_{\mathbf{v}} \right] = \int [\mathcal{D}\mathbf{a}_0] F_0[\mathbf{a}_0] \exp \left[\int_{\Sigma} d^3 \mathbf{S}_{\mathbf{u}} [\mathbf{a}_0 \cdot \mathbb{T}_{\mathbf{u}}] \right] , \quad (5.17)$$

with⁶

$$F_0[\mathbf{a}_0] \propto \exp \left[-\frac{1}{2} \int_{\Sigma} d^3 \mathbf{S}_{\mathbf{u}} d^3 \mathbf{S}_{\mathbf{v}} \mathbf{a}_0(\mathbf{u}) \Gamma_2^{-1}(\mathbf{u}, \mathbf{v}) \mathbf{a}_0(\mathbf{v}) \right] . \quad (5.18)$$

In eq. (5.17), the measure $[\mathcal{D}\mathbf{a}_0]$ contains one functional integration for each gauge field component and each electric field component involved in the initial condition on Σ . Thus, one can rewrite:

$$\mathbb{T}_{\text{resummed}}^{\mu\nu}(\mathbf{x}) = \int [\mathcal{D}\mathbf{a}_0] F_0[\mathbf{a}_0] \mathbb{T}_{\text{Lo}}^{\mu\nu}[\mathbb{A}_0[\tilde{\rho}_{1,2}] + \mathbf{a}_0; \mathbf{x}] . \quad (5.19)$$

In other words, the resummation of the terms that give the leading contribution at the time τ_{\max} can equivalently be performed by adding a fluctuating component to the initial condition of the classical field⁷ on Σ , with a Gaussian distribution. The previous formula can also be rewritten as

$$\mathbb{T}_{\text{resummed}}^{\mu\nu}(\mathbf{x}) = \int [\mathcal{D}\mathbb{A}_0] \mathcal{F}_0[\mathbb{A}_0; \tilde{\rho}_{1,2}] \mathbb{T}_{\text{Lo}}^{\mu\nu}[\mathbb{A}_0; \mathbf{x}] , \quad (5.20)$$

⁵An elementary form of this identity,

$$e^{\frac{\alpha}{2} \partial_x^2} f(x) = \int_{-\infty}^{+\infty} dz \frac{e^{-z^2/2\alpha}}{\sqrt{2\pi\alpha}} f(x+z) ,$$

can be proven by doing a Taylor expansion of the exponential in the left hand side and of $f(x+z)$ in the right hand side. In this simple example, one sees that an operator which is Gaussian in derivatives is a *smearing operator* that amounts to convoluting the target function with a Gaussian.

⁶The unwritten constant prefactor, proportional to $[\det(\Gamma_2)]^{-1/2}$, is such that the distribution $F_0[\mathbf{a}_0]$ has an integral over \mathbf{a}_0 normalized to unity.

⁷The same conclusion was reached in [4, 181], via different approaches.

where $\mathcal{F}_0[\mathbb{A}_0; \tilde{\rho}_{1,2}]$ is now a Gaussian functional whose center value depends on the configuration of $\tilde{\rho}_{1,2}$ of the fast sources:

$$\mathcal{F}_0[\mathbb{A}_0; \tilde{\rho}_{1,2}] \equiv F_0[\mathbb{A}_0 - \mathbb{A}_0[\tilde{\rho}_{1,2}]] . \quad (5.21)$$

The result obtained in eq. (5.20) is quite remarkable: the resummation of the loop corrections (i.e. quantum corrections) that lead to the most unstable behavior is equivalent to an average over a Gaussian ensemble of classical field configurations.

At this stage, it is easy to see why eq. (5.20) cures the problems encountered in a fixed loop order expansion. Indeed, the secular divergences at NLO are due to the fact that the strict g^2 expansion amounts to linearizing the equation of motion for perturbations around the classical field. The resummation that we have performed restores all the non-linearities in the dynamics of these perturbations –this is done by promoting the perturbation into a shift of the initial conditions for the non-linear evolution of the classical field– and as a consequence, eq. (5.20) does not contain secular divergences anymore. Indeed, since the Yang-Mills potential is bounded from below, the classical field \mathcal{A} whose initial condition is \mathbb{A}_0 leads to an energy-momentum tensor whose components are bounded at all times. Averaging over \mathbb{A}_0 with a Gaussian ensemble does not alter this conclusion.

5.3 Initial spectrum of fluctuations

5.3.1 Gauge invariance

For applications to heavy ion collisions, it is necessary to know the spectrum of fluctuations described by the distribution $F_0[\alpha_0]$ on a surface Σ at some very small proper time $\tau \rightarrow 0^+$. Before doing this, let us discuss some formal properties of these fluctuations, starting with gauge invariance.

From eq. (5.19), one can check that the resummed energy-momentum tensor is invariant under gauge transformations of the background classical gauge field:

$$\mathcal{A}_0[\tilde{\rho}_{1,2}] \rightarrow \Omega^\dagger \mathcal{A}_0^\mu[\tilde{\rho}_{1,2}] \Omega + \frac{i}{g} \Omega^\dagger \partial^\mu \Omega . \quad (5.22)$$

We already know that the energy-momentum tensor calculated in a given configuration of classical field is invariant under gauge transformations of this classical field. Therefore, $T_{\text{lo}}^{\mu\nu}[\mathbb{A}_0[\tilde{\rho}_{1,2}] + \alpha_0; \chi]$ is invariant under the transformation

$$\mathcal{A}_0[\tilde{\rho}_{1,2}] + \alpha_0 \rightarrow \Omega^\dagger \left[\mathcal{A}_0^\mu[\tilde{\rho}_{1,2}] + \alpha_0 \right] \Omega + \frac{i}{g} \Omega^\dagger \partial^\mu \Omega . \quad (5.23)$$

For the left hand side of eq. (5.19) to have the announced invariance property, it is sufficient that the distribution of fluctuations $\mathcal{F}_0[\mathbb{A}_0; \tilde{\rho}_{1,2}]$ be invariant when we simultaneously perform the transformation of eq. (5.22) for the background field and the transformation

$$\alpha_0 \rightarrow \Omega^\dagger \alpha_0 \Omega \quad (5.24)$$

for the fluctuation. Note that this is the expression of the gauge transformation when α_0 is expressed in the fundamental representation. Using $\Omega^\dagger t_r^a \Omega = t_r^b \Omega_{b\alpha}^\dagger$ (where the index r

denotes an arbitrary representation, and Ω_{ab} the components of Ω in the *adjoint* representation), this transformation law is equivalent to⁸

$$a_0^a \rightarrow \Omega_{ab}^\dagger a_0^b. \quad (5.25)$$

Formally, the invariance of the distribution of fluctuations under this transformation is satisfied provided the kernel $\Gamma_2(\mathbf{u}, \mathbf{v})$ transforms as

$$\Gamma_{2ab}(\mathbf{u}, \mathbf{v}) \rightarrow \Omega_{ac}^\dagger(\mathbf{u}) \Gamma_{2cd}(\mathbf{u}, \mathbf{v}) \Omega_{db}(\mathbf{v}) \quad (5.26)$$

when the classical field $\mathcal{A}_0[\tilde{\rho}_{1,2}]$ is gauge rotated according to eq. (5.22). Note that eq. (5.22) is nothing but the gauge transformation of the propagator of a small fluctuation on top of the background $\mathcal{A}_0[\tilde{\rho}_{1,2}]$, so it should be satisfied by construction, given the definition (5.4).

5.3.2 Ultraviolet divergences

Another important aspect of eq. (5.20) is the fact that it is potentially plagued by ultraviolet divergences. Indeed, since one is resumming quantum fluctuations, the energy-momentum tensor should receive a contribution from the (infinite) zero point energy. In order to regularize these divergences, one should temporarily limit by a cutoff Λ the largest momentum mode of the fluctuation a_0 . Since the energy-momentum tensor has a canonical dimension four, we expect that its dependence on this cutoff can be organized as follows:

$$T_{\text{resummed}}^{\mu\nu}(x) = c_1 \Lambda^4 + c_2 \Lambda^2 + c_3, \quad (5.27)$$

where $c_{1,2,3}$ are finite quantities. It is easy to renormalize the energy-momentum tensor by subtraction if one can prove that the divergences are truly a property of the vacuum and do not depend on the background classical field $\mathcal{A}_0[\tilde{\rho}_{1,2}]$. The coefficient c_1 is dimensionless – it is therefore a pure number, that cannot depend on the background field. The case of c_2 is a bit more tricky. Indeed, its dimension two a priori allows a dependence on the background field. However, since we know that the left hand side in eq. (5.27) is invariant under gauge transformations of the background field, we conclude that the coefficient c_2 must be a gauge invariant, local (because the left hand side is a local quantity), dimension two quantity. There is no such quantity in Yang-Mills theory, except for $c_2 = 0$. Thus, on the basis of gauge symmetry and locality, we expect that the only ultraviolet divergence in our expression for the resummed energy-momentum tensor is a quartic divergence, with a coefficient that does not depend on the background field. Because of this, it can in principle be computed once for all (by taking $\tilde{\rho}_{1,2} = 0$) and subtracted.

5.3.3 Locality of the spectrum

From the definition in eq. (5.18), it appears that the distribution of fluctuations on the initial surface is a Gaussian that is entirely determined by the 2-point function $\Gamma_2(\mathbf{u}, \mathbf{v})$. In eq. (5.4), this 2-point function is expressed in terms of the small fluctuations $a_{\pm k\lambda a}^\mu$, that are plane waves that have evolved from $x^0 = -\infty$ to the time of interest, over the classical background field \mathcal{A}_0 . This formula suggests that the spectrum of fluctuations on the Cauchy surface Σ depends on the entire past history of the system, from $x^0 = -\infty$ to the proper time τ of the

⁸The a_0^a (\mathbb{C} -number) introduced here is related to the a_0 (matrix in the representation r of $SU(3)$) of eq. (5.24) by $a_0 = a_0^a t_r^a$.

surface Σ . However, this spectrum is in fact a local (in time) property of the system, that depends only on the background field in the vicinity of the surface Σ and on a basis of small fluctuations over the background in that neighborhood.

Consider the equation for the propagation of small fluctuations on top of a classical field configuration \mathcal{A} ,

$$\frac{1}{\sqrt{-g}} \mathcal{D}_\alpha (\sqrt{-g} g^{\alpha\beta} g^{\nu\mu} (\mathcal{D}_\beta a_\mu - \mathcal{D}_\mu a_\beta)) - i g^{\alpha\beta} g^{\nu\mu} \mathcal{F}_{\mu\beta} a_\alpha = 0. \quad (5.28)$$

written here for a generic system of coordinates, possibly curvilinear. $g^{\mu\nu}$ is the metric tensor in this system of coordinates, and g denotes its determinant (negative since the signature of the metric is chosen to be $(+, -, -, -)$).

Since the equations of motion (5.28) of the small fluctuations are linear, the set of its solutions is a vector space, and it is sufficient to know a basis of this space in order to be able to construct any solution. For a real background field such as the classical field \mathcal{A}^μ , the evolution in time of the small fluctuations is unitary⁹. Therefore, there should be an inner product between pairs of solutions of eq. (5.28) that remains invariant during the evolution of these solutions. To construct this inner product, rewrite eq. (5.28) as

$$\mathcal{O}^{\nu\mu} a_\mu = 0, \quad (5.29)$$

with

$$\mathcal{O}^{\nu\mu} \equiv \mathcal{D}_\alpha \sqrt{-g} (g^{\nu\mu} g^{\alpha\beta} - g^{\nu\beta} g^{\mu\alpha}) \mathcal{D}_\beta - i g \sqrt{-g} g^{\nu\alpha} g^{\mu\beta} \mathcal{F}_{\alpha\beta}. \quad (5.30)$$

Consider now two solutions a_μ and b_μ of eq. (5.29), and start from the identity

$$0 = \int_\Omega d^4x a_\nu^*(x) \left[\overrightarrow{\mathcal{O}^{\nu\mu}} - \overleftarrow{\mathcal{O}^{\nu\mu}*} \right] b_\mu(x), \quad (5.31)$$

where Ω is some domain of space-time. This identity is a trivial consequence of the equations of motion for a^* and b . A remarkable property of the integrand in the right hand side is that it is a total derivative¹⁰,

$$\begin{aligned} a_\nu^*(x) \left[\overrightarrow{\mathcal{O}^{\nu\mu}} - \overleftarrow{\mathcal{O}^{\nu\mu}*} \right] b_\mu(x) &= \\ &= \partial_\alpha \left[\sqrt{-g} (g^{\nu\mu} g^{\alpha\beta} - \frac{1}{2} g^{\nu\beta} g^{\mu\alpha} - \frac{1}{2} g^{\nu\alpha} g^{\mu\beta}) (a_\nu^*(x) \overleftrightarrow{\mathcal{D}}_\beta b_\mu(x)) \right]. \end{aligned} \quad (5.32)$$

Therefore, one can use Stokes' theorem,

$$\int_\Omega d^4x \partial_\alpha F^\alpha = \int_{\partial\Omega} d^3\mathbf{S}_u n_\alpha F^\alpha \quad (5.33)$$

where $d^3\mathbf{S}_u$ is the measure on the boundary $\partial\Omega$, and n_α is a normal vector to the boundary, oriented outwards. Let us assume that the boundary $\partial\Omega$ is made of two locally space-like

⁹In event of confusion from the apparent structure of the last term of eq. (5.28), note that the components of the adjoint generators are purely imaginary, and therefore the function that multiplies a^μ in this term is real.

¹⁰For this property to be true, it is crucial that the last term in eq. (5.30) is real and one should properly take the complex conjugate of the covariant derivatives when they act on the left. This property is in fact closely related to the operator $\mathcal{O}^{\nu\mu}$ being Hermitian; the evolution of the fluctuations is unitary.

surfaces Σ_1 and Σ_2 , and a third boundary located at infinity in the spatial directions on which all the fields are vanishing. Then eq. (5.31) is equivalent to

$$\begin{aligned} & \int_{\Sigma_1} d^3 \mathbf{S}_u \sqrt{-g} \left(g^{\nu\mu} g^{\alpha\beta} - \frac{1}{2} g^{\nu\beta} g^{\mu\alpha} - \frac{1}{2} g^{\nu\alpha} g^{\mu\beta} \right) n_\alpha \left(a_\nu^*(u) \overleftrightarrow{\mathcal{D}}_\beta b_\mu(u) \right) \\ &= \int_{\Sigma_2} d^3 \mathbf{S}_u \sqrt{-g} \left(g^{\nu\mu} g^{\alpha\beta} - \frac{1}{2} g^{\nu\beta} g^{\mu\alpha} - \frac{1}{2} g^{\nu\alpha} g^{\mu\beta} \right) n_\alpha \left(a_\nu^*(u) \overleftrightarrow{\mathcal{D}}_\beta b_\mu(u) \right). \end{aligned} \quad (5.34)$$

We have thus proved, most generally, that an inner product defined as

$$(a|b) \equiv i \int_{\Sigma} d^3 \mathbf{S}_u \sqrt{-g} \left(g^{\nu\mu} g^{\alpha\beta} - \frac{1}{2} g^{\nu\beta} g^{\mu\alpha} - \frac{1}{2} g^{\nu\alpha} g^{\mu\beta} \right) n_\alpha \left(a_\nu^*(u) \overleftrightarrow{\mathcal{D}}_\beta b_\mu(u) \right), \quad (5.35)$$

is independent of the Cauchy surface Σ used to define it, provided a_μ and b_μ obey the equation of motion of small fluctuations. Note that we have added a factor i to its definition to ensure that it is Hermitian,

$$\begin{aligned} (a|b)^* &= (b|a), \\ (a^*|b^*) &= -(b|a) = -(a|b)^*. \end{aligned} \quad (5.36)$$

In the special case where Σ is a surface of constant τ and we work in the Fock-Schwinger gauge $A^\tau = 0$, we have $n \cdot \mathcal{D} = \partial_\tau$, and $n \cdot a = 0$, $n \cdot b = 0$. Therefore the inner product simplifies into

$$(a|b) \equiv i \int_{\tau=\text{const}} d^3 \mathbf{S}_u \sqrt{-g} g^{\nu\mu} \left(a_\nu^*(u) \overleftrightarrow{\partial}_\tau b_\mu(u) \right). \quad (5.37)$$

Now let us evaluate the inner product for pairs of field fluctuations taken from the set of the $a_{\pm k\lambda a}$. Since the inner product does not depend on the chosen time surface and since we know these fields at $x^0 \rightarrow -\infty$ (because they are defined via their initial condition in the remote past), we can evaluate the inner product by using plane wave initial conditions for these fluctuation fields. This gives

$$\begin{aligned} (a_{+k\lambda a} | a_{-l\rho b}) &= 0 \\ (a_{+k\lambda a} | a_{+l\rho b}) &= \delta_{\lambda\rho} \delta_{ab} (2\pi)^3 2k \delta(\mathbf{k} - \mathbf{l}) \\ (a_{-k\lambda a} | a_{-l\rho b}) &= -\delta_{\lambda\rho} \delta_{ab} (2\pi)^3 2k \delta(\mathbf{k} - \mathbf{l}). \end{aligned} \quad (5.38)$$

Thus this particular basis of the space of solutions of eq. (6.44) is orthonormal with respect to the invariant inner product defined in eq. (5.35). Note also that the $a_{+k\lambda a}$'s represent only one *half of the basis* of the vector space of solutions of eq. (5.28) –namely the solutions that have a positive frequency in the remote past. The other half is simply obtained by complex conjugation. It is easy to check that any unitary transformation of the positive energy solutions (and a concomitant change to the negative energy ones, that are their complex conjugates) transforms an orthonormal basis into another orthonormal basis, and leaves the formula eq. (5.4) unchanged. This remark is useful because it leaves us the freedom to label

the elements of the basis by other quantities than the Cartesian 3-momentum. This will be true in our specific case where we are interested in a basis in a curvilinear co-ordinate system.

It is important to note that the prefactor in front of the δ functions in eq. (5.38) exactly cancels the factors that are included in the integration measure in eq. (5.4), namely one has

$$\int \frac{d^3\mathbf{k}}{(2\pi)^3 2k} (a_{+\mathbf{k}\lambda\mathbf{a}} | a_{+\mathbf{l}\rho\mathbf{b}}) = 1 . \quad (5.39)$$

This remark in fact defines uniquely how the inner product of the basis elements should be normalized given a generic choice for the integration measure in eq. (5.4). Moreover, this makes clear that eq. (5.4) is just one particular representation of the correlator Γ_2 ; there exists such a representation for any orthonormal basis of the space of solutions of eq. (5.28), as we shall explain now. Thanks to the above inner product, one can spell out a general procedure¹¹ for constructing the correlator Γ_2 :

- i. Find a complete set of independent *positive energy* solutions $a_{\mathbf{k}}$ of eq. (5.28), where \mathbf{K} denotes collectively (usually a mix of continuous and discrete labels) all the labels necessary to index these solutions.
- ii. This set of solutions should obey the orthogonality condition,

$$(a_{\mathbf{k}} | a_{\mathbf{k}'}) = N_{\mathbf{k}} \delta_{\mathbf{k}\mathbf{k}'} \quad (5.40)$$

with $N_{\mathbf{k}}$ real and positive definite¹²,

- iii. The correlator Γ_2 is then given by

$$\Gamma_2(\mathbf{u}, \mathbf{v}) = \int d\mu_{\mathbf{k}} a_{\mathbf{k}}(\mathbf{u}) a_{\mathbf{k}}^*(\mathbf{v}) , \quad (5.41)$$

where the measure $d\mu_{\mathbf{k}}$ (a mix of integrals and discrete sums) is such that

$$\int d\mu_{\mathbf{k}} N_{\mathbf{k}} \delta_{\mathbf{k}\mathbf{k}'} = 1 . \quad (5.42)$$

It is clear from eqs. (5.40) and (5.42) that the Γ_2 given by eq. (5.41) is independent of how we normalize the solutions, provided we choose the integration measure accordingly. Moreover, the correlator Γ_2 does not depend on the orthonormal basis of solutions one chooses, and we only need to know the solutions at the time of interest (and thus we can avoid the complication of evolving the plane waves from the past through the forward light-cone).

A further simplification is possible because in practice we won't need to use directly eq. (5.41) for Γ_2 . Indeed, an ensemble of real-valued field fluctuations a^{μ} that have a 2-point equal-time correlation given by Γ_2 can be generated by the following formula,

$$a^{\mu}(\mathbf{x}) = \int d\mu_{\mathbf{k}} \left[c_{\mathbf{k}} a_{\mathbf{k}}^{\mu}(\mathbf{x}) + c_{\mathbf{k}}^* a_{\mathbf{k}}^{\mu*}(\mathbf{x}) \right] , \quad (5.43)$$

¹¹In this light, eq. (5.4) which represents Γ_2 in terms of the $a_{\pm\mathbf{k}\lambda\mathbf{a}}$'s, exploits one possible method of constructing such an orthonormal basis. In this case, one starts at $x^0 = -\infty$ with the plane waves, that are known to form an orthonormal basis, and evolves them forward to the time of interest. The time invariance of the inner product then guarantees us that we get an orthonormal basis on the forward light-cone.

¹²This means that the solutions $a_{\mathbf{k}}$ will in general be complex solutions.

where the coefficients c_k are random Gaussian-distributed complex numbers whose variance is given by

$$\begin{aligned}\langle c_k c_{k'}^* \rangle &= \frac{N_k}{2} \delta_{kk'} \\ \langle c_k c_{k'} \rangle &= \langle c_k^* c_{k'}^* \rangle = 0.\end{aligned}\tag{5.44}$$

Based on these ideas, we have constructed in [13] an orthonormal basis of positive frequency solutions, that can be used in order to generate an appropriate ensemble of fluctuations. Naturally, since the background field A^μ is known analytically only at $\tau = 0^+$ (and in a small neighborhood of this surface by performing an expansion in powers of τ), the solutions we have obtained are themselves only valid at small τ . This is however sufficient in practice, provided one starts the time evolution at a time $\tau_0 \ll Q_s^{-1}$.

5.4 Time evolution of the distribution of initial conditions

5.4.1 Liouville equation

So far, we have not specified the initial surface Σ . To be able to use the power counting rules that led to the exponentiation of the 1-loop result, i.e. to a Gaussian distribution for the initial value of the classical field, it is necessary that this surface be located before the instabilities develop. For instance, eq. (5.20) is valid with a Gaussian \mathcal{F}_0 if the surface Σ is taken just above the light-cone, at a fixed proper time $\tau = 0^+$. If the initial surface Σ was taken at a time where the instabilities are already fully developed, then our power counting would be unable to pick up all the important contributions.

However, one should also be able to recover the left hand side of eq. (5.20) with any initial surface, provided one modifies appropriately the distribution of initial fields. In particular, it may be useful to start at a surface Σ_τ located at a later proper time τ , i.e. we would like to rewrite eq. (5.20) as

$$T_{\text{resummed}}^{\mu\nu}(x) = \int [\mathcal{D}A_\tau] \mathcal{F}_\tau[A_\tau; \tilde{\rho}_{1,2}] T_{\text{LO}}^{\mu\nu}[A_\tau; x],\tag{5.45}$$

For observables measured at the point x to be independent of this initial time, the distribution \mathcal{F}_0 must be replaced by a distribution \mathcal{F}_τ , in order to compensate the fact that the evolution with the Yang-Mills equations is now shortened¹³. In order to derive the renormalization group equation for \mathcal{F}_τ that realizes this invariance, it is useful to view $\mathcal{F}_0[A_0; \tilde{\rho}_{1,2}]$ as a classical phase-space density for a statistical ensemble of systems. The evolution equation for \mathcal{F}_τ describes how this ensemble of systems flows under the classical Yang-Mills equations. This equation is nothing but the Liouville equation:

$$\frac{\partial \mathcal{F}_\tau}{\partial \tau} + \{\mathcal{F}_\tau, \mathcal{H}_{\text{YM}}\} = 0,\tag{5.46}$$

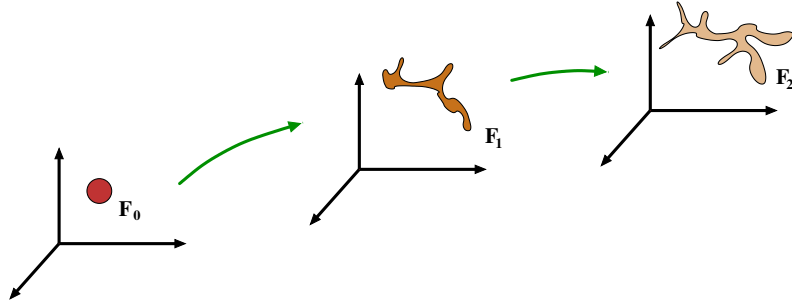
¹³If one knew the distribution \mathcal{F}_τ at the time when the observable is measured, one could avoid entirely the step that consists in solving the Yang-Mills equations.

where \mathcal{H}_{YM} is the Hamiltonian corresponding to the classical Yang-Mills equations¹⁴. The symbol $\{\cdot, \cdot\}$ denotes the classical Poisson bracket, i.e.

$$\{A, B\} \equiv \int d^3\mathbf{x} \left(\frac{\delta A}{\delta \mathcal{A}(\mathbf{x})} \frac{\delta B}{\delta \mathcal{E}(\mathbf{x})} - \frac{\delta A}{\delta \mathcal{E}(\mathbf{x})} \frac{\delta B}{\delta \mathcal{A}(\mathbf{x})} \right), \quad (5.47)$$

where \mathcal{E} is the canonical momentum associated to \mathcal{A} . It is indeed easy to check that if

Figure 5.4: Illustration of the Hamiltonian flow of the ensemble of initial conditions described by the distribution $\mathcal{F}_0[\mathcal{A}_0; \bar{\rho}_{1,2}]$.



eq. (5.46) is satisfied, then any observable that depends solely on the value of the classical field at some later time is independent on the time at which one sets the initial conditions if its expectation value is given by eq. (5.45).

Note that in the regime where the self-interactions of the gauge fields cannot be neglected, especially at early times when the field amplitude is large, the Yang-Mills Hamiltonian has large cubic and quartic terms in the fields and their conjugate momenta. In eq. (5.46), these non quadratic terms of H_{YM} generate non-gaussianities in the distribution of fields. In other words, the distribution of fields \mathcal{F}_τ remains Gaussian only if the Hamiltonian in the Liouville equation is quadratic.

From eq. (5.46), one can prove that the phase-space density $\mathcal{F}_\tau[\mathcal{A}; \bar{\rho}_{1,2}]$ is conserved along a given trajectory (Liouville theorem¹⁵). This result has another, particularly intuitive, formulation: if one sees the evolution of \mathcal{F}_τ as that of a fluid in phase-space (see the figure 5.4), then the Liouville theorem is equivalent to the incompressibility of this “fluid”. The initial distribution \mathcal{F}_0 (droplet of fluid in this analogy) gets deformed under the time evolution, but the volume it occupies in phase-space remains constant.

¹⁴If \mathcal{E} is the canonical momentum associated to the field \mathcal{A} , then the classical Yang-Mills equations read:

$$\dot{\mathcal{A}} = \partial \mathcal{H}_{\text{YM}} / \partial \mathcal{E} \quad , \quad \dot{\mathcal{E}} = -\partial \mathcal{H}_{\text{YM}} / \partial \mathcal{A} \quad .$$

¹⁵Liouville’s theorem can be proven as follows. Denote $f(\tau) = \mathcal{F}_\tau[\mathcal{A}(\tau); \bar{\rho}_{1,2}]$ where $\mathcal{A}(\tau)$ obeys the Yang-Mills equations and \mathcal{F}_τ the Liouville equation. We have

$$\dot{f}(\tau) = \frac{\partial \mathcal{F}_\tau}{\partial \tau} + \mathcal{A} \frac{\delta \mathcal{F}_\tau}{\delta \mathcal{A}} + \dot{\mathcal{E}} \frac{\delta \mathcal{F}_\tau}{\delta \mathcal{E}} = -\{\mathcal{F}_\tau, H_{\text{YM}}\} + \{\mathcal{F}_\tau, H_{\text{YM}}\} = 0 \quad .$$

5.4.2 Ergodicity and thermalization?

Numerical simulations of the classical Yang-Mills equations have shown that they have positive Lyapunov exponents [28, 29, 178], i.e. that phase-space trajectories that start very close tend to diverge exponentially in time, making the dynamics chaotic. From numerical simulations on small lattices, it has also been argued that the phase-space trajectories of classical Yang-Mills equations are ergodic: most of the trajectories fill densely the manifold corresponding to energy conservation, spending in a given area a time proportional to the measure of that area.

At this time, the precise implications of this behavior on the thermalization of the system of color fields are not known and one can only speculate. If the system was contained into in a fixed sized box, then it would be very plausible that a micro-canonical equilibrium ensemble is reached in a time determined by the inverse of the largest Lyapunov exponent. To make the argument a bit more precise, recall that for a classical configuration of color fields the components of the energy-momentum tensor read:

$$\begin{aligned} T^{00} &= \frac{1}{2} (E_a^i E_a^i + B_a^i B_a^i) , \\ T^{0i} &= \epsilon^{ijk} E_a^j B_a^k , \\ T^{ij} &= T^{00} \delta^{ij} - E_a^i E_a^j - B_a^i B_a^j . \end{aligned} \quad (5.48)$$

If one assumes that the energy density T^{00} is conserved along a classical trajectory¹⁶ and that the ergodicity of a typical trajectory¹⁷ implies that all the configurations of the fields E_a^i, B_a^i compatible with a given T^{00} are equally likely¹⁸, then one obtains trivially the following results for the averages over the distribution $\mathcal{F}_0[A_0; \tilde{\rho}_{1,2}]$:

$$\begin{aligned} \langle T^{0i} \rangle &= 0 , \\ \langle T^{ij} \rangle &= \frac{\delta^{ij}}{3} \langle T^{00} \rangle . \end{aligned} \quad (5.49)$$

This form of $\langle T^{\mu\nu} \rangle$ would justify the applicability of ideal hydrodynamics to the system, since we have now an energy momentum tensor that has the form expected for an ideal fluid. Moreover, we see that the equation of state of the system would be $\epsilon = 3p$, as expected from its scale invariance. However, in the case of a rapidly expanding system, as is the case for heavy ion collisions, the conclusion is far from clear since the expansion may hinder the isotropization.

¹⁶Strictly speaking, only the total (i.e. integrated over space) energy is conserved. However, on short time-scales, the energy cannot move very far because of causality and its local density should remain approximately constant.

¹⁷The average over fluctuating initial conditions implied by eq. (5.20) is crucial for this argument. Indeed, the phase-space trajectory corresponding to the plain Glasma fields is not ergodic: it remains confined to the subspace of fields that are independent of rapidity, which have a negative longitudinal pressure. By allowing fluctuations of the initial field on the light-cone, one frees the phase-space trajectories from this constraint, and they can now explore in full the manifold allowed by energy conservation.

¹⁸This is indeed what one expects of ergodicity: all the micro-states corresponding to the same energy are equally likely.

Chapter 6

Toy model study: Scalar fields in a box



In the previous chapter, we have argued that in order to cure the problem posed by secular divergences in higher order corrections, one should add Gaussian fluctuations to the initial conditions on the light-cone for the classical Glasma fields. Although it is easy to see that this cures the problem of secular divergences, the consequences of this resummation on the energy-momentum tensor are at best speculative at this point, because the implementation of this resummation in QCD is technically challenging. The hope is that this resummation includes all the physical processes that are important for the equilibration of the system, but a complete proof of this statement is still out of sight.

Here, we propose to apply the same ideas to a much simpler quantum field theory, in which one can study these questions numerically in great detail. This model will serve as a concrete realization of the resummation program we have proposed in the previous chapter. This toy model shares many of the features of the CGC, in particular the evolution of the system is driven by a strong external source, and it also has instabilities that call for a resummation identical to the one advocated in the previous chapter.

In the first section of the chapter, we setup the model. We also compute its energy-momentum tensor at LO and NLO, and observe explicitly the secular divergences in the NLO correction. Then, we resum the secular terms, and obtain a formula with Gaussian fluctuations for the initial conditions at $t = 0$ of the classical field.

In the section 6.2, we first look at the effect of the zero-mode –spatially uniform– fluctuations. We show that they make the pressure relax towards the equilibrium pressure, and that they lead to a micro-canonical phase-space density. Due to the great simplicity of the model, it is possible to interpret these effects as a decoherence phenomenon due to the non-linear couplings between the fields. We also show that the same relaxation occurs in a system which is longitudinally expanding, as would be the case in a collision.

In the section 6.3, we describe the results of numerical simulations with the complete spectrum of fluctuations, including spatially dependent fluctuations. We again observe that the pressure relaxes towards the equilibrium pressure, in a time that decreases with increasing coupling constant. We also compute the fluctuations of the energy density, and show a qualitative change of shape as time increases.

Then, we compute the spectral density of the system. This tells us that, after a brief transient regime, it is populated by massive quasi-particles. Next, we perform a direct computation of the occupation number in the system. After a rather short transient regime dominated by resonance phenomena, we observe a scaling regime reminiscent of turbulence over some range of k . At late times, the system appears to approach thermal equilibrium with a slowly varying number of particles, and a Bose condensate forms at $\mathbf{k} = 0$ due to a particle excess.

6.1 Model setup

6.1.1 CGC-like scalar model

Our aim is to set up a scalar field model that mimics the main features of the Color Glass Condensate applied to the description of the early stages of heavy ion collisions. To achieve this, we couple a scalar field to an external source J , via the following Lagrangian:

$$\mathcal{L} \equiv \frac{1}{2}(\partial_\mu \phi)(\partial^\mu \phi) - \frac{g^2}{4!}\phi^4 + J\phi. \quad (6.1)$$

In the CGC framework, the source J coupled to the gauge fields represents the color charge current carried by the two colliding projectiles, and therefore this current is zero at positive proper time (i.e. after the collision has taken place). In order to mimic this feature while keeping a simple coordinate system, we assume here that the source J is nonzero only for Cartesian time $x^0 < 0$, and we parameterize it as¹

$$J(x) \sim \theta(-x^0) \frac{Q^3}{g}. \quad (6.2)$$

At $x^0 > 0$, the external source J is zero, and the fields evolve solely via their self-interactions, like the color fields radiated in the collision of two hadrons or nuclei in the CGC framework.

In eq. (6.2), we have incorporated two additional features that are also present in the CGC. The external current J is strong in the sense that it contains a power of the inverse coupling (that we assume to be small, in order to legitimate an expansion in powers of g^2), and its dimension is provided by the parameter Q (that plays in this model the role of the saturation scale in the Color Glass Condensate).

Note that a scalar field theory with a ϕ^4 coupling in four space-time dimensions is scale invariant at the classical level (one can see this from the fact that the coupling constant g is dimensionless for this theory). In our model, this scale invariance is broken solely by the coupling to the external source J , that introduces the scale Q . Thus, we should expect that all physical quantities will simply be given by some power of Q times a prefactor that depends on the coupling g .

6.1.2 $T^{\mu\nu}$ at leading order

Like in the CGC, the leading order (tree level) contribution to the energy-momentum tensor can be expressed solely in terms of a classical solution φ of the field equation of motion. Namely, one has

$$T_{\text{Lo}}^{\mu\nu}(x) = \partial^\mu \varphi \partial^\nu \varphi - g^{\mu\nu} \left[\frac{1}{2}(\partial_\alpha \varphi)^2 - \frac{g^2}{4!}\varphi^4 \right], \quad (6.3)$$

¹In the actual numerical implementation of the model, the time dependent prefactor also contains a factor that makes it vanish when $x^0 \rightarrow -\infty$ in order to have a free theory in the remote past.

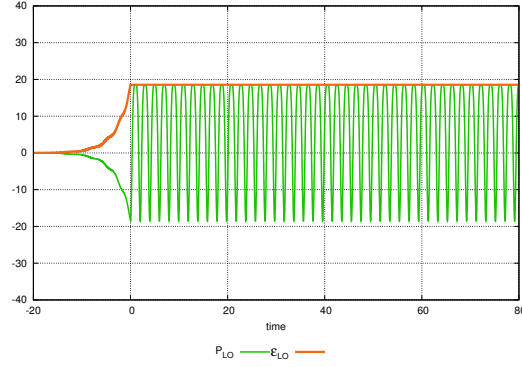
where

$$\begin{aligned} \square\varphi + \frac{g^2}{3!}\varphi^3 &= J, \\ \lim_{x^0 \rightarrow -\infty} \varphi(x^0, \mathbf{x}) &= 0. \end{aligned} \quad (6.4)$$

Clearly, due to the non-linear term in the equation of motion, the solution φ (and hence the coefficient c_0) depends on gJ to all orders. This LO energy momentum tensor is conserved²,

$$\partial_\mu T_{LO}^{\mu\nu} = 0. \quad (6.5)$$

Figure 6.1: Components of $T_{LO}^{\mu\nu}$ for a spatially uniform external source. To perform this calculation, we have taken in eq. (6.4) a source $J = g^{-1}Q^3\theta(-x^0)e^{aQx^0}$ (with $g = 1$, $a = 0.1$ and $Q = 2.5$), that disappears adiabatically in the remote past.



If the source J is taken spatially homogeneous, then the energy-momentum tensor evaluated at leading order takes the simple form:

$$T_{LO}^{\mu\nu}(x) = \begin{pmatrix} \epsilon_{LO} & 0 & 0 & 0 \\ 0 & p_{LO} & 0 & 0 \\ 0 & 0 & p_{LO} & 0 \\ 0 & 0 & 0 & p_{LO} \end{pmatrix}, \quad (6.6)$$

with the leading order energy density and pressure given by

$$\begin{aligned} \epsilon_{LO} &= \frac{1}{2}\dot{\varphi}^2 + \frac{g^2}{4!}\varphi^4 \\ p_{LO} &= \frac{1}{2}\dot{\varphi}^2 - \frac{g^2}{4!}\varphi^4. \end{aligned} \quad (6.7)$$

It is trivial to check that the energy density ϵ_{LO} is constant in time at $x^0 > 0$ (after the external source J has been switched off), while the pressure p_{LO} is a periodic function of time at $x^0 > 0$, as illustrated in the figure 6.1. Clearly, at this order of the calculation of ϵ_{LO} and p_{LO} , one does not have a well defined (single-valued) relationship $\epsilon_{LO} = f(p_{LO})$: in other words, *there is no equation of state at leading order in g^2 .*

²Strictly speaking, this is true only at $x^0 > 0$. At negative times, some energy is injected into the system by the external source J .

6.1.3 $T^{\mu\nu}$ at next to leading order

At next to leading order, the energy momentum tensor can be written as

$$\begin{aligned} T_{\text{NLO}}^{\mu\nu} = & c_1 Q^4 = \partial^\mu \varphi \partial^\nu \beta + \partial^\mu \beta \partial^\nu \varphi - g^{\mu\nu} \left[\partial_\alpha \beta \partial^\alpha \varphi - \beta U'(\varphi) \right] + \\ & + \int \frac{d^3 \mathbf{k}}{(2\pi)^3 2k} \left[\partial^\mu a_{-\mathbf{k}} \partial^\nu a_{+\mathbf{k}} - \frac{g^{\mu\nu}}{2} \left(\partial_\alpha a_{-\mathbf{k}} \partial^\alpha a_{+\mathbf{k}} - U''(\varphi) a_{-\mathbf{k}} a_{+\mathbf{k}} \right) \right], \end{aligned} \quad (6.8)$$

where for brevity we use the notation $U(\varphi) \equiv g^2 \varphi^4 / 4!$ (and the prime denotes a derivative with respect to φ). In this formula, β and $a_{\pm\mathbf{k}}$ are small field perturbations, that are defined by the following equations:

$$\begin{aligned} & \left[\square + U''(\varphi) \right] a_{\pm\mathbf{k}} = 0 \\ & \lim_{x^0 \rightarrow -\infty} a_{\pm\mathbf{k}}(x) = e^{\pm i\mathbf{k} \cdot \mathbf{x}}, \\ & \left[\square + U''(\varphi) \right] \beta = -\frac{1}{2} U'''(\varphi) \int \frac{d^3 \mathbf{k}}{(2\pi)^3 2k} a_{-\mathbf{k}} a_{+\mathbf{k}} \\ & \lim_{x^0 \rightarrow -\infty} \beta(x) = 0. \end{aligned} \quad (6.9)$$

Note that since in our model the classical field φ is spatially homogeneous, the equation of motion of $a_{\pm\mathbf{k}}$ simplifies into

$$\ddot{a}_{\pm\mathbf{k}} + (\mathbf{k}^2 + U''(\varphi)) a_{\pm\mathbf{k}} = 0. \quad (6.10)$$

Moreover, for the same reason, the field fluctuation β depends only on time.

After some algebra, it is easy to check that the energy-momentum tensor is also conserved at NLO³ for $x^0 > 0$,

$$\partial_\mu T_{\text{NLO}}^{\mu\nu} = 0. \quad (6.11)$$

The 00 component of $T_{\text{NLO}}^{\mu\nu}$ gives us the energy density at NLO,

$$\epsilon_{\text{NLO}} = \dot{\beta} \dot{\varphi} + \beta U'(\varphi) + \frac{1}{2} \int \frac{d^3 \mathbf{k}}{(2\pi)^3 2k} \left[\dot{a}_{-\mathbf{k}} \dot{a}_{+\mathbf{k}} + (\mathbf{k}^2 + U''(\varphi)) a_{-\mathbf{k}} a_{+\mathbf{k}} \right]. \quad (6.12)$$

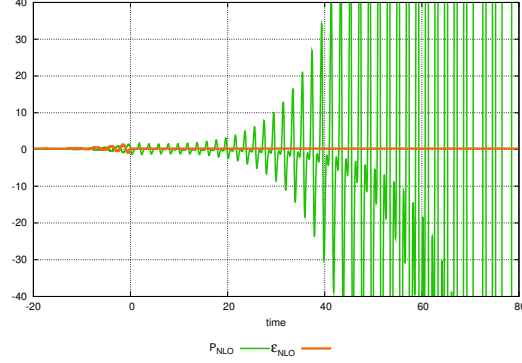
Given eqs. (6.9), it is straightforward to verify that this correction is also constant in time, $\dot{\epsilon}_{\text{NLO}} = 0$, in agreement with eq. (6.11). The 11 component of eq. (6.8) –the NLO pressure in the x direction– reads

$$p_{\text{NLO}} = \dot{\beta} \dot{\varphi} - \beta U'(\varphi) + \frac{1}{2} \int \frac{d^3 \mathbf{k}}{(2\pi)^3 2k} \left[\dot{a}_{-\mathbf{k}} \dot{a}_{+\mathbf{k}} - (\mathbf{k}^2 - 2k_x^2 + U''(\varphi)) a_{-\mathbf{k}} a_{+\mathbf{k}} \right]. \quad (6.13)$$

We have evaluated numerically ϵ_{NLO} and p_{NLO} for a coupling constant $g = 1$, by first solving eqs. (6.9) for β and for the $a_{\mathbf{k}}$'s (for a discretized set of \mathbf{k} 's). The results of this calculation are shown in the figure 6.2. From this evaluation, we see that the energy density at NLO is

³Naturally, this was obvious from the start. Indeed, since the conservation equation $\partial_\mu T^{\mu\nu} = 0$ is linear in the components of $T^{\mu\nu}$, it does not mix the different g^2 orders and therefore the conservation equation must be satisfied by each order separately.

Figure 6.2: Components of $T_{\text{NLO}}^{\mu\nu}$ for a spatially uniform external source. This calculation has been done for $g = 1$.



constant at $\chi^0 > 0$, as we expected⁴. We also notice that for $g = 1$, the NLO correction to the energy density is very small, of the order of 1.4% of the LO result⁵. Thus, we conclude from this that for such a value of the coupling, we have a well behaved perturbative expansion for ϵ . However, the NLO pressure behaves quite differently: not only it is not constant (and hence there is no equation of state at NLO), but it also has oscillations whose amplitude grows exponentially at large χ^0 . Therefore, the NLO correction to the pressure eventually becomes larger than the LO contribution, and the perturbative expansion in powers of g^2 breaks down. Another noticeable fact is that at $\chi^0 = 0$, p_{NLO} is still a small correction to p_{LO} ; it is only later that it becomes large.

6.1.4 Interpretation of the NLO result

The divergence of the pressure at NLO can be understood as a consequence of the unstable behavior of $\alpha_{\pm\mathbf{k}}(\chi)$ for some values of \mathbf{k} . The stability properties of the small fluctuations in ϕ^4 field theory are well known:

- i. There is a range in $|\mathbf{k}|$ where the $\alpha_{\mathbf{k}}$'s diverge exponentially in time, due to *parametric resonance*. On the figure 6.3, we have represented the Lyapunov exponent as a function of the spatial momentum of the fluctuation⁶.
- ii. The zero mode $\mathbf{k} = 0$ fluctuation, α_0 , diverges linearly in time, a phenomenon closely related to the fact that the oscillation frequency in a non-harmonic potential depends on the amplitude of the oscillations.

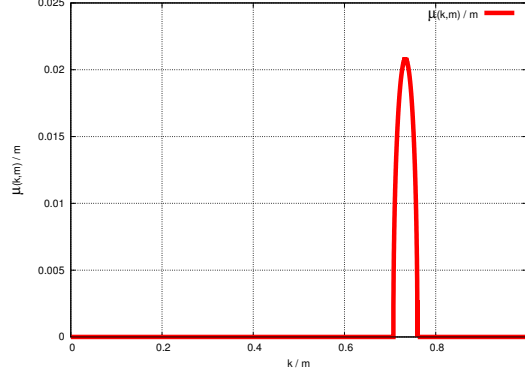
In addition, one observes numerically that the fluctuation modes in the vicinity of $\mathbf{k} = 0$, although they are not mathematically unstable, can reach quite large values (they appear to

⁴This time independence can be seen as a test of the accuracy of the numerical calculation, because it results from a cancellation between several terms that grow with time.

⁵Indeed, since there is a prefactor $1/4!$ in our definition of the interaction potential, $g = 1$ corresponds to fairly weak interactions.

⁶For a discussion of parametric resonance in other approaches and contexts (in particular inflationary cosmology), see [181–185].

Figure 6.3: *Lyapunov exponent for small fluctuations in a ϕ^4 scalar theory.*

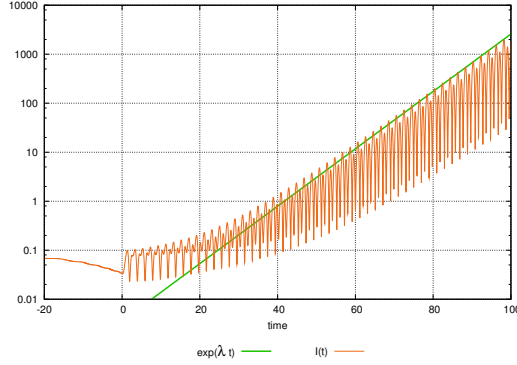


grow linearly for some time, before going down again). Because of the existence of these modes that grow in time, integrals such as

$$I(\chi^0) \equiv \int \frac{d^3\mathbf{k}}{(2\pi)^3 2k} a_{-\mathbf{k}}(\chi) a_{+\mathbf{k}}(\chi), \quad (6.14)$$

that appear in the components of $T_{\text{NLO}}^{\mu\nu}$ or in the right hand side of the equation for β , have secular divergences as illustrated in the figure 6.4. In this plot, one can check that the en-

Figure 6.4: *Numerical evaluation of the integral defined in eq. (6.14). We also show an exponential fit of the envelope.*



velope of the oscillations grows exponentially, with a growth rate $\lambda \approx 2 * \mu_{\text{max}}$ where μ_{max} is the maximal Lyapunov exponent in the resonance band. Note that, if the same integral is evaluated with an upper cutoff that excludes the resonance band from the integration domain, then $I(\chi^0)$ grows only linearly, because now its behavior is dominated by the soft fluctuation modes whose growth is only linear.

Secular divergences in integrals such as eq. (6.14) cancel in the calculation of ϵ_{NLO} because the energy density is protected by the conservation of the energy momentum tensor. However,

they do not cancel in p_{NLO} , and this is why we have the divergent behavior displayed in the figure 6.2.

6.1.5 Resummation of the NLO corrections

Like in the CGC framework, one can formally express the NLO correction to the energy-momentum tensor as the action of a certain operator on the LO contribution,

$$T_{\text{NLO}}^{\mu\nu}(x) = \left[\int d^3\mathbf{u} \beta \cdot \mathbb{T}_{\mathbf{u}} + \frac{1}{2} \int d^3\mathbf{u} d^3\mathbf{v} \int \frac{d^3\mathbf{k}}{(2\pi)^3 2k} [\mathbf{a}_{+\mathbf{k}} \cdot \mathbb{T}_{\mathbf{u}}] [\mathbf{a}_{-\mathbf{k}} \cdot \mathbb{T}_{\mathbf{v}}] \right] T_{\text{LO}}^{\mu\nu}(x), \quad (6.15)$$

where the operator $\mathbb{T}_{\mathbf{u}}$ is the generator of shifts of the initial conditions φ_0 , $\partial_0 \varphi_0$ (at $x^0 = 0$) of the classical field:

$$\mathbf{a} \cdot \mathbb{T}_{\mathbf{u}} \equiv \mathbf{a}(0, \mathbf{u}) \frac{\delta}{\delta \varphi_0(\mathbf{u})} + \dot{\mathbf{a}}(0, \mathbf{u}) \frac{\delta}{\delta \partial_0 \varphi_0(\mathbf{u})}. \quad (6.16)$$

As we have seen in the Yang-Mills case, a simple resummation that leads to an energy-momentum tensor which is finite at all times consists in starting from eq. (6.15) and in exponentiating the quadratic part⁷ of the operator inside the square brackets,

$$T_{\text{resummed}}^{\mu\nu}(x) \equiv \exp \left[\frac{1}{2} \int d^3\mathbf{u} d^3\mathbf{v} \int \frac{d^3\mathbf{k}}{(2\pi)^3 2k} [\mathbf{a}_{+\mathbf{k}} \cdot \mathbb{T}_{\mathbf{u}}] [\mathbf{a}_{-\mathbf{k}} \cdot \mathbb{T}_{\mathbf{v}}] \right] T_{\text{LO}}^{\mu\nu}(x). \quad (6.17)$$

Here also, this formula can be recasted as a functional integral over fluctuations⁸ for the initial condition of the classical field φ ,

$$T_{\text{resummed}}^{\mu\nu} = \int [D\alpha(x) D\dot{\alpha}(x)] F[\alpha, \dot{\alpha}] T_{\text{LO}}^{\mu\nu}[\varphi_0 + \alpha], \quad (6.18)$$

where the distribution $F[\alpha, \dot{\alpha}]$ is Gaussian in $\alpha(x)$ and $\dot{\alpha}(x)$, with 2-point correlations given by:

$$\begin{aligned} \langle \alpha(x) \alpha(y) \rangle &= \int \frac{d^3\mathbf{k}}{(2\pi)^3 2k} \mathbf{a}_{+\mathbf{k}}(0, x) \mathbf{a}_{-\mathbf{k}}(0, y), \\ \langle \dot{\alpha}(x) \dot{\alpha}(y) \rangle &= \int \frac{d^3\mathbf{k}}{(2\pi)^3 2k} \dot{\mathbf{a}}_{+\mathbf{k}}(0, x) \dot{\mathbf{a}}_{-\mathbf{k}}(0, y). \end{aligned} \quad (6.19)$$

When the background field is zero (i.e. in the vacuum), the $\mathbf{a}_{\pm\mathbf{k}}$'s are equal to the ordinary plane waves. In this case, it is easy to check that the expression in Fourier space of this distribution reads

$$F[\alpha_{\mathbf{k}}, \dot{\alpha}_{\mathbf{k}}] = \exp \left[- \int \frac{d^2\mathbf{k}}{(2\pi)^3} \frac{|\dot{\alpha}_{\mathbf{k}}|^2 + k^2 |\alpha_{\mathbf{k}}|^2}{k} \right], \quad (6.20)$$

where $\alpha_{\mathbf{k}}, \dot{\alpha}_{\mathbf{k}}$ are the spatial Fourier transforms of $\alpha(x), \dot{\alpha}(x)$ respectively. This expression of the vacuum quantum fluctuations is identical to the one derived in [4] by using the path integral formulation of the problem.

⁷One could also include the linear term $\beta \cdot \mathbb{T}_{\mathbf{u}}$ in the resummation simply by shifting by an amount $\beta(0, x)$ the central value of the Gaussian ensemble of initial conditions. However, since this central value is of order $\mathcal{O}(g^{-1})$ while $\beta(0, x) \sim \mathcal{O}(g)$, such a shift can be safely neglected.

⁸This formula was first proposed in [181], and applied to the reheating problem in cosmology in [186]. In field theories at finite temperature in equilibrium, similar classical approximations have been studied in [187, 188].

6.2 Toy calculation with uniform fluctuations

6.2.1 Introduction

Before presenting the full results of an actual numerical evaluation of eq. (6.18), let us first present the results of a calculation in which one includes only spatially homogeneous fluctuations. Even though this is not realistic, this much simpler calculation will be very instructive regarding the possible effect of these fluctuations on the behavior of the energy-momentum tensor.

When we consider spatially homogeneous fluctuations only, the main simplification is that the functional integrations over the fields α and $\dot{\alpha}$ in eq. (6.18) become ordinary integrals over a pair of real numbers, with a Gaussian weight :

$$Z(\alpha, \dot{\alpha}) \equiv \exp \left[- \left(\frac{\alpha^2}{2\sigma_1} + \frac{\dot{\alpha}^2}{2\sigma_2} \right) \right] . \quad (6.21)$$

The two parameters $\sigma_{1,2}$ can be used in this toy calculation in order to control the magnitude of the fluctuations: in the limit $\sigma_{1,2} \rightarrow 0$, we recover the leading order case that has no fluctuations at all.

The second important simplification in this toy calculation is that, since both the underlying classical field and the fluctuations are spatially homogeneous, the field equation of motion is not a true partial differential equation but an ordinary differential equation. Therefore, we do not need to use a lattice in order to solve it numerically. The expressions for the energy density and the pressure read

$$\begin{aligned} \epsilon &= \left\langle \frac{1}{2} \dot{\varphi}^2 + \mathcal{U}(\varphi) \right\rangle_{\alpha, \dot{\alpha}} , \\ p &= \left\langle \frac{1}{2} \dot{\varphi}^2 - \mathcal{U}(\varphi) \right\rangle_{\alpha, \dot{\alpha}} , \end{aligned} \quad (6.22)$$

where φ is the solution of the classical equation of motion whose value at $x^0 = 0$ is $\varphi_0 + \alpha$ (and $\dot{\varphi}_0 + \dot{\alpha}$ for its time derivative). The brackets $\langle \dots \rangle_{\alpha, \dot{\alpha}}$ denote an averaging over all possible values of $\alpha, \dot{\alpha}$ with the distribution of eq. (6.21).

6.2.2 Energy momentum tensor

In the figure 6.5, we display the result of this calculation in the limit where we do not have fluctuations ($\sigma_{1,2} \rightarrow 0$), and naturally we get a result which is equivalent to the one displayed in the figure 6.1 for the plain leading order calculation. Note that in this figure, for reasons that will become obvious shortly, we have represented the energy density divided by three. In the figure 6.6, we show the results of the same calculation performed with non-zero widths $\sigma_{1,2}$ for the Gaussian distribution of fluctuations. We observe a striking difference compared to the previous (LO) figure: now, the oscillations of the pressure are damped and the value of the pressure relaxes to $\epsilon/3$. In other words, we now have a single-valued relationship between the pressure and the energy density, i.e. an *equation of state*. Moreover, this equation of state, $\epsilon = 3p$, is that of a scale invariant system in $1 + 3$ dimensions.

Figure 6.5: Components of $T^{\mu\nu}$ when no fluctuations are included (i.e. at leading order).

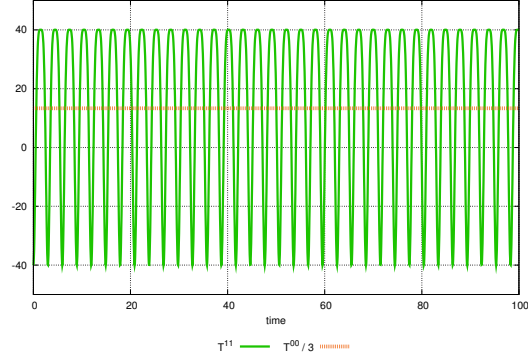


Figure 6.6: Components of $T^{\mu\nu}$ with a Gaussian ensemble of spatially uniform initial conditions.

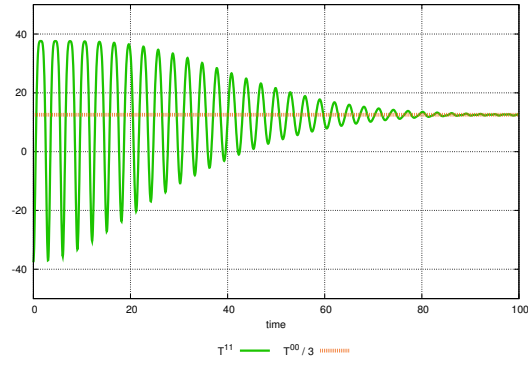
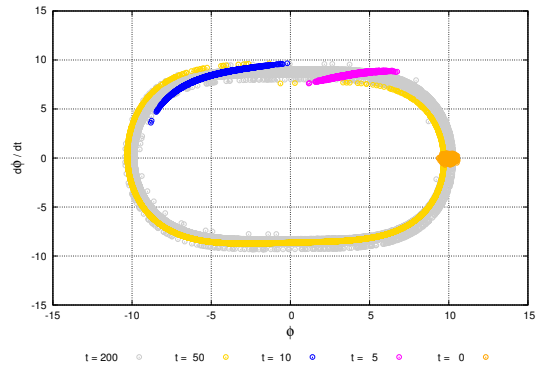


Figure 6.7: Phase-space distribution of the ensemble of classical fields, at various stages of the time evolution.



6.2.3 Phase-space density

It is also instructive to look at the phase-space density $\mathcal{F}_t(\varphi, \dot{\varphi})$ of the points $(\varphi, \dot{\varphi})$ as the system evolves in time. This is shown in the figure 6.7. At $t = 0$, we start with a Gaussian distribution of the initial conditions, with a small dispersion around the average values ($\varphi = 10$ and $\dot{\varphi} = 0$ in our example).

Each initial condition then evolves independently according to the classical equation of motion, and the corresponding trajectory in the $(\varphi, \dot{\varphi})$ plane is a closed loop⁹ due to the periodicity of classical solutions. One observes that the initially Gaussian-shaped cloud of points starts spreading around a closed loop, to eventually fill it entirely in the limit of large times. When this asymptotic regime is reached, the density $\mathcal{F}_t(\varphi, \dot{\varphi})$ depends only on the energy (i.e. roughly speaking on the radial coordinate in the plot of figure 6.7) and no longer on the angular coordinate.

A more formal way of phrasing the same result is to first note that the time evolution of the phase-space density \mathcal{F}_t obeys the Liouville equation,

$$\frac{\partial \mathcal{F}_t}{\partial t} + \{\mathcal{F}_t, H\} = 0, \quad (6.23)$$

($\{\cdot, \cdot\}$ is the classical Poisson bracket) and that if a stationary distribution is reached at late times, it can only depend on φ and $\dot{\varphi}$ via $H(\varphi, \dot{\varphi})$.

The asymptotic behavior of the phase-space density in our toy model is reminiscent of a micro-canonical equilibrium state, in which the phase-space density is uniform on a constant energy manifold. In other words, all the micro-states that have the same energy are equally likely.

6.2.4 Interpretation of the results

Of the previous numerical observations, the easiest to understand is the spreading of the phase-space density around a closed orbit. Because the oscillations are non-harmonic¹⁰, the various points rotate at different speeds: in a φ^4 potential, the outer points rotate faster than the inner ones. Therefore, as time increases, the cloud of points spreads more and more due to this effect.

One can estimate the time necessary for the clouds of points to spread over a complete orbit. This happens when the angular spread of the points reaches the value 2π . For one field configuration, this angular variable is (up to a phase that depends on the initial condition, small in our case if we start from a narrow Gaussian distribution) $\theta = \omega t$, and the angular velocity ω depends only on the energy of that particular field configuration. If we consider two field configurations, their angular variable difference $\Delta\theta$ drifts apart linearly in time, $\Delta\theta = \Delta\omega t$, where $\Delta\omega$ is the difference between their angular velocities. In the case of a $g^2\varphi^4/4!$ potential, it is easy to prove that

$$\omega = \frac{\pi}{2\sqrt{3}} \frac{g\varphi_{\max}}{\int_{-1}^{+1} \frac{dx}{\sqrt{1-x^4}}} \approx 0.346 g\varphi_{\max}, \quad (6.24)$$

⁹These loops are constant energy curves $\frac{1}{2}\dot{\varphi}^2 + U(\varphi) = H$.

¹⁰The assumption of a scale invariant theory simplifies the expressions here, but is not crucial to the argument. The only requirement for this phenomenon is that the frequency of the oscillations depends on their amplitude; thus any non-harmonic potential will lead to similar results.

where φ_{\max} is amplitude of the oscillations of φ . Thus, the angular shift between the pair of field configurations is also $\Delta\theta \approx 0.346 g\Delta\varphi_{\max} t$, and this shift reaches 2π in a time

$$t \approx \frac{18.2}{g\Delta\varphi_{\max}} . \quad (6.25)$$

After this time, the two fields have become completely incoherent. We see that this time is inversely proportional to the coupling constant g , and to the difference of the field amplitudes. Thus a narrow initial Gaussian distribution will need a longer time to spread around the orbit than a broader initial distribution.

Once we know that the phase-space density spreads uniformly on constant energy curves, it is easy to understand why the pressure relaxes towards $\epsilon/3$ when we let the initial conditions for the classical field fluctuate. The trace of the energy-momentum tensor (assuming 4 dimensions of space-time) is

$$T^\mu{}_\mu = \varphi \left(\square\varphi + 4 \frac{U(\varphi)}{\varphi} \right) - \partial_\alpha(\varphi \partial^\alpha \varphi) . \quad (6.26)$$

A scale invariant theory in four dimensions is a theory in which the interaction potential obeys $U'(\varphi) = 4U(\varphi)/\varphi$. This is the case of a φ^4 interaction. Therefore, the first term in the right hand side of the previous equation vanishes thanks to the equation of motion of the classical field φ . This results shows that the energy-momentum tensor of a single configuration of classical field is not zero in our model, but is a total derivative. In our simplified toy model where the fields are spatially homogeneous, the previous relation simplifies into

$$T^\mu{}_\mu = - \frac{d(\varphi\dot{\varphi})}{dt} . \quad (6.27)$$

When integrated over one period, the trace of the energy-momentum of one classical field configuration vanishes, because the classical field is a periodic function of time,

$$\overline{T^\mu{}_\mu} \equiv \frac{1}{T} \int_t^{t+T} d\tau T^\mu{}_\mu(\varphi(\tau), \dot{\varphi}(\tau)) = 0 . \quad (6.28)$$

(The result of the integral is in fact independent of the starting time t used to compute the average.) When we calculate the energy-momentum tensor averaged over fluctuations of the initial conditions, we are in fact performing an ensemble average weighted by the phase-space density $\mathcal{F}_t(\varphi, \dot{\varphi})$,

$$\langle T^\mu{}_\mu \rangle_{\alpha, \alpha} = \int d\varphi d\dot{\varphi} \mathcal{F}_t(\varphi, \dot{\varphi}) T^\mu{}_\mu(\varphi, \dot{\varphi}) , \quad (6.29)$$

and the time dependence of the left hand side comes from that of the density \mathcal{F}_t . In order to use the previous observation about the long time behavior of the density \mathcal{F}_t , it is convenient to trade the integration variables $\varphi, \dot{\varphi}$ for energy/angle variables E, θ ,

$$\langle T^\mu{}_\mu \rangle_{\alpha, \alpha} = \int dE d\theta \tilde{\mathcal{F}}_t(E, \theta) T^\mu{}_\mu(E, \theta) , \quad (6.30)$$

where $\tilde{\mathcal{F}}_t$ is the phase-space density in the new system of coordinates (it is equal to the original \mathcal{F}_t times the Jacobian of the change of variables). Our first result can be stated as the fact that $\tilde{\mathcal{F}}_t(E, \theta)$ becomes a function of only E (let us denote it by $\tilde{\mathcal{F}}_\infty(E)$) when the time is large enough. When this happens, we can rewrite the previous equation as

$$\langle T^\mu{}_\mu \rangle_{\alpha, \alpha} \underset{t \rightarrow \infty}{\approx} \int dE \tilde{\mathcal{F}}_\infty(E) \int d\theta T^\mu{}_\mu(E, \theta) . \quad (6.31)$$

The crucial point here is that the integral over θ is nothing but the integral over one orbit for a single classical field configuration,

$$\int d\theta T^\mu{}_\mu(E, \theta) = \frac{2\pi}{T} \int_t^{t+T} d\tau T^\mu{}_\mu(\varphi(\tau), \dot{\varphi}(\tau)) = 0 . \quad (6.32)$$

Thus, we have proven that

$$\epsilon - 3p = \langle T^\mu{}_\mu \rangle_{\alpha, \dot{\alpha}} \underset{t \rightarrow \infty}{\approx} 0 , \quad (6.33)$$

in agreement with what we have observed numerically. Moreover, from the derivation of this result, it is clear that the time necessary to reach this limit is the same as the time necessary for the phase-space density to become independent of the angular variable θ (given in eq. (6.25)).

6.3 Equation of state

6.3.1 Implementation of the full spectrum of fluctuations

In the previous section, we have shown that averaging over an ensemble of initial conditions for classical fields can lead the pressure to relax towards one third of the energy density. However, this study was oversimplified since we used only fluctuations that are uniform in space, and their Gaussian distribution was set by hand. However, quantum field theory *predicts* what the spectrum of these fluctuations should be, in the form of eqs. (6.19) and (6.18), and leaves no freedom to handpick what fluctuations we use. Indeed, from these formulas, we can make an ab initio calculation of the behavior of the pressure. The only tunable quantities in the calculation are the scale Q (or more generally the source J) that controls the amount of energy injected into the system at $t < 0$, and the coupling constant g .

Note that this spectrum of fluctuations for the initial condition for the field φ can be obtained by parameterizing the initial field as

$$\varphi(0, \mathbf{x}) \equiv \varphi_0(\mathbf{x}) + \int \frac{d^3\mathbf{k}}{(2\pi)^3 2k} \left[c_{\mathbf{k}} a_{+\mathbf{k}}(0, \mathbf{x}) + c_{\mathbf{k}}^* a_{-\mathbf{k}}(0, \mathbf{x}) \right] , \quad (6.34)$$

where the $c_{\mathbf{k}}$ are random Gaussian numbers with the following variance

$$\langle c_{\mathbf{k}} c_{\mathbf{l}} \rangle = 0 , \quad \langle c_{\mathbf{k}} c_{\mathbf{l}}^* \rangle = (2\pi)^3 |\mathbf{k}| \delta(\mathbf{k} - \mathbf{l}) . \quad (6.35)$$

This is the representation we adopt for the initial fluctuating fields. In order to implement it, we must follow the following steps:

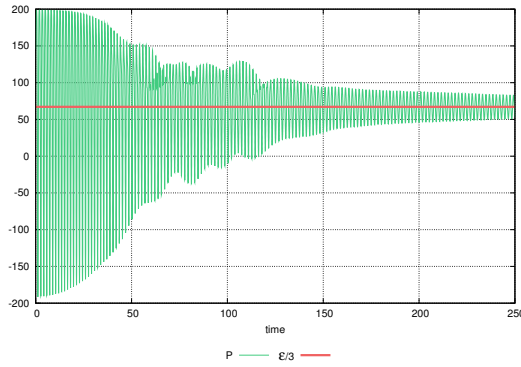
- i. solve the classical equation of motion (6.4) from $t = -\infty$ (in practice some large and negative time) to $t = 0$ in order to obtain $\varphi_0(\mathbf{x})$,
- ii. solve the evolution equation (6.9) for the $a_{\pm\mathbf{k}}$'s from $t = -\infty$ to $t = 0$,
- iii. generate Gaussian random complex coefficients according to eq. (6.35) to construct an initial field via eq. (6.34)
- iv. evolve this field to the time of interest by using the classical equation of motion (6.4) with $J = 0$,
- v. repeat steps iii. and iv. in order to perform a Monte-Carlo average over the fluctuations of the initial field.

6.3.2 Relaxation of the pressure

Unless stated otherwise, the numerical results in this section have been obtained on a 12^3 lattice¹¹. The functional integration in eq. (6.18) is approximated by a Monte-Carlo average over 1000 configurations of the initial conditions, distributed according to eqs. (6.19).

In the figure 6.8, we show the result of the computation of the pressure averaged over the Gaussian ensemble of initial conditions, for a value of the coupling¹² $g = 0.5$. We also show the energy density divided by three on the same plot. All the quantities in this plot

Figure 6.8: Time evolution of the pressure averaged over the initial fluctuations. All the resonant modes are included in the simulation. The coupling constant is $g = 0.5$.



are expressed in lattice units, which means that the horizontal axis is t/a (where a is the lattice spacing) and the vertical axis should be understood as ϵa^4 or $p a^4$. Note that the lattice cutoff in this simulation is chosen to be just above the upper limit of the parametric resonance window – therefore, all the resonant modes take part in the dynamics of the system.

We observe that the ensemble averaged pressure relaxes towards $\epsilon/3$. This plot, obtained with the actual spectrum of fluctuations predicted by quantum field theory, is one of the central results of this section. One can qualitatively identify two stages in this relaxation: (1) in the range $0 \leq t \lesssim 50$, the amplitude of the pressure oscillations decreases very quickly to a moderate value and, (2) from time 50 onwards, one has a slower approach of the pressure to $\epsilon/3$ that gets slowly rid of the residual oscillations. We will observe again this two-stage time evolution when we look at the fluctuations of the energy density.

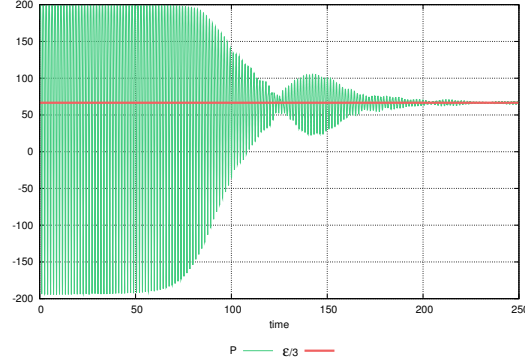
6.3.3 Influence of the resonant modes

In the section 6.3, we have seen that the pressure relaxes to $\epsilon/3$ even if only the mode $\mathbf{k} = 0$ is included in the simulation. This was understood as an effect of the phase decoherence that exists in a non-harmonic potential between classical solutions that have slightly different

¹¹In some instances, we have also performed simulations on 20^3 , 32^3 and 64^3 lattices, and found only small differences as long as the physical scales are below the lattice cutoff.

¹²Because of the prefactor $g^2/4!$ in the interaction potential, a value $g = 0.5$ corresponds to a very weak coupling strength.

Figure 6.9: Time evolution of the pressure averaged over the initial fluctuations. The lattice cutoff is located below the resonance band in order to exclude them from the simulation. The coupling constant is $g = 0.5$.



amplitudes. When we include all the \mathbf{k} -modes of the fluctuations, the situation becomes arguably more complicated. In particular, the stability analysis of these fluctuations indicates that in addition to a linear instability of the soft modes due to the above mentioned decoherence phenomenon, there are also exponentially unstable modes in a narrow band of values \mathbf{k} .

In order to assess the role played in the time evolution by the modes of the resonance band, we have performed a second simulation with the same physical parameters, but where the lattice cutoff is now placed just below the lower end of the resonance band. When one does this, none of the modes that exist on this lattice has an exponential instability. Since the resonance band is quite narrow, this is a small change of the cutoff in physical units (in the first simulation, the cutoff was just above the upper end of the resonance band). However, one can see in the figure 6.9 that excluding the resonant modes leads to some significant changes.

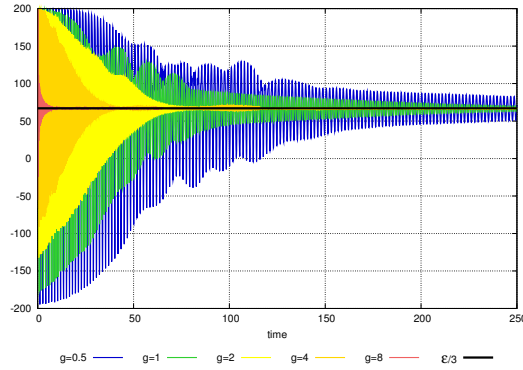
The final outcome, i.e. the relaxation towards $\epsilon/3$, is not changed, but the details of the time evolution of the pressure are modified. Firstly, one observes a rather long delay during which the oscillations of the pressure remain almost constant in amplitude. Then, at a time of order 75 in lattice units, these oscillations are damped very quickly to very small wiggles around $\epsilon/3$. Except for a brief relapse, the oscillations remain very small after this time. In particular, the two-stage evolution that we observed with the full spectrum is now replaced by the following two stages: (1) nothing happens and, (2) very rapid relaxation that leaves almost no residual oscillations.

Therefore, it appears that the resonant modes, even if their presence or absence in the resummation is not crucial for the final outcome, can alter significantly the time evolution of the pressure. At this point, the precise role of the resonant modes is somewhat unclear, and it appears that the dynamics of the complete system is much richer than what one can learn by studying the linearized evolution of a single mode: the non-linear couplings between the various modes (once the instabilities have made them large enough) seem to play an important role in the evolution of the system.

6.3.4 Dependence on the coupling constant

The simulation that led to the result of the figure 6.8 has been performed with a value $g = 0.5$ for the coupling constant – a very small value for our scalar field theory since there is also a factor $1/4!$ in the interaction potential. We have studied the time evolution of the pressure

Figure 6.10: Time evolution of the pressure averaged over the initial fluctuations for various values of the coupling constant: $g = 0.5, 1, 2, 4, 8$. All the resonant modes are included in the simulation.



for larger values of the coupling constant: $g = 1, 2, 4, 8$, and the results are shown in the figure 6.10. Note that this fluctuation is done at fixed energy density. Indeed, since Q is the only dimensionful parameter of our model and since there is a factor $1/g$ in the source J , the energy density behaves at leading order as $\epsilon \propto Q^4/g^2$. Thus, if we increase g at constant Q , the energy density decreases. Since our goal is to assess the time at which the pressure obeys an equation of state in order to justify a hydrodynamical description of the system, the comparison of the relaxation for various couplings should be done for systems that have the same energy density. Therefore, in the comparison shown in the figure 6.10, the value of Q has been adjusted in each simulation so that the energy density is always the same.

One can see in the figure 6.10 that the relaxation time decreases with increasing coupling constants g . In the figure 6.11, we have represented the relaxation time –defined as the time necessary to reduce the initial oscillations of the pressure by a factor 4– as a function of the coupling constant g for our set of values of g . One can fit all the points except the last one ($g = 8$) by a power law that suggest the following dependence

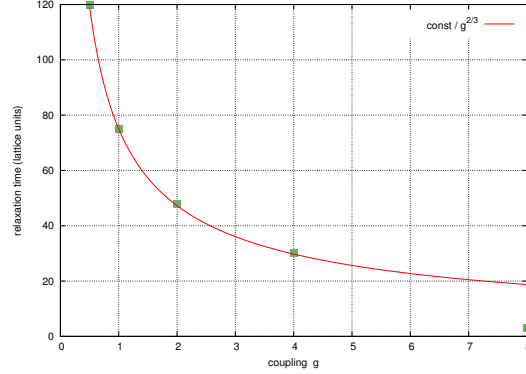
$$t_{\text{relax}} = \frac{\text{const}}{g^{2/3}} . \quad (6.36)$$

The last point in this plot is an outlier that does not follow this power law, possibly because this value of the coupling is too extreme for our approximations/resummations to make sense.

6.3.5 Energy density fluctuations

The results we have shown so far indicate that the pressure in the system relaxes towards the equation of state $p = \epsilon/3$, in time that decreases as the coupling constant increases.

Figure 6.11: Points: relaxation time (see the text for the definition used here) as a function of the coupling g . Line: fit by a power law.



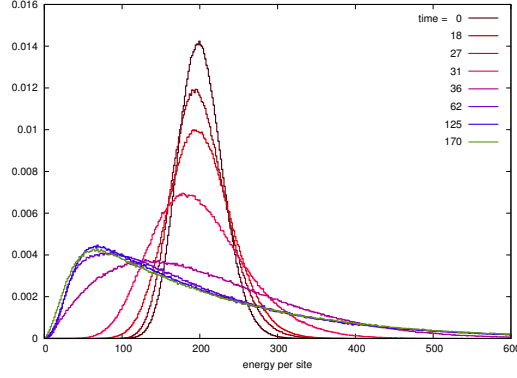
However, this study by itself does not tell much about the precise nature of the state reached by the system. In particular, it does not tell whether the system reaches a state of local thermal equilibrium, although this is quite plausible given the behavior. Then comes the question of how to characterize the internal state of the system: since we have strong fields, it is likely that the system cannot be described in terms of quasi-particles with a momentum distribution that would follow e.g. a Bose-Einstein law. In the section 6.3, we have seen in a very simple case that the phase-space density reaches a stationary form reminiscent of the micro-canonical equilibrium ensemble. Unfortunately, now that we are looking at a full fledged quantum field theory, the phase-space is infinite dimensional and whether the same happens is difficult to assess numerically.

There are however also signs of thermalization in the fluctuations of the energy distribution in the system. Of course, for the whole system the energy is constrained by conservation laws and will not fluctuate, regardless of whether the system is in thermal equilibrium or not. But by looking the energy fluctuations in a small subsystem, one can learn something about the energy exchanges between this subsystem and the rest of the system – that now acts as a thermal bath. Indeed, the energy in the subsystem is not fixed, and its fluctuations do not have the same form depending of whether the subsystem is in equilibrium or not with its surroundings. In particular, if a subsystem is in thermal equilibrium with a thermal bath, its fluctuations are those of the canonical ensemble, that has a density operator $\rho \equiv \exp(-\beta H)$.

We have computed these energy fluctuations for the smallest subsystem one can conceive on a lattice, i.e. a single lattice site. In the figure 6.12, we display histograms of the values of the energy on one site¹³, at various times in the evolution. These curves have been normalized so that their integral is equal to one, hence they can be interpreted as probability distributions for the value of the energy on one lattice site. At $t = 0$, this distribution is very close to a Gaussian, centered on the mean energy density in the system. The width of this Gaussian is entirely determined by the Gaussian spectrum of fluctuations in eq. (6.19). As early times, the distribution first remains Gaussian-like, but tends to broaden with time. Then, around $t \approx 30$ in lattice units, we observe a rapid change of shape of this distribution: the peak of the distribution shifts to lower values of the energy and the tail extends much further at large

¹³In lattice units, this is simply the value of T^{00} at one given site.

Figure 6.12: *Distribution of energy density on one lattice site, at various times of the evolution. The coupling constant is $g = 0.5$.*



energy. Once this dramatic change of shape has taken place, the evolution of the distribution is rather slow and a stationary distribution is reached at late times.

It is interesting to compare the evolution of the energy distribution on one lattice site with the time evolution of the pressure in the figure 6.8. The initial rapid decrease of the pressure oscillations is concomitant with the change of shape of the energy distribution. The subsequent (slower) relaxation of the residual oscillations of the pressure occurs while the energy has already reached an almost stationary distribution.

6.4 Spectral properties and thermalization

6.4.1 Introduction

In the previous section, we have seen that after a proper resummation of the leading secular terms, the pressure converges towards its equilibrium value in a fairly short time –something that would not happen with the unresummed expression of the energy-momentum tensor. However, this study does not tell us much about the microscopic evolution of the system: indeed, since the energy density and the pressure of the system are intensive quantities that integrate over all the modes of the system, the existence of an equation of state identical to the equilibrium one does not imply that the system is in full equilibrium. Equilibrium requires a much more stringent microscopic arrangement of the system, in which the energy is distributed among the various modes in a very specific way.

In this section, we pursue the study in order to elucidate the microscopic state of the system. In particular, we would like to know whether the system is thermalized when its pressure has relaxed to its equilibrium value, or whether on the contrary one could have an equilibrium-like pressure tensor while the system is still far from equilibrium¹⁴. A natural quantity to study in order to address this question is the occupation number in the system, and

¹⁴In the 2 Particle Irreducible approach [185, 189–193] to the relaxation of a linear sigma model, it has already been observed that an equation of state can be obtained much earlier than the complete thermalization of the system [194].

its time evolution. However, even before computing the occupation number, it is interesting to ask whether the system can be described in terms of quasi-particles (this is not trivial: although the system is weakly coupled, it is also very dense, and strong collective effects may render the quasi-particles completely unstable). We first compute the spectral density of the system, after having justified that it can be resummed in the same way as the energy-momentum tensor. Then, we continue our study with the occupation number. We compute it as a function of momentum up to very large times, and identify several stages in its time evolution. From the occupation number, we perform several tests of the quasi-particle picture (e.g. compare the measured mass of the quasi-particles, with its value at 1-loop, including medium effects) and compute how the entropy of the system evolves with time. We end the section with a discussion of some aspects of the classical field theory to which the original quantum field theory is equivalent in our resummation scheme.

6.4.2 Lattice setup for the study of thermalization

A crucial ingredient in this process is the parametric resonance that exists in the ϕ^4 scalar field theory, and therefore it is important that the ultraviolet lattice cutoff be large enough to comprise the resonance band. If the source J is parametrically

$$J \sim \frac{Q^3}{g}, \quad (6.37)$$

then the resonance band is located at momenta of order $k \sim Q$, and the UV cutoff Λ must therefore obey $Q \lesssim \Lambda$. Setting up the lattice cutoff in this way is sufficient to study the evolution of the system at short times, because on these time scales the occupation number remains small above the resonance region, as we shall see later.

This is however not sufficient if we want to study the approach of the system to thermal equilibrium. In order to see this, recall that the energy density in the system is parametrically

$$\epsilon \sim \frac{Q^4}{g^2}. \quad (6.38)$$

If thermal equilibrium is achieved, this energy density must also be given by the Stefan-Boltzmann formula (at least for reasonably weak couplings),

$$\epsilon \sim T^4, \quad (6.39)$$

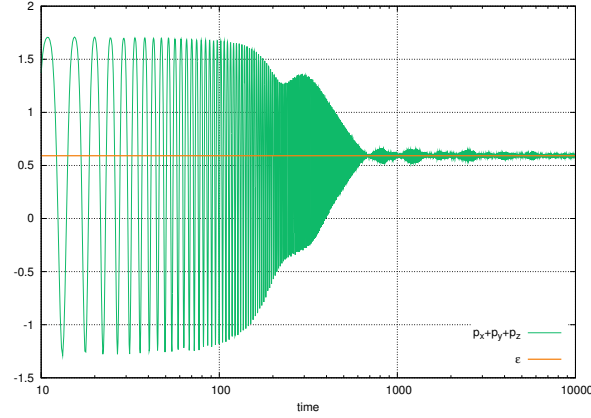
which tells us that the system would equilibrate at a temperature

$$T \sim \frac{Q}{\sqrt{g}}. \quad (6.40)$$

For a numerical simulation to be able to approach the equilibrium state, the lattice ultraviolet cutoff must be large enough to include modes of the order of the temperature, which is a more stringent constraint than simply having the resonance band below the cutoff. At weak coupling, this implies that the resonance band should be located towards the soft sector of the lattice spectrum, i.e. in a region where the lattice mode density is rather low. In order to still have a significant number of lattice modes inside the resonance band, we used a larger lattice (of size 20^3), and we have chosen the value of the parameter Q so that the resonance band is located near $k \approx 1$ (in lattice units, where the ultraviolet cutoff is at $\Lambda = \sqrt{12}$).

This choice of Q is significantly lower than the value used in the previous section (where we were only interested in the early stages of the time evolution, dominated by the resonant modes). This means a lower energy density, and larger time scales. Indeed, since our system is scale invariant, energy density scales like Q^4 and all the times scale like $1/Q$. The resulting time evolution of the pressure, for this choice of Q and a coupling constant $g = 1$, is shown in the figure 6.13.

Figure 6.13: Relaxation of the pressure tensor towards the equilibrium value.



6.4.3 Spectral function and quasi-particles

Definition and leading order

Before we study the time evolution of the occupation number in the system, it is interesting to ask an even more elementary question: can the system be described in terms of quasi-particles, or on the contrary does it interact so strongly that no identifiable quasi-particles show up in its spectrum? To that effect, one can compute the spectral function, defined as the imaginary part of the Fourier transform of the retarded propagator¹⁵:

$$\rho(\omega, \mathbf{k}; y^0) \equiv 2 \operatorname{Im} \int_0^{+\infty} dt d^3\mathbf{x} e^{i\omega t} e^{-i\mathbf{k}\cdot\mathbf{x}} G_{\text{r}}(y^0 + t, \mathbf{x}, y^0, \mathbf{0}) . \quad (6.41)$$

In this formula, the retarded propagator is normalized so that

$$\left[\square_x + U''(\varphi(x)) \right] G_{\text{r}}(x, y) = \delta(x - y) \quad (6.42)$$

for a classical field configuration φ . A system in equilibrium is invariant under translations in time, and therefore its spectral function defined in this way is in fact independent of the time y^0 . However, for transient systems that are not yet in equilibrium, the spectral function will evolve with time and the y^0 dependence is important.

¹⁵We assume here that the system is spatially homogeneous. This is the case in our setup since the source J does not depend on \mathbf{x} .

At leading order, we simply need to obtain the retarded propagator in a classical background field $\varphi(x)$,

$$G_R^{LO}(x, y) = \sum \text{diagram} , \quad (6.43)$$


where the grey blobs denote the retarded classical field $\varphi(x)$ and the lines with an arrow the bare retarded propagator (the sum is over the number of insertions of the classical field, from 0 to $+\infty$). In a numerical calculation, the simplest way to compute this propagator is to consider a small field perturbation $a(x)$ in that background, that obeys the following equation of motion

$$\left[\square_x + U''(\varphi(x)) \right] a(x) = 0 . \quad (6.44)$$

The fluctuation $a(x)$ can be related to its value at the time y^0 by the following Green's formula

$$a(x) = \int d^3 \mathbf{y} \left[G_R^{LO}(x, y) (\partial_y^0 a(y)) - (\partial_y^0 G_R^{LO}(x, y)) a(y) \right] , \quad (6.45)$$

that involves precisely the propagator we are looking for. Thus, by choosing the following initial conditions at time y^0 ,

$$a(y^0, \mathbf{y}) = 0 , \quad \partial_y^0 a(y^0, \mathbf{y}) = \delta(\mathbf{y}) , \quad (6.46)$$

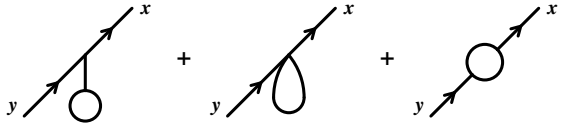
the perturbation $a(x)$ is precisely the propagator we need in eq. (6.41),

$$G_R^{LO}(x^0, \mathbf{x}, y^0, \mathbf{0}) = a(x^0, \mathbf{x}) . \quad (6.47)$$

Thanks to this observation, we reduce the problem of finding the retarded propagator at leading order to that of solving the equation (6.44) with the initial conditions of eq. (6.46), which is easily doable numerically¹⁶.

Next to leading order and resummation

At next to leading order, three topologies must be evaluated¹⁷:

$$G_R^{NLO}(x, y) = \text{diagram 1} + \text{diagram 2} + \text{diagram 3} , \quad (6.48)$$


where the both the propagators and the vertices are dressed by the classical field $\varphi(x)$. The first topology is the same as the retarded propagator at leading order, in which one of the φ

¹⁶On a lattice, the delta function that appears in the initial condition for $\partial_y^0 a(y^0, \mathbf{y})$ becomes a Kronecker symbol: the derivative is zero at all points of the lattice except at the origin (0,0,0) where it is equal to one.

¹⁷Although these diagrams seem to involve cubic vertices, this is not the case. These vertices where three lines merge are in fact proportional to $U'''(\varphi(x))$, and are thus proportional to an extra $\varphi(x)$ that does not appear explicitly in the diagrammatic representation.

insertions has been replaced by a 1-loop tadpole β defined in eq. (6.9). Given that this tadpole is given by (see the eq. (39) in [5])

$$\beta(x) = \left[\int d^3\mathbf{u} \beta \cdot \mathbb{T}_{\mathbf{u}} + \frac{1}{2} \int d^3\mathbf{u} d^3\mathbf{v} \int \frac{d^3\mathbf{k}}{(2\pi)^3 2k} [a_{+\mathbf{k}} \cdot \mathbb{T}_{\mathbf{u}}] [a_{-\mathbf{k}} \cdot \mathbb{T}_{\mathbf{v}}] \right] \varphi(x), \quad (6.49)$$

it is easy to check that this contribution is related to the leading order one by the following functional identity

$$G_{\mathbf{r}}^{\text{NLOI}}(x, y) = \left[\int d^3\mathbf{u} \beta \cdot \mathbb{T}_{\mathbf{u}} + \frac{1}{2} \int d^3\mathbf{u} d^3\mathbf{v} \int \frac{d^3\mathbf{k}}{(2\pi)^3 2k} [a_{+\mathbf{k}} \cdot \mathbb{T}_{\mathbf{u}}] [a_{-\mathbf{k}} \cdot \mathbb{T}_{\mathbf{v}}] \right]_{=\varphi} G_{\mathbf{r}}^{\text{LO}}(x, y), \quad (6.50)$$

where the subscript ‘= φ ’ indicates that the two operators $\mathbb{T}_{\mathbf{u}}\mathbb{T}_{\mathbf{v}}$ in the second term should act on the same field φ , i.e.

$$\begin{aligned} & \left[\mathbb{T}_{\mathbf{u}}\mathbb{T}_{\mathbf{v}} \right]_{\text{same } \varphi} \varphi(x_1) \cdots \varphi(x_n) \equiv \\ & \equiv \sum_{i=1}^n \varphi(x_1) \cdots \varphi(x_{i-1}) \left[\left[\mathbb{T}_{\mathbf{u}}\mathbb{T}_{\mathbf{v}} \right] \varphi(x_i) \right] \varphi(x_{i+1}) \cdots \varphi(x_n). \end{aligned} \quad (6.51)$$

By using the formula

$$G_{+-}^{\text{LO}}(x, y) = \int \frac{d^3\mathbf{k}}{(2\pi)^3 2k} a_{+\mathbf{k}}(x) a_{-\mathbf{k}}(y), \quad (6.52)$$

the second topology can be written as follows,

$$G_{\mathbf{r}}^{\text{NLO2}}(x, y) = \left[\frac{1}{2} \int d^3\mathbf{u} d^3\mathbf{v} \int \frac{d^3\mathbf{k}}{(2\pi)^3 2k} [a_{+\mathbf{k}} \cdot \mathbb{T}_{\mathbf{u}}] [a_{-\mathbf{k}} \cdot \mathbb{T}_{\mathbf{v}}] \right]_{\text{same } \mathcal{U}''(\varphi)} G_{\mathbf{r}}^{\text{LO}}(x, y), \quad (6.53)$$

where the subscript ‘same $\mathcal{U}''(\varphi)$ ’ indicates that the two operators $\mathbb{T}_{\mathbf{u}}\mathbb{T}_{\mathbf{v}}$ should act on the same compound $\mathcal{U}''(\varphi)$ –one operator on each field of $\mathcal{U}''(\varphi)$. The third topology can first be written as

$$G_{\mathbf{r}}^{\text{NLO3}}(x, y) = \int d^4w d^4z G_{\mathbf{r}}^{\text{LO}}(x, w) \Sigma_{\mathbf{r}}^{\text{1loop}}(w, z) G_{\mathbf{r}}^{\text{LO}}(z, y), \quad (6.54)$$

where $\Sigma_{\mathbf{r}}^{\text{1loop}}$ is the 1-loop retarded self-energy,

$$\Sigma_{\mathbf{r}}^{\text{1loop}}(w, z) = \Sigma_{++}^{\text{1loop}}(w, z) - \Sigma_{+-}^{\text{1loop}}(w, z). \quad (6.55)$$

Next, one can rewrite this self-energy as

$$\Sigma_{\mathbf{r}}^{\text{1loop}}(w, z) = \frac{1}{2} \mathcal{U}'''(\varphi(w)) \mathcal{U}'''(\varphi(z)) G_{\mathbf{r}}^{\text{LO}}(w, z) \left[G_{+-}^{\text{LO}}(w, z) + G_{-+}^{\text{LO}}(w, z) \right], \quad (6.56)$$

where the prefactor 1/2 is the symmetry factor of the loop. By combining eqs. (6.54) and (6.56) and by using (6.52), one can finally prove

$$G_{\mathbf{r}}^{\text{NLO2}}(x, y) = \left[\frac{1}{2} \int d^3\mathbf{u} d^3\mathbf{v} \int \frac{d^3\mathbf{k}}{(2\pi)^3 2k} [a_{+\mathbf{k}} \cdot \mathbb{T}_{\mathbf{u}}] [a_{-\mathbf{k}} \cdot \mathbb{T}_{\mathbf{v}}] \right]_{\text{distinct } \varphi's} G_{\mathbf{r}}^{\text{LO}}(x, y), \quad (6.57)$$

where the qualifier ‘distinct φ ’s’ indicates that the two operators $\mathbb{T}_{\mathbf{u}}\mathbb{T}_{\mathbf{v}}$ must act on two fields φ ’s that are inserted at different points on the LO propagator $G_{\mathbf{r}}^{\text{LO}}$. Adding eqs. (6.50), (6.53) and (6.57) therefore simply lifts any restriction on the action of these operators, and we obtain

$$G_{\mathbf{r}}^{\text{NLO}}(\mathbf{x}, \mathbf{y}) = \left[\int d^3\mathbf{u} \beta \cdot \mathbb{T}_{\mathbf{u}} + \frac{1}{2} \int d^3\mathbf{u} d^3\mathbf{v} \int \frac{d^3\mathbf{k}}{(2\pi)^3 2k} [\mathbf{a}_{+\mathbf{k}} \cdot \mathbb{T}_{\mathbf{u}}] [\mathbf{a}_{-\mathbf{k}} \cdot \mathbb{T}_{\mathbf{v}}] \right] G_{\mathbf{r}}^{\text{LO}}(\mathbf{x}, \mathbf{y}) . \quad (6.58)$$

This formula is formally identical to the formula we have obtained previously for the energy-momentum tensor at NLO, and it leads to the same pathologies due to the presence of secular divergences. Likewise, the problem can be cured here by performing the same resummation as in the case of the energy-momentum tensor, that amounts to exponentiating the quadratic part of the operator in the square brackets in eq. (6.58) (as in eq. (6.17)):

$$G_{\mathbf{r}}^{\text{resummed}}(\mathbf{x}, \mathbf{y}) \equiv \exp \left[\frac{1}{2} \int d^3\mathbf{u} d^3\mathbf{v} \int \frac{d^3\mathbf{k}}{(2\pi)^3 2k} [\mathbf{a}_{+\mathbf{k}} \cdot \mathbb{T}_{\mathbf{u}}] [\mathbf{a}_{-\mathbf{k}} \cdot \mathbb{T}_{\mathbf{v}}] \right] G_{\mathbf{r}}^{\text{LO}}(\mathbf{x}, \mathbf{y}) . \quad (6.59)$$

This resummation amounts to a functional average over Gaussian fluctuations of the initial condition of the classical field at $\mathbf{x}^0 = 0$,

$$G_{\mathbf{r}}^{\text{resummed}} = \int [D\alpha(\mathbf{x}) D\dot{\alpha}(\mathbf{x})] F[\alpha, \dot{\alpha}] G_{\mathbf{r}}^{\text{LO}}[\varphi_0 + \alpha] \quad (6.60)$$

where the Gaussian distribution $F[\alpha, \dot{\alpha}]$ is defined in eq. (6.19). Therefore, in order to compute the resummed retarded propagator, we should repeat the procedure outlined in the section 6.4.3 for every classical field φ obtained from an ensemble of initial conditions $\varphi_0 + \alpha$, where α samples the Gaussian distribution $F[\alpha, \dot{\alpha}]$.

Numerical results

At the initial time (see the figure 6.14), the spectral function has a fairly complicated structure. Although the large \mathbf{k} modes have a single spectral peak at $\omega \approx |\mathbf{k}|$, the situation is richer in the soft sector. There, besides the main branch that continues to large \mathbf{k} , the spectral density exhibits additional branches. One of them corresponds to a higher mass excitation, and another one has a mass comparable to the main branch but an anomalous dispersion such that the frequency decreases while the momentum increases. Therefore, at early times, the quasi-particle picture is not a good description of the degrees of freedom in the system.

As the time increases, these extra branches in the spectral function decrease in amplitude and eventually disappear, starting with the higher mass excitation. Ultimately, only the main excitation remains, as one can see in the plot on the right of the figure 6.15 at a time $y^0 = 3000$. At intermediate times (such as $y^0 = 400$, represented on the plot on the left of the figure 6.15), one gets closer to the spectral function of a system made of quasi-particles, with only small remnants of the structures that existed at early times. It is interesting to note that the characteristic time for the disappearance of the extra branches in $\rho(\omega, \mathbf{k}; y^0)$ is comparable to the relaxation time of the pressure, that we have found in the previous section to start at a time of the order of $y^0 \sim 100$.

Quasi-particle mass

In order to further assess the existence of quasi-particles in the system, one can fit the main branch of the spectral function by a function of the form $\omega = \sqrt{\mathbf{k}^2 + m^2}$. The result

Figure 6.14: Spectral function $\rho(\omega, \mathbf{k}; y^0 = 0.0)$ at the initial time. The computation is done on a 20^3 lattice, for a coupling constant $g = 1$. In this plot, \mathbf{k} denotes the lattice momentum, i.e. $\sqrt{2(3 - \cos(2\pi l/L) - \cos(2\pi m/L) - \cos(2\pi n/L))}$ on a L^3 lattice (l, m, n is the triplet of integers in the range $[0, L - 1]$ that labels a given momentum state).

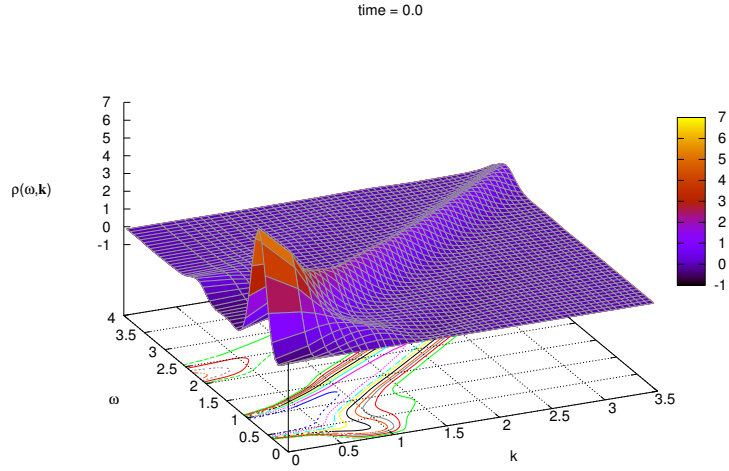
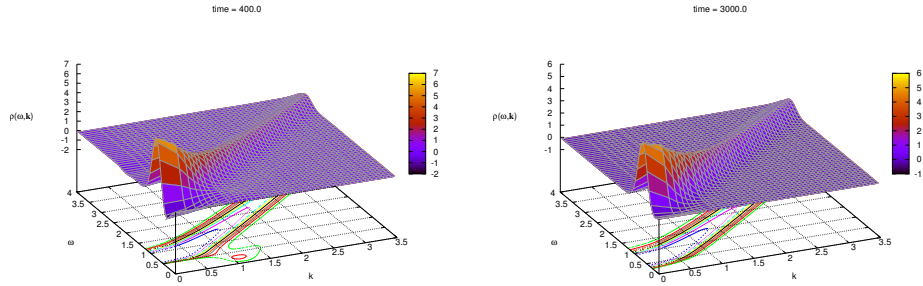
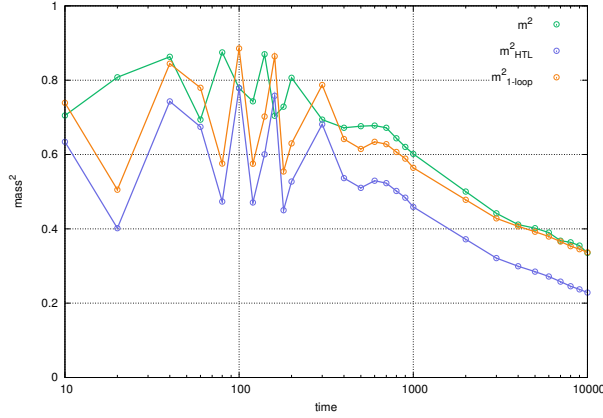


Figure 6.15: Spectral function $\rho(\omega, \mathbf{k}; y^0)$ at the times $y^0 = 400$ (left) and $y^0 = 3000$ (right). The computation is done on a 20^3 lattice, for a coupling constant $g = 1$.



of this fit is shown in the figure 6.16. One sees that the mass m resulting from this fit is not stable until a time $y^0 \approx 100$, and becomes much more regular afterwards. This is in agreement with the previous qualitative observation that only the main branch of the spectral function survives after this time. Moreover, after $y^0 \geq 1000$, the mass of the quasi-particles that populate the system decreases slowly with time, indicating that the system is not yet completely equilibrated (the change in the mass of the quasi-particles reflects a change in the occupation number of the various modes of the system, that we will study more directly in the following section). If one takes as a crude estimate the Hard Thermal Loop [195, 196]

Figure 6.16: Green line: quasi-particle mass obtained by a fit of the main dispersion branch with a function of the form $\omega = \sqrt{k^2 + m^2}$. Blue line: 1-loop analytic calculation from the occupation number. Red line: 1-loop gap equation that resums recursively all the daisy diagrams. (See the text in section 6.4.5 for explanations regarding the curves labelled m_{HTL}^2 and $m_{1\text{-loop}}^2$.)



expression of the medium-generated mass (see for instance [197], pp 41–45),

$$m_{\text{HTL}}^2 = g^2 \int \frac{d^3k}{(2\pi)^3 2k} f_k, \quad (6.61)$$

as a function of the occupation number f_k , we can interpret the decrease of the mass as a shift of the occupation number from low k to higher k 's. In other words, while our system starts with most of its energy contained in the soft modes, higher- k modes are progressively populated by a top-down (in length scale) cascade process, which makes the medium-generated mass decrease with time.

A word of caution should be added about the width of the quasi-particles. The width of the spectral peak in the figures 6.14 and 6.15 is probably not the physical width: for practical reasons the numerical computation of the Fourier transform in time in eq. (6.41) cannot integrate up to very large times¹⁸. Thus the width we see in the resulting plots is to a large extent contaminated by the fact that the time interval is finite in the numerical calculation (for the physical width to be visible unambiguously in these plots, the length of the time interval would have to be much larger than the lifetime of the quasi-particles).

¹⁸One can check in the free case that this is a very singular Fourier transform. At $k = 0$, it is of the form $\int_0^{+\infty} dt t \exp(i\omega t) \sim \delta'(\omega)$.

6.4.4 Occupation number

Expression in terms of G_{+-} and G_{-+}

Now that we know that at times $x^0 \geq 100$, the spectral content of the system reduces to simple quasi-particles, it makes sense to compute their occupation number. Recall that the creation and annihilation operators a_k^\dagger, a_k are related to the field operator $\hat{\phi}$ via

$$\begin{aligned} a_k &= i \int d^3x e^{ik \cdot x} \overleftrightarrow{\partial}_{x^0} \hat{\phi}(x) \\ a_k^\dagger &= -i \int d^3x e^{-ik \cdot x} \overleftrightarrow{\partial}_{x^0} \hat{\phi}(x) . \end{aligned} \quad (6.62)$$

From this, we get the following two reduction formulas

$$\begin{aligned} \langle a_k^\dagger a_k \rangle &= \int d^3x d^3y e^{ik \cdot (x-y)} \overleftrightarrow{\partial}_{x^0} \overleftrightarrow{\partial}_{y^0} G_{+-}(x, y)|_{x^0=y^0} \\ \langle a_k a_k^\dagger \rangle &= \int d^3x d^3y e^{ik \cdot (x-y)} \overleftrightarrow{\partial}_{x^0} \overleftrightarrow{\partial}_{y^0} G_{-+}(x, y)|_{x^0=y^0} , \end{aligned} \quad (6.63)$$

with the understanding that the times x^0 and y^0 are set equal only after the derivatives have been evaluated.

It turns out to be more straightforward to calculate the sum of these two expectation values,

$$\langle a_k^\dagger a_k + a_k a_k^\dagger \rangle = \int d^3x d^3y e^{ik \cdot (x-y)} \overleftrightarrow{\partial}_{x^0} \overleftrightarrow{\partial}_{y^0} G_s(x, y)|_{x^0=y^0} \quad (6.64)$$

where $G_s \equiv G_{+-} + G_{-+}$, because in our framework the symmetric propagator G_s is easier to compute than the separate $G_{\pm\mp}$. The occupation number f_k is related to the left hand side of eq. (6.64) by

$$2\omega_k V(1 + 2f_k) = \langle a_k^\dagger a_k + a_k a_k^\dagger \rangle , \quad (6.65)$$

where V is the volume of the system and ω_k the dispersion relation of the quasi-particles.

Calculation of G_s

Let us now see how to compute the symmetric propagator $G_s(x, y)$ at LO, NLO and in the re-summation scheme we have developed to cure the pathologies related to secular divergences. At leading order, it is simply given by the product of two classical fields at the points x and y ,

$$G_s^{\text{LO}}(x, y) = 2\varphi(x)\varphi(y) . \quad (6.66)$$

At next to leading order, G_s is made of two pieces:

- i. a 1-loop correction β to one of the factors φ of the LO result,
- ii. a connected tree contribution $\mathcal{G}_s \equiv \mathcal{G}_{+-} + \mathcal{G}_{-+}$ that links the points x and y ,

$$G_s^{\text{NLO}}(x, y) = 2 \left[\beta(x) \varphi(y) + \varphi(x) \beta(y) \right] + \mathcal{G}_s(x, y) . \quad (6.67)$$

The second term is given by

$$\mathcal{G}_s(x, y) = \int \frac{d^3 \mathbf{k}}{(2\pi)^3 2k} \left[a_{+\mathbf{k}}(x) a_{-\mathbf{k}}(y) + a_{-\mathbf{k}}(x) a_{+\mathbf{k}}(y) \right] . \quad (6.68)$$

The $a_{\pm \mathbf{k}}$'s can be formally related to the classical field $\varphi(x)$ by (see eq. (2.98))

$$a_{\pm \mathbf{k}}(x) = \int d^3 \mathbf{u} [a_{\pm \mathbf{k}} \cdot \mathbb{T}_{\mathbf{u}}] \varphi(x) , \quad (6.69)$$

while for the tadpole β we can use eq. (6.49). Then, it is straightforward to combine the two terms to obtain

$$G_s^{\text{NLO}}(x, y) = \left[\int d^3 \mathbf{u} \beta \cdot \mathbb{T}_{\mathbf{u}} + \frac{1}{2} \int d^3 \mathbf{u} d^3 \mathbf{v} \int \frac{d^3 \mathbf{k}}{(2\pi)^3 2k} [a_{+\mathbf{k}} \cdot \mathbb{T}_{\mathbf{u}}] [a_{-\mathbf{k}} \cdot \mathbb{T}_{\mathbf{v}}] \right] G_s^{\text{LO}}(x, y) . \quad (6.70)$$

From here, it is clear that one can perform the same resummation, where one exponentiates the quadratic part of the operator in the square brackets. This amounts to an average over Gaussian fluctuations of the initial classical field at $x^0 = 0$,

$$G_s^{\text{resummed}}(x, y) = 2 \int [D\alpha D\dot{\alpha}] F[\alpha, \dot{\alpha}] \left[\varphi(x) \varphi(y) \right]_{\varphi_0 + \alpha} , \quad (6.71)$$

where the subscript $\varphi_0 + \alpha$ indicates the initial condition used at $x^0 = 0$ to start the evolution of the classical field φ . $F[\alpha, \dot{\alpha}]$ is the Gaussian distribution of fluctuations defined in eqs. (6.18) and (6.19).

Time evolution of $f_{\mathbf{k}}$

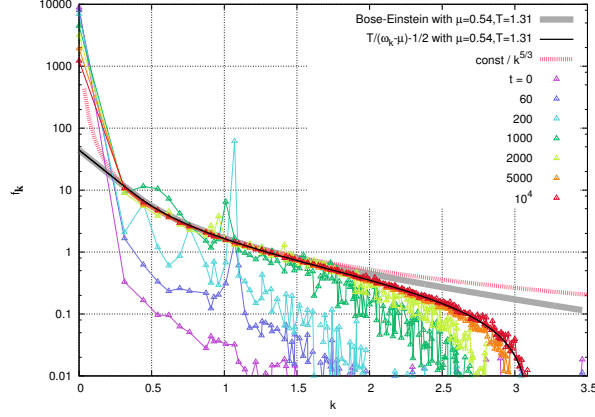
By combining the previous results, the occupation number obtained in this resummation scheme can be written as

$$f_{\mathbf{k}} + \frac{1}{2} = \frac{1}{2\omega_{\mathbf{k}} V} \int [D\alpha D\dot{\alpha}] F[\alpha, \dot{\alpha}] \left| \int d^3 \mathbf{x} e^{i\mathbf{k} \cdot \mathbf{x}} (\dot{\varphi}(x^0, \mathbf{x}) + i\omega_{\mathbf{k}} \varphi(x^0, \mathbf{x})) \right|_{\varphi_0 + \alpha}^2 . \quad (6.72)$$

In the evaluation of this formula, we use for the energy $\omega_{\mathbf{k}} = \sqrt{\mathbf{k}^2 + m^2}$ with the mass fitted in the previous section (thus, we use a different mass at each time x^0). The result of this calculation is displayed in the figure 6.17, where we show the occupation number at various stages of the time evolution, as well as three fits that we shall discuss shortly.

Let us first briefly describe the main stages of the time evolution. At the initial time $t = 0$, only the zero mode is occupied and the higher modes have a negligible occupation number. This is a direct consequence of our setup, where the classical field is initially driven by a spatially homogeneous source. Then, shortly afterwards (this is already visible in the spectrum at $t = 20$) one sees an increase of the occupation in the non-zero modes, concomitant with a decrease of the occupation in the zero mode (barely visible in the figure, due to the logarithmic vertical scale). The increase of the non-zero modes is most pronounced in a narrow

Figure 6.17: Occupation number f_k at various times in the evolution of the system. The grey band represents a fit by a Bose-Einstein distribution. The dashed red band is a fit by a pure power law $k^{-5/3}$. The thin black line is a fit by a distribution of the form given in eq. (6.74).



band of k , where it peaks more than an order of magnitude above the rest of the curve. One can check¹⁹ that this band of k coincides with the band of parametric resonance that we have discussed in detail in [11]. Thus, it appears that the dominant physics at early times is that of resonance, which leads to a quick increase of the occupation number in a narrow region of k . After $t = 1000$, the resonance peak has disappeared and the evolution becomes fairly slow.

Let us now discuss fits of the occupation number, that are represented in the figure 6.17. The first two are a fit by a Bose-Einstein distribution,

$$f_{\text{BE}}(k) = \frac{1}{e^{\beta(\omega_k - \mu)} - 1}, \quad (6.73)$$

and a fit by a classical distribution of the form

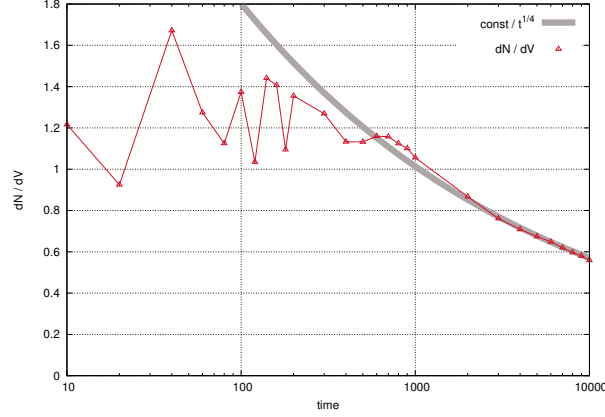
$$f_{\text{class}}(k) = \frac{T}{\omega_k - \mu} - \frac{1}{2}. \quad (6.74)$$

Interestingly, the best fit we could achieve with a Bose-Einstein distribution required a non-zero chemical potential. Although the particle number has no reason to be conserved in this theory (there is no symmetry protecting it), this suggests that changes of the particle number are slow compared to the evolution of the distribution in momentum space: a chemical potential at the latest times we have considered indicates that the particle number has not yet reached its equilibrium value (and its positive sign means that we have a particle excess). At weak coupling, this is rather natural: inelastic processes have a much smaller rate than the elastic ones²⁰, and therefore at intermediate time scales the number of particles is an approximately conserved quantity. In order to check this hypothesis, we can evaluate the number density by summing the occupation number over all the modes k . This has been done in the figure 6.18. One sees indeed that, after a period of somewhat erratic evolution (that roughly

¹⁹See the appendix B of [11].

²⁰For the ϕ^4 scalar theory that we consider here, $\sigma_{\text{el}} \sim g^4$, while $\sigma_{\text{inel}} \sim g^8$. The hierarchy between the elastic and inelastic time-scales is certainly less pronounced in QCD (see [198]) and there it is unclear whether there is enough time for the formation of a transient state that has a non-zero chemical potential.

Figure 6.18: Time evolution of the quasi-particle density in the system. Gray band: fit of the tail with a power law $t^{-1/4}$.



corresponds to the time necessary to have well defined quasi-particles in the system), the number density decreases very slowly at late times, as a small negative power of time.

It is also obvious from the figure 6.17 that a Bose-Einstein distribution does not fit well the occupation number in the tail at large k . In fact, the contrary would have been surprising, since this computation is essentially semi-classical. Naively, one may expect to obtain a classical distribution of the form $T/(\omega_k - \mu)$ (again, a non-zero μ is allowed if number changing processes are very slow), but one can check that such a distribution does not produce a better fit of the tail²¹. It turns out that this drop has a rather trivial explanation. Firstly, note that a very good fit is obtained with the distribution given in eq. (6.74) (the thin black line in the figure 6.17), that differs from the naive classical distribution by an extra $-1/2$ term. This extra term, that makes the fit considerably better, has a trivial origin: it comes from the $-1/2$ in the equation (6.72), which in the derivation of the formula for f_k can be traced back to the non-zero commutator between creation and annihilation operators. Keeping this $-1/2$ correction in the definition of the occupation number for a semi-classical calculation is to a large extent an arbitrary choice. Indeed, such an approximation is expected to reproduce correctly the underlying quantum theory only in the region where the occupation number is sufficiently large. When this is the case, one has $f_k + 1/2 \approx f_k$, and therefore this $1/2$ is not very significant. This also means that the drop of the occupation number at $k \geq 2$ in the figure 6.17, although perfectly understandable in our semi-classical approximation, is obviously not a physical feature of the underlying quantum theory²². In our setup, there is one advantage in keeping the $-1/2$ in eq. (6.72) though: if one does the same computation with a vanishing source $J = 0$, one gets identically $f_k = 0$, which is of course the exact answer. Without this $-1/2$, one would have obtained $f_k = 1/2$.

²¹At first sight, one could be tempted to blame this drop in the tail on the rarefaction of the lattice modes at large k . However, this hypothesis does not hold if one does the same simulation with lower physical scales: this leads to a similar drop, but at a smaller value of k . If the drop was caused by lattice artifacts, one would expect it to occur at a fixed value of k (in lattice units), no matter what the physical scales are.

²²Interestingly however, the $-1/2$ term in eq. (6.74) is nothing but the second term in the expansion of the Bose-Einstein distribution in powers of $(\omega_k - \mu)/T$. Therefore, at a formal level, keeping this $1/2$ correction in the present semi-classical computation gives a better approximation of the full quantum theory. This point was already discussed extensively in [199, 200] in the context of the Boltzmann equation.

Kolmogorov turbulence

At $t \approx 200$, the modes in the resonance band reach their maximal occupancy, and start to subside afterwards, while the other non-zero modes continue to increase. While the resonance peak progressively disappears, one sees in the figure 6.17 that the occupation curves tend to accumulate in the intermediate k range on a fixed line that is well fitted by a power law $k^{-5/3}$. In this regime, the zero mode continues to decrease, while the occupation curve extends slowly into the hard region.

Such a scaling with an exponent $-5/3$ in the power law is well known in the physics of turbulence (see the first part of [201] for instance). Typically, in Kolmogorov's turbulence, the energy cascades to the hard modes from a source localized in the soft sector, with an intermediate stationary distribution in between, that follows a power law $k^{-5/3}$. In our case, the zero mode plays the role of this source, since it was initially the only occupied mode. In contrast to the usual setup in the study of Kolmogorov's turbulence [201], our system is closed and eventually the zero mode will run out of energy and will not be able to feed the cascade anymore. However, in our simulation, we have not reached the time at which this starts to happen.

Bose-Einstein condensation

In the figure 6.17, we saw that the occupation number at late times is best fitted by a distribution of the form of eq. (6.74). This fit however calls for two comments:

- i. the occupation number of the zero mode is well above the curve provided by this fit,
- ii. the best value of the chemical potential ($\mu = 0.54$) is very close to the mass of the quasi-particles at this time, $m = 0.58$.

These two seemingly unrelated facts have in fact a common interpretation. As we have seen before, a chemical potential arises because the number of quasi-particles evolves very slowly in this theory, and a positive μ is the reaction of the system to accommodate an excess of particles. However, it is clear from eqs. (6.73) and (6.74) that μ cannot be larger than the mass m – otherwise, the occupation number would become negative near $k = 0$. But having an upper bound on the chemical potential implies an upper bound on the particle density that these distributions can describe. What if the particle excess in the system is so large that the density is larger than this upper bound? When this happens, the excess of particles condense on the zero mode, a phenomenon known as Bose-Einstein condensation. Dynamically, the collisions lead to a distribution that has two components²³,

$$f_{\mathbf{k}} = \frac{1}{e^{\beta(\omega_{\mathbf{k}} - \mu)} - 1} + f_0 \delta(\mathbf{k}), \quad (6.75)$$

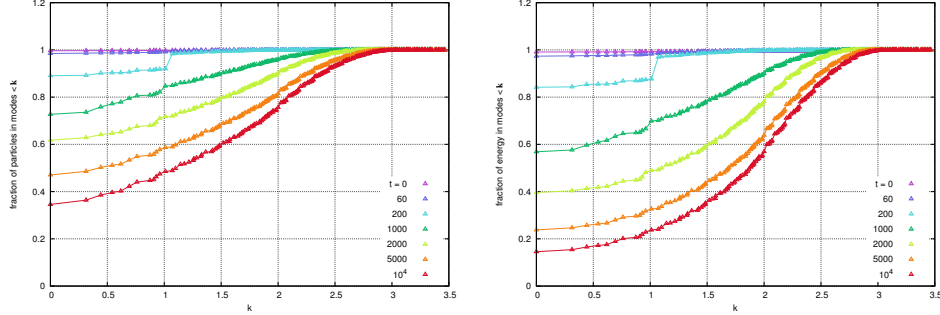
i.e. the chemical potential settles to the maximal value $\mu = m$, and the extra particles go into the zero mode²⁴ $\mathbf{k} = 0$. As one can see from the fit of the figure 6.17, the occupation number appears to be precisely of the form of eq. (6.75).

From the knowledge of the occupation number, it is easy to compute what fraction of the number of particles and what fraction of the total energy are contained in the zero mode at various times. This information is provided in the two plots of the figure 6.19. At early

²³Here we have written the quantum version of the distribution, but it has an analogue in our semi-classical approximation, where the first term is replaced by $f_{\text{class}}(\mathbf{k})$. This is discussed in more detail in the appendix 6.4.7.

²⁴By using the Boltzmann equation, it is easy to see that $\mathbf{k} = 0$ is the only mode where the extra particles can go. If the particles in excess occupy non-zero modes, then one does not have a fixed point of the Boltzmann equation.

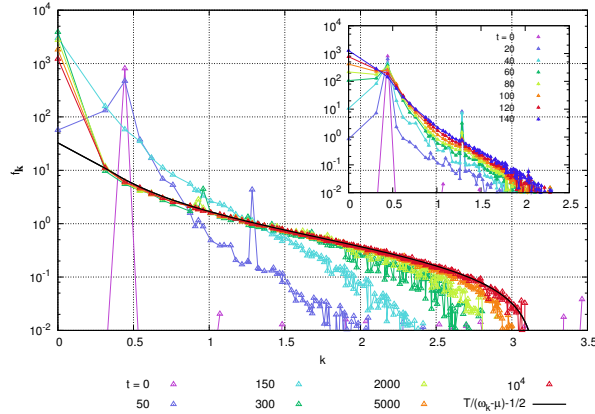
Figure 6.19: Left: fraction of particles contained in the modes $|\mathbf{l}| \leq |\mathbf{k}|$, at various stages of the time evolution. Right: fraction of energy contained in the modes $|\mathbf{l}| \leq |\mathbf{k}|$.



times (up to $t \sim 100$), all the particles and all the energy is stored in the zero mode, as a consequence of our initial condition. At intermediate times (e.g. at $t = 200$), a large fraction of the energy is still in the zero mode, and the remainder is almost entirely in the resonance band. At the latest time we have considered ($x^0 = 10^4$ lattice units), the zero mode still contains about 35% of the particles and 15% of the energy.

One could argue that our computation does not demonstrate Bose-Einstein condensation, because we started from an initial condition in which all the energy is already stored in the zero mode. What if we start from a situation where the zero mode is empty? We have done that in the figure 6.20, in which the energy of the system is initially contained in the modes $(k_x, k_y, k_z) = (1, 1, 0)$ and $(-1, -1, 0)$ (the total energy being exactly the same as in the figure 6.17). Thus, at the initial time, the occupation number has a delta peak at a single,

Figure 6.20: Occupation number $f_{\mathbf{k}}$ at various times, for a system initialized in the modes $(k_x, k_y, k_z) = (1, 1, 0)$ and $(-1, -1, 0)$. Top right inset: behavior at short times.



non-zero, energy. But then, one sees that a non-zero occupation number develops in the zero mode (and in other modes as well), to reach very large values in a rather short time. After this rapid transient regime, all trace of the original peak has been washed out. At late times,

the distribution has become identical to the one encountered in the figure 6.17: all the modes but the zero mode are described by a function of the form of eq. (6.74), and there is a particle excess in the zero mode. This study strongly suggests that Bose-Einstein condensation indeed occurs in this system²⁵, when it is initially over-occupied.

6.4.5 Further tests of the quasi-particle description

Quasi-particle mass

From the occupation number, we can further test the quasi-particle description of the system. A simple check is to compute the medium-induced mass of the quasi-particles, assuming that perturbation theory applies. The Hard Thermal Loop contribution to this mass has already been given in eq. (6.61), and we have represented this quantity in the figure 6.16 (blue curve), along with the mass obtained by fitting the location of the peak in the spectral function. In the region where quasi-particles are well defined ($y^0 \geq 100$), we see that the HTL value of the mass is systematically lower than the observed one. We can improve this result by including also the 1-loop vacuum contribution to the mass. At 1-loop in a ϕ^4 theory, this is given by a tadpole graph whose expression can be written as

$$m_{1\text{-loop}}^2 = g^2 \int \frac{d^3\mathbf{k}}{(2\pi)^3 2k} \left(\frac{1}{2} + f_{\mathbf{k}} \right). \quad (6.76)$$

Including the vacuum contribution to the mass improves significantly (see the red curve in the figure 6.16) the agreement between the theoretical prediction and the fit, indicating that higher-order corrections are presumably rather small for this value of the coupling ($g = 1$). Thus, it appears that the quasi-particle description is quite consistent: indeed, the occupation number computed from the fields themselves, when inserted into the 1-loop formula for the effective mass, reproduces very well the mass measured by fitting the peak in the spectral function.

Residual interaction energy

A quasi-particle description of a system is useful only if the residual interactions between the quasi-particles are weak – in other words, if the main effect of the interactions is simply to alter the properties of the particles (e.g. by generating an effective mass). This can be tested by computing the energy density of the system by summing the energies of its quasi-particles, i.e. by assuming that they have no residual interactions²⁶,

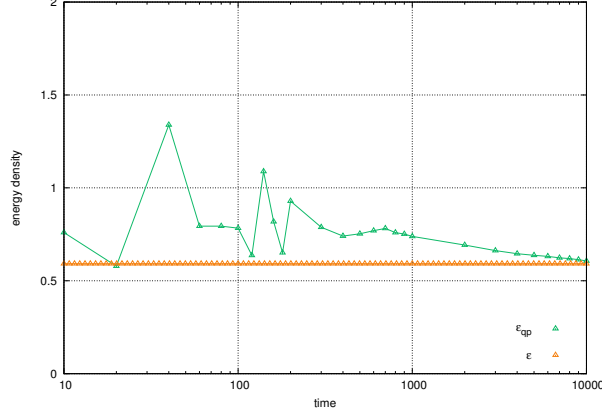
$$\epsilon_{\text{qp}} \equiv \int \frac{d^3\mathbf{k}}{(2\pi)^3} f_{\mathbf{k}} \sqrt{\mathbf{k}^2 + m^2}. \quad (6.77)$$

By comparing this quasi-particle energy to the actual energy density, $\epsilon \equiv \langle T^{00} \rangle$, we can estimate the interaction energy of the quasi-particles and therefore the strength of their residual interactions. The result of this comparison is shown in the figure 6.21. We see that the

²⁵Of course, since the study is performed on a lattice, that has by definition a discrete spectrum, it is impossible to tell whether the distribution has a true $\delta(\mathbf{k})$ term at the origin or whether it is a strongly peaked but otherwise regular function.

²⁶In our framework, replacing the true energy density by ϵ_{qp} is equivalent to substituting the expectation value of the interaction energy $\langle U(\varphi) \rangle$ by $\frac{1}{2} m^2 \langle \varphi^2 \rangle$, i.e. to a mean-field approximation.

Figure 6.21: Comparison between the actual energy density of the system (ϵ) and the energy carried by the quasi-particles (ϵ_{qp}) if one neglects their interactions.



true energy of the system is always below the energy of its quasi-particles, indicating that the residual interactions are attractive – which is indeed a standard result of a ϕ^4 field theory. Moreover, as the time increases, the energy of the quasi-particles gets closer to the true energy, meaning that the quasi-particle description is better at late times.

Entropy production

From the occupation number, it is also possible to compute the entropy density,

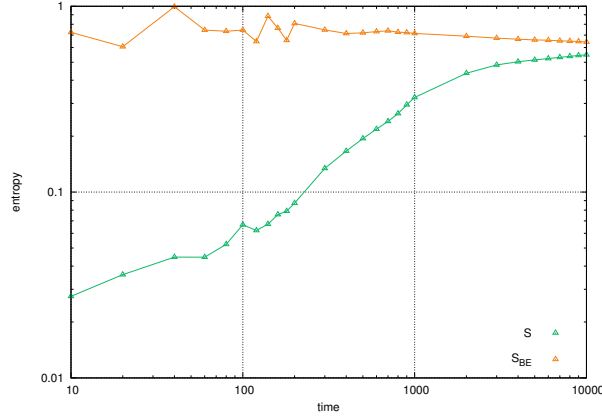
$$s \equiv \int \frac{d^3\mathbf{k}}{(2\pi)^3} \left[(1 + f_{\mathbf{k}}) \ln(1 + f_{\mathbf{k}}) - f_{\mathbf{k}} \ln f_{\mathbf{k}} \right]. \quad (6.78)$$

The time evolution of this quantity is shown in the figure 6.22 (green curve). One sees that the entropy density is multiplied roughly by a factor 20 during the evolution of the system (the initial value is low in our setup because the occupancy is entirely localized in the zero mode at $t = 0$). In the red curve, we have displayed the entropy that would have a gas of free bosons of equal energy density at thermal equilibrium²⁷. The true entropy of the system gets close to the equilibrium entropy, but not exactly equal even at the largest times we have considered (the discrepancy remains of the order of 10–20%). This difference is presumably a combination of two factors: (i) the fact that the system is not yet fully equilibrated, and (ii) the residual interactions of its quasi-particles.

The increase of the entropy defined by eq. (6.78) may seem paradoxical at first sight, given the way it has been obtained in our framework. Indeed, at the microscopic level, our system is described as an ensemble of classical field configurations that evolve according to the Euler-Lagrange equation of motion. This equation of motion is invariant under time reversal $t \rightarrow -t$, yet the entropy s computed in this system is clearly not invariant under this transformation – despite the fact that it is a functional of classical fields that have a time-reversible evolution. Let us recall here that the ensemble of classical field configurations that

²⁷Its small variations with time are due to the fact that the mass of the quasi-particles is not constant.

Figure 6.22: Green curve (S): time evolution of the entropy density s defined in eq. (6.78). Red curve (S_{BE}): entropy of a non-interacting gas of bosons of equal energy density, in thermal equilibrium.



describe the system in our framework evolves according to the Liouville equation,

$$\partial_t \mathcal{F}_t + \{\mathcal{F}_t, H\} = 0. \quad (6.79)$$

Instead of eq. (6.78), one could have defined an entropy based on the probability distribution $\mathcal{F}_t[\varphi, \dot{\varphi}]$ of the field configurations in phase-space,

$$S \equiv - \int [D\varphi D\dot{\varphi}] \mathcal{F}_t[\varphi, \dot{\varphi}] \ln \mathcal{F}_t[\varphi, \dot{\varphi}]; \quad (6.80)$$

and it is easy to see that it is constant in time thanks to Liouville's theorem (see the appendix F). This means that, if one were able to determine the field configuration of the system at a given time, there would be no entropy increase because everything would be known about the microscopic state of the system. In contrast, the definition (6.78) is the appropriate definition when one knows only the single particle distribution in the system. Compared to eq. (6.80), a lot of information about the microscopic state of the system has been discarded by doing this. This coarse graining is the reason why the entropy given by (6.78) increases with time, while at the microscopic level the field configurations evolve via time reversible equations.

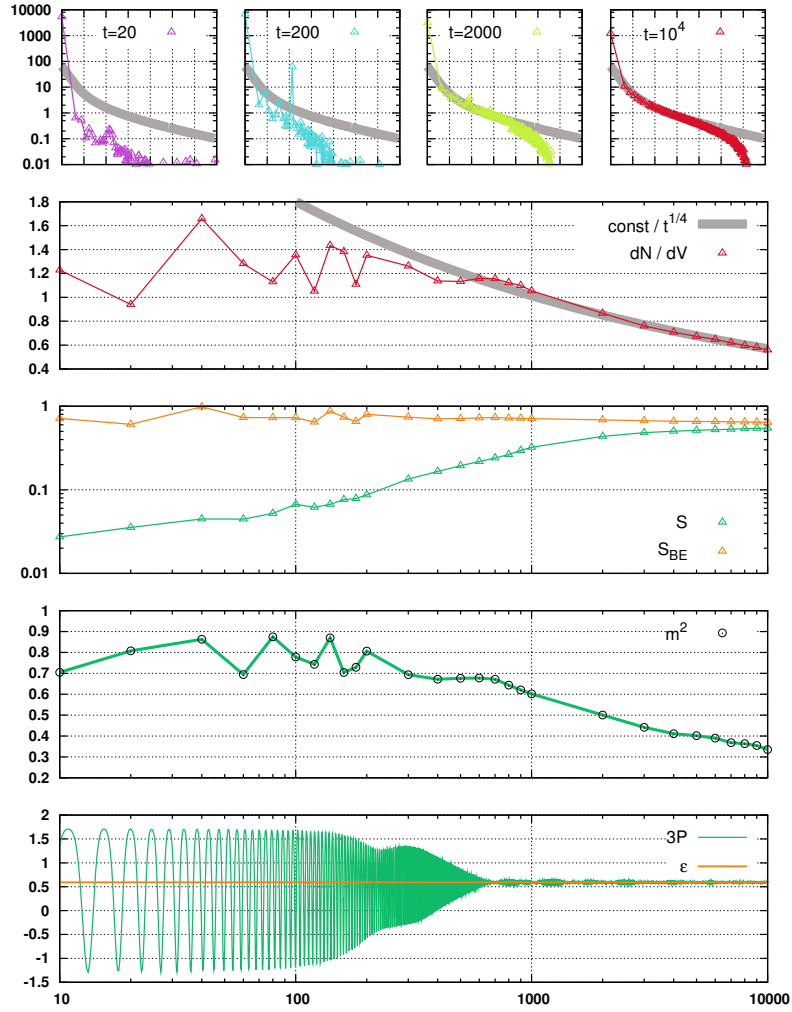
6.4.6 Time evolution at a glance

Let us summarize the main results of this section in a synthetic way, by displaying in parallel the time evolutions of the various quantities that we have considered separately so far. This is shown in the figure 6.23. From these plots, it appears that one can divide the time evolution in three stages that are qualitatively distinct²⁸:

- i. $0 \leq t \leq 100$: at these early times, the pressure of the system has not yet started to relax towards its equilibrium value $p = \epsilon/3$. Moreover, quasi-particles are not

²⁸The numerical values of the times quoted here are not absolute, but depend on the energy density in the system. Indeed, in a scale invariant theory, all the time-scales vary like $\epsilon^{-1/4}$. Moreover, these time-scales depend on the coupling constant g^2 , and decrease as the coupling increases.

Figure 6.23: (Panels numbered 1 to 5 from the bottom to the top.) Panel 1: time evolution of the pressure. Panel 2: time evolution of the quasi-particle mass. Panel 3: time evolution of the entropy, compared to the entropy of a gas of same energy density at thermal equilibrium. Panel 4: time evolution of the quasi-particle density. Panel 5: occupation number at various stages of the time evolution (the gray band is a fit at the latest time by a Bose-Einstein distribution with a chemical potential).



a good description of the system (their mass is not well defined, and there are extra spurious branches in the spectral function). The entropy displays only a very moderate growth during this era, the occupation number starts rising in the resonance band almost immediately, but the energy is still almost entirely contained in the zero mode,

- ii. $100 \leq t \leq 600$: this intermediate period starts when the occupancy in the resonance band reaches its maximum and starts to subside, while the occupation number rises in the other momentum modes. During this stage, the zero mode still contains the largest share of the total energy, and the remainder is contained predominantly in the resonant modes. The main features of this era are the relaxation of the pressure towards its equilibrium value, and an important growth of the entropy. In this era, there are well defined quasi-particles, with a mass that is almost constant in time,
- iii. $600 \leq t$: in the late stages of the time evolution, the pressure is the equilibrium one, and the entropy displays only a marginal growth. However, the system is not yet fully equilibrated: the mass of the quasi-particles shows a clear decrease, while the occupation number continues to slowly expand towards higher momenta. During this stage, the occupation number shows some signs of Kolmogorov scaling, but perhaps even more compelling is the fact that it seems to evolve as would a system dominated by elastic collisions and which is overpopulated compared to equilibrium – i.e. by developing a chemical potential equal to the mass and a Bose condensate at zero momentum. At the same time, the energy initially contained in the zero mode is progressively distributed among the higher modes.

A very interesting observation is the appearance of a chemical potential, that we interpreted as resulting from a particle excess (compared to the value the particle density should have in equilibrium) combined to a fairly slow rate of inelastic processes. Eventually, the inelastic processes will wipe out the initial particle excess. However, because they are slow, there is an extended regime where the occupation number settles on a form that has a chemical potential. Moreover, for the bosonic quantum statistics, the chemical potential cannot be larger than the mass of the quasi-particles. This implies that if the particle excess is too large, it cannot be accommodated solely by a chemical potential and the system stabilizes itself by the formation of a condensate at zero momentum. This is consistent with our numerical results, where we observe a large occupancy in the zero mode, that persists until late times while the chemical potential remains close to the mass of the quasi-particles. Interestingly, the condition of overpopulation is also realized for the gluons produced initially in heavy ion collisions. Indeed, at a time Q_s^{-1} (where Q_s is the saturation momentum), the energy density is $\epsilon \sim Q_s^4/g^2$ and the gluon number density is $n \sim Q_s^3/g^2$. Thus one has the dimensionless ratio $ne^{-3/4} \sim g^{-1/2} \gg 1$, that should be of order 1 in chemical equilibrium. Depending on the strength of the number-changing processes, one may also expect the (transient) appearance of a gluonic chemical potential and the formation of a gluon condensate at zero momentum.

6.4.7 Evolution of the classical phase-space density

In the figure 6.17, we have obtained a very good fit of the occupation number at late times by a function of the form

$$f_k = \frac{T}{\omega_k - \mu} - \frac{1}{2}. \quad (6.81)$$

This fit works except for the zero mode, that is over occupied with respect to this distribution. We interpreted this distribution as the classical approximation of a Bose-Einstein distribution, and the $-1/2$ term was simply due to our definition of the occupation number.

However, it is also interesting to forget the underlying quantum field theory we started from, and to consider in its own right the classical problem by which it is approximated. This reformulation is equivalent to solving the Liouville equation,

$$\partial_t \mathcal{F}_t + \{\mathcal{F}_t, \mathcal{H}\} = 0, \quad (6.82)$$

given some Gaussian initial distribution. Therefore, if we adopt this point of view, we just have a (large) collection of coupled classical oscillators, and we follow their Hamiltonian flow in phase-space. Let us now discuss some aspects of this classical dynamical system, that are relevant to the topics discussed previously.

Effective Hamiltonian

Motivated by the observation of quasi-particles in the system, we may assume that there is a transformation of the fields and their conjugate momenta such that the Hamiltonian becomes a sum of quasi-free harmonic oscillators coupled only by some weak residual interactions. In practice, this amounts to writing

$$\begin{aligned} \mathcal{H} &= \int d^3\mathbf{x} \frac{1}{2} \left(\dot{\varphi}^2 + (\nabla \varphi)^2 \right) + \frac{g^2}{4!} \varphi^4 \\ &= \int d^3\mathbf{x} \underbrace{\frac{1}{2} \left(\dot{\varphi}^2 + (\nabla \varphi)^2 + m^2 \varphi^2 \right)}_{\mathcal{H}_0} + \underbrace{\frac{g^2}{4!} \varphi^4 - \frac{1}{2} m^2 \varphi^2}_{\mathcal{H}'_{\text{int}}}. \end{aligned} \quad (6.83)$$

So far, we have just added and subtracted a mass term by hand, and the parameter m^2 is still arbitrary. In order to make the residual interactions small, one can choose the mean field value for m^2 ,

$$m^2 = \frac{g^2}{2} \langle \varphi^2(\mathbf{x}) \rangle, \quad (6.84)$$

where the angle brackets denote an ensemble average²⁹. The first part of this Hamiltonian can be rewritten as a sum of independent harmonic oscillators by going to Fourier space,

$$\mathcal{H}_0 = \int \frac{d^3\mathbf{k}}{(2\pi)^3} \underbrace{\frac{1}{2} |\dot{\varphi}_{\mathbf{k}}|^2 + \frac{1}{2} \omega_{\mathbf{k}}^2 |\varphi_{\mathbf{k}}|^2}_{h_{\mathbf{k}}}, \quad (6.85)$$

where $\omega_{\mathbf{k}} \equiv (\mathbf{k}^2 + m^2)^{1/2}$ and where $\varphi_{\mathbf{k}}$ is the spatial Fourier transform of φ .

This decomposition of the classical Hamiltonian into elementary harmonic oscillators plus residual interactions is a good starting point to make connections with the study of the occupation number in the previous sections. Indeed, it is easy to check that eq. (6.72) is equivalent to

$$\frac{1}{2} + f_{\mathbf{k}} = \frac{\langle h_{\mathbf{k}} \rangle}{V \omega_{\mathbf{k}}}. \quad (6.86)$$

²⁹One can check numerically that this mean field expression of the mass is in very good agreement with the measured mass of the quasi-particles.

In other words, $\langle h_k \rangle$ is the occupancy of the mode k times ω_k times the volume, plus a constant *vacuum contribution* $V\omega_k/2$. This means that one should find a non-zero average value for $\langle h_k \rangle$ even in the vacuum – actual particles in the mode k correspond to an excess of $\langle h_k \rangle$ over $V\omega_k/2$.

Time evolution of the classical distribution

In order to start the discussion, we first plot in the figure 6.24 the distribution $\mathcal{F}_t[\varphi, \dot{\varphi}]$ of the classical field configurations at various stages of the evolution. Since we obviously cannot plot a functional, we have represented several *Fourier slices*: a slice being defined as the distribution of configurations in the plane³⁰ $(\sqrt{\omega_k/V}|\varphi_k|, |\dot{\varphi}_k|/\sqrt{\omega_k V})$. In the figure 6.24, we have represented this distribution for three values of k : the zero mode, a mode in the resonance band, and a mode at some higher momentum. At the initial time, the zero mode of the fields is highly coherent, and its distribution is concentrated around a single point. In contrast, all the higher modes contain only fluctuations centered around the origin $(0, 0)$, with a width which is that of the vacuum fluctuations (i.e. the width that gives $\langle h_k \rangle = \omega_k/2$). At the next time, $t = 200$, the zero mode has decohered and now fills almost uniformly a curve³¹ of constant energy. We also see that the distribution of the resonant modes has expanded due to parametric resonance, while the harder modes still have the same distribution as the $t = 0$ one. At later times, the expansion of the resonant modes reaches a maximum and then subsides, while the distribution of the hard modes begins to expand as well. Simultaneously, the zero mode distribution shrinks slowly, while remaining on a curve of constant energy (i.e. this seemingly constant energy is in fact slowly decreasing, due to a transfer of energy from the soft to the hard modes).

To summarize these observations, the Fourier modes that initially have a large amplitude quickly decohere. If there are many such modes (instead of only one as in our numerical example), what happens then depends on whether the classical dynamics is chaotic or on the contrary integrable: in a chaotic system, all these modes mix and fill uniformly an energy shell, while in the integrable case these modes would evolve independently and cover an invariant torus of much smaller dimension (for N modes, an energy shell is a manifold of dimension $2N - 1$, while an invariant torus has dimension N only). On larger time scales, the energy carried by these initially large modes decreases slowly, and is transferred to the higher modes whose distribution expands as a consequence of this transfer.

Asymptotic behavior

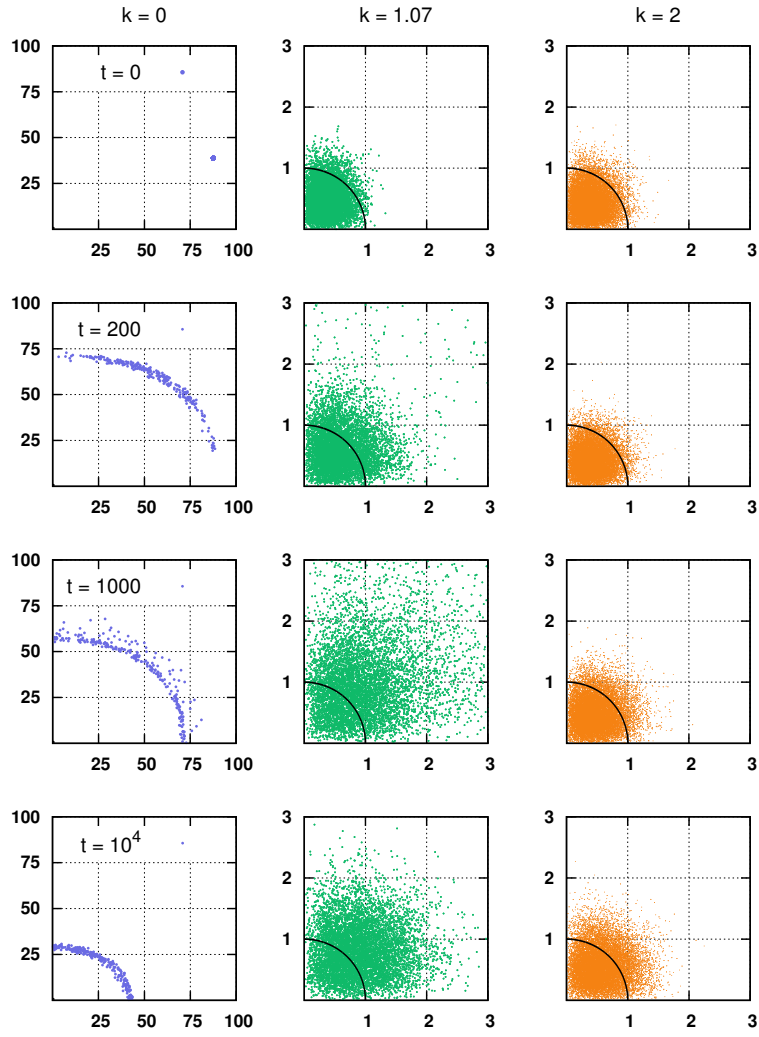
What is then the asymptotic distribution $\mathcal{F}_\infty[\varphi, \dot{\varphi}]$ of these classical fields? Let us assume first that the only quantity that is invariant under the Hamiltonian flow is the energy itself³². From the Liouville equation, it is clear that the asymptotic distribution must have a vanishing Poisson bracket with the Hamiltonian. This property is satisfied by any distribution that depends on $\varphi, \dot{\varphi}$ only through the Hamiltonian $\mathcal{H}[\varphi, \dot{\varphi}]$. Such an asymptotic form for the distribution \mathcal{F}_∞ has strong implications on the average value of $\langle h_k \rangle$. Indeed, if we can

³⁰We rescale the Fourier components in this way so that the vacuum fluctuations look the same for all k . A value of $\langle h_k \rangle$ proportional to ω_k corresponds to a circle of fixed radius (of order unity) in this plane.

³¹This is not exactly a curve of constant h_0 , as one can see from the fact that it is not a circle. This deviation from a circle is due to the fact that there is a large correction $g^2\varphi_0^4/4!$ coming from the interaction energy. Indeed, the zero mode, because of its large amplitude, is strongly interacting with itself.

³²The total spatial momentum of the system is also conserved, but it does not play any role here because we analyze the problem in the rest frame of the system.

Figure 6.24: Phase-space density in the $(\sqrt{\omega_k/V}|\varphi_k|, |\dot{\varphi}_k|/\sqrt{\omega_k V})$ plane. From left to right: $k = 0, 1.07$ (resonant mode), and 2. From top to bottom: $t = 0, 200, 10^3$ and 10^4 . Note the vastly different scale used for the zero mode (left column). The black circle represents the radius of the pure vacuum fluctuations.



neglect the interaction energy (e.g. assuming that most of the interaction energy can be absorbed into an effective mass), then a distribution that depends only on \mathcal{H} implies the equipartition of the energy among the modes,

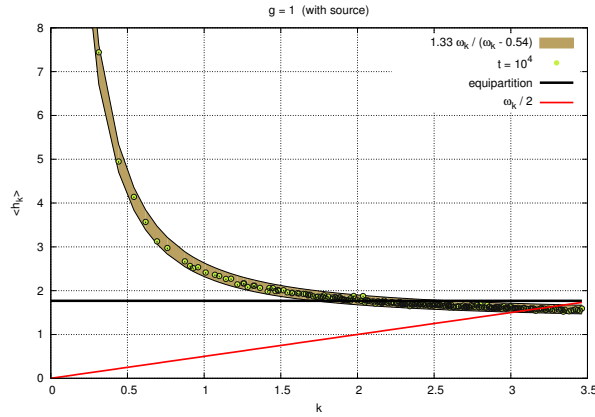
$$\langle h_k \rangle = \text{const (independent of } k) . \quad (6.87)$$

Note that this conclusion holds no matter what is the precise form of the function of \mathcal{H} that \mathcal{F}_∞ is equal to. When equipartition in the classical phase-space is reached, the occupation number becomes of the form:

$$f_k = \frac{\text{const}}{\omega_k} - \frac{1}{2} . \quad (6.88)$$

Asymptotic behavior with constraints

Figure 6.25: Average value $\langle h_k \rangle$ of the energy in the mode k . The brown band is a fit of the form $T\omega_k/(\omega_k - \mu)$, and its width reflects the expected statistical error in our Monte-Carlo simulation. The horizontal line shows the expected result if equipartition is reached. The red line represents the zero point energy of the vacuum, i.e. $\omega_k/2$.



When we try to fit the late time curves of the figure 6.17 by an expression of the form (6.88), that lacks the chemical potential μ , the result is not good. This is best seen by plotting $\langle h_k \rangle$ (see the figure 6.25), since eq. (6.88) would correspond to an horizontal line in this plot. In contrast, the much better fit of the figure 6.17 could be explained if the average value of h_k at late times was of the form

$$\langle h_k \rangle = \text{const} \frac{\omega_k}{\omega_k - \mu} . \quad (6.89)$$

This is obvious in the figure 6.25, where we obtain a good fit to $\langle h_k \rangle$ by an expression of this form.

It is possible to understand eq. (6.89) if one assumes that the Hamiltonian flow not only conserves energy (exactly), but also (to a good degree of approximation) the following quan-

tity³³

$$\mathcal{N}[\varphi, \dot{\varphi}] \equiv \int \frac{d^3\mathbf{k}}{(2\pi)^3} \frac{h_{\mathbf{k}}}{\omega_{\mathbf{k}}} . \quad (6.90)$$

It is obvious that this quantity has a vanishing Poisson bracket with the free quasi-particle part of the Hamiltonian \mathcal{H}_0 , and that only the residual quasi-particle interactions $\mathcal{H}'_{\text{int}}$ can possibly make this quantity change. If both \mathcal{H} and \mathcal{N} are invariants, then the most general asymptotic solution of the Liouville equation must depend on $\varphi, \dot{\varphi}$ only through some combination of the form $\mathcal{H} - \mu\mathcal{N}$. For any distribution of this form, equipartition is replaced by

$$\left\langle h_{\mathbf{k}} - \mu \frac{h_{\mathbf{k}}}{\omega_{\mathbf{k}}} \right\rangle = \text{const (independent of } \mathbf{k} \text{)} , \quad (6.91)$$

which leads to eq. (6.89). Therefore, in the classical system of fields, it seems that the very slow variation of \mathcal{N} is what explains that we observed an energy distribution that differs considerably from the naive equipartition.

Note that when k is large, eq. (6.91) is equivalent to $\langle h_{\mathbf{k}} \rangle = \text{const}$. This implies that the constant in the right hand side must be positive. Considering now $\mathbf{k} = 0$, this imposes $\mu \leq m$. Inserting now eq. (6.91) in the definition of \mathcal{N} ,

$$\langle \mathcal{N} \rangle = \int \frac{d^3\mathbf{k}}{(2\pi)^3} \frac{\text{const}}{\omega_{\mathbf{k}} - \mu} , \quad (6.92)$$

we see that it increases with μ , and reaches a finite (because the singularity at $\mathbf{k} = 0$ is integrable) maximum when $\mu = m$. However, it may happen that the initial value of $\langle \mathcal{N} \rangle$ is larger than this maximum. In this situation, the $\langle h_{\mathbf{k}} \rangle$'s must be altered in order to accommodate this excess, but in such a way that eq. (6.91) remains valid. Any modification of $\langle h_{\mathbf{k}} \rangle$ for $\mathbf{k} \neq 0$ will violate eq. (6.91), so the only possibility is to modify $\langle h_0 \rangle$. Then, we see that the only way to change $\langle h_0 \rangle$ without violating eq. (6.91) is to add to have $\mu = m$. Thus, when there is an excess of $\langle \mathcal{N} \rangle$, the equilibrium value of $\langle h_{\mathbf{k}} \rangle$ takes the form

$$\langle h_{\mathbf{k}} \rangle = A \delta(\mathbf{k}) + B \frac{\omega_{\mathbf{k}}}{\omega_{\mathbf{k}} - m} . \quad (6.93)$$

This explains why we found a chemical potential whose value is very close to the mass of the quasi-particles (within statistical errors). This phenomenon can be seen as an analogue in classical Hamiltonian dynamics of *Bose condensation* in quantum mechanics.

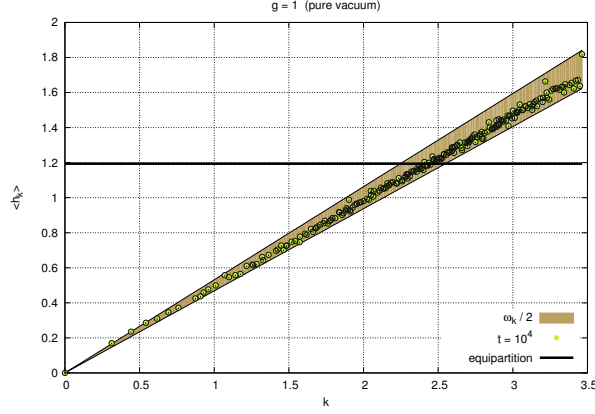
Do vacuum fluctuations thermalize?

The fact that the Liouville evolution makes the distribution \mathcal{F}_t evolve towards a classical thermal equilibrium leads to an interesting question: does the same happen if there is no source coupled to the quantum fields, i.e. for pure vacuum fluctuations? In this case, the initial distribution is

$$\mathcal{F}_0[\varphi, \dot{\varphi}] = \exp \left[- \int \frac{d^2\mathbf{k}}{(2\pi)^3} \frac{|\dot{\varphi}_{\mathbf{k}}|^2 + k^2 |\varphi_{\mathbf{k}}|^2}{k} \right] , \quad (6.94)$$

corresponding to $\langle h_{\mathbf{k}} \rangle = k/2$. The consistency of our approach requires that the vacuum does not change over time. However, since eq. (6.94) is not a function of \mathcal{H} , our previous

Figure 6.26: Average value of the energy \bar{h}_k in the mode k for pure vacuum fluctuations. The center of the brown band is $\omega_k/2$, and its width reflects the expected statistical error in our Monte-Carlo simulation). The horizontal line corresponds to equipartition.



considerations suggest that equipartition may also occur if we start from the pure vacuum fluctuations given by eq. (6.94). We have computed $\langle \bar{h}_k \rangle$ numerically for the pure vacuum case, by starting from the distribution of eq. (6.94) and by evolving the corresponding classical field configurations also to a large time $t = 10^4$. As shown in the figure 6.26, this computation shows no sign of equipartition of the vacuum energy, indicating that the vacuum is stable in our framework.

This is at first sight an intriguing result. Indeed, how does the purely classical Liouville equation know that the distribution of eq. (6.94) represents the ground state of the corresponding quantum theory? In a sense, the Liouville equation seems to know more than what its “classical” qualifier might suggest. This result can be qualitatively explained by recalling the formal connection that exists between quantum mechanics and the classical Liouville equation. In quantum mechanics, a system can be described by a density operator $\hat{\rho}$, whose evolution is driven by the Von Neumann equation,

$$i\partial_t \hat{\rho} + [\hat{\rho}, H] = 0. \quad (6.95)$$

It was noted by Wigner and Moyal that this quantum mechanical problem can be formulated equivalently as an evolution in the classical phase-space (see [202] for a recent review). To do this, one should first introduce the Wigner distribution associated to the density operator $\hat{\rho}$. For a single degree of freedom, this is defined as

$$W(q, p) \equiv \int dx e^{ipx} \langle q + x/2 | \hat{\rho} | q - x/2 \rangle. \quad (6.96)$$

The Von Neumann equation can then be shown to be equivalent to the Moyal equation for W ,

$$\partial_t W + \{\{W, \mathcal{H}\}\} = 0, \quad (6.97)$$

³³The average $\langle \mathcal{N} \rangle$ in the classical field theory is the counterpart of the number of quasi-particles in the quantum theory.

where $\{\{\cdot, \cdot\}\}$ is the Moyal bracket, obtained as the Wigner transform of the commutator. At this stage, one has a formulation of quantum mechanics that involves only quantities defined on the classical phase-space (the quantum mechanical aspects are hidden in the fact that the Moyal bracket depends on \hbar). The connection to the classical Liouville equation follows from the following two properties,

- i. the Moyal bracket $\{\{\cdot, \mathcal{H}\}\}$ is equal to the Poisson bracket $\{\cdot, \mathcal{H}\}$ if the Hamiltonian \mathcal{H} is quadratic in the coordinates and momenta,
- ii. for any quantities A and B defined on the classical phase-space, one has

$$\{\{A, B\}\} = \{A, B\} + \mathcal{O}(\hbar^2) . \quad (6.98)$$

If the quantum system is in its ground state $|0\rangle$, its density operator $\hat{\rho}_0 \equiv |0\rangle\langle 0|$ is invariant under the Von Neumann equation. Equivalently, the corresponding Wigner distribution W_0 is invariant under the Moyal equation. Since \mathcal{F}_0 is the Wigner distribution of the same vacuum state, it is thus natural that it is left invariant by the Liouville evolution, since it is the $\hbar \rightarrow 0$ limit of the invariant Moyal evolution.

Conclusions and Perspectives



he central result of this manuscript is the proof that, for inclusive observables in heavy ion collisions, the logarithms of the collision energy are universal and can be factorized into the JIMWLK evolution of distributions that describe the content of the two projectiles. This universality establishes a rigorous connection between Deep Inelastic Scattering off nuclei and heavy ion collisions: these distributions can be constrained in DIS experiments, and then used to compute observables in nucleus-nucleus collisions.

A consequence of this factorization theorem is that –at leading logarithmic accuracy– all the dependence on energy and rapidity in inclusive observables is inherited from the evolution of the color charge distributions of the projectiles prior to the collision. This is also true of the rapidity correlations in multigluon spectra: all the leading correlations pre-exist in the wavefunctions of the projectiles. The correlations that are produced during the collision itself are a subleading effect.

Thus, from the JIMWLK equation for the projectile evolution, one can make predictions (at leading logarithmic accuracy) for the energy and rapidity dependence of observables in heavy ion collisions, that can be tested in experiments. A key observation is the existence of correlations between pairs of particles separated by a large rapidity interval. From causality, one can trace this effect back to the state of the system at a very short time after the impact, i.e. when its dynamics was still dominated by the physics of gluon saturation. This long range correlation has a natural explanation in the framework we have presented in this manuscript, related to the fact that the strong color fields produced in the collision have a very weak rapidity dependence. In fact, the JIMWLK equation predicts how this correlation should decrease when the rapidity separation increases, a prediction that will be testable at the LHC thanks to the large rapidity acceptance available in detectors such as CMS and ATLAS. The Color Glass Condensate also predicts that the multiplicity distribution should be close to a negative binomial distribution, a fact compatible with experimental observations.

The results on factorization presented in this manuscript can be extended in several directions. Firstly, it would be interesting to study whether it also applies to the production of other particles, such as light quarks (for heavy quarks –with a large mass compared to the saturation momentum–, the multiple scattering corrections that make factorization non-trivial are suppressed, and this case should fall back to the much simpler k_T -factorization). A second extension, technically more complicated, is to study the next-to-leading logarithmic contributions in order to assess whether they also factorize via a NLO-improved JIMWLK equation.

Our proof of factorization highlights the special status of inclusive observables, such as inclusive spectra or the energy-momentum tensor. It is easy to see that our proof fails for exclusive observables, because constraints imposed on the content of the final state modify the boundary conditions of the fields. At the moment, it seems clear that the CGC formalism must be altered if one wants to describe exclusive reactions –such as diffraction–, but the precise nature and extent of these modifications is so far unknown. In phenomenological models of diffraction in hadronic collisions, one introduces the so-called *survival probability* – the probability that no inelastic process happens besides the hard process of interest– in order to account for the breakdown of factorization in diffractive processes when going from DIS to hadronic collisions. However, a QCD-based justification of these models is still missing. Because of its ability to cope with situations where multiparton processes matter, the CGC seems to be a promising framework for studying these questions. This is definitely an interesting theoretical problem, that has also a phenomenological interest in other areas such as the central diffractive production of the Higgs boson in proton-proton collisions at the LHC.

The main outstanding problem in the study of the early stages of heavy ion collisions is that of thermalization. The comparison between experimental results and hydrodynamical models tends to favor a fast thermalization, a result which is notoriously hard to justify on the theory side. In the Color Glass Condensate framework, our best hope towards the resolution of this issue is the resummation that we have developed in the last part of this manuscript in order to cure the secular divergences that appear in higher loop orders. This resummation amounts to a classical Yang-Mills evolution with a Gaussian ensemble of initial conditions. Combined with the known fact that the Yang-Mills equations have positive Lyapunov exponents, this suggests that thermalization in heavy ion collisions may be related to the chaotic behavior of classical QCD.

In order to explore these ideas in a simpler setting, we have studied in detail a scalar field theory by using the same techniques. In this context, we were able to conclude that this resummation indeed leads to the expected equilibrium equation of state. In fact, the initial condition is a coherent state and the equation of state is obtained as soon as the initial coherence is destroyed. In addition, we have shown that, although the system is made of strong fields configurations, quasi-particles emerge once decoherence is achieved. Later on, the occupation number of these quasi-particles evolve to an equilibrium distribution. If the initial condition is made of large enough fields, this distribution has a positive chemical potential and even a Bose-Einstein condensate (BEC) in the zero mode. In the Color Glass Condensate framework, the initial condition immediately after the collision of two heavy ions is also characterized by large fields that could possibly lead to the formation of a condensate, but whether a BEC forms or not depends crucially on the rate of inelastic processes.

Moreover, these results raise further questions regarding the precise state of the matter formed in heavy ion collisions, and in particular whether it reaches complete local thermal equilibrium or not. At the most fundamental level, the full thermalization of the system requires that the correlation functions obey the *Kubo-Martin-Schwinger relations* [203, 204], and it would be interesting to assess to what extent they are satisfied (or violated) by the fields produced in the early stages of heavy ion collisions. Given the possible formation of a BEC, it would also be very instructive to compute the transport coefficients –especially the shear viscosity– of the matter produced in these collisions.

Another interesting, more formal, direction would be to investigate possible connections between the resummation presented in the final part of this work and older ideas in the field of quantum chaos, such as *Berry's conjecture* [205–207] and Srednicki's hypothesis of *eigenstate thermalization* [208, 209]. These works consider quantum mechanical systems whose classical limit is chaotic, and try to uncover the relationships that exist between the chaoticity of the classical system and the mechanisms by which the quantum system reaches thermal equilibrium. To some extent, similar questions arise when one tries to understand the thermalization of the matter produced in heavy ion collisions.

Part IV

Appendices

Appendix A

Schwinger-Keldysh formalism



As is well known, Feynman perturbation theory in quantum field theory is the tool of choice for computing transition amplitudes such as $\langle \mathbf{p}' \mathbf{q}'_{\text{out}} | \mathbf{p} \mathbf{q}_{\text{in}} \rangle$. The calculation of these matrix elements is amenable via the Lehmann–Symanzik–Zimmermann reduction formulas to the expectation value of time-ordered products of field operators, between the in- and out- vacuum states, for instance $\langle 0_{\text{out}} | T \phi(x_1) \phi(x_2) \phi(x_3) \phi(x_4) | 0_{\text{in}} \rangle$, the calculation of which can be performed with the usual Feynman rules that we shall review in the first section of this appendix.

However, there is a class of more general problems that cannot be addressed by this standard perturbation theory. One of the simplest problems of that kind is the evaluation of the expectation value of the number operator $\langle 0_{\text{in}} | a_{\text{out}}^\dagger(\mathbf{p}) a_{\text{out}}(\mathbf{p}) | 0_{\text{in}} \rangle$, which counts the particles of momentum \mathbf{p} in the final state, given that the initial state was the in- vacuum. To evaluate this matrix element, one needs to calculate the amplitude $\langle 0_{\text{in}} | \phi(x) \phi(y) | 0_{\text{in}} \rangle$, that has no time ordering, and where one has the in- vacuum state on both sides. More generally, one often needs the amplitudes $\langle 0_{\text{in}} | \bar{T} \phi(x_1) \cdots \phi(x_n) T \phi(y_1) \cdots \phi(y_p) | 0_{\text{in}} \rangle$, where \bar{T} denotes the anti-time ordering. This is what the Schwinger-Keldysh formalism is designed for. We will derive the rules for the perturbative expansion of this kind of matrix elements in section A.2.

A.1 Standard perturbation theory

Let $\phi(x)$ be the field operator in Heisenberg's representation. It can be formally related to the field operator in the interaction representation, $\phi_{\text{in}}(x)$, by the relation

$$\phi(x) = U(-\infty, x^0) \phi_{\text{in}}(x) U(x^0, -\infty) , \quad (\text{A.1})$$

where $U(x_2, x_1)$ is an evolution operator defined as

$$U(x_2, x_1) \equiv T \exp i \int_{x_1^0}^{x_2^0} d^4x \mathcal{L}_{\text{int}}(\phi_{\text{in}}(x)) . \quad (\text{A.2})$$

(In this definition, \mathcal{L}_{int} is the part of the Lagrangian containing the interaction terms, i.e. the terms of degree three or higher in the field operator.) The evolution operator $U(x_2, x_1)$ obeys

the following properties :

$$\begin{aligned}
U(x, y) & \text{ is unitary ,} \\
U(x, x) & = \mathbf{1} , \\
U(x, y) U(y, x) & = \mathbf{1} , \\
U(x, y) U(y, z) & = U(x, z) .
\end{aligned} \tag{A.3}$$

Note that in the definition of the field in the interaction picture, we have decided to make $\phi(x)$ and $\phi_{\text{in}}(x)$ coincide at $x^0 = -\infty$. This choice is conventional, and by no means a necessity. A crucial advantage of $\phi_{\text{in}}(x)$ over $\phi(x)$ is that it behaves like a free field. This can be seen from the following relation :

$$\Box_x \phi(x) - \frac{\partial \mathcal{L}_{\text{int}}(\phi(x))}{\partial \phi(x)} = U(-\infty, x^0) \left[\Box_x \phi_{\text{in}}(x) \right] U(x^0, -\infty) . \tag{A.4}$$

In other words, if $\phi(x)$ obeys the equation of motion that includes the interactions of \mathcal{L}_{int} , then $\phi_{\text{in}}(x)$ obeys the free Klein-Gordon equation.

Let us now consider a matrix element $\langle 0_{\text{out}} | T \phi(x_1) \cdots \phi(x_n) | 0_{\text{in}} \rangle$. Let us first substitute every Heisenberg field by the corresponding field in the interaction picture, by using repeatedly eq. (A.1). This leads to

$$\begin{aligned}
\langle 0_{\text{out}} | T \phi(x_1) \cdots \phi(x_n) | 0_{\text{in}} \rangle & = \langle 0_{\text{out}} | U(-\infty, +\infty) T \phi_{\text{in}}(x_1) \cdots \phi_{\text{in}}(x_n) \\
& \times \exp i \int_{-\infty}^{+\infty} d^4x \mathcal{L}_{\text{int}}(\phi_{\text{in}}(x)) | 0_{\text{in}} \rangle ,
\end{aligned} \tag{A.5}$$

where we have used the properties of the evolution operators in order to rearrange them¹. The next step is to notice that $U(-\infty, +\infty)$ is precisely the evolution operator that transforms the in- vacuum into the out- vacuum, so that we have

$$\langle 0_{\text{out}} | U(-\infty, +\infty) = \langle 0_{\text{in}} | . \tag{A.6}$$

Therefore, the matrix element of interest can be rewritten as

$$\begin{aligned}
\langle 0_{\text{out}} | T \phi(x_1) \cdots \phi(x_n) | 0_{\text{in}} \rangle & = \langle 0_{\text{in}} | T \phi_{\text{in}}(x_1) \cdots \phi_{\text{in}}(x_n) \\
& \times \exp i \int_{-\infty}^{+\infty} d^4x \mathcal{L}_{\text{int}}(\phi_{\text{in}}(x)) | 0_{\text{in}} \rangle .
\end{aligned} \tag{A.7}$$

Now, everything in the right hand side is expressed in terms of the in- fields, which are free fields, and of the in- vacuum state. Moreover, all the interaction terms have been collected in the exponential that appears in the second line. Therefore, the perturbative expansion is obtained as a Taylor expansion of this exponential.

It is customary to collect the values of these correlators into a unique generating functional,

$$Z[\eta] \equiv \langle 0_{\text{out}} | T \exp i \int_{-\infty}^{+\infty} d^4x \eta(x) \phi(x) | 0_{\text{in}} \rangle , \tag{A.8}$$

¹We have used the fact that the ordering of the operators inside a T-product is irrelevant: $T A(x) B(y) = T B(y) A(x)$.

such that

$$\langle 0_{\text{out}} | T \phi(x_1) \cdots \phi(x_n) | 0_{\text{in}} \rangle = \frac{\delta}{i\delta\eta(x_1)} \cdots \frac{\delta}{i\delta\eta(x_n)} Z[\eta] \Big|_{\eta=0} . \quad (\text{A.9})$$

From eq. (A.7), this generating functional can be rewritten as

$$\begin{aligned} Z[\eta] &= \langle 0_{\text{in}} | T \exp i \int_{-\infty}^{+\infty} d^4x [\mathcal{L}_{\text{int}}(\phi_{\text{in}}(x)) + \eta(x)\phi_{\text{in}}(x)] | 0_{\text{in}} \rangle \\ &= \exp i \int_{-\infty}^{+\infty} d^4x \mathcal{L}_{\text{int}} \left(\frac{\delta}{i\delta\eta(x)} \right) \underbrace{\langle 0_{\text{in}} | T \exp i \int_{-\infty}^{+\infty} d^4x \eta(x)\phi_{\text{in}}(x) | 0_{\text{in}} \rangle}_{Z_0[\eta]} . \end{aligned} \quad (\text{A.10})$$

In the second line, the interactions have been completely factorized: evaluating their effect at a given order merely amounts to taking enough functional derivatives of the free generating functional $Z_0[\eta]$. The evaluation of $Z_0[\eta]$ is a standard calculation in free field theory, that we shall not repeat here. The result is a Gaussian functional of the current $\eta(x)$:

$$Z_0[\eta] = \exp -\frac{1}{2} \int_{-\infty}^{+\infty} d^4x d^4y \eta(x) G_{\text{f}}^0(x, y) \eta(y) , \quad (\text{A.11})$$

where $G_{\text{f}}^0(x, y)$ is the free Feynman propagator,

$$G_{\text{f}}^0(x, y) \equiv \langle 0_{\text{in}} | T \phi_{\text{in}}(x) \phi_{\text{in}}(y) | 0_{\text{in}} \rangle = i \int \frac{d^4p}{(2\pi)^4} \frac{e^{-ip \cdot (x-y)}}{p^2 + i\epsilon} . \quad (\text{A.12})$$

From the above results, it is clear that the perturbative expansion for correlators such as eq. (A.5) is obtained as a diagrammatic expansion, where the links between the vertices are Feynman propagators.

Let us close this section by mentioning the *vacuum-vacuum diagrams*. These are diagrams without any external legs, that appear quite naturally in the expansion of eq. (A.10) as disconnected factors. Their sum is nothing but the vacuum to vacuum transition amplitude

$$Z[0] = \langle 0_{\text{out}} | 0_{\text{in}} \rangle , \quad (\text{A.13})$$

hence their name. The vacuum-vacuum diagrams are not zero. However, in a stable theory, their sum is a pure phase that appears in front of every transition amplitude. Thanks to this property, the vacuum-vacuum diagrams have no effect on transition probabilities, and it is therefore common to simply disregard them.

A.2 Schwinger-Keldysh perturbation theory

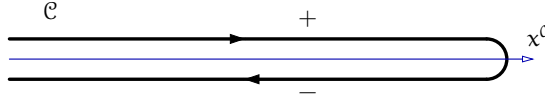
Consider now correlators of the type $\langle 0_{\text{in}} | \bar{T} \phi(x_1) \cdots \phi(x_n) T \phi(y_1) \cdots \phi(y_p) | 0_{\text{in}} \rangle$. One must again replace each Heisenberg field operator by its counterpart in the interaction repre-

sensation, using eq. (A.1). After some rearrangement of the evolution operators, we get :

$$\begin{aligned}
\langle 0_{\text{in}} | \bar{T} \phi(x_1) \cdots \phi(x_n) T \phi(y_1) \cdots \phi(y_p) | 0_{\text{in}} \rangle &= \\
&= \langle 0_{\text{in}} | \bar{T} \left[\phi_{\text{in}}(x_1) \cdots \phi_{\text{in}}(x_n) \exp i \int_{-\infty}^{+\infty} d^4x \mathcal{L}_{\text{int}}(\phi_{\text{in}}(x)) \right] \\
&\quad \times T \left[\phi_{\text{in}}(y_1) \cdots \phi_{\text{in}}(y_p) \exp i \int_{-\infty}^{+\infty} d^4x \mathcal{L}_{\text{int}}(\phi_{\text{in}}(x)) \right] | 0_{\text{in}} \rangle .
\end{aligned} \tag{A.14}$$

Here, we have exploited the fact that the factor $U(-\infty, +\infty)$ that appears in these manipulations is the anti-time ordered exponential of the interaction term, in order to write this formula in a more symmetric way. To go further, it is useful to imagine that the time axis is in fact a contour \mathcal{C} made of two branches labelled $+$ and $-$ running parallel to the real axis, as illustrated in figure A.1. This contour is oriented, with the $+$ branch running in the direction of

Figure A.1: Time contour in the Schwinger-Keldysh formalism.



increasing time, followed by the $-$ branch running in the direction of decreasing time. Then, it is convenient to introduce a *path ordering*, denoted by P and defined as a standard ordering along the contour \mathcal{C} . In more detail, one has

$$P A(x) B(y) = \begin{cases} T A(x) B(y) & \text{if } x^0, y^0 \in \mathcal{C}_+ , \\ \bar{T} A(x) B(y) & \text{if } x^0, y^0 \in \mathcal{C}_- , \\ A(x) B(y) & \text{if } x^0 \in \mathcal{C}_- , y^0 \in \mathcal{C}_+ , \\ B(y) A(x) & \text{if } x^0 \in \mathcal{C}_+ , y^0 \in \mathcal{C}_- . \end{cases} \tag{A.15}$$

One can use this contour ordering to write the previous equations in a much more compact way. In particular, eq. (A.14) can be generalized into :

$$\begin{aligned}
\langle 0_{\text{in}} | P \phi^-(x_1) \cdots \phi^-(x_n) \phi^+(y_1) \cdots \phi^+(y_p) | 0_{\text{in}} \rangle &= \\
&= \langle 0_{\text{in}} | P \phi_{\text{in}}^-(x_1) \cdots \phi_{\text{in}}^-(x_n) \phi_{\text{in}}^+(y_1) \cdots \phi_{\text{in}}^+(y_p) \exp i \int_{\mathcal{C}} d^4x \mathcal{L}_{\text{int}}(\phi_{\text{in}}(x)) | 0_{\text{in}} \rangle .
\end{aligned} \tag{A.16}$$

The differences compared to eq. (A.14) are threefold :

- i. A single overall path ordering takes care automatically of both the time ordering and the anti-time ordering contained in the original formula,
- ii. For this trick to work, one must (temporarily) assume that the fields on the upper and lower branch of the contour \mathcal{C} are distinct: ϕ^+ and ϕ^- respectively,

- iii. The time integration in the exponential is now running over both branches of the contour \mathcal{C} .

The advantage of having introduced this more complicated time contour is that it leads to a formula which is formally identical to eq. (A.7), provided one replaces the time ordering by the path ordering and provided one extends the time integration from \mathbb{R} to \mathcal{C} . In particular, all the subsequent manipulations can be generalized straightforwardly. One can first define a generating functional,

$$Z^{\text{SK}}[\eta] \equiv \langle 0_{\text{in}} | T \exp i \int_{\mathcal{C}} d^4x \eta(x) \phi(x) | 0_{\text{in}} \rangle, \quad (\text{A.17})$$

that encodes all the correlators considered in this section, provided the external source η has distinct values η^+ and η^- on the two branches of the contour (the superscript SK is used to distinguish this generating functional from the standard one). As in the standard case, one can write this generating functional as:

$$Z^{\text{SK}}[\eta] = \exp i \int_{\mathcal{C}} d^4x \mathcal{L}_{\text{int}} \left(\frac{\delta}{i\delta\eta(x)} \right) \underbrace{\langle 0_{\text{in}} | T \exp i \int_{\mathcal{C}} d^4x \eta(x) \phi_{\text{in}}(x) | 0_{\text{in}} \rangle}_{Z_0^{\text{SK}}[\eta]}, \quad (\text{A.18})$$

with

$$\begin{aligned} Z_0^{\text{SK}}[\eta] &= \exp -\frac{1}{2} \int_{\mathcal{C}} d^4x d^4y \eta(x) G_{\mathcal{C}}^0(x, y) \eta(y) \\ G_{\mathcal{C}}^0(x, y) &\equiv \langle 0_{\text{in}} | P \phi_{\text{in}}(x) \phi_{\text{in}}(y) | 0_{\text{in}} \rangle. \end{aligned} \quad (\text{A.19})$$

The free propagator $G_{\mathcal{C}}^0$, defined on the contour \mathcal{C} , is a natural extension of the Feynman propagator (in particular, it coincides with the Feynman propagator if the two time arguments are on the $+$ branch of the contour). Besides the propagator, the other change to the perturbative expansion in the Schwinger-Keldysh formalism is that the time integration at the vertices of a diagram must run over the contour \mathcal{C} instead of the real axis.

It is common to break down the propagator into 4 components $G_{\pm\pm}^0(x, y)$, depending on whether the times x^0, y^0 are on the upper or lower branch of the contour. An explicit calculation of these free propagators leads to

$$\begin{aligned} G_{++}^0(x, y) &= i \int \frac{d^4p}{(2\pi)^4} \frac{e^{-ip \cdot (x-y)}}{p^2 + i\epsilon}, \\ G_{--}^0(x, y) &= -i \int \frac{d^4p}{(2\pi)^4} \frac{e^{-ip \cdot (x-y)}}{p^2 - i\epsilon}, \\ G_{+-}^0(x, y) &= \int \frac{d^4p}{(2\pi)^4} e^{-ip \cdot (x-y)} 2\pi\theta(-p^0) \delta(p^2), \\ G_{-+}^0(x, y) &= \int \frac{d^4p}{(2\pi)^4} e^{-ip \cdot (x-y)} 2\pi\theta(+p^0) \delta(p^2). \end{aligned} \quad (\text{A.20})$$

This formulation of the Schwinger-Keldysh formalism leads to the following diagrammatic rules :

- i. Draw all the diagrams that contribute to the correlator of interest at a given order (the power counting is identical to that of standard perturbation theory),
- ii. For each diagram, assign an index $+$ or $-$ to all the vertices in all the possible combinations; a $+$ vertex is given a coupling $-ig$ and a $-$ vertex has the coupling $+ig$,
- iii. Connect the vertices by the appropriate propagators $G_{\pm\pm}^0$,
- iv. Integrate the time at each vertex on the real axis (one should not integrate over \mathcal{C} here, since the fact that there are two branches has been explicitly taken into account by doubling the vertices); if working in momentum space, integrate over the four momentum running in each independent loop.

In the Schwinger-Keldysh formalism, the discussion of the vacuum-vacuum diagrams is even simpler than in conventional perturbation theory. Here, one has

$$Z^{\text{SK}}[0] = \langle 0_{\text{in}} | 0_{\text{in}} \rangle = 1, \quad (\text{A.21})$$

which means that all the connected vacuum-vacuum diagrams are zero. This is due to the fact that in this formalism one is calculating correlators that have the in- vacuum on both sides. This cancellation works individually for each diagram topology, and results from a cancellation between the various ways of assigning the $+$ and $-$ indices to the vertices of a diagram (a vacuum-vacuum diagram with a fixed assignment of $+$ and $-$ vertices is not zero in general).

A.3 Relation between the functionals $Z[\eta]$ and $Z^{\text{SK}}[\eta]$

There is a useful functional relation between the generating functionals of conventional perturbation theory, and that of the Schwinger-Keldysh formalism. Let us first state this relation, and we will then prove it in the rest of the section :

$$Z^{\text{SK}}[\eta_+, \eta_-] = \exp \left[\int d^4x d^4y G_{+-}^0(x, y) \square_x \square_y \frac{\delta^2}{\delta \eta_+(x) \delta \eta_-(y)} \right] Z[\eta_+] Z^*[\eta_-]. \quad (\text{A.22})$$

(Here, in order to avoid any confusion, we write explicitly the two components $+$ and $-$ of the source η in the Schwinger-Keldysh generating functional.) Thanks to this formula, one can construct diagrams in the Schwinger-Keldysh formalism by *stitching* an ordinary Feynman diagram and the complex conjugate of another Feynman diagram.

In order to prove this relation, first notice that it is sufficient to establish it for a free theory, since the interactions are always trivially factorizable (see eqs. (A.10) and (A.18)). Therefore, we need to compute the functional

$$\begin{aligned} W[\eta_+, \eta_-] &\equiv \exp \left(\int d^4x d^4y G_{+-}^0(x, y) \square_x \square_y \frac{\delta^2}{\delta \eta_+(x) \delta \eta_-(y)} \right) \\ &\times \exp \left(-\frac{1}{2} \int d^4x d^4y \eta_+(x) G_{++}^0(x, y) \eta_+(y) \right) \\ &\times \exp \left(-\frac{1}{2} \int d^4x d^4y \eta_-(x) G_{--}^0(x, y) \eta_-(y) \right). \end{aligned} \quad (\text{A.23})$$

Our goal is to show that this functional is equal to $Z_0^{\text{sk}}[\eta_+, \eta_-]$. In this formula, we have used the fact that the Feynman propagator is the $++$ component of the Schwinger-Keldysh propagator, and that its complex conjugate is the $--$ component. In order to simplify the notations, let us rewrite this formula in the following compact way

$$W[\eta_+, \eta_-] = e^{\frac{\delta}{\delta\eta_+} \otimes A_{+-} \otimes \frac{\delta}{\delta\eta_-}} e^{-\frac{1}{2}(\eta_+ \otimes G_{++}^0 \otimes \eta_+ + \eta_- \otimes G_{--}^0 \otimes \eta_-)} , \quad (\text{A.24})$$

where all the convolutions over space-time have been replaced by the symbol \otimes , and where we denote $A_{+-}(x, y) \equiv \overleftarrow{\square}_x G_{+-}^0(x, y) \overrightarrow{\square}_y$ (the arrows are important because the \square_x should not act on the x -dependence of G_{+-}^0). In order to compute this functional, it is convenient to write the last two Gaussian factors as Fourier integrals :

$$\begin{aligned} W[\eta_+, \eta_-] &= e^{\frac{\delta}{\delta\eta_+} \otimes A_{+-} \otimes \frac{\delta}{\delta\eta_-}} \int [D\pi_+ D\pi_-] e^{i(\pi_+ \otimes \eta_+ + \pi_- \otimes \eta_-)} \\ &\quad \times e^{-\frac{1}{2}(\pi_+ \otimes G_{++}^{0,-1} \otimes \pi_+ + \pi_- \otimes G_{--}^{0,-1} \otimes \pi_-)} \\ &= \int [D\pi_+ D\pi_-] e^{i\pi_+ \otimes [\eta_+ + A_{+-} \otimes \frac{\delta}{\delta\eta_-}]} e^{i\pi_- \otimes \eta_-} \\ &\quad \times e^{-\frac{1}{2}(\pi_+ \otimes G_{++}^{0,-1} \otimes \pi_+ + \pi_- \otimes G_{--}^{0,-1} \otimes \pi_-)} \\ &= \int [D\pi_+ D\pi_-] e^{i(\pi_+ \otimes \eta_+ + \pi_- \otimes \eta_-)} \\ &\quad \times e^{-\frac{1}{2}(\pi_+ \otimes G_{++}^{0,-1} \otimes \pi_+ + \pi_- \otimes G_{--}^{0,-1} \otimes \pi_- - 2\eta_+ \otimes A_{+-} \otimes \eta_-)} . \end{aligned} \quad (\text{A.25})$$

In order to obtain the second and third equalities, we have exploited the fact that the exponential of a derivative is a translation operator. At this point, we simply need to perform the Fourier transform in reverse, which is straightforward because it is a Gaussian integral. The result reads

$$W[\eta_+, \eta_-] = e^{-\frac{1}{2}(\eta_+ \otimes G_{++}^0 \otimes \eta_+ + \eta_- \otimes G_{--}^0 \otimes \eta_- - \eta_+ \otimes G_{+-}^0 \otimes \eta_- - \eta_- \otimes G_{-+}^0 \otimes \eta_+)} , \quad (\text{A.26})$$

which is nothing but eq. (A.18), where the argument of the exponential has been broken down into all the possible combinations of $+$ and $-$ indices. This ends the proof of eq. (A.22).

A.4 Propagators in a background field

A recurrent problem encountered in this manuscript is to compute the Schwinger-Keldysh propagators in the presence of a background field φ . In section 2.6.2, this problem is solved by writing the equations of motion obeyed by the various propagators, as well as their boundary conditions, and by exhibiting an expression that fulfills both. In this appendix, we present an alternate derivation of this result, that does not require to guess what the solution is. The method proposed here simply amounts to performing explicitly the resummation of the background field insertions. As one will see, this approach is arguably more tedious, but is in a sense much more elementary.

The equation that performs this resummation is

$$\mathcal{G}_{\epsilon\epsilon'}(x, y) = G_{\epsilon\epsilon'}^0(x, y) - i \sum_{\eta=\pm} \eta \int d^4z G_{\epsilon\eta}^0(x, z) \mathcal{U}''(\varphi(z)) \mathcal{G}_{\eta\epsilon'}(z, y) . \quad (\text{A.27})$$

In this form, the equation is fairly complicated to solve because the four components of the Schwinger-Keldysh propagator get mixed already after the first insertion of the background field. However, there is a simple way to simplify these equations. It is based on the observation that the four propagators are not independent, but satisfy a linear relation,

$$\begin{aligned} G_{++}^0 + G_{--}^0 &= G_{+-}^0 + G_{-+}^0, \\ \mathcal{G}_{++} + \mathcal{G}_{--} &= \mathcal{G}_{+-} + \mathcal{G}_{-+}, \end{aligned} \quad (\text{A.28})$$

which follows immediately from their definition as path-ordered products of two fields, and from the identity $\theta(x) + \theta(-x) = 1$. It is possible to exploit this relation as follows: perform a rotation on the matrix made of the four propagators so that one component of the rotated matrix becomes zero². Having a zero in the matrix of propagators make the resummation of the background field considerably simpler. Therefore, let us define

$$\mathbb{G}_{\alpha\beta} \equiv \sum_{\epsilon, \epsilon' = \pm} \Omega_{\alpha\epsilon} \Omega_{\beta\epsilon'} \mathcal{G}_{\epsilon\epsilon'}. \quad (\text{A.29})$$

(The same rotation is applied to the free propagators.) There is not a unique choice of the matrix $\Omega_{\alpha\epsilon}$ that gives a zero component in $\mathbb{G}_{\alpha\beta}$, but the following choice is convenient:

$$\Omega_{\alpha\epsilon} \equiv \frac{1}{\sqrt{2}} \begin{pmatrix} 1 & -1 \\ 1 & 1 \end{pmatrix}. \quad (\text{A.30})$$

The rotated propagators read

$$\mathbb{G}_{\alpha\beta}^0 = \begin{pmatrix} 0 & G_{\Lambda}^0 \\ G_{\text{R}}^0 & G_{\text{S}}^0 \end{pmatrix}, \quad \mathbb{G}_{\alpha\beta} = \begin{pmatrix} 0 & \mathcal{G}_{\Lambda} \\ \mathcal{G}_{\text{R}} & \mathcal{G}_{\text{S}} \end{pmatrix}, \quad (\text{A.31})$$

where we have introduced

$$\begin{aligned} G_{\text{R}}^0 &= G_{++}^0 - G_{+-}^0, & \mathcal{G}_{\text{R}} &= \mathcal{G}_{++} - \mathcal{G}_{+-}^0, \\ G_{\Lambda}^0 &= G_{++}^0 - G_{-+}^0, & \mathcal{G}_{\Lambda} &= \mathcal{G}_{++} - \mathcal{G}_{-+}^0, \\ G_{\text{S}}^0 &= G_{++}^0 + G_{--}^0, & \mathcal{G}_{\text{S}} &= \mathcal{G}_{++} + \mathcal{G}_{--}^0. \end{aligned} \quad (\text{A.32})$$

(The subscripts R, A and S stand respectively for *retarded*, *advanced* and *symmetric*.) After having performed this rotation, eq. (A.27) is transformed into

$$\mathbb{G}_{\alpha\beta}(x, y) = \mathbb{G}_{\alpha\beta}^0(x, y) - i \sum_{\delta, \gamma} \int d^4 z \mathbb{G}_{\alpha\delta}^0(x, z) \mathcal{U}''(\varphi(z)) \sigma_{\delta\gamma} \mathbb{G}_{\gamma\beta}(z, y), \quad (\text{A.33})$$

where we denote

$$\sigma \equiv \begin{pmatrix} 0 & 1 \\ 1 & 0 \end{pmatrix}. \quad (\text{A.34})$$

In order to make the notations more compact, let us introduce the following shorthand,

$$[\mathbb{A} \circ \mathbb{B}]_{\alpha\beta}(x, y) \equiv -i \sum_{\delta, \gamma} \int d^4 z \mathbb{A}_{\alpha\delta}(x, z) \mathcal{U}''(\varphi(z)) \sigma_{\delta\gamma} \mathbb{B}_{\gamma\beta}(z, y). \quad (\text{A.35})$$

²This trick was invented in the context of Quantum Field Theory at finite temperature [210–213].

With this notation, eq. (A.33) takes a very compact form,

$$\mathbb{G} = \mathbb{G}^0 + \mathbb{G}^0 \circ \mathbb{G} , \quad (\text{A.36})$$

and its solution is

$$\mathbb{G} = \sum_{n=0}^{\infty} \left[\mathbb{G}^0 \right]^{\circ n} , \quad \text{with } A^{\circ n} \equiv \underbrace{A \circ \dots \circ A}_{n \text{ times}} . \quad (\text{A.37})$$

What makes the calculation of this infinite sum easy after the rotation we have performed is the fact that the elementary object $\mathbb{G}^0 \sigma$ is the sum of a diagonal and a nilpotent matrix:

$$\mathbb{G}^0 \sigma = \mathbb{D} + \mathbb{N} , \quad \mathbb{D} \equiv \begin{pmatrix} G_A^0 & 0 \\ 0 & G_R^0 \end{pmatrix} , \quad \mathbb{N} \equiv \begin{pmatrix} 0 & 0 \\ G_S^0 & 0 \end{pmatrix} . \quad (\text{A.38})$$

One has $\mathbb{N}^2 = 0$, which simplifies a lot the calculation of the n -th power of $\mathbb{G}^0 \sigma$. From this observation, it is easy to obtain

$$\left[\mathbb{G}^0 \right]^{\circ(n+1)} = \begin{pmatrix} 0 & \left[G_A^0 \right]^{\star(n+1)} \\ \left[G_R^0 \right]^{\star(n+1)} & \sum_{i=0}^n \left[G_R^0 \right]^{\star i} \star G_S^0 \star \left[G_A^0 \right]^{\star(n-i)} \end{pmatrix} , \quad (\text{A.39})$$

with the notation

$$[A \star B](x, y) \equiv -i \int d^4 z A(x, z) U''(\varphi(z)) B(z, y) , \quad (\text{A.40})$$

(and an obvious definition for the \star -exponentiation.) By looking at the off-diagonal components of eq. (A.39), one sees that their resummation is trivial because they do not mix. Moreover, the resummed \mathcal{G}_S propagator has a simple expression in terms of the resummed retarded and advanced propagators. These results can be summarized by

$$\begin{aligned} \mathcal{G}_R &= \sum_{n=0}^{\infty} \left[G_R^0 \right]^{\star n} , \\ \mathcal{G}_A &= \sum_{n=0}^{\infty} \left[G_A^0 \right]^{\star n} , \\ \mathcal{G}_S &= \mathcal{G}_R (G_R^0)^{-1} G_S^0 (G_A^0)^{-1} \mathcal{G}_A . \end{aligned} \quad (\text{A.41})$$

At this stage, we know all the components of the resummed propagator in the rotated basis. In order to obtain them in the original basis, we just have to invert the rotation of eq. (A.29). We obtain:

$$\begin{aligned} \mathcal{G}_{-+} &= \mathcal{G}_R (G_R^0)^{-1} G_{-+}^0 (G_A^0)^{-1} \mathcal{G}_A , \\ \mathcal{G}_{+-} &= \mathcal{G}_R (G_R^0)^{-1} G_{+-}^0 (G_A^0)^{-1} \mathcal{G}_A , \\ \mathcal{G}_{++} &= \frac{1}{2} \left[\mathcal{G}_R (G_R^0)^{-1} G_S^0 (G_A^0)^{-1} \mathcal{G}_A + \mathcal{G}_R + \mathcal{G}_A \right] , \\ \mathcal{G}_{--} &= \frac{1}{2} \left[\mathcal{G}_R (G_R^0)^{-1} G_S^0 (G_A^0)^{-1} \mathcal{G}_A - \mathcal{G}_R - \mathcal{G}_A \right] . \end{aligned} \quad (\text{A.42})$$

After some more massaging, it is easy to check that the first two of these equations are equivalent to eqs. (2.96), and that third and fourth equations are equivalent to eqs. (2.93).

Appendix B

Green's formulas



Because of causality, retarded solutions of partial differential equations are fully determined from the value of the unknown function and some of its derivatives on an initial surface chosen to set the initial conditions. It is often useful to have formulas that express, even formally, the solution as a functional of this initial data. This can be achieved by means of Green's formulas. In this appendix, we present the derivation of a Green's formula first in the simple case of the Klein-Gordon equation with some arbitrary interaction potential, and initial conditions set on a surface of constant time. This Green's formula is then generalized to an arbitrary initial Cauchy surface. Finally, we derive some useful Green's formulas that will help us in summing tree diagrams in the Schwinger-Keldysh formalism.

B.1 Green's formula for a retarded classical scalar field

Consider the following partial differential equation¹,

$$\square_x \phi(x) + U'(\phi(x)) = j(x) , \quad (\text{B.1})$$

where $U(\phi)$ is some interaction potential and $j(x)$ a source that drives the evolution of the function $\phi(x)$.

Since this equation contains time derivatives up to second order, it is necessary to specify the initial value of ϕ itself as well as that of its first time derivative. Let us assume that we know these values on the surface $t = 0$. We wish to obtain a formula for $\phi(x)$ at a time $x^0 > 0$ in terms of this initial data. In order to do this, we must introduce the retarded Green's function of the operator \square_x , defined by² :

$$\begin{aligned} \square_x G_r^0(x, y) &= -i\delta(x - y) , \\ G_r^0(x, y) &= 0 \quad \text{if } x^0 < y^0 . \end{aligned} \quad (\text{B.2})$$

¹This equation is the classical equation of motion in the scalar field theory of Lagrangian

$$\mathcal{L} \equiv \frac{1}{2}(\partial_\mu \phi)(\partial^\mu \phi) - U(\phi) + j\phi .$$

²The normalization of the first equation is consistent with our general convention for propagators, that have an i in the numerator. For instance, the free retarded propagator in Fourier space reads: $G_r^0(p) \equiv i/(p^2 + ip^0\epsilon)$.

(The superscript 0 is a reminder of the fact that this is a *free* Green's function, that does not depend on the interaction potential $U(\phi)$.) Note that $G_r^0(x, y)$ obeys the same equation if acted upon with $\overleftarrow{\square}_y$ instead.

Now, from the equations obeyed by ϕ and by G_r^0 , we can write the following equations,

$$\begin{aligned} G_r^0(x, y) \overrightarrow{\square}_y \phi(y) &= G_r^0(x, y) \left[j(y) - U'(\phi(y)) \right], \\ G_r^0(x, y) \overleftarrow{\square}_y \phi(y) &= -i\delta(x - y)\phi(y), \end{aligned} \quad (B.3)$$

where the arrows on the d'Alembertian operators indicate on which side they act. By integrating these equations over y above the initial surface $t = 0$, and by subtracting them, we get the following relation

$$\phi(x) = i \int_{y^0 > 0} d^4 y G_r^0(x, y) \left[(\overleftarrow{\square}_y - \overrightarrow{\square}_y) \phi(y) + j(y) - U'(\phi(y)) \right]. \quad (B.4)$$

The last step is to show that the term that involves the difference between the two d'Alembertian operators is in fact a boundary term that depends only on the initial conditions. Note first the following identity,

$$A(\overleftarrow{\square} - \overrightarrow{\square})B = \partial^\mu A(\overleftarrow{\partial}_\mu - \overrightarrow{\partial}_\mu)B, \quad (B.5)$$

where the leftmost ∂^μ acts on everything on its right. In other words, the left hand side is a total derivative, and its integral over $d^4 y$ can be rewritten as a surface integral thanks to Stokes' theorem. The integration domain defined by $y^0 > 0$ has three boundaries:

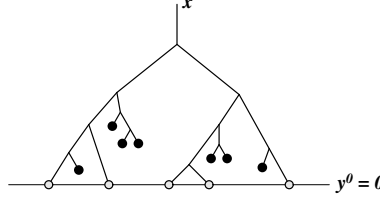
- i. $y^0 = +\infty$: this boundary at infinite time does not contribute, by virtue of the definition of the retarded Green's function G_r^0 . Indeed, $G_r^0(x, y) = 0$ if $y^0 > x^0$.
- ii. $y^0 = 0$: this boundary gives a non zero contribution, that depends only on the initial conditions for the field ϕ .
- iii. Boundary at spatial infinity : this boundary does not contribute if we assume that the field vanishes when $|x| \rightarrow \infty$, or if we adopt periodic boundary conditions in the spatial directions.

Therefore, we obtain

$$\begin{aligned} \phi(x) &= i \int_{y^0 > 0} d^4 y G_r^0(x, y) \left[j(y) - U'(\phi(y)) \right] \\ &\quad + i \int_{y^0 = 0} d^3 y G_r^0(x, y) (\overrightarrow{\partial}_{y^0} - \overleftarrow{\partial}_{y^0}) \phi(y). \end{aligned} \quad (B.6)$$

This is the Green's formula we were looking for. The second term in the right hand side tells us how $\phi(x)$ depends on the initial values of $\phi(x)$ and of its first time derivative. We see that it is not necessary to know anything else on the initial surface in order to uniquely determine the solution. The first term in the right hand side provides the dependence on the source j , and on the interactions.

Figure B.1: Typical contribution to $\phi(x)$ in the diagrammatic representation of eq. (B.6), in the case of cubic interactions. The solid dots represent the sources j , the open circles represent the initial value of the field or field derivatives on the surface $y^0 = 0$. The lines are retarded propagators G_R^0 .



Except in the trivial case where the potential $U(\phi)$ is zero, eq. (B.6) does not provide an explicit result for $\phi(x)$, since the right hand side depends on $\phi(y)$ at points above the initial surface. Despite this limitation, this is a very useful tool in order to perform formal manipulations involving retarded solutions of eq. (B.1). To end this section, let us mention a diagrammatic interpretation of eq. (B.6), illustrated in figure B.1. One can expand the right hand side of eq. (B.6) in powers of the interactions. The starting point is the zeroth order approximation, obtained by setting the potential to $U = 0$, and then by proceeding recursively in order to keep higher orders in U . The outcome of this expansion is an infinite series of terms that have a tree structure. The root of this tree is the point x where the field is evaluated, and its leaves are either sources j (if there are any above the surface $y^0 = 0$) or the initial data on the surface $y^0 = 0$. In particular, if the source $j(x)$ vanishes at $y^0 > 0$, then all the j dependence of the classical field is implicitly hidden in the $\phi(y)$ that appears in the boundary term.

B.2 Extension to a generic initial surface

In the previous section, the initial conditions for the field ϕ have been set on the surface of constant time $y^0 = 0$. However, there are many situations in which this initial data is known on a different initial surface³. Let us consider a generic surface Σ , on which the field ϕ and its derivatives are known. As before, we wish to obtain a formula that expresses $\phi(x)$ at some point x above Σ in terms of these initial conditions on Σ .

Most of the derivation is identical to the case of a constant time initial surface, with all the integrals over the domain $y^0 > 0$ replaced by integrals over the domain Ω located above Σ . The only significant change occurs when we apply Stokes' theorem in order to transform the 4-dimensional integral of a total derivative into an integral over the boundary of Ω . Like in the previous case, the boundaries at infinite time, and at infinity in the spatial directions do not contribute, and we have only a contribution from the surface Σ . Stokes' theorem can then be written as

$$\int_{\Omega} d^4 y \partial_{\mu} F^{\mu}(y) = - \int_{\Sigma} d^3 S_y n_{\mu} F^{\mu}(y) , \quad (B.7)$$

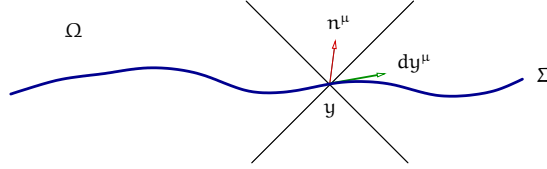
³Many applications of Green's formulas in this manuscript require that we take the light-cone as the initial surface.

where d^3S_y is the measure on the surface Σ , and n^μ is a 4-vector normal to the surface Σ at the point y , pointing above the surface Σ . In the important case where the initial surface is invariant by translation in the transverse directions, the proper normalization for n^μ and d^3S_y can be obtained as follows. Parameterize an arbitrary displacement dy^μ on the surface Σ about the point y as $dy^\mu = (\beta dy^3, dy^1, dy^2, dy^3)$, where β is the local slope of the surface Σ in the (y^3, y^0) plane. Then, we have:

$$\begin{aligned} n_\mu dy^\mu &= 0, \\ n_\mu n^\mu &= 1, \quad n^0 > 0, \\ d^3S_y &= \sqrt{1 - \beta^2} dy^1 dy^2 dy^3. \end{aligned} \tag{B.8}$$

The second and third conditions require to have $\beta < 1$ in order to make sense. This implies that the surface Σ must be locally space-like. Physically, this means that a signal emitted from a point of the surface Σ cannot reach the surface again in the future. The relations (B.8)

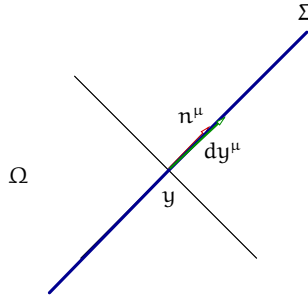
Figure B.2: Illustration of eqs. (B.8).



are illustrated in figure B.2. Note that the orthogonality defined by $n_\mu dy^\mu = 0$ does not correspond to the Euclidean concept of orthogonality.

The limiting case of a surface Σ parallel to the light-cone can be handled as the limit $\beta \rightarrow 1^-$ in the above equations. In this limit, the vectors n^μ and dy^μ are both parallel to the light-cone (and therefore tangential to the surface Σ in the Euclidean sense), as illustrated in figure B.3. Moreover, this limit is a bit pathological since the vector n^μ would need to

Figure B.3: Illustration of eqs. (B.8) in the limiting case of a surface Σ parallel to the light-cone.



have infinite components in order to fulfill $n_\mu n^\mu = 1$. This problem is easily circumvented, because the vanishing prefactor $\sqrt{1 - \beta^2}$ from the measure d^3S_y can be absorbed into the definition of the vector n^μ , which makes its components finite. For this particular case of

surface Σ , Stokes' theorem can be rewritten more simply in terms of light-cone coordinates as:

$$\int_{\Omega} d^4 y \partial_{\mu} F^{\mu}(y) = - \int_{\Sigma} dy^+ dy^1 dy^2 F^{-}(y) . \quad (\text{B.9})$$

Thanks to eq. (B.7), it is possible to write the Green's formula for an arbitrary initial surface Σ as

$$\begin{aligned} \phi(x) &= i \int_{\Omega} d^4 y G_{\text{r}}^0(x, y) \left[j(y) - U'(\phi(y)) \right] \\ &\quad + i \int_{\Sigma} d^3 \mathbf{S}_y G_{\text{r}}^0(x, y) (\mathbf{n} \cdot \vec{\partial}_y - \mathbf{n} \cdot \overleftarrow{\partial}_y) \phi(y) . \end{aligned} \quad (\text{B.10})$$

For an arbitrary surface Σ , the second term in the right hand side of this formula tells us explicitly what information about ϕ we must provide on the initial surface in order to determine it uniquely above the surface: at every point $y \in \Sigma$, one must specify the values of the field $\phi(y)$ and of its *normal derivative* $\mathbf{n} \cdot \partial_y \phi(y)$.

B.3 Green's formula for small field fluctuations

Consider now a small perturbation $a(x)$ to the classical field, and assume that $a(x) \ll \phi(x)$. Therefore, one can linearize the equation of motion of $a(x)$, and we get

$$\left[\square_x + U''(\phi(x)) \right] a(x) = 0 . \quad (\text{B.11})$$

Treating the term $U''(\phi(x))a(x)$ as an interaction, we can easily derive a Green's formula that expresses the field fluctuation $a(x)$ in terms of its initial conditions on a surface Σ ,

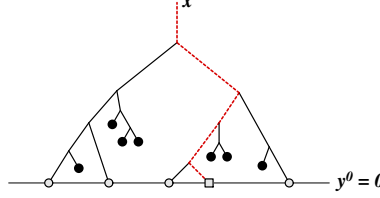
$$\begin{aligned} a(x) &= i \int_{\Omega} d^4 y G_{\text{r}}^0(x, y) \left[-U''(\phi(y))a(y) \right] \\ &\quad + i \int_{\Sigma} d^3 \mathbf{S}_y G_{\text{r}}^0(x, y) (\mathbf{n} \cdot \vec{\partial}_y - \mathbf{n} \cdot \overleftarrow{\partial}_y) a(y) . \end{aligned} \quad (\text{B.12})$$

Eq. (B.12) is illustrated in the figure B.4. Every diagram contributing to $a(x)$ has exactly one instance of the initial value of $a(y)$ (represented by an open square in the figure) on the initial surface. Indeed, it is easy to see from eq. (B.12) that $a(x)$ depends linearly on its value $a(y)$ on the initial surface. This is a consequence of the fact that equation of motion for a small fluctuation is a linear equation.

By comparing the figures B.1 and B.4, one sees that they differ only by the fact that one instance of the field $\phi(y)$ has been replaced by the small fluctuation $a(y)$ on the initial surface. Therefore, we expect a linear relationship between $a(x)$ and $\phi(x)$, of the form

$$a(x) = \mathcal{T} \phi(x) , \quad (\text{B.13})$$

Figure B.4: Typical contribution to $\alpha(x)$ in the diagrammatic representation of eq. (B.12), in the case of cubic interactions. The solid dots represent the sources j , the open circles represent the initial data for $\phi(y)$ on the surface $y^0 = 0$, and the open square the initial data for $\alpha(y)$. The lines are retarded propagators G_r^0 . The red dashed line is the retarded propagator of the fluctuation in the background ϕ , i.e. an inverse of the operator $\square + U''(\phi)$.



where \mathcal{T} is a linear operator that substitutes one power of $\phi(y)$ by $\alpha(y)$ on Σ (i.e. an operator that involves first derivatives with respect to the initial conditions on Σ). It is easy to prove this relation by using eqs. (B.10) and (B.12). In order to do so and at the same time determine what the operator \mathcal{T} is, let us apply \mathcal{T} to the Green's formula that gives $\phi(x)$. We get⁴

$$\begin{aligned} \mathcal{T}\phi(x) &= i \int_{\Omega} d^4y G_r^0(x, y) \left[-U''(\phi(y)) \mathcal{T}\phi(y) \right] \\ &\quad + i \mathcal{T} \int_{\Sigma} d^3\mathbf{S}_y G_r^0(x, y) (n \cdot \vec{\partial}_y - n \cdot \overleftarrow{\partial}_y) \phi(y). \end{aligned} \quad (\text{B.14})$$

If the boundary term in this formula can be made identical to the boundary term in the Green's formula for $\alpha(x)$, then we will have proven the announced relationship between $\alpha(x)$ and $\phi(x)$. This is the case if the operator \mathcal{T} is chosen as

$$\mathcal{T} \equiv \int_{\Sigma} d^3\mathbf{S}_y \underbrace{\left[\alpha(y) \frac{\delta}{\delta\phi(y)} + (n \cdot \partial\alpha(y)) \frac{\delta}{\delta(n \cdot \partial\phi(y))} \right]}_{\alpha \cdot \mathbb{T}_y}, \quad (\text{B.15})$$

which is nothing but the operator that substitutes $\alpha(y)$ to $\phi(y)$ on the initial surface Σ , as announced. We will use frequently the notation $\alpha \cdot \mathbb{T}_y$, in which \mathbb{T}_y is the generator of the translations of the initial field⁵ at the point $y \in \Sigma$. Thus, we will write:

$$\alpha(x) = \int_{\Sigma} d^3\mathbf{S}_y [\alpha \cdot \mathbb{T}_y] \phi(x). \quad (\text{B.16})$$

This formula is useful in situations where the classical field $\phi(x)$ is not known analytically (usually because the non-linear interactions prevent one from finding explicit solutions). Not

⁴Since \mathcal{T} acts only on the initial fields on Σ , we have $\mathcal{T}j = 0$.

⁵In particular, if we denote by $\phi[\phi_0]$ the classical field whose initial value on Σ is ϕ_0 , then we have

$$\exp \left\{ \int_{\Sigma} d^3\mathbf{S}_y [\alpha_0 \cdot \mathbb{T}_y] \right\} \phi[\phi_0] = \phi[\phi_0 + \alpha_0].$$

knowing $\phi(x)$ explicitly means that one cannot solve explicitly the equation of motion of the fluctuation $\alpha(x)$ either. However, many manipulations involving the fluctuations can be performed thanks to eq. (B.16), without knowing explicit solutions.

Let us also mention another useful representation of the small fluctuation $\alpha(x)$, in terms of the retarded propagator \mathcal{G}_r over the background ϕ . This dressed propagator is defined by

$$\begin{aligned} [\square_x + \mathcal{U}''(\phi(x))] \mathcal{G}_r(x, y) &= -i\delta(x - y) , \\ \mathcal{G}_r(x, y) &= 0 \quad \text{if } x^0 < y^0 . \end{aligned} \quad (\text{B.17})$$

In terms of this propagator, the Green's formula for $\alpha(x)$ is a pure boundary term,

$$\alpha(x) = i \int_{\Sigma} d^3 \mathbf{S}_y \mathcal{G}_r(x, y) (\mathbf{n} \cdot \vec{\partial}_y - \mathbf{n} \cdot \overleftarrow{\partial}_y) \alpha(y) . \quad (\text{B.18})$$

In other words, the interactions with the background field ϕ –that appear in the first term of eq. (B.12)– are now entirely resummed in the dressed propagator \mathcal{G}_r . Note also that this relation implies

$$i \int_{\Sigma} d^3 \mathbf{S}_y \mathcal{G}_r(x, y) (\mathbf{n} \cdot \vec{\partial}_y - \mathbf{n} \cdot \overleftarrow{\partial}_y) \alpha(y) = \int_{\Sigma} d^3 \mathbf{S}_y [\alpha \cdot \mathbb{T}_y] \phi(x) . \quad (\text{B.19})$$

In particular, this identity implies:

$$\begin{aligned} \mathcal{G}_r(x, y) &= -i \frac{\delta\phi(x)}{\delta(\mathbf{n} \cdot \partial\phi(y))} , \\ (\mathbf{n} \cdot \partial_y) \mathcal{G}_r(x, y) &= i \frac{\delta\phi(x)}{\delta\phi(y)} . \end{aligned} \quad (\text{B.20})$$

B.4 Schwinger-Keldysh formalism

In some problems related to heavy ion collisions at high energy, one needs to compute sums of tree diagrams in the Schwinger-Keldysh formalism. As we shall explain in the next section, these sums can be expressed in terms of solutions of the classical equations of motion with boundary conditions that depend on the details of the tree diagrams being summed. The determination of the boundary conditions is done by comparison with some appropriate Green's formulas.

In the case of the Schwinger-Keldysh formalism, one is considering a pair of fields $\phi_{\pm}(x)$, that are both solutions of the classical equation of motion

$$\square_x \phi_{\pm}(x) + \mathcal{U}'(\phi_{\pm}(x)) = j(x) . \quad (\text{B.21})$$

(For simplicity we take the same source $j(x)$ for the two fields, but this limitation is easily circumvented if necessary.) Since the Schwinger-Keldysh propagator G_{++}^0 is also a Green's function of the operator \square_x , we can reproduce the previous derivation of Green's formula, which leads to⁶

$$\begin{aligned} \phi_+(x) &= i \int d^4 y G_{++}^0(x, y) [j(y) - \mathcal{U}'(\phi_+(y))] \\ &\quad + i \int d^3 \mathbf{y} \left[G_{++}^0(x, y) (\overleftarrow{\partial}_{y^0} - \vec{\partial}_{y^0}) \phi_+(y) \right]_{y^0=-\infty}^{y^0=+\infty} , \end{aligned} \quad (\text{B.22})$$

⁶Here also, the prefactors i follow from our convention for the propagators of the Schwinger-Keldysh formalism (see eqs. (A.20)).

where we used the notation $[f(y^0)]_{y^0=a}^{y^0=b} \equiv f(b) - f(a)$. The only difference with the Green's formula derived with retarded propagators is the boundary term: since $G_{++}^0(x, y)$ does not vanish when $y^0 > x^0$, there is also a non-zero contribution from the boundary at $y^0 = +\infty$.

Then, by using the fact that $\square_y G_{+-}^0(x, y) = 0$, we obtain in a similar way :

$$\begin{aligned} 0 &= i \int d^4 y G_{+-}^0(x, y) [j(y) - U'(\phi_-(y))] \\ &\quad + i \int d^3 y \left[G_{+-}^0(x, y) (\overleftrightarrow{\partial}_{y^0} \phi_-(y)) \right]_{y^0=-\infty}^{y^0=+\infty}. \end{aligned} \quad (\text{B.23})$$

Subtracting this equation from eq. (B.22), we obtain

$$\begin{aligned} \phi_+(x) &= i \int d^4 y G_{++}^0(x, y) [j(y) - U'(\phi_+(y))] - G_{+-}^0(x, y) [j(y) - U'(\phi_-(y))] \\ &\quad - i \int d^3 y \left[G_{++}^0(x, y) \overleftrightarrow{\partial}_{y^0} \phi_+(y) - G_{+-}^0(x, y) \overleftrightarrow{\partial}_{y^0} \phi_-(y) \right]_{y^0=-\infty}^{y^0=+\infty}, \end{aligned} \quad (\text{B.24})$$

where $A \overleftrightarrow{\partial}_{y^0} B \equiv A(\overrightarrow{\partial}_{y^0} - \overleftarrow{\partial}_{y^0})B$. Similarly, we obtain for $\phi_-(x)$:

$$\begin{aligned} \phi_-(x) &= i \int d^4 y G_{-+}^0(x, y) [j(y) - U'(\phi_+(y))] - G_{--}^0(x, y) [j(y) - U'(\phi_-(y))] \\ &\quad - i \int d^3 y \left[G_{-+}^0(x, y) \overleftrightarrow{\partial}_{y^0} \phi_+(y) - G_{--}^0(x, y) \overleftrightarrow{\partial}_{y^0} \phi_-(y) \right]_{y^0=-\infty}^{y^0=+\infty}. \end{aligned} \quad (\text{B.25})$$

At this point, these formulas are rather formal, and it is not clear why we have gone through the trouble of subtracting the quantity given by eq. (B.23), since it is identically zero. This will become transparent in the next section, where we show that these formulas enable one to sum series of tree diagrams encountered in the Schwinger-Keldysh formalism.

Note also that the only property of the propagators G_{-+}^0 and G_{+-}^0 that we have used in this derivation is the fact that they are annihilated by the operator \square_y . Therefore, the equations (B.24) and (B.25) remain valid if we replace these propagators by any other pair of propagators sharing the same property. For instance, one can replace the propagators G_{+-}^0 and G_{-+}^0 of eqs. (A.20) by the following objects

$$\begin{aligned} \overline{G}_{+-}^0(x, y) &= \int \frac{d^4 p}{(2\pi)^4} e^{-ip \cdot (x-y)} u(\mathbf{p}) 2\pi\theta(-p^0)\delta(p^2), \\ \overline{G}_{-+}^0(x, y) &= \int \frac{d^4 p}{(2\pi)^4} e^{-ip \cdot (x-y)} v(\mathbf{p}) 2\pi\theta(+p^0)\delta(p^2), \end{aligned} \quad (\text{B.26})$$

where $u(\mathbf{p})$ and $v(\mathbf{p})$ are some arbitrary functions of the momentum \mathbf{p} , without altering any of the formulas in this section. We will make use of this freedom in the next section.

B.5 Summing tree diagrams using Green's formulas

In heavy ion collisions at high energy, observables at leading order involve sums of tree diagrams. These sums of diagrams can in general be expressed in terms of solutions of the classical equations of motion. However, in order to determine them uniquely, one must know the boundary conditions obeyed by these classical solutions. The strategy in order to obtain them is to write the sum of tree diagrams as a recursive integral equation. Then, by comparing this integral equation with a Green's formula such as eq. (B.6), one can read off the boundary conditions easily.

B.5.1 Sum of retarded trees

Let us illustrate this first in the simplest case, where one must sum all the tree diagrams built with retarded propagators, and whose *leaves* are a source $j(x)$. Let us call $\phi(x)$ the sum of all such tree diagrams. Given the recursive structure of such trees, one can write immediately :

$$\phi(x) = i \int d^4y G_{\text{r}}^0(x, y) [j(y) - U'(\phi(y))] , \quad (\text{B.27})$$

where the integration over d^4y is extended to the entire⁷ space-time. Therefore, we see that this formula is identical to a Green's formula like (B.6), where the initial surface would be at $y^0 = -\infty$ instead of $y^0 = 0$, and where the boundary term would be identically zero. This means that the sum of these tree diagrams is a retarded solution of the classical equation of motion with a null boundary condition in the remote past

$$\begin{aligned} \square_x \phi(x) + U'(\phi(x)) &= j(x) , \\ \lim_{y^0 \rightarrow -\infty} \phi(y^0, \mathbf{y}) &= 0 . \end{aligned} \quad (\text{B.28})$$

B.5.2 Sum of trees in the Schwinger-Keldysh formalism

Consider now a more complicated example, in which one must sum tree diagrams in the Schwinger-Keldysh formalism. Now, each vertex in a diagram is carrying an index $\epsilon = \pm$. For simplicity, we assume that the $+$ and $-$ sources are identical, so that we still have a single source $j(x)$. Because this is necessary in certain applications, we are going to use the modified propagators \bar{G}_{+-}^0 and \bar{G}_{-+}^0 defined in eqs. (B.26), instead of the propagators G_{+-}^0 and G_{-+}^0 defined in eqs. (A.20) (the propagators G_{++}^0 and G_{--}^0 are kept unchanged). In addition to summing over all the possible trees, we sum over all the combinations of \pm indices at every internal vertex. Again, it is easy to write the sum of these trees as two coupled integral equations (there are now two fields $\phi_{\pm}(x)$ depending on the index carried by the root of the tree) :

$$\begin{aligned} \phi_+(x) &= i \int d^4y G_{++}^0(x, y) [j(y) - U'(\phi_+(y))] \\ &\quad - i \int d^4y \bar{G}_{+-}^0(x, y) [j(y) - U'(\phi_-(y))] , \\ \phi_-(x) &= i \int d^4y \bar{G}_{-+}^0(x, y) [j(y) - U'(\phi_+(y))] \\ &\quad - i \int d^4y G_{--}^0(x, y) [j(y) - U'(\phi_-(y))] . \end{aligned} \quad (\text{B.29})$$

⁷This is because in the Feynman rules the integration at each vertex is extended to the full space-time \mathbb{R}^4 .

At this point, we recognize that the right hand side of these equations is identical to the first term in the right hand side of eqs. (B.24) and (B.25). From this observation, we conclude that $\phi_+(x)$ and $\phi_-(x)$ are solutions of the classical equation of motion,

$$\square_x \phi_{\pm}(x) + \mathcal{U}'(\phi_{\pm}(x)) = j(x) , \quad (\text{B.30})$$

and that they obey the following boundary conditions

$$\begin{aligned} \int d^3 \mathbf{y} \left[G_{++}^0(x, y) \overleftrightarrow{\partial}_{y^0} \phi_+(y) - \overline{G}_{+-}^0(x, y) \overleftrightarrow{\partial}_{y^0} \phi_-(y) \right]_{y^0=-\infty}^{y^0=+\infty} &= 0 , \\ \int d^3 \mathbf{y} \left[\overline{G}_{-+}^0(x, y) \overleftrightarrow{\partial}_{y^0} \phi_+(y) - G_{--}^0(x, y) \overleftrightarrow{\partial}_{y^0} \phi_-(y) \right]_{y^0=-\infty}^{y^0=+\infty} &= 0 . \end{aligned} \quad (\text{B.31})$$

As one can see, we have now coupled boundary conditions for the fields ϕ_+ and ϕ_- . More importantly, the boundary conditions involve the value of the fields both at $y^0 = -\infty$ and at $y^0 = +\infty$.

These boundary conditions are non-local in coordinate space, since they involve integrals over $d^3 \mathbf{y}$ on the surfaces $y^0 = \pm\infty$. However, they can be simplified considerably if one uses the following Fourier representations for the propagators

$$\begin{aligned} G_{++}^0(x, y) &= \int \frac{d^3 \mathbf{p}}{(2\pi)^3 2p} \left[\theta(x^0 - y^0) e^{-i\mathbf{p} \cdot (x-y)} + \theta(y^0 - x^0) e^{+i\mathbf{p} \cdot (x-y)} \right] , \\ G_{--}^0(x, y) &= \int \frac{d^3 \mathbf{p}}{(2\pi)^3 2p} \left[\theta(x^0 - y^0) e^{+i\mathbf{p} \cdot (x-y)} + \theta(y^0 - x^0) e^{-i\mathbf{p} \cdot (x-y)} \right] , \\ \overline{G}_{+-}^0(x, y) &= \int \frac{d^3 \mathbf{p}}{(2\pi)^3 2p} u(\mathbf{p}) e^{+i\mathbf{p} \cdot (x-y)} , \\ \overline{G}_{-+}^0(x, y) &= \int \frac{d^3 \mathbf{p}}{(2\pi)^3 2p} v(\mathbf{p}) e^{-i\mathbf{p} \cdot (x-y)} . \end{aligned} \quad (\text{B.32})$$

Compared to the expressions of these propagators in eqs. (A.20) and (B.26), we have performed explicitly the integration over p^0 in order to obtain these formulas. Thus, whenever p^0 appears in these expressions, it should be replaced by the positive on-shell value $p^0 = |\mathbf{p}|$. The other ingredient we need in order to simplify the boundary conditions is a Fourier representation for the fields $\phi_{\pm}(y)$,

$$\phi_{\epsilon}(y) \equiv \int \frac{d^3 \mathbf{p}}{(2\pi)^3 2p} \left[f_{\epsilon}^{(+)}(y^0, \mathbf{p}) e^{-i\mathbf{p} \cdot y} + f_{\epsilon}^{(-)}(y^0, \mathbf{p}) e^{+i\mathbf{p} \cdot y} \right] . \quad (\text{B.33})$$

The superscripts (\pm) on the Fourier coefficients serve to distinguish the positive and negative energy modes. Note that because the fields $\phi_{\pm}(y)$ are not free fields, these Fourier coefficients are time dependent. In practice, one may assume that the interactions are switched off at $y^0 = \pm\infty$, so that the coefficients $f_{\epsilon}^{(\pm)}(y^0, \mathbf{p})$ tend to constants when $y^0 \rightarrow \pm\infty$. However, these limiting values are different at $y^0 = +\infty$ and at $y^0 = -\infty$, and we must keep the y^0 argument to distinguish them. To proceed further, one needs the following result,

$$\int d^3 \mathbf{y} e^{i\epsilon \mathbf{p} \cdot (x-y)} \overleftrightarrow{\partial}_{y^0} e^{i\epsilon' \mathbf{p}' \cdot y} = i\delta_{\epsilon\epsilon'} e^{i\epsilon \mathbf{p} \cdot x} (2\pi)^3 2p \delta(\mathbf{p} - \mathbf{p}') , \quad (\text{B.34})$$

valid for $\epsilon, \epsilon' = \pm$. It is then straightforward to rewrite the boundary conditions as

$$\begin{aligned} \int \frac{d^3\mathbf{p}}{(2\pi)^3 2p} \left[e^{+ip \cdot x} \left(f_+^{(-)}(+\infty, \mathbf{p}) - u(\mathbf{p}) [f_-^{(-)}(+\infty, \mathbf{p}) - f_-^{(-)}(-\infty, \mathbf{p})] \right) \right. \\ \left. - e^{-ip \cdot x} f_+^{(+)}(-\infty, \mathbf{p}) \right] = 0, \\ \int \frac{d^3\mathbf{p}}{(2\pi)^3 2p} \left[e^{-ip \cdot x} \left(f_-^{(+)}(+\infty, \mathbf{p}) - v(\mathbf{p}) [f_+^{(+)}(+\infty, \mathbf{p}) - f_+^{(+)}(-\infty, \mathbf{p})] \right) \right. \\ \left. - e^{+ip \cdot x} f_-^{(-)}(-\infty, \mathbf{p}) \right] = 0. \end{aligned} \quad (\text{B.35})$$

These relations must be satisfied at any point x in \mathbb{R}^4 . Therefore, one can exploit the fact that the plane waves $\exp(\pm ip \cdot x)$ are linearly independent in order to get separate conditions for each mode \mathbf{p} :

$$\begin{aligned} f_+^{(+)}(-\infty, \mathbf{p}) &= f_-^{(-)}(-\infty, \mathbf{p}) = 0, \\ f_+^{(-)}(+\infty, \mathbf{p}) &= u(\mathbf{p}) f_-^{(-)}(+\infty, \mathbf{p}), \\ f_-^{(+)}(+\infty, \mathbf{p}) &= v(\mathbf{p}) f_+^{(+)}(+\infty, \mathbf{p}). \end{aligned} \quad (\text{B.36})$$

One sees that the boundary conditions have a very compact expression in terms of the Fourier coefficients of the fields ϕ_{\pm} . At $y^0 = -\infty$, $\phi_+(y)$ has no positive energy modes and $\phi_-(y)$ has no negative energy modes. At $y^0 = +\infty$, the negative energy modes of $\phi_+(y)$ and $\phi_-(y)$ are proportional (with a proportionality relation that involves the function $u(\mathbf{p})$). A similar relation, that involves the function $v(\mathbf{p})$, holds between their positive energy modes at $y^0 = +\infty$. Eqs. (B.36), together with the equations of motion (B.30), determine uniquely the fields $\phi_{\pm}(x)$ and therefore provide the solution to our original problem of summing tree diagrams in the Schwinger-Keldysh formalism. One should however keep in mind that this solution is somewhat formal, because it is extremely difficult to solve a non-linear field equation of motion⁸ with boundary conditions specified both at $y^0 = -\infty$ and $y^0 = +\infty$.

Let us also mention that these boundary conditions become considerably simpler in the case where $u(\mathbf{p}) = v(\mathbf{p}) \equiv 1$, i.e. when one is summing tree diagrams in the unmodified Schwinger-Keldysh formalism. Indeed, from the second and third of eqs. (B.36), we see that the fields $\phi_{\pm}(y)$ have identical Fourier coefficients at $y^0 = +\infty$. Therefore, the two fields must be equal in the limit $y^0 \rightarrow +\infty$. Then, by solving their equation of motion backwards in time, one sees trivially that they are equal at all times (since they obey identical equations of motion),

$$\text{if } u(\mathbf{p}) = v(\mathbf{p}) \equiv 1, \quad \phi_+(x) = \phi_-(x), \quad \forall x \in \mathbb{R}^4. \quad (\text{B.37})$$

Finally, the first of eqs. (B.36) tells us that

$$\text{if } u(\mathbf{p}) = v(\mathbf{p}) \equiv 1, \quad \lim_{x^0 \rightarrow -\infty} \phi_{\pm}(x) = 0. \quad (\text{B.38})$$

To summarize, when $u(\mathbf{p}) = v(\mathbf{p}) \equiv 1$, the two fields $\phi_{\pm}(x)$ are equal to the retarded field that vanishes when $x^0 \rightarrow -\infty$. This result could in fact have been obtained by a much more

⁸If one were dealing with an ordinary differential equation (i.e. with zero spatial dimensions), this problem can be solved by an iterative *point and shoot* technique. This method is difficult to generalize with guaranteed convergence in the case of field equations.

elementary argument. Indeed, in the unmodified Schwinger-Keldysh formalism, one sees easily that the summation over the \pm indices at the vertices of tree diagrams always leads to the following combinations of propagators,

$$G_{++}^0 - G_{+-}^0 = G_{-+}^0 - G_{--}^0 = G_{\text{r}}^0 . \quad (\text{B.39})$$

In other words, summing over these indices amounts to replacing all the propagators in a given tree by retarded propagators, and one is thus led to the problem discussed in section [B.5.1](#).

Appendix C

Small fluctuations in a background field



Calculating next-to-leading-order corrections in the Color Glass Condensate framework involves small field fluctuations propagating over a classical field. In this appendix, we derive some useful properties of these small fluctuations. In order to keep the notations simple, the derivation is illustrated for the case of scalar fields, but the generalization to gauge fields is immediate.

C.1 Basis of retarded small fluctuations

Fluctuations occur in the problems discussed in this manuscript as variations around some classical field configuration. It may happen that these fluctuations obey non retarded boundary conditions (see the section 2.6.4 for instance), which makes them rather complicated to handle. However, because the equation of motion of small fluctuations is linear, it is always possible to write them as a linear superposition of small fluctuations that obey retarded boundary conditions. Let us introduce $\alpha_k(x)$, defined by the equation of motion

$$\left[\square_x + U''(\phi(x)) \right] \alpha_k(x) = 0, \quad (\text{C.1})$$

and the retarded boundary condition

$$\lim_{x^0 \rightarrow -\infty} \alpha_k(x) = e^{-ik \cdot x}. \quad (\text{C.2})$$

We must also introduce their complex conjugate $\alpha_k^*(x)$, which obeys the same equation of motion (because the potential $U(\phi)$ is real), and the following retarded boundary condition,

$$\lim_{x^0 \rightarrow -\infty} \alpha_k^*(x) = e^{+ik \cdot x}. \quad (\text{C.3})$$

The $\alpha_k(x)$, combined to their complex conjugates $\alpha_k^*(x)$, form a basis of the space of small field fluctuations. Therefore, any solution of the equation of motion for small fluctuations can be written as

$$\alpha(x) = \int \frac{d^3k}{(2\pi)^3 2k} \left[\alpha_+^k \alpha_k(x) + \alpha_-^k \alpha_k^*(x) \right], \quad (\text{C.4})$$

where the α_{\pm}^k are constant coefficients that must be determined from the boundary conditions (the boundary conditions in general lead to a set of linear equations for the coefficients).

C.2 Completeness relations

The set of small fluctuations $\{\alpha_k(x), \alpha_k^*(x)\}$ obey some useful relations, that are a consequence of unitarity. Consider first two generic solutions $\alpha_1(x)$ and $\alpha_2(x)$ of the equation of small fluctuations. In order to make the notations more compact in the rest of this appendix, it is useful to introduce the following notations

$$|\alpha\rangle \equiv \begin{pmatrix} \alpha(x) \\ \dot{\alpha}(x) \end{pmatrix} \quad , \quad \langle \alpha| \equiv (\alpha^*(x) \quad \dot{\alpha}^*(x)) \sigma_2 \quad , \quad (\text{C.5})$$

where the dot denotes a time derivative and σ_2 is the second Pauli matrix. Thanks to the fact that the background potential $U''(\phi(x))$ is real, one can construct from α_1 and α_2 an inner product which is an invariant of the time evolution of the two fluctuations. This quantity is reminiscent of the Wronskian for two solutions of a second order ordinary differential equations, and it is defined as follows

$$(\alpha_1 | \alpha_2) \equiv i \int d^3x \left[\dot{\alpha}_1^*(x) \alpha_2(x) - \alpha_1^*(x) \dot{\alpha}_2(x) \right] \quad , \quad (\text{C.6})$$

where σ_2 is the second Pauli matrix. Although $(\alpha_1 | \alpha_2)$ could possibly depend on time (since one integrates only over space in its definition), it is immediate to verify that

$$\frac{\partial}{\partial x^0} (\alpha_1 | \alpha_2) = 0 \quad . \quad (\text{C.7})$$

Since it is a constant in time, one can compute this inner product from the value of the field fluctuations in the remote past. This is particularly handy when the fluctuations under consideration are specified by retarded boundary conditions, as is the case for $\alpha_k(x)$ and $\alpha_k^*(x)$. One finds

$$\begin{aligned} (\alpha_k | \alpha_l) &= (2\pi)^3 2k \delta(k-l) \quad , \\ (\alpha_k^* | \alpha_l^*) &= -(2\pi)^3 2k \delta(k-l) \quad , \\ (\alpha_k^* | \alpha_l) &= (\alpha_k | \alpha_l^*) = 0 \quad . \end{aligned} \quad (\text{C.8})$$

Consider now a generic solution $\alpha(x)$ of eq. (C.1). Since the α_k and α_k^* provide a basis of the linear space of solutions, one can write $\alpha(x)$ as a linear superposition of α_k and α_k^* ,

$$|\alpha\rangle = \int \frac{d^3k}{(2\pi)^3 2k} \left[\alpha_+^k |\alpha_k\rangle + \alpha_-^k |\alpha_k^*\rangle \right] \quad , \quad (\text{C.9})$$

where the coefficients α_{\pm}^k do not depend on time or space. By using the orthogonality relations obeyed by the vectors $|\alpha_k\rangle$ and $|\alpha_k^*\rangle$, one gets easily

$$\alpha_+^k = (\alpha_k | \alpha) \quad , \quad \alpha_-^k = -(\alpha_k^* | \alpha) \quad . \quad (\text{C.10})$$

By inserting these relations back into eq. (C.9), and by using the fact that it is valid for any small fluctuation $\alpha(x)$ solution of eq. (C.1), we obtain the following identity

$$\int \frac{d^3k}{(2\pi)^3 2k} \left[|\alpha_k\rangle (\alpha_k | - |\alpha_k^*\rangle (\alpha_k^* | \right] = 1 \quad . \quad (\text{C.11})$$

This identity is valid at all times over the space of solutions of eq. (C.1). It is a manifestation of the fact that, when the background field is real, the time evolution preserves the completeness of the set of states $|\mathbf{a}_k\rangle, |\mathbf{a}_k^*\rangle$.

Eq. (C.11) can also be written in a more explicit form in terms of the Fourier coefficients of the field fluctuations $\mathbf{a}_k, \mathbf{a}_k^*$. Let us decompose these fluctuations as

$$\begin{aligned}\mathbf{a}_k(x) &= \int \frac{d^3\mathbf{p}}{(2\pi)^3 2p} \left[\mathbf{a}_k^{(+)}(x^0, \mathbf{p}) e^{-ip \cdot x} + \mathbf{a}_k^{(-)}(x^0, \mathbf{p}) e^{+ip \cdot x} \right], \\ \mathbf{a}_k^*(x) &= \int \frac{d^3\mathbf{p}}{(2\pi)^3 2p} \left[\mathbf{a}_k^{*(+)}(x^0, \mathbf{p}) e^{-ip \cdot x} + \mathbf{a}_k^{*(-)}(x^0, \mathbf{p}) e^{+ip \cdot x} \right].\end{aligned}\quad (\text{C.12})$$

(Note that we obviously have $\mathbf{a}_k^{(\pm)}(x^0, \mathbf{p}) = [\mathbf{a}_k^{(\mp)}(x^0, \mathbf{p})]^*$.) The Fourier coefficients at $x^0 = +\infty$ can be obtained as *scalar products* between the states $|\mathbf{a}_k\rangle, |\mathbf{a}_k^*\rangle$ and free states,

$$\begin{aligned}\mathbf{a}_k^{(+)}(+\infty, \mathbf{p}) &= -(\mathbf{a}_{0k}^* | \mathbf{a}_k) \quad , \quad \mathbf{a}_k^{(-)}(+\infty, \mathbf{p}) = (\mathbf{a}_{0k} | \mathbf{a}_k) \quad , \\ \mathbf{a}_k^{*(+)}(+\infty, \mathbf{p}) &= -(\mathbf{a}_{0k}^* | \mathbf{a}_k^*) \quad , \quad \mathbf{a}_k^{*(-)}(+\infty, \mathbf{p}) = (\mathbf{a}_{0k} | \mathbf{a}_k^*) \quad ,\end{aligned}\quad (\text{C.13})$$

where \mathbf{a}_{0k} and \mathbf{a}_{0k}^* are defined in a similar way to \mathbf{a}_k and \mathbf{a}_k^* , except that they obey the in-vacuum equation of motion (i.e. with $U''(\phi) = 0$). In the previous formulas, all the scalar products must be evaluated at $x^0 = +\infty$. By multiplying eq. (C.11) by $(\mathbf{a}_{0p} |$ or $(\mathbf{a}_{0p}^* |$ on the left and by $| \mathbf{a}_{0q})$ or $| \mathbf{a}_{0q}^*)$ on the right, we obtain the following relations among the Fourier coefficients at $x^0 = +\infty$ of the fluctuations $\mathbf{a}_k, \mathbf{a}_k^*$,

$$\begin{aligned}\int \frac{d^3\mathbf{k}}{(2\pi)^3 2k} \left[\mathbf{a}_k^{*(+\epsilon)}(+\infty, \mathbf{p}) \mathbf{a}_k^{(-\epsilon')}(+\infty, \mathbf{q}) - \mathbf{a}_k^{(+\epsilon)}(+\infty, \mathbf{p}) \mathbf{a}_k^{*(-\epsilon')}(+\infty, \mathbf{q}) \right] \\ = \epsilon \delta_{\epsilon\epsilon'} (2\pi)^3 2p \delta(\mathbf{p} - \mathbf{q}) \quad .\end{aligned}\quad (\text{C.14})$$

A similar relation holds for the Fourier coefficients at $x^0 = -\infty$, but there it is somewhat trivial because the fluctuations $\mathbf{a}_k, \mathbf{a}_k^*$ are simple plane waves. The interest of this relation is that it remains true after the time evolution of the fluctuations over a non trivial background.

C.3 $\mathcal{G}_{+-}(x, y) = \mathcal{G}_{-+}(x, y)$ for $(x - y)^2 < 0$

In the section 2.6, we need to evaluate the propagators \mathcal{G}_{+-} and \mathcal{G}_{-+} of the Schwinger-Keldysh formalism in the presence of a background field. These propagators were conveniently expressed in terms of the fluctuations \mathbf{a}_k and \mathbf{a}_k^* , via the relations:

$$\begin{aligned}\mathcal{G}_{+-}(x, y) &= \int \frac{d^3\mathbf{k}}{(2\pi)^3 2k} \mathbf{a}_k^*(x) \mathbf{a}_k(y) \quad , \\ \mathcal{G}_{-+}(x, y) &= \int \frac{d^3\mathbf{k}}{(2\pi)^2 2k} \mathbf{a}_k(x) \mathbf{a}_k^*(y) \quad .\end{aligned}\quad (\text{C.15})$$

From their definition as expectation values of field operators,

$$\mathcal{G}_{+-}(x, y) \equiv \langle \phi(y) \phi(x) \rangle \quad , \quad \mathcal{G}_{-+}(x, y) \equiv \langle \phi(x) \phi(y) \rangle \quad ,\quad (\text{C.16})$$

it seems that these two propagators should be equal when evaluated for a space-like interval, i.e. for $(x - y)^2 < 0$. However, this property is not obvious in eq. (C.15). The goal of this section is to show in more detail how this property comes about.

C.3.1 Elementary proof for equal times

For the particular case of equal times, $x^0 = y^0$, and different locations, $\mathbf{x} \neq \mathbf{y}$, this property of the dressed $\mathcal{G}_{\pm\mp}$ propagators can be proven by a very elementary method.

First of all, it is easy to check that the corresponding free propagators obey this property:

$$G_{+-}^0(x, y) = G_{-+}^0(x, y) \quad \text{if } x^0 = y^0 \quad \text{and } \mathbf{x} \neq \mathbf{y} . \quad (\text{C.17})$$

(This can be checked by an explicit calculation of these free propagators in coordinate space.) Note that as $\mathbf{x} = \mathbf{y}$, these two propagators are not equal. In fact, their difference at equal times is proportional to $\delta(\mathbf{x} - \mathbf{y})$.

Let us now construct the dressed propagators \mathcal{G}_{+-} and \mathcal{G}_{-+} iteratively, order by order in the background field. Here, it is important to assume that the two Schwinger-Keldysh components of the background field are equal ($\mathcal{A}_+ = \mathcal{A}_- \equiv \mathcal{A}$). Consider the order 1 for $\mathcal{G}_{\pm\mp}(x, y)$:

$$\begin{aligned} \mathcal{G}_{+-}^{(1)}(x, y) &= i \int d^4 z \mathcal{A}(z) \left[G_{++}^0(x, z) G_{+-}^0(z, y) - G_{+-}^0(x, z) G_{--}^0(z, y) \right] \\ \mathcal{G}_{-+}^{(1)}(x, y) &= i \int d^4 z \mathcal{A}(z) \left[G_{-+}^0(x, z) G_{++}^0(z, y) - G_{--}^0(x, z) G_{-+}^0(z, y) \right] . \end{aligned} \quad (\text{C.18})$$

The next step is to decompose the free propagators G_{++}^0 and G_{--}^0 in terms of the off-diagonal components:

$$\begin{aligned} G_{++}^0(x, y) &= \theta(x^0 - y^0) G_{-+}^0(x, y) + \theta(y^0 - x^0) G_{+-}^0(x, y) \\ G_{--}^0(x, y) &= \theta(x^0 - y^0) G_{+-}^0(x, y) + \theta(y^0 - x^0) G_{-+}^0(x, y) . \end{aligned} \quad (\text{C.19})$$

If we assume that $x^0 = y^0$, the integration over z^0 in eqs. (C.18) can be split into the ranges $z^0 < x^0$ and $z^0 > x^0$, and in each of these ranges one can replace the $++$ or $--$ propagators by either the $+-$ or $-+$ propagator. This substitution leads to

$$\begin{aligned} \mathcal{G}_{+-}^{(1)}(x, y) &= i \int_{z^0 < x^0} d^4 z \mathcal{A}(z) \left[G_{-+}^0(x, z) G_{+-}^0(z, y) - G_{+-}^0(x, z) G_{-+}^0(z, y) \right] , \\ \mathcal{G}_{-+}^{(1)}(x, y) &= i \int_{z^0 < x^0} d^4 z \mathcal{A}(z) \left[G_{-+}^0(x, z) G_{+-}^0(z, y) - G_{+-}^0(x, z) G_{-+}^0(z, y) \right] . \end{aligned} \quad (\text{C.20})$$

Thus, we see explicitly that $\mathcal{G}_{+-}^{(1)}(x, y) = \mathcal{G}_{-+}^{(1)}(x, y)$ if $x^0 = y^0$. Note also that the contribution coming from the range $z^0 > x^0$ has identically cancelled out in the integrals. This is a consequence of our assumption that $\mathcal{A}_+ = \mathcal{A}_-$.

In order to generalize these results to any order in the background field, it is sufficient to notice that the decomposition of eqs. (C.19) is also valid for the propagators at order n in the

background field. Then, by writing the order $n + 1$ as the convolution of the order n and a free propagator, one arrives easily at

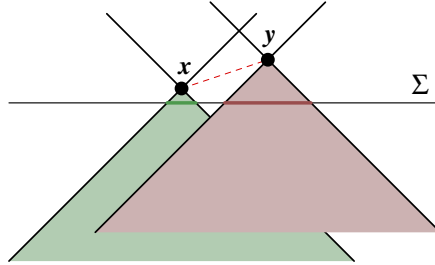
$$\begin{aligned}\mathcal{G}_{+-}^{(n+1)}(x, y) &= i \int_{z^0 < x^0} d^4 z \mathcal{A}(z) \left[\mathcal{G}_{-+}^{(n)}(x, z) G_{+-}^0(z, y) - \mathcal{G}_{+-}^{(n)}(x, z) G_{-+}^0(z, y) \right], \\ \mathcal{G}_{-+}^{(n+1)}(x, y) &= i \int_{z^0 < x^0} d^4 z \mathcal{A}(z) \left[\mathcal{G}_{-+}^{(n)}(x, z) G_{+-}^0(z, y) - \mathcal{G}_{+-}^{(n)}(x, z) G_{-+}^0(z, y) \right].\end{aligned}\tag{C.21}$$

This proves the identity $\mathcal{G}_{+-}^{(n+1)}(x, y) = \mathcal{G}_{-+}^{(n+1)}(x, y)$ at equal time, and by induction completes the proof of this identity for the dressed propagator.

One can also note an additional property, valid if the background field $\mathcal{A}(z)$ is real. In this case, the propagators $\mathcal{G}_{+-}(x, y)$ and $\mathcal{G}_{-+}(x, y)$ are mutually complex conjugate for any points x and y (this is obvious either from eqs. (C.15) or iteratively¹ from eqs. (C.21) after checking that the property holds for the free propagators). Therefore, since they are equal at equal times, they must also be purely real at $x^0 = y^0$.

C.3.2 Extension to generic space-like intervals

Figure C.1: Backward light-cones of summits x and y for a space-like interval $(x - y)^2 < 0$. The darker green and red segments on Σ represent the support of $\mathbb{T}_u \varphi(x)$ and $\mathbb{T}_u \varphi(y)$ respectively. Since they have no point in common, the integral in eq. (C.25) is zero.



The case of a generic space-like interval between the points x and y is not so elementary, but it can be derived from our previous result for equal times. To do so, we must go back to the representation of eqs. (C.15) for the $\mathcal{G}_{\pm\mp}$ propagators, and recall eq. (2.98),

$$\alpha_k(x) = \int_{\Sigma} d^3 \mathbf{S}_u \left[\alpha_k \cdot \mathbb{T}_u \right] \varphi(x). \tag{C.22}$$

For the integration surface Σ , we will chose a constant time surface, so that the measure $d^3 \mathbf{S}_u$

¹The i in front of the integral is crucial (i.e. the insertion of the background field should be $i\mathcal{A}(z)$ with a real $\mathcal{A}(z)$).

is simply the usual 3-volume element $d^3\mathbf{u}$. Thanks to this formula, we can write

$$\begin{aligned}\mathcal{G}_{+-}(\mathbf{x}, \mathbf{y}) &= \int \frac{d^3\mathbf{k}}{(2\pi)^3 2k} \int_{\Sigma} d^3\mathbf{u} d^3\mathbf{v} \left[[\mathbf{a}_{\mathbf{k}}^* \cdot \mathbb{T}_{\mathbf{u}}] \varphi(\mathbf{x}) \right] \left[[\mathbf{a}_{\mathbf{k}} \cdot \mathbb{T}_{\mathbf{v}}] \varphi(\mathbf{y}) \right] \\ \mathcal{G}_{-+}(\mathbf{x}, \mathbf{y}) &= \int \frac{d^3\mathbf{k}}{(2\pi)^3 2k} \int_{\Sigma} d^3\mathbf{u} d^3\mathbf{v} \left[[\mathbf{a}_{\mathbf{k}} \cdot \mathbb{T}_{\mathbf{u}}] \varphi(\mathbf{x}) \right] \left[[\mathbf{a}_{\mathbf{k}}^* \cdot \mathbb{T}_{\mathbf{v}}] \varphi(\mathbf{y}) \right].\end{aligned}\tag{C.23}$$

The result of the previous subsection tells us that since the points \mathbf{u} and \mathbf{v} both lie on the same equal-time surface Σ , we have

$$\int \frac{d^3\mathbf{k}}{(2\pi)^3 2k} \left[\mathbf{a}_{\mathbf{k}}^*(\mathbf{u}) \mathbf{a}_{\mathbf{k}}(\mathbf{v}) - \mathbf{a}_{\mathbf{k}}(\mathbf{u}) \mathbf{a}_{\mathbf{k}}^*(\mathbf{v}) \right] \propto \delta(\mathbf{u} - \mathbf{v}),\tag{C.24}$$

from which we get

$$\mathcal{G}_{+-}(\mathbf{x}, \mathbf{y}) - \mathcal{G}_{-+}(\mathbf{x}, \mathbf{y}) \propto \int_{\Sigma} d^3\mathbf{u} \left[\mathbb{T}_{\mathbf{u}} \varphi(\mathbf{x}) \right] \left[\mathbb{T}_{\mathbf{u}} \varphi(\mathbf{y}) \right].\tag{C.25}$$

From causality, $\mathbb{T}_{\mathbf{u}} \varphi(\mathbf{x})$ is non-zero only if the point \mathbf{u} is located inside the backward light-cone of summit \mathbf{x} . Likewise for $\mathbb{T}_{\mathbf{u}} \varphi(\mathbf{y})$. Thus, the above integral is zero if we can find a constant time surface Σ such that the intersections of the light-cones of summits \mathbf{x} and \mathbf{y} with Σ have no point in common. This is the case if the interval $\mathbf{x} - \mathbf{y}$ is space-like, as illustrated in the figure C.1.

Appendix D

Light-cone coordinates, Light-cone gauge



ynamical aspects of high energy scattering simplify when expressed in the so-called *light-cone coordinates*. Indeed, they make some of the kinematical properties of such collisions more manifest – in particular, the invariance under Lorentz boosts in the longitudinal direction. Similarly, the *light-cone gauge* is the gauge that makes the parton interpretation of the structure of a fast hadron manifest. In this appendix, we first define light-cone coordinates. Then, we define the light-cone gauge, and compute the gluon propagator in the gauge $A^+ = 0$. Finally, we derive the Green's formula for a retarded classical field in the gauge $A^+ = 0$, in order to obtain the LC gauge expression of the operator \mathbb{T}_u introduced in the section 2.6 of this manuscript.

D.1 Light-cone coordinates

The light-cone coordinates v^+, v^- are defined from the standard Cartesian coordinates by choosing a reference axis. If one takes the z axis as the reference, their definition reads:

$$v^+ \equiv \frac{v^0 + v^3}{\sqrt{2}}, \quad v^- \equiv \frac{v^0 - v^3}{\sqrt{2}}, \quad (\text{D.1})$$

where v^μ is an arbitrary 4-vector. The transverse coordinates \mathbf{v}^\perp are left unchanged.

The main advantage of light-cone coordinates is that they simplify the kinematics in situations that involve fast moving objects in the z direction. For instance, light-cone coordinates lead to a particularly simple form for Lorentz boosts in the z direction:

$$\begin{aligned} v^+ &\rightarrow \sqrt{\frac{1+\beta}{1-\beta}} v^+, \\ v^- &\rightarrow \sqrt{\frac{1-\beta}{1+\beta}} v^-, \\ \mathbf{v}_\perp &\rightarrow \mathbf{v}_\perp, \end{aligned} \quad (\text{D.2})$$

where β is the velocity of the boost. Thus, a longitudinal boost just amounts to a rescaling of the components v^\pm , with no mixing. For a boost in the $+z$ direction, with a velocity close to the speed of light, the $+$ components become large while the $-$ component shrinks to zero.

Another place where a simplification due to light-cone coordinates is manifest is in the expression of the d'Alembertian operator:

$$\square = 2\partial^+\partial^- - \nabla_\perp^2, \quad (\text{D.3})$$

where we denote¹ $\partial^+ \equiv \partial/\partial x^-$ and $\partial^- \equiv \partial/\partial x^+$. One sees that this operator becomes first order in derivatives with respect to either of the longitudinal coordinates, contrary to its expression in Cartesian coordinates.

Finally, in light-cone coordinates, the covariant product of two vectors u^μ and v^μ takes the form:

$$u \cdot v = u^+v^- + u^-v^+ - \mathbf{u}_\perp \cdot \mathbf{v}_\perp, \quad (\text{D.4})$$

and the 4-volume element is

$$d^4v = dv^+ dv^- d^2\mathbf{v}_\perp. \quad (\text{D.5})$$

D.2 Gluon propagator in LC gauge

The light-cone gauge is a particular case of axial gauge $\tilde{n} \cdot A = 0$ in which the vector \tilde{n}^μ is light-like. Typically, this gauge is used in problems involving a fast moving color charge, with a vector \tilde{n}^μ aligned with the velocity of the projectile. The importance of this gauge is due to the fact that it makes manifest the parton model of hadrons.

Consider the QCD Lagrangian to which we add a gauge fixing term proportional to $(\tilde{n} \cdot A)^2$,

$$\mathcal{L} \equiv -\frac{1}{4}F_{\mu\nu}^a F_{\mu\nu}^a + \frac{1}{2\alpha}(\tilde{n} \cdot A)^2. \quad (\text{D.6})$$

We are mostly interested in the case where $\tilde{n} \cdot A = A^+$, but in fact most of the discussion is valid for any vector \tilde{n}^μ . In order to determine the free propagator in this gauge, we need first to isolate the quadratic part of the Lagrangian,

$$\mathcal{L}_{\text{quad}} = \frac{1}{2}A_\mu^a \left[\square g^{\mu\nu} - \partial^\mu \partial^\nu + \frac{1}{\alpha} \tilde{n}^\mu \tilde{n}^\nu \right] A_\nu^a. \quad (\text{D.7})$$

The free propagator we are looking for is a Green's function of the operator in the square brackets. Its calculation is best performed in momentum space, where we need to invert

$$-g^{\mu\nu}k^2 + k^\mu k^\nu + \frac{1}{\alpha} \tilde{n}^\mu \tilde{n}^\nu. \quad (\text{D.8})$$

Because this tensor is symmetric in (μ, ν) , its inverse must be a linear combination of $g^{\mu\nu}$, $k^\mu k^\nu$, $\tilde{n}^\mu \tilde{n}^\nu$ and $k^\mu \tilde{n}^\nu + k^\nu \tilde{n}^\mu$. Writing the most general linear combination of these elementary tensors, and multiplying it with eq. (D.8), we finally obtain the following expression for the propagator in momentum space :

$$D_0^{\mu\nu}(k) = i \left[-\frac{g^{\mu\nu}}{k^2} + \frac{k^\mu k^\nu}{(\tilde{n} \cdot k)^2} \left(\alpha - \frac{\tilde{n}^2}{k^2} \right) + \frac{k^\mu \tilde{n}^\nu + k^\nu \tilde{n}^\mu}{k^2(\tilde{n} \cdot k)} \right]. \quad (\text{D.9})$$

¹These notations have been chosen because ∂^+ (resp. ∂^-) transforms like the $+$ (resp. $-$) component of a 4-vector under a Lorentz boost in the z direction.

Note that this expression is still incomplete, because we need to add $i\epsilon$'s to the denominators in order to make the propagator regular on the real energy axis. Doing so amounts to choosing certain boundary conditions for the fields that evolve according to this propagator. The central object in the studies presented in this manuscript is the retarded propagator, which has all its poles below the real energy axis. This amounts to writing:

$$D_{0,r}^{\mu\nu}(k) = i \left[-\frac{g^{\mu\nu}}{k^2 + ik^0\epsilon} + \frac{k^\mu k^\nu}{(\tilde{n} \cdot k + i\epsilon)^2} \left(\alpha - \frac{\tilde{n}^2}{k^2 + ik^0\epsilon} \right) + \frac{k^\mu \tilde{n}^\nu + k^\nu \tilde{n}^\mu}{(k^2 + ik^0\epsilon)(\tilde{n} \cdot k + i\epsilon)} \right]. \quad (D.10)$$

(This choice for the $i\epsilon$ prescription of the $\tilde{n} \cdot k$ denominators is indeed retarded if $n^0 > 0$. We will assume that this is the case.)

In the case of the light-cone gauge $A^+ = 0$, this amounts to choosing a vector \tilde{n}^μ that has $\tilde{n}^- = 1$ and all its other components zero. Moreover, we work in the *strict* light cone gauge, that corresponds to the limit $\alpha \rightarrow 0$ for the gauge fixing parameter. The propagator simplifies somewhat in this limit :

$$D_{0,r}^{\mu\nu}(k) = -\frac{i}{k^2 + ik^0\epsilon} \left[g^{\mu\nu} - \frac{k^\mu \tilde{n}^\nu + k^\nu \tilde{n}^\mu}{\tilde{n} \cdot k + i\epsilon} \right]. \quad (D.11)$$

Note that this propagator is zero if any of its Lorentz indices is equal to $+$.

D.3 Green's formulas in LC gauge

An essential ingredient in our discussion is the Green's formula that expresses a field fluctuation in terms of its value on some initial surface. In this appendix, this initial surface will be the light-like plane defined by $x^- = 0$, but our derivation is more general than that and applies to any (locally space-like or light-like) initial surface.

D.3.1 Green's formula for a small fluctuation in the vacuum

Consider first a small field fluctuation a^μ propagating in the vacuum. In the strict light-cone gauge, it obeys

$$\begin{aligned} a^+(y) &= 0, \\ [\Box_y g^{\mu\nu} - \partial_y^\mu \partial_y^\nu] a_\nu(y) &= 0. \end{aligned} \quad (D.12)$$

It is easy to check that the free propagator $D_{0,r}^{\rho\mu}(x, y)$ obeys

$$D_{0,r}^{\rho\mu}(x, y) [\overleftarrow{\Box}_y g^{\mu\nu} - \overleftarrow{\partial}_y^\mu \overleftarrow{\partial}_y^\nu] = i \left[g^{\rho\nu} - \frac{\partial^\rho \tilde{n}^\nu}{\tilde{n} \cdot \partial} \right] \delta(x - y), \quad (D.13)$$

where the arrows indicate that the derivatives act on the left. Now, multiply eq. (D.12) by $D_{0,r}^{\rho\mu}(x, y)$ on the left, eq. (D.13) by $a_\nu(y)$ on the right², integrate y over all the domain defined by $y^- > 0$, and subtract the two equations. One obtains

$$a^\rho(x) = -i \int_{y^- > 0} d^4 y D_{0,r}^{\rho\mu}(x, y) [\overleftrightarrow{\partial}_y^\mu \overleftrightarrow{\partial}_y^\nu - \overleftarrow{\Box}_y g^{\mu\nu}] a_\nu(y), \quad (D.14)$$

²When we multiply eq. (D.13) by a_ν on the right, the second term vanishes thanks to the gauge condition $\tilde{n} \cdot a = 0$ obeyed by the gauge field fluctuation.

where $\overleftrightarrow{A} \equiv \overrightarrow{A} - \overleftarrow{A}$. Using the relations

$$\begin{aligned} A \overleftrightarrow{\square} B &= \partial^\mu [A \overleftrightarrow{\partial}_\mu B], \\ A \overleftrightarrow{\partial}^\mu \overleftrightarrow{\partial}^\nu B &= \frac{1}{2} \partial^\mu [A \overleftrightarrow{\partial}^\nu B] + \frac{1}{2} \partial^\nu [A \overleftrightarrow{\partial}^\mu B], \end{aligned} \quad (\text{D.15})$$

we see that the integrand in eq. (D.14) is a total derivative. Therefore, we can rewrite this integral as an integral on the boundary of the integration domain. If the derivative we integrate by parts is a ∂^i or ∂^- , then the corresponding boundary is located at infinity in the direction y^i or y^+ respectively. We assume here that the field fluctuation under consideration has a compact enough support so that these contributions vanish. We are thus left with the terms coming from the derivative ∂^+ . The contribution from the boundary at $y^- = +\infty$ is zero, because of our choice of the retarded prescription for the propagator. Therefore, the only contribution is from the boundary at $y^- = 0$,

$$\alpha^\rho(x) = -i \int_{y^-=0} dy^+ d^2 \mathbf{y}_\perp D_{\mu 0, \text{R}}^\rho(x, y) \left[g^{\mu\nu} (n \cdot \overleftrightarrow{\partial}_y) - \frac{1}{2} (n^\mu \overleftrightarrow{\partial}^\nu_y + n^\nu \overleftrightarrow{\partial}^\mu_y) \right] \alpha_\nu(y), \quad (\text{D.16})$$

where n^μ is a vector such that $n \cdot dy = 0$ for any infinitesimal displacement dy^μ on the surface $y^- = 0$ (it is the unit vector normal to the surface $y^- = 0$, in the sense of the Minkowsky scalar product). This formula indicates how the value of the fluctuation at the point x is related to its value on an initial surface located at $y^- = 0$ (Note that this dependence is linear since small fluctuations obey a linear equation of motion). A priori, it involves the values of all the components of the fluctuation on this surface, as well as that of its first derivatives. However, some of this information is not necessary because the propagator vanishes when $\mu = +$ and because of the gauge condition $\alpha^+(y) = 0$. If one eliminates from the previous formula all the terms that are obviously zero and integrate some terms by parts³, we get $\alpha^\rho(x) \equiv \mathcal{B}_0^\rho[\alpha](x)$, where $\mathcal{B}_0^\rho[\alpha](x)$ is an integral that depends only on the value of the field and of some of its derivatives on the initial surface,

$$\begin{aligned} \mathcal{B}_0^\rho[\alpha](x) &= -i \int_{y^-=0} dy^+ d^2 \mathbf{y}_\perp \left\{ \left[\partial_\mu^y D_{0, \text{R}}^{\rho\mu}(x, y) \right] \alpha^-(y) \right. \\ &\quad \left. - D_{0, \text{R}}^{\rho-}(x, y) \left[\partial_y^\mu \alpha_\mu(y) \right] - D_{0, \text{R}}^{\rho i}(x, y) 2 \partial_y^- \alpha^i(y) \right\}. \end{aligned} \quad (\text{D.17})$$

Therefore, it appears that in the light-cone gauge $A^+ = 0$, and for an initial surface $y^- = 0$, we need to know the initial value of α^- , $\partial^- \alpha^i$ and $\partial_\mu \alpha^\mu$ in order to fully determine the value of the fluctuation at the point x . This fact is the reason why there are only three terms in the definition of the operator \mathbb{T}_u in eq. (3.39) (but we postpone until the end of this section the explanation of why one needs to include the Wilson line Ω in this definition).

Moreover, the first term in the right hand side of eq. (D.17) can be simplified by using the explicit expression of the free propagators in light cone gauge :

$$\partial_\mu^y D_{0, \text{R}}^{\rho\mu}(x, y) = \delta^{\rho-} \theta(x^- - y^-) \delta(x^+ - y^+) \delta(\mathbf{x}_\perp - \mathbf{y}_\perp). \quad (\text{D.18})$$

³The antisymmetric derivatives $\overleftrightarrow{\partial}^-_y$ and $\overleftrightarrow{\partial}^i_y$ can be eliminated by integration by parts. This is not possible for $\overleftrightarrow{\partial}^+_y$ since the boundary term does not contain an integral with respect to y^- . This is why we have a term involving the derivative $\partial_y^+ D_{0, \text{R}}^{\rho-}$.

D.3.2 Green's formula for classical solutions

There is also a similar Green's formula for retarded classical solutions of the Yang-Mills equations. Contrary to the case of small fluctuations, we do not assume that the gauge field is small, and we keep all the self-interactions as well as the interactions with some external source. Formally, we can write the Lagrangian as

$$\mathcal{L} = \mathcal{L}_{\text{quad}} - \mathcal{U}(\mathcal{A}) , \quad (\text{D.19})$$

where $\mathcal{U}(\mathcal{A})$ is a local polynomial of the gauge field. It contains the 3- and 4-gluon couplings and the coupling to the external source. In the $\mathcal{A}^+ = 0$ gauge, the corresponding classical equation of motion is

$$[\Box_y g^{\mu\nu} - \partial_y^\mu \partial_y^\nu] \mathcal{A}_\nu(y) = \frac{\partial \mathcal{U}(\mathcal{A})}{\partial \mathcal{A}_\mu(y)} . \quad (\text{D.20})$$

Then one can follow the same procedure as in the case of small fluctuations, to obtain

$$\mathcal{A}^\rho(x) = -i \int_{y^- > 0} d^4 y \, D_{0,r}^{\rho\mu}(x, y) \frac{\partial \mathcal{U}(\mathcal{A})}{\partial \mathcal{A}_\mu(y)} + \mathcal{B}_0^\rho[\mathcal{A}](x) , \quad (\text{D.21})$$

where the boundary term is the same as in eq. (D.17) with \mathcal{A}^μ instead of α^μ . Of course, the dependence of the classical field on its initial conditions is no longer linear because of the first term in the right hand side; the self interactions of the gauge fields lead to an involved dependence on the initial conditions.

D.3.3 Green's formula for α^μ in a background field

Finally, the Green's formula of eq. (D.17) can be extended to the situation where the fluctuation $\alpha^\mu(x)$ propagates on top of a classical background field \mathcal{A}^μ rather than the vacuum. The only change is the addition of a bulk term that takes into account the interactions of the fluctuation $\alpha^\mu(x)$ with the background field \mathcal{A}^μ above the initial surface,

$$\alpha^\rho(x) = -i \int_{y^- > 0} d^4 y \, D_{0,r}^{\rho\nu}(x, y) \frac{\partial^2 \mathcal{U}(\mathcal{A})}{\partial \mathcal{A}_\nu(y) \partial \mathcal{A}^\sigma(y)} \alpha^\sigma(y) + \mathcal{B}_0^\rho[\alpha](x) . \quad (\text{D.22})$$

The derivation of this formula is very similar to that for the classical field \mathcal{A}^μ .

In the derivation of the JIMWLK equation, the fluctuations $\alpha^\mu(x)$ one considers are fluctuations whose initial condition at $x^0 \rightarrow -\infty$ are plane waves of momentum k . One can calculate explicitly their value on the initial surface, which means that we know analytically the quantities α^- , $\partial^- \alpha^i$ and $\partial_\mu \alpha^\mu$ in the r.h.s. of eq. (D.17). A crucial property is that the initial values of α^- and $\partial^- \alpha^i$ are suppressed by an extra factor $k^- \sim 1/k^+$, and thus any term containing them cannot have a divergence when $k^+ \rightarrow +\infty$.

Our goal is to calculate the logarithms that occur when $k^+ \rightarrow +\infty$ solely by inspecting the boundary term in eq. (D.17). For this to work, no logarithms should be produced by the interactions of the fluctuation with the background field above the initial surface. The simplest way to achieve this is to be in a gauge where the background field is zero above the initial

surface. It is very simple to achieve this in the specific situation encountered in the derivation of the JIMWLK equation, because this background field is a pure gauge: $\mathcal{A}^\mu \equiv ig^{-1}\Omega^\dagger\partial^\mu\Omega$. In this special case, the Green's formula that gives the fluctuation at the point x takes a very simple form,

$$\begin{aligned} a^\rho(x) = & -i\Omega^\dagger(x) \int_{y^-=0} dy^+ d^2y_\perp \left\{ \left[\partial_\mu^y D_{0,r}^{\rho\mu}(x,y) \right] \Omega(y) a^-(y) \right. \\ & \left. - D_{0,r}^{\rho-}(x,y) \left[\partial_y^\mu \Omega(y) a_\mu(y) \right] - D_{0,r}^{\rho i}(x,y) 2\partial_y^- \Omega(y) a^i(y) \right\}, \end{aligned} \quad (D.23)$$

in which there is no bulk term. All the interactions of the fluctuation with the pure gauge background field are taken into account by the Wilson lines Ω and Ω^\dagger . To obtain this expression, one should apply a gauge transformation Ω that eliminates the background field above the initial surface (this is possible because it is a pure gauge), and perform the inverse transformation at the endpoint x . This is why the most convenient definition of \mathbb{T}_u in eq. (3.45) involves functional derivatives with respect to the background field transformed by Ω rather than the background field itself⁴.

D.4 Propagation through a shockwave background

A common problem involving small fluctuations in the context of high energy collisions in QCD is to study the propagation of the fluctuation on top of the classical field created by a fast moving charge. Let us assume a color charge distribution $\rho(x^-, \mathbf{x}_\perp)$, corresponding to a projectile moving in the $+z$ direction. At high energy, this distribution of charge is localized near $x^- = 0$, for instance in the strip $0 \leq x^- \leq \epsilon$ with ϵ infinitesimal. It is well known that in the Lorenz gauge ($\partial_\mu A^\mu = 0$), the classical solution of Yang-Mills equations that vanishes in the remote past is:

$$\begin{aligned} \tilde{\mathcal{A}}^-(x) &= 0, \\ \tilde{\mathcal{A}}^i(x) &= 0, \\ \tilde{\mathcal{A}}^+(x) &= -\frac{1}{\nabla_\perp^2} \tilde{\rho}(x^-, \mathbf{x}_\perp). \end{aligned} \quad (D.24)$$

(The tilde indicate objects expressed in the Lorenz gauge, to distinguish them from the LC gauge ones.)

We are now going to solve the equation of motion for a small fluctuation propagating on top of this classical field. The source $\tilde{\rho}$ being almost a delta function at $x^- = 0$, this is also the case for the only non-zero component of the classical field, i.e. $\tilde{\mathcal{A}}^+$. Obviously, the propagation of the fluctuation is trivial in the regions where all the components of the classical field are zero since the equation of motion there is the Klein-Gordon equation. Therefore, we need only to determine the change of the fluctuation when it crosses the strip $0 \leq x^- \leq \epsilon$. Since the background field behaves as a delta function in this strip, we expect a discontinuity for the fluctuation.

⁴Of course, the two ways of defining \mathbb{T}_u —with and without the Ω — are exactly equivalent. But if we did not include the Ω in the definition, the logarithmic divergences would come from a combination of the second and third terms of eq. (3.39), instead of being limited to the third term if we include the Ω in the definition of \mathbb{T}_u .

The difficulty in solving the equation of motion of the fluctuation in this strip varies widely depending on the choice of the gauge for the fluctuation. It turns out to be very complicated in the Lorenz gauge⁵. However, there is a trick that consists in noticing that eqs. (D.24) can also be interpreted as the classical solution in the $\mathcal{A}^- = 0$ gauge. The great advantage of this gauge, compared to any other gauge, is that the incoming fluctuation does not alter the color charge distribution on the $+z$ axis. Indeed, from the covariant conservation of the current, $[\mathcal{D}_\mu, J^\mu] = 0$, we see that only a non-zero minus component of the fluctuation can have an influence on the current whose only non-zero component is the $+$ component. Therefore, in this gauge the color current J^+ is fixed once for all, and does not receive any correction due to the incoming fluctuation.

By writing the Yang-Mills equations for the field $\tilde{\mathcal{A}}^\mu + \tilde{a}^\mu$ in the $\mathcal{A}^- = 0$ gauge and expanding to order one in the fluctuation \tilde{a}^μ , one obtains the following equations of motion for the fluctuation:

$$\begin{aligned} \partial^- \tilde{a}^+ - \partial^i \tilde{a}^i &= 0, \\ \square \tilde{a}^i - 2ig[\tilde{\mathcal{A}}^+, \partial^- \tilde{a}^i] &= 0, \\ \square \tilde{a}^+ - 2ig[\tilde{\mathcal{A}}^+, \partial^- \tilde{a}^i] &= 2ig[\partial^i \tilde{\mathcal{A}}^+, \tilde{a}^i]. \end{aligned} \quad (\text{D.25})$$

The first of these equations does not contain any derivative with respect to x^- . Therefore, it can be seen as a constraint that relates \tilde{a}^+ and \tilde{a}^i at each x^- . The second equation contains only the transverse components of the fluctuation, and should be solved first. In the strip $0 \leq x^- \leq \epsilon$, one can check that its solution is⁶

$$\tilde{a}^i(x^+, x^-, \mathbf{x}_\perp) = \mathcal{U}(x^-, \mathbf{x}_\perp) \tilde{a}^i(x^+, 0, \mathbf{x}_\perp), \quad (\text{D.26})$$

where \mathcal{U} is a Wilson line defined by

$$\mathcal{U}(x^-, \mathbf{x}_\perp) = T_- \exp \left[ig \int_0^{x^-} dz^- \tilde{\mathcal{A}}^+(z^-, \mathbf{x}_\perp) \right]. \quad (\text{D.27})$$

(T_- denotes an ordering of the formula in z^- .) Eq. (D.26) tells us the value of the discontinuity of the fluctuation \tilde{a}^i when it goes from $x^- = 0$ to $x^- = \epsilon$. In order to obtain the same information for the component \tilde{a}^+ , we can either solve the constraint (first equation), or solve the third equation. Both calculations give the same result:

$$\tilde{a}^+(x^+, x^-, \mathbf{x}_\perp) = \mathcal{U}(x^-, \mathbf{x}_\perp) \tilde{a}^+(x^+, 0, \mathbf{x}_\perp) + [\partial^i \mathcal{U}(x^-, \mathbf{x}_\perp)] \frac{1}{\partial^-} \tilde{a}^i(x^+, 0, \mathbf{x}_\perp). \quad (\text{D.28})$$

We see that the components $+$ and i mix while they are propagating through the strip where the background field is non-zero.

⁵See the appendix of [1].

⁶Note that one relies here on the fact that ϵ is infinitesimal. This would not be an exact solution for a finite ϵ .

Appendix E

Laplacian Green's function in two dimensions



qualities involving the Green's function of the Laplacian operator in two dimensions (or its derivatives) are very useful in the derivation of the JIMWLK equation. The formulas we present in this appendix are scattered in the original works discussing the JIMWLK equation. We compile them here, with their derivation, as a convenience for the reader.

E.1 Definition

Let us denote $G(\mathbf{x}_\perp - \mathbf{y}_\perp)$ a Green's function of the 2-dimensional Laplacian operator,

$$\partial_\perp^2 G(\mathbf{x}_\perp - \mathbf{y}_\perp) = \delta(\mathbf{x}_\perp - \mathbf{y}_\perp) . \quad (\text{E.1})$$

It admits a simple Fourier representation,

$$G(\mathbf{x}_\perp - \mathbf{y}_\perp) = - \int \frac{d^2 \mathbf{k}_\perp}{(2\pi)^2} e^{i \mathbf{k}_\perp \cdot (\mathbf{x}_\perp - \mathbf{y}_\perp)} \frac{1}{\mathbf{k}_\perp^2} . \quad (\text{E.2})$$

Note that this object suffers from an infrared problem, which is obvious for dimensional reasons: this propagator is a dimensionless object in coordinate space, invariant under translations and rotations, and therefore it must be a function of $\mu |\mathbf{x}_\perp - \mathbf{y}_\perp|$ where μ is some mass scale that was not present in the previous equation.

E.2 Derivatives of the Green's function

Derivatives of this propagator do not suffer from this infrared ambiguity. Consider for instance¹

$$\partial_x^i G(\mathbf{x}_\perp - \mathbf{y}_\perp) = i \int \frac{d^2 \mathbf{k}_\perp}{(2\pi)^2} e^{i \mathbf{k}_\perp \cdot (\mathbf{x}_\perp - \mathbf{y}_\perp)} \frac{k_\perp^i}{\mathbf{k}_\perp^2} . \quad (\text{E.3})$$

¹Let us recall that $\partial_x^i = \frac{\partial}{\partial x_i} = -\frac{\partial}{\partial x^i}$.

From its symmetries and dimension, it is obvious that this derivative can be written as

$$\partial_x^i G(\mathbf{x}_\perp - \mathbf{y}_\perp) = C \frac{\mathbf{x}_\perp^i - \mathbf{y}_\perp^i}{(\mathbf{x}_\perp - \mathbf{y}_\perp)^2}, \quad (\text{E.4})$$

where the prefactor C is dimensionless. Because the derivative of the propagator is not infrared singular, the cutoff μ cannot appear in its expression and C must be a pure number (otherwise it would have to be a function of $\mu|\mathbf{x}_\perp - \mathbf{y}_\perp|$ to have the correct dimension). In order to determine the constant, take another derivative ∂_x^i and integrate over \mathbf{x}_\perp the resulting equation over some domain Ω of the plane that contains the point \mathbf{y}_\perp . On the left hand side, we get the integral of $\delta(\mathbf{x}_\perp - \mathbf{y}_\perp)$ since G is a Green's function of ∂_\perp^2 . We then get

$$1 = C \int_\Omega d^2\mathbf{x}_\perp \partial_x^i \frac{\mathbf{x}_\perp^i - \mathbf{y}_\perp^i}{(\mathbf{x}_\perp - \mathbf{y}_\perp)^2}. \quad (\text{E.5})$$

The right hand side can be transformed by using the 2-dimensional Stokes theorem, leading to an integral on the boundary of Ω (oriented counter-clockwise)

$$1 = -C \int_{\partial\Omega} \frac{\epsilon^{ij} (\mathbf{x}_\perp^i - \mathbf{y}_\perp^i) dx^j}{(\mathbf{x}_\perp - \mathbf{y}_\perp)^2}, \quad (\text{E.6})$$

where ϵ^{ij} is completely antisymmetric (with $\epsilon^{12} = 1$). The contour integral in this equation is a topological invariant, that depends only on the winding number of the contour $\partial\Omega$ around the point \mathbf{y}_\perp . It is best calculated by deforming $\partial\Omega$ into the unit circle around the point \mathbf{y}_\perp . We get easily

$$1 = -2\pi C. \quad (\text{E.7})$$

Thus we have

$$\partial_x^i G(\mathbf{x}_\perp - \mathbf{y}_\perp) = -\frac{1}{2\pi} \frac{\mathbf{x}_\perp^i - \mathbf{y}_\perp^i}{(\mathbf{x}_\perp - \mathbf{y}_\perp)^2}. \quad (\text{E.8})$$

The second derivative of the propagator is also useful in the derivation of the JIMWLK equation. By applying ∂_x^j to the previous equation, one obtains

$$\begin{aligned} \partial_x^i \partial_x^j G(\mathbf{x}_\perp - \mathbf{y}_\perp) &= -\frac{1}{2\pi} \partial_x^j \frac{\mathbf{x}_\perp^i - \mathbf{y}_\perp^i}{(\mathbf{x}_\perp - \mathbf{y}_\perp)^2} \\ &= \frac{1}{2\pi(\mathbf{x}_\perp - \mathbf{y}_\perp)^2} \left[\delta^{ij} - 2 \frac{(\mathbf{x}_\perp^i - \mathbf{y}_\perp^i)(\mathbf{x}_\perp^j - \mathbf{y}_\perp^j)}{(\mathbf{x}_\perp - \mathbf{y}_\perp)^2} \right]. \end{aligned} \quad (\text{E.9})$$

This formula, although perfectly correct for $\mathbf{x}_\perp \neq \mathbf{y}_\perp$, is incorrect at the point $\mathbf{x}_\perp = \mathbf{y}_\perp$. In order to see this, take the trace over the indices i and j . In the left hand side, we have the Laplacian of the propagator, i.e. $\delta(\mathbf{x}_\perp - \mathbf{y}_\perp)$, while the right hand side would give zero. The full formula for the second derivative is

$$\partial_x^i \partial_x^j G(\mathbf{x}_\perp - \mathbf{y}_\perp) = \frac{\delta^{ij}}{2} \delta(\mathbf{x}_\perp - \mathbf{y}_\perp) + \frac{1}{2\pi} \Delta^{ij}(\mathbf{x}_\perp - \mathbf{y}_\perp), \quad (\text{E.10})$$

with

$$\Delta^{ij}(\mathbf{x}_\perp - \mathbf{y}_\perp) \equiv \frac{1}{(\mathbf{x}_\perp - \mathbf{y}_\perp)^2} \left[\delta^{ij} - 2 \frac{(\mathbf{x}_\perp^i - \mathbf{y}_\perp^i)(\mathbf{x}_\perp^j - \mathbf{y}_\perp^j)}{(\mathbf{x}_\perp - \mathbf{y}_\perp)^2} \right]. \quad (\text{E.11})$$

E.3 Useful identities

This function Δ^{ij} obeys an interesting identity. By integration by parts, one can check that

$$\begin{aligned} \int \frac{d^2 \mathbf{u}_\perp}{(2\pi)^2} \frac{d^2 \mathbf{v}_\perp}{(2\pi)^2} \frac{(\mathbf{x}_\perp^i - \mathbf{u}_\perp^i)(\mathbf{y}_\perp^j - \mathbf{v}_\perp^j)}{(\mathbf{x}_\perp - \mathbf{u}_\perp)^2 (\mathbf{y}_\perp - \mathbf{v}_\perp)^2} \partial_u^i \partial_v^j G(\mathbf{u}_\perp - \mathbf{v}_\perp) = \\ = \frac{1}{(2\pi)^2} \int \frac{d^2 \mathbf{u}_\perp}{(2\pi)^2} \frac{(\mathbf{x}_\perp^i - \mathbf{u}_\perp^i)(\mathbf{y}_\perp^i - \mathbf{u}_\perp^i)}{(\mathbf{x}_\perp - \mathbf{u}_\perp)^2 (\mathbf{y}_\perp - \mathbf{u}_\perp)^2} \\ = \int \frac{d^2 \mathbf{u}_\perp}{(2\pi)^2} \frac{d^2 \mathbf{v}_\perp}{(2\pi)^2} \frac{(\mathbf{x}_\perp^i - \mathbf{u}_\perp^i)(\mathbf{y}_\perp^j - \mathbf{v}_\perp^j)}{(\mathbf{x}_\perp - \mathbf{u}_\perp)^2 (\mathbf{y}_\perp - \mathbf{v}_\perp)^2} \delta^{ij} \delta(\mathbf{u}_\perp - \mathbf{v}_\perp). \end{aligned} \quad (\text{E.12})$$

Using now eq. (E.10), we obtain the following identity,

$$\int \frac{d^2 \mathbf{u}_\perp}{(2\pi)^2} \frac{d^2 \mathbf{v}_\perp}{(2\pi)^2} \frac{(\mathbf{x}_\perp^i - \mathbf{u}_\perp^i)(\mathbf{y}_\perp^j - \mathbf{v}_\perp^j)}{(\mathbf{x}_\perp - \mathbf{u}_\perp)^2 (\mathbf{y}_\perp - \mathbf{v}_\perp)^2} \left[\frac{\delta^{ij}}{2} \delta(\mathbf{u}_\perp - \mathbf{v}_\perp) - \frac{1}{2\pi} \Delta^{ij}(\mathbf{u}_\perp - \mathbf{v}_\perp) \right] = 0. \quad (\text{E.13})$$

Let us also provide an alternate representation of the 2-dimensional propagator that is sometimes helpful. Start with the integral

$$\int \frac{d^2 \mathbf{u}_\perp}{(2\pi)^2} \frac{\mathbf{u}_\perp^i - \mathbf{x}_\perp^i}{(\mathbf{u}_\perp - \mathbf{x}_\perp)^2} \frac{\mathbf{u}_\perp^i - \mathbf{y}_\perp^i}{(\mathbf{u}_\perp - \mathbf{y}_\perp)^2} = \int d^2 \mathbf{u}_\perp \left[\partial_u^i G(\mathbf{u}_\perp - \mathbf{x}_\perp) \right] \left[\partial_u^i G(\mathbf{u}_\perp - \mathbf{y}_\perp) \right]. \quad (\text{E.14})$$

The integral in the right hand side can be performed by parts, since it leads to the Laplacian of a propagator, which is a delta function. Thus, we obtain the identity

$$G(\mathbf{x}_\perp - \mathbf{y}_\perp) = - \int \frac{d^2 \mathbf{u}_\perp}{(2\pi)^2} \frac{\mathbf{u}_\perp^i - \mathbf{x}_\perp^i}{(\mathbf{u}_\perp - \mathbf{x}_\perp)^2} \frac{\mathbf{u}_\perp^i - \mathbf{y}_\perp^i}{(\mathbf{u}_\perp - \mathbf{y}_\perp)^2}. \quad (\text{E.15})$$

Note that the integral over \mathbf{u}_\perp suffers from the same infrared problem (when $|\mathbf{u}_\perp| \rightarrow \infty$ in this representation) that we have already mentioned at the beginning of this appendix.

Appendix F

Liouville equation



Fluctuations on top of a classical field configuration may be instable and lead to secular terms in observables, making them divergent at late times. Such fluctuations arise via loop corrections, and need to be resummed in order to obtain expressions that remain finite at all times. In the last part of this manuscript, we have shown that the resummation of the most divergent loop corrections is equivalent to a Gaussian average over the initial conditions for the classical field encountered at leading order. Equivalently, this resummation can be performed by solving the classical Liouville equation with a Gaussian initial condition. In this appendix, we recall some well known properties of the Liouville equation.

F.1 Hamilton's equations

In this appendix, we denote generically the canonical coordinates by \mathbf{Q} , the corresponding canonical momenta by \mathbf{P} , and the Hamiltonian by \mathcal{H} . Hamilton's equations read

$$\dot{\mathbf{Q}} = \frac{\partial \mathcal{H}}{\partial \mathbf{P}}, \quad \dot{\mathbf{P}} = -\frac{\partial \mathcal{H}}{\partial \mathbf{Q}}. \quad (\text{F.1})$$

Let us introduce a few useful notations :

$$\mathbf{x} \equiv \begin{pmatrix} \mathbf{Q} \\ \mathbf{P} \end{pmatrix}, \quad \nabla \equiv \begin{pmatrix} \partial/\partial \mathbf{Q} \\ \partial/\partial \mathbf{P} \end{pmatrix}, \quad \mathbf{V} \equiv \begin{pmatrix} \partial \mathcal{H} / \partial \mathbf{P} \\ -\partial \mathcal{H} / \partial \mathbf{Q} \end{pmatrix}. \quad (\text{F.2})$$

Hamilton's equations can now be rewritten in the following compact form

$$\dot{\mathbf{x}} = \mathbf{V}. \quad (\text{F.3})$$

This notation is suggestive of the fact that \mathbf{V} is the velocity field induced on phase-space by the Hamiltonian. A crucial property of Hamiltonian flows is that they are incompressible,

$$\nabla \cdot \mathbf{V} = 0. \quad (\text{F.4})$$

This identity is the essence of Liouville's equation.

F.2 Liouville's equation

Consider an ensemble of such dynamical systems, all described by the same Hamiltonian \mathcal{H} . At the time t , their distribution in phase-space is described by a density $\mathcal{F}_t[\mathbf{Q}, \mathbf{P}]$, and we wish to derive an equation that describes the time evolution of this distribution. Naturally, the number of systems in the ensemble is not changing since each system evolves independently of the others. Thus, \mathcal{F}_t is the density for a locally conserved quantity. We have seen before that each point in phase-space moves with the velocity \mathbf{V} . Therefore, we can write a continuity equation that expresses this conservation,

$$\partial_t \mathcal{F}_t + \nabla \cdot (\mathcal{F}_t \mathbf{V}) = 0 . \quad (\text{F.5})$$

By using eq. (F.4), we can rewrite this equation as¹

$$\underbrace{\left[\partial_t + \mathbf{V} \cdot \nabla \right]}_{D_t} \mathcal{F}_t = 0 . \quad (\text{F.6})$$

Note that the term $\mathbf{V} \cdot \nabla \mathcal{F}_t$ is nothing but the Poisson bracket $\{\mathcal{F}_t, \mathcal{H}\}$. Thus, we see that both eqs (F.5) and (F.6) are equivalent to the usual form of the Liouville equation,

$$\partial_t \mathcal{F}_t + \{\mathcal{F}_t, \mathcal{H}\} = 0 . \quad (\text{F.7})$$

The forms (F.5) and (F.6) of the Liouville equation are a useful reminder of its origin as the continuity equation for the density of systems in phase-space, and because they make some properties of Hamiltonian flows more transparent – in particular thanks to the *flow derivative* D_t introduced in eq. (F.6).

F.3 Basic properties

In this section, we derive some elementary properties of Liouville's equation. To state some of these properties, it will be useful to denote $[d\Gamma]$ the measure on phase-space.

The most elementary property,

$$\int [d\Gamma] \mathcal{F}_t = \text{const} , \quad (\text{F.8})$$

is in fact just the integral version of Liouville's equation itself. It is simply another way of stating that the number of systems in the ensemble does not change over time. A similar statement can be made about the energy if we note that²

$$D_t \mathcal{H} = 0 . \quad (\text{F.9})$$

(which means that the Hamiltonian does not vary if we follow the flow). Then, by multiplying eq. (F.6) by \mathcal{H} , and by integrating over phase-space, we get

$$\int [d\Gamma] \mathcal{F}_t \mathcal{H} = \text{const} . \quad (\text{F.10})$$

This equation simply says that the total energy of our ensemble of systems is conserved.

¹In the form $D_t \mathcal{F}_t = 0$, the Liouville equation leads easily to the *Liouville theorem*, that states that \mathcal{F}_t is constant along flow lines.

²This is due to $\partial_t \mathcal{H} = 0$ and $\mathbf{V} \cdot \nabla \mathcal{H} = \{\mathcal{H}, \mathcal{H}\} = 0$.

Bibliography

- [1] F. Gelis, Y. Mehtar-Tani, Phys. Rev. **D 73**, 034019 (2006).
- [2] F. Gelis, R. Venugopalan, Nucl. Phys. **A 776**, 135 (2006).
- [3] F. Gelis, R. Venugopalan, Nucl. Phys. **A 779**, 177 (2006).
- [4] K. Fukushima, F. Gelis, L. McLerran, Nucl. Phys. **A 786**, 107 (2007).
- [5] F. Gelis, T. Lappi, R. Venugopalan, Phys. Rev. **D 78**, 054019 (2008).
- [6] F. Gelis, T. Lappi, R. Venugopalan, Phys. Rev. **D 78**, 054020 (2008).
- [7] F. Gelis, T. Lappi, R. Venugopalan, Phys. Rev. **D 79**, 094017 (2009).
- [8] A. Dumitru, F. Gelis, L. McLerran, R. Venugopalan, Nucl. Phys. **A 810**, 91 (2008).
- [9] K. Dusling, F. Gelis, T. Lappi, R. Venugopalan, Nucl. Phys. **A 836**, 159 (2010).
- [10] F. Gelis, T. Lappi, L. McLerran, Nucl. Phys. **A 828**, 149 (2009).
- [11] K. Dusling, T. Epelbaum, F. Gelis, R. Venugopalan, Nucl. Phys. **A 850**, 69 (2011).
- [12] K. Fukushima, F. Gelis, arXiv:1106.1396, to appear in Nucl. Phys. A.
- [13] K. Dusling, F. Gelis, R. Venugopalan, Nucl. Phys. **A 872**, 161 (2011).
- [14] T. Epelbaum, F. Gelis, Nucl. Phys. **A 872**, 210 (2011).
- [15] A.J. Baltz, L.D. McLerran, Phys. Rev. **C 58**, 1679 (1998).
- [16] A.J. Baltz, F. Gelis, L.D. McLerran, A. Peshier, Nucl. Phys. **A 695**, 395 (2001).
- [17] F. Gelis, R. Venugopalan, Phys. Rev. **D 69**, 014019 (2004).
- [18] J.P. Blaizot, F. Gelis, R. Venugopalan, Nucl. Phys. **A 743**, 13 (2004).
- [19] J.P. Blaizot, F. Gelis, R. Venugopalan, Nucl. Phys. **A 743**, 57 (2004).
- [20] A. Krasnitz, R. Venugopalan, Nucl. Phys. **B 557**, 237 (1999).
- [21] A. Krasnitz, R. Venugopalan, Phys. Rev. Lett. **84**, 4309 (2000).
- [22] A. Krasnitz, R. Venugopalan, Phys. Rev. Lett. **86**, 1717 (2001).
- [23] A. Krasnitz, Y. Nara, R. Venugopalan, Phys. Rev. Lett. **87**, 192302 (2001).

- [24] A. Krasnitz, Y. Nara, R. Venugopalan, Nucl. Phys. **A 717**, 268 (2003).
- [25] A. Krasnitz, Y. Nara, R. Venugopalan, Nucl. Phys. **A 727**, 427 (2003).
- [26] T. Lappi, Phys. Rev. **C 67**, 054903 (2003).
- [27] A. Dumitru, K. Dusling, F. Gelis, J. Jalilian-Marian, T. Lappi, R. Venugopalan, Phys. Lett. **B 697**, 21 (2011).
- [28] T.S. Biro, C. Gong, B. Muller, A. Trayanov, Int. J. Mod. Phys. **C 5**, 113 (1994).
- [29] U.W. Heinz, C.R. Hu, S. Leupold, S.G. Matinyan, B. Muller, Phys. Rev. **D 55**, 2464 (1997).
- [30] T. Kunihiro, B. Muller, A. Ohnishi, A. Schafer, T.T. Takahashi, A Yamamoto, Phys. Rev. **D 82**, 114015 (2010).
- [31] P. Romatschke, R. Venugopalan, Phys. Rev. **D 74**, 045011 (2006).
- [32] S. Mrowczynski, M.H. Thoma, Phys. Rev. **D 62**, 036011 (2000).
- [33] S. Mrowczynski, Phys. Lett. **B 314**, 118 (1993).
- [34] S. Mrowczynski, Phys. Lett. **B 393**, 26 (1997).
- [35] S. Mrowczynski, Acta Phys. Polon. **B 37**, 427 (2006).
- [36] S. Mrowczynski, Acta Phys. Polon. **B 39**, 1665 (2008).
- [37] P. Arnold, J. Lenaghan, G.D. Moore, JHEP **0308**, 002 (2003).
- [38] P. Arnold, J. Lenaghan, G.D. Moore, L.G. Yaffe, Phys. Rev. Lett. **94**, 072302 (2005).
- [39] P. Arnold, G.D. Moore, L.G. Yaffe, Phys. Rev. **D 72**, 054003 (2005).
- [40] P. Romatschke, M. Strickland, Phys. Rev. **D 68**, 036004 (2003).
- [41] P. Romatschke, M. Strickland, Phys. Rev. **D 70**, 116006 (2004).
- [42] A.K. Rebhan, P. Romatschke, M. Strickland, Phys. Rev. Lett. **94**, 102303 (2005).
- [43] A.K. Rebhan, P. Romatschke, M. Strickland, JHEP **0509**, 041 (2005).
- [44] P. Arnold, G.D. Moore, Phys. Rev. **D 73**, 025006 (2006).
- [45] P. Arnold, G.D. Moore, Phys. Rev. **D 73**, 025013 (2006).
- [46] P. Arnold, G.D. Moore, Phys. Rev. **D 76**, 045009 (2007).
- [47] A.H. Mueller, A.I. Shoshi, S.M.H. Wong, Nucl. Phys. **B 760**, 145 (2007).
- [48] P. Romatschke, A. Rebhan, Phys. Rev. Lett. **97**, 252301 (2006).
- [49] D. Bodeker, K. Rummukainen, JHEP **0707**, 022 (2007).
- [50] J. Berges, S. Scheffler, D. Sexty, Phys. Lett. **B 681**, 362 (2009).
- [51] A.K. Rebhan, M. Strickland, M. Attems, Phys. Rev. **D 78**, 045023 (2008).
- [52] A.K. Rebhan, D. Steineder, Phys. Rev. **D 81**, 085044 (2010).

- [53] F. Karsch, et al. [RBC and HotQCD Collaboration], J. Phys. **G35**, 104096 (2008).
- [54] P. Huovinen, P.V. Ruuskanen, Ann. Rev. Nucl. Part. Sci. **56**, 163 (2006).
- [55] P. Romatschke, Int. J. Mod. Phys. E **19**, 1 (2010).
- [56] D. Teaney, Prog. Part. Nucl. Phys. **62**, 451 (2009).
- [57] P. Romatschke, U. Romatschke, Phys. Rev. Lett. **99**, 172301 (2007).
- [58] J.P. Blaizot, E. Iancu, A. Rebhan, Phys. Lett. **B 470**, 181 (1999).
- [59] J.P. Blaizot, E. Iancu, A. Rebhan, Phys. Rev. Lett. **83**, 2906 (1999).
- [60] F.D. Aaron, et al, [H1 and ZEUS Collaborations] JHEP **1001**, 109 (2010).
- [61] E.A. Kuraev, L.N. Lipatov, V.S. Fadin, Sov. Phys. JETP **45**, 199 (1977).
- [62] I. Balitsky, L.N. Lipatov, Sov. J. Nucl. Phys. **28**, 822 (1978).
- [63] M. Froissart, Phys. Rev. **123**, 1053 (1961).
- [64] L.V. Gribov, E.M. Levin, M.G. Ryskin, Phys. Rept. **100**, 1 (1983).
- [65] A.M. Stasto, K. Golec-Biernat, J. Kwiecinski, Phys. Rev. Lett. **86**, 596 (2001).
- [66] F. Gelis, R. Peschanski, L. Schoeffel, G. Soyez, Phys. Lett. B. **647**, 376 (2007).
- [67] H. Kowalski, T. Lappi, R. Venugopalan, Phys. Rev. Lett. **100**, 022303 (2008).
- [68] H. Kowalski, D. Teaney, Phys. Rev. **D 68**, 114005 (2003).
- [69] A. Deshpande, R. Ent, R. Milner, CERN Courier, October 2009.
- [70] L.D. McLerran, R. Venugopalan, Phys. Rev. **D 49**, 2233 (1994).
- [71] L.D. McLerran, R. Venugopalan, Phys. Rev. **D 49**, 3352 (1994).
- [72] L.D. McLerran, R. Venugopalan, Phys. Rev. **D 50**, 2225 (1994).
- [73] L.D. McLerran, R. Venugopalan, Phys. Rev. **D 59**, 094002 (1999).
- [74] L.D. McLerran, R. Venugopalan, Phys. Lett. **B 424**, 15 (1998).
- [75] A. Ayala, J. Jalilian-Marian, L.D. McLerran, R. Venugopalan, Phys. Rev. **D 53**, 458 (1996).
- [76] J. Jalilian-Marian, A. Kovner, L.D. McLerran, H. Weigert, Phys. Rev. **D 55**, 5414 (1997).
- [77] J. Jalilian-Marian, A. Kovner, A. Leonidov, H. Weigert, Nucl. Phys. **B 504**, 415 (1997).
- [78] J. Jalilian-Marian, A. Kovner, A. Leonidov, H. Weigert, Phys. Rev. **D 59**, 014014 (1999).
- [79] J. Jalilian-Marian, A. Kovner, A. Leonidov, H. Weigert, Phys. Rev. **D 59**, 034007 (1999).
- [80] J. Jalilian-Marian, A. Kovner, A. Leonidov, H. Weigert, Phys. Rev. **D 59**, 099903 (1999).

- [81] E. Iancu, A. Leonidov, L.D. McLerran, Nucl. Phys. **A 692**, 583 (2001).
- [82] E. Iancu, A. Leonidov, L.D. McLerran, Phys. Lett. **B 510**, 133 (2001).
- [83] E. Ferreira, E. Iancu, A. Leonidov, L.D. McLerran, Nucl. Phys. **A 703**, 489 (2002).
- [84] I. Balitsky, Nucl. Phys. **B 463**, 99 (1996).
- [85] Yu.V. Kovchegov, Phys. Rev. **D 60**, 034008 (1999).
- [86] Yu.V. Kovchegov, Phys. Rev. **D 61**, 074018 (2000).
- [87] J.P. Blaizot, E. Iancu, H. Weigert, Nucl. Phys. **A 713**, 441 (2003).
- [88] K. Rummukainen, H. Weigert, Nucl. Phys. **A 739**, 183 (2004).
- [89] T. Lappi, Phys. Lett. **B 703**, (325 (2011)).
- [90] A. Dumitru, J. Jalilian-Marian, T. Lappi, B. Schenke, R. Venugopalan, arXiv:1108.4764.
- [91] E. Iancu, R. Venugopalan, Quark Gluon Plasma 3, Eds. R.C. Hwa and X.N. Wang, World Scientific, hep-ph/0303204.
- [92] F. Gelis, E. Iancu, J. Jalilian-Marian, R. Venugopalan, Ann. Rev. Part. Nucl. Sci. **60**, 463 (2010).
- [93] T. Lappi, Int. J. Mod. Phys. **E20**, 1 (2011).
- [94] R.E. Cutkosky, J. Math. Phys. **1**, 429 (1960).
- [95] G. 't Hooft, M.J.G. Veltman, CERN report 73-9.
- [96] J. Schwinger, J. Math. Phys. **2**, 407 (1961).
- [97] L.V. Keldysh, Sov. Phys. JETP **20**, 1018 (1964).
- [98] M.J.G. Veltman, Physica **29**, 186 (1963).
- [99] S.K. Kauffmann, M. Gyulassy, J. Phys. **A 11**, 1715 (1978).
- [100] E.A. De Wolf, I.M. Dremin, W. Kittel, Phys. Rept. **270**, 1 (1996).
- [101] C. Itzykson, J.B. Zuber, *Quantum field theory*, McGraw-Hill (1980).
- [102] K. Fukushima, F. Gelis, T. Lappi, Nucl. Phys. **A 831**, 184 (2009).
- [103] A. Kovner, L.D. McLerran, H. Weigert, Phys. Rev. **D 52**, 3809 (1995).
- [104] A. Kovner, L.D. McLerran, H. Weigert, Phys. Rev. **D 52**, 6231 (1995).
- [105] Yu.V. Kovchegov, D.H. Rischke, Phys. Rev. **C 56**, 1084 (1997).
- [106] Yu.V. Kovchegov, Nucl. Phys. **A 692**, 557 (2001).
- [107] I. Balitsky, Phys. Rev. **D 70**, 114030 (2004).
- [108] R.J. Fries, J.I. Kapusta, Y. Li, nucl-th/0604054.
- [109] J.P. Blaizot, Y. Mehtar-Tani, Nucl. Phys. **A 818**, 97 (2009).

- [110] Yu.V. Kovchegov, Phys. Rev. **D 54**, 5463 (1996).
- [111] T. Lappi, Phys. Lett. **B 643**, 11 (2006).
- [112] A. Krasnitz, Y. Nara, R. Venugopalan, Phys. Lett. **B 554**, 21 (2003).
- [113] T. Lappi, R. Venugopalan, Phys. Rev. **C 74**, 054905 (2006).
- [114] T. Lappi, Eur. Phys. J. **C 55**, 285 (2008).
- [115] M. Hentschinski, H. Weigert, A. Schafer, Phys. Rev. **D 73**, 051501 (2006).
- [116] A. Makhlin, hep-ph/9608259.
- [117] A. Makhlin, hep-ph/9608261.
- [118] A.H. Mueller, Lectures given at the International Summer School on Particle Production Spanning MeV and TeV Energies (Nijmegen 99), Nijmegen, Netherlands, 8-20, Aug 1999, hep-ph/9911289.
- [119] A. Dumitru, L.D. McLerran, Nucl. Phys. **A 700**, 492 (2002).
- [120] F. Gelis, S. Jeon, R. Venugopalan, Nucl. Phys. **A 817**, 61 (2009).
- [121] E. Iancu, D.T. Triantafyllopoulos, Nucl. Phys. **A 756**, 419 (2005).
- [122] E. Iancu, D.T. Triantafyllopoulos, Phys. Lett. **B 610**, 253 (2005).
- [123] A.H. Mueller, A.I. Shoshi, S.M.H. Wong, Nucl. Phys. **B 715**, 440 (2005).
- [124] A. Kovner, M. Lublinsky, Phys. Rev. **D 71**, 085004 (2005).
- [125] A. Kovner, M. Lublinsky, Phys. Rev. Lett. **94**, 181603 (2005).
- [126] Y. Hatta, E. Iancu, L. McLerran, A. Stasto, D.N. Triantafyllopoulos, Nucl. Phys. **A 764**, 423 (2006).
- [127] I. Balitsky, Phys. Rev. **D 72**, 074027 (2005).
- [128] H. Weigert, Prog. Part. Nucl. Phys. **55**, 461 (2005).
- [129] T. Lappi, L.D. McLerran, Nucl. Phys. **A 772**, 200 (2006).
- [130] E. Iancu, K. Itakura, L.D. McLerran, Nucl. Phys. **A 724**, 181 (2003).
- [131] B. Andersson, G. Gustafson, G. Ingelman, T. Sjostrand, Phys. Rept. **97**, 31 (1983).
- [132] T.S. Biro, H.B. Nielsen, J. Knoll, Nucl. Phys. **B 245**, 449 (1984).
- [133] H. Ehtamo, J. Lindfors, L.D. McLerran, Z. Phys. **C 18**, 341 (1983).
- [134] G. Gatoff, A.K. Kerman, T. Matsui, Phys. Rev. **D 36**, 114 (1987).
- [135] B.I. Abelev, et al., [STAR Collaboration] Phys. Rev. **C 80**, 064912 (2009).
- [136] J. Adams, et al., [STAR Collaboration] Phys. Rev. Lett. **95**, 152301 (2005).
- [137] J. Adams, et al., [STAR Collaboration] Phys. Rev. **C 73**, 064907 (2006).

- [138] F. Wang, [STAR Collaboration] talk at Quark Matter 2004, J. Phys. G **30**, S1299 (2004).
- [139] A. Adare, et al., [PHENIX Collaboration] Phys. Rev. C **78**, 014901 (2008).
- [140] B. Wosiek, [PHOBOS Collaboration], Quark Matter 2008, J. Phys. **G35**, 104005 (2008).
- [141] [CMS Collaboration], JHEP **1009**, 091 (2010).
- [142] T. Lappi, S. Srednyak, R. Venugopalan, JHEP **1001**, 066 (2010).
- [143] K. Fukushima, Phys. Rev. D **77**, 074005 (2008).
- [144] J.F. Gunion, G. Bertsch, Phys. Rev. D **25**, 746 (1982).
- [145] M. Gyulassy, L.D. McLerran, Phys. Rev. C **56**, 2219 (1997).
- [146] M. Daugherty, [STAR Collaboration] PoS C **FRNC2006**, 005 (2006).
- [147] A. Kiyomichi, [PHENIX collaboration] Lake Louise Winter Institute: Fundamental Interactions, Lake Louise, Alberta, Canada, Feb 2005.
- [148] D. Kharzeev, M. Nardi, Phys. Lett. B **507**, 121 (2001).
- [149] D. Kharzeev, E. Levin, Phys. Lett. B **523**, 79 (2001).
- [150] H.J. Drescher, A. Dumitru, A. Hayashigaki, Y. Nara, Phys. Rev. C **74**, 044905 (2006).
- [151] H.J. Drescher, Y. Nara, Phys. Rev. C **75**, 034905 (2007).
- [152] E.V. Shuryak, Phys. Rev. C **76**, 047901 (2007).
- [153] S. Gavin, L. McLerran, G. Moschelli, Phys. Rev. C **79**, 051902 (2009).
- [154] Yu.V. Kovchegov, H. Weigert, Nucl. Phys. A **784**, 188 (2007).
- [155] E. Gardi, J. Kuokkanen, K. Rummukainen, H. Weigert, Nucl. Phys. A **784**, 282 (2007).
- [156] J.L. Albacete, N. Armesto, J.G. Milhano, C.A. Salgado, U.A. Wiedemann, Phys. Rev. D **71**, 014003 (2005).
- [157] J.L. Albacete, Y. Kovchegov, Phys. Rev. D **75**, 125021 (2007).
- [158] J.L. Albacete, N. Armesto, J.G. Milhano, C.A. Salgado, Phys. Rev. D **80**, 034031 (2009).
- [159] J.L. Albacete, N. Armesto, J.G. Milhano, C.A. Salgado, arXiv:0906.2721.
- [160] I. Balitsky, Phys. Rev. D **75**, 014001 (2007).
- [161] I. Balitsky, G.A. Chirilli, Phys. Rev. D **77**, 014019 (2008).
- [162] B. Alver, et al., [PHOBOS Collaboration] arXiv:0903.2811.
- [163] G. Arnison, et al., [UA1 Collaboration] Phys. Lett. B **123**, 108 (1983).
- [164] G.J. Alner, et al., [UA5 Collaboration] Phys. Lett. B **160**, 193 (1985).

- [165] G.J. Alner, et al., [UA5 Collaboration] Phys. Lett. **B 160**, 199 (1985).
- [166] R.E. Ansorge, et al., [UA5 Collaboration] Z. Phys. **C 37**, 191 (1988).
- [167] S.S. Adler, et al., [PHENIX Collaboration] Phys. Rev. **C 76**, 034903 (2007).
- [168] A. Adare, et al., [PHENIX Collaboration] Phys. Rev. **C 78**, 044902 (2008).
- [169] D. Kharzeev, Yu. Kovchegov, K. Tuchin, Phys. Rev. **D 68**, 094013 (2003).
- [170] A. Giovannini, L. Van Hove, Z. Phys.C **30**, 391 (1986).
- [171] C.S. Lindsey, et al., [E735 Collaboration] Nucl. Phys. **A 544**, 343 (1992).
- [172] M.A. Braun, C. Pajares, V.V. Vechernin, Phys. Lett. **B 493**, 54 (2000).
- [173] J. Dias de Deus, E.G. Ferreira, C. Pajares, R. Ugoccioni, Phys. Lett. **B 581**, 156 (2004).
- [174] I.M. Dremin, J.W. Gary, Phys. Rep. **349**, 301, (2001).
- [175] I.M. Dremin, V.A. Nechitailo, Phys. Rev. **D 70**, 034005 (2004).
- [176] P. Romatschke, R. Venugopalan, Phys. Rev. Lett. **96**, 062302 (2006).
- [177] P. Romatschke, R. Venugopalan, Eur. Phys. J. **A 29**, 71 (2006).
- [178] J. Bolte, B. Müller, A. Schäfer, Phys. Rev. **D 61**, 054506.
- [179] H. Fujii, K. Itakura, Nucl. Phys. **A 809**, 88 (2008).
- [180] H. Fujii, K. Itakura, A. Iwazaki, Nucl. Phys. **A 828**, 178 (2009).
- [181] D.T. Son, hep-ph/9601377.
- [182] P.B. Greene, L. Kofman, A.D. Linde, A.A. Starobinsky, Phys. Rev. **D 56**, 6175 (1997).
- [183] R. Allahverdi, R. Brandenberger, F. Cyr-Racine, A. Mazumdar, arXiv:1001.2600.
- [184] A.V. Frolov, JCAP **0811**, 009 (2008).
- [185] J. Berges, J. Serreau, Phys. Rev. Lett. **91**, 111601 (2003).
- [186] S.Yu. Khlebnikov, I.I. Tkachev, Phys. Rev. Lett. **77**, 219 (1996).
- [187] G. Aarts, J. Smit, Phys. Lett. **B 393**, 395 (1997).
- [188] G. Aarts, J. Smit, Nucl. Phys. **B 511**, 451 (1998).
- [189] J. Serreau, hep-ph/0410330.
- [190] J. Berges, S. Borsányi, J. Serreau, Nucl. Phys. **B 660**, 51 (2003).
- [191] G. Aarts, J. Berges, Phys. Rev. Lett. **88**, 041603 (2002).
- [192] G. Aarts, J. Berges, Phys. Rev. **D 64**, 105010 (2001).
- [193] G. Aarts, N. Laurie, A. Tranberg, Phys. Rev. **D 78** 125028 (2008).
- [194] J. Berges, S. Borsanyi, C. Wetterich, Phys. Rev. Lett. **93**, 142002 (2004).

- [195] R.D. Pisarski, Phys. Rev. Let. **63**, 1129 (1989).
- [196] E. Braaten, R.D. Pisarski, Nucl. Phys. **B 337**, 569 (1990).
- [197] J. Kapusta, C. Gale, *Finite temperature field theory; Principles and applications (2nd Edition)*, Cambridge University Press (2006).
- [198] P. Arnold, C. Dogan, G.D. Moore, Phys. Rev. **D 74**, 085021 (2006).
- [199] A.H. Mueller, D.T. Son, Phys. Lett. **B 582**, 279 (2004).
- [200] S. Jeon, Phys. Rev. **C 72**, 014907 (2005).
- [201] D. Bernard, cond-mat/0007106, Lectures given at IPhT, Saclay, France (2000).
- [202] A. Polkovnikov, Annals Phys. **325**, 1790 (2010).
- [203] R. Kubo, J. Phys. Soc. Japan **12**, 570 (1957).
- [204] P.C. Martin, J. Schwinger, Phys. Rev. **115**, 1342 (1959).
- [205] M.V. Berry, J. Phys. A: Math. Gen. **1012**, 2083 (1977).
- [206] C. Jarzynski, Phys. Rev. E **56**, 2254 (1997).
- [207] J.M. Deutsch, Phys. Rev. **A 43**, 2046 (1991).
- [208] M. Srednicki, Phys. Rev. E **50**, 888 (1994).
- [209] M. Rigol, V. Dunjko, M. Olshanii, Nature **452**, 854 (2008).
- [210] P. Aurenche, T. Becherrawy, Nucl. Phys. **B 379**, 259 (1992).
- [211] P. Aurenche, T. Becherrawy, E. Petitgirard, hep-ph/9403320.
- [212] M.A. van Eijck, R. Kobes, Ch.G. van Weert, Phys. Rev. **D 50**, 4097 (1994).
- [213] M.A. van Eijck, Ch.G. van Weert, Phys. Lett. **B 278**, 305 (1992).

Index

- Balitsky-Kovchegov equation, 16, 112
- Berry's conjecture, 182
- BFKL equation, v, 10, 112
- Blast wave model, 102
- Bose condensation, 176
- Bose Einstein condensation, 165, 166, 171, 182
- Boundary conditions, *see* Classical field
 - generator of translations, 39, 45, 62, 64, 69, 83, 156, 199, 218
- Bremsstrahlung, 13

- Chemical potential, 165, 171, 176
- Chiral symmetry restoration, 5
- Classical field, 34, 119
 - boundary conditions, 34, 44, 54, 57, 203, 204
 - instabilities, 121
 - retarded, 34, 52, 54, 83, 196, 203, 205
- Classical source, 3, 13, 17, 18, 21, 52, 77
 - covariant conservation, 53
- Color Glass Condensate, 3, 7, 10, 15, 51, 63, 68, 76, 77, 87
- Confinement, 6, 12, 14
 - Λ_{QCD} , 6
 - transition, 5
- Connected graph, 18, 22, 26
- Contour ordering, 188
- Critical energy density, 5
- Cutkosky, *see* Cutting rules
- Cutting rules, 23

- Decoherence, 147
- Deep Inelastic Scattering, 9, 15

- E735 experiment, 114
- Eigenstate thermalization, 182
- Eikonal coupling, 13
- Energy
 - center of mass, 8
- Energy-momentum tensor, 6, 81, 82, 87, 119
- Entropy, 168
- Equation of state, 6, 135, 139, 144, 148

- Equilibrium, 121, 146
 - canonical, 152
- Ergodicity, 135
- Evolution operator, 185
- Exclusive observables, 36, 60
- External source, *see* Classical source

- Factorization, 3, 59, 78, 84, 86
 - in time, 46
 - role of causality, 59
- Fluctuations, 9, 43, 65, 67, 107, 127, 143, 148, 176, 207
 - basis, 39, 44, 207–209
 - classical field variation, 39
 - energy, 152
 - lifetime, 9
 - propagator, 38, 66, 191
- Flux tube, 91, 96, 101, 109, 113, 119
- Fock-Schwinger gauge, 54, 56, 61, 63
- Fragmentation function, 51
- Froissart bound, 10

- Gauge condition, *see* Fock-Schwinger gauge, Light-cone gauge, Lorenz gauge
- Gauge invariance, 14, 128
- Generating functional
 - Feynman amplitudes, 31, 186, 190
 - multiplicity, *see* Particle spectrum
 - Schwinger-Keldysh, 31, 189, 190
- Glasma, 91, 96, 101, 109, 113, 119, 122
- Gluon
 - cascade, 10
 - density, v, 8, 10, 17
 - propagator, 217
 - recombination, v, 11
 - saturation, v, 7, 10, 12, 16
 - spectrum, *see* Particle spectrum
- Green's formula, 39, 40, 195, 196
 - for small fluctuations, 74, 199, 200
 - light-cone gauge, 215
 - on a generic Cauchy surface, 197
 - on the light-cone, 198, 216
 - Schwinger-Keldysh formalism, 201, 203

- Hamilton equations, 225
- Hanbury-Brown-Twiss interferometry, 6
- Heavy ion collisions, v, 5, 7, 15, 49, 81, 87
- Hydrodynamics, 6
 - initial conditions, 6, 51, 81, 87

- Inclusive observable, *see* Particle spectrum; Energy momentum tensor
- Interaction representation, 185

- JIMWLK
 - equation, 15, 59, 68, 69, 76, 78, 217
 - Hamiltonian, 76–79, 83, 86
 - Langevin formulation, 16
- Laplacian Green’s function, 70, 71, 221
- Large Hadron Collider, 12
- Lattice QCD, 5, 6
- Leading Order, 33, 34, 52, 82, 84, 138
- Light-cone
 - coordinates, 213
 - gauge, 53, 64, 69, 214
- Liouville
 - equation, 133, 169, 225, 226
 - theorem, 134, 226
- Logarithms, 15, 63, 65, 66, 68, 69, 72, 73, 76, 84, 86
- Loop correction, *see* Next to Leading Order
- Lorentz
 - contraction, 11, 13, 54
 - time dilation, 9, 13
- Lorenz gauge, 55
- LSZ, *see* Reduction formulas
- Lyapunov exponent, 122, 135, 141
- McLerran-Venugopalan model, 3, 10, 12, 15, 58, 98, 112
- Momentum fraction, 7, 8, 10
- Moyal equation, 177
- Multiplicity, 7, 107
 - Bose-Einstein distribution, 114
 - clustering, 26, 28, 87
 - generating function, 27, 108
 - moments, 27, 109, 113
 - negative binomial distribution, 107, 114
 - Poisson distribution, 28, 29, 87, 107
 - probability distribution, 21, 25, 26, 30, 36
- Next to Leading Order, 37–43, 46, 61, 62, 68–74, 76, 83–85, 123, 140
- Occupation number, 161
- Parametric resonance, 141, 150, 162, 171
- Particle correlations, 26, 84, 87, 94–97, 107
- Particle spectrum
 - generating functional, 29, 32, 43, 45, 52, 87
 - multiple inclusive, 30, 35, 42, 43, 46, 84–86
 - single inclusive, 21, 30, 33, 34, 37–39, 42, 51, 52, 58, 61, 62, 76, 77
- Parton
 - model, v, 9
 - valence, 9, 10, 12
- Perfect fluid, 6
- Phase diagram, 5

PHENIX experiment, 102, 114
 Poisson distribution, *see* Multiplicity
 Polarization vector, 52
 Power counting, 14, 18, 20, 22, 124, 125
 Pressure, *see* Equation of state
 Pure gauge field, 56

 Quantum Chromo-Dynamics, 3, 5, 49
 Quark Gluon Plasma, 6
 Quasiparticles, 158, 167

 Radial flow, 101
 Reduction formulas, 31, 161, 185
 Relativistic Heavy Ion Collider, 7, 12
 Renormalization, 129
 Retarded propagator, 40, 192, 195, 201, 214, 217

 Saturation scale, 6, 11
 Scalar field theory, 3, 17
 Schwinger mechanism, 37, 93
 Schwinger-Keldysh
 formalism, 17, 23, 32, 38, 83, 185, 187
 propagators, 24, 38, 189, 191
 retarded basis, 192
 Secular divergences, 121, 123, 142
 Small x , *see* Momentum fraction
 Spectral density, 155
 STAR experiment, 7, 102

 Thermal equilibrium, *see* Equilibrium
 Turbulence, 165, 171

 UA5 experiment, 114
 Unitarity, 10, 21, 27, 30, 44
 Universality, 16, 59, 60, 78, 84, 86

 Vacuum fluctuations, *see* Fluctuations
 Vacuum-vacuum diagrams, 21, 25, 30, 187, 190
 Valence partons, *see* Parton
 Viscosity, 6
 Von Neumann equation, 177

 Wigner distribution, 177
 Wilson line, 15, 56, 64, 66, 78, 86

 Yang-Mills equation, 14, 52, 55, 58, 82, 85, 121, 122